The Role of Peroxisomes in Chronic Obstructive Pulmonary Disease

Inaugural Dissertation

Submitted to the
Faculty of Medicine
in partial fulfilment of the requirements
for the PhD-Degree
of the Faculties of Veterinary Medicine and Medicine
of the Justus Liebig University Giessen

by
Natalia El-Merhie
of
Minsk, Belarus

Giessen 2016

From the Institute for Anatomy and Cell Biology,
Division of Medical Cell Biology
Director/Chairperson: Prof. Dr. Eveline Baumgart-Vogt
of the Faculty of Medicine of Justus Liebig University Giessen

First Supervisor and Committee Member: Prof. Dr. Eveline Baumgart-Vogt
Second Supervisor and Committee Member: Prof. Christiane Herden
Committee Members: Prof. Dr. Norbert Weissmann

Date of Doctoral Defense: July 24, 2017

Declaration

“I declare that I have completed this dissertation single-handedly without the unauthorized help of a second party and only with the assistance acknowledged therein. I have appropriately acknowledged and referenced all text passages that are derived literally from or are based on the content of published or unpublished work of others, and all information that relates to verbal communications. I have abided by the principles of good scientific conduct laid down in the charter of the Justus Liebig University of Giessen in carrying out the investigations described in the dissertation.”

Giessen, December 15, 2016 Natalia El-Merhie

List of Abbreviations

α1AT, Alpha-1-antitrypsin
AECI, Alveolar type I cells
AECII, Alveolar type II cells
APS, Ammonium persulfate
ARE, Antioxidant response element
BSA, Bovine serum albumin
CAT, Catalase
CCL2, CC-chemokine ligand 2
CCR2, CC-chemokine receptor 2
cDNA, Complementary deoxyribonucleic acid
COPD, Chronic obstructive pulmonary disease
CSE, Cigarette smoke extract
DBD, DNA binding domain
DHA, Docosahexaenoic acid
DHAPAT (GNPAT), Dihydroxyacetone phosphate acyltransferase
DMSO, Dimethyl sulfoxide
DNA, Deoxyribonucleic acid
DTT, 1,4-dithio-DL-threitol
EDTA, Ethylenediamine tetraacetate
$FEV_{1,}$ Forced expiratory volume in one second
FGF, Fibroblast growth factors
FVC, Forced vital capacity
GOLD, Global initiative for chronic obstructive lung disease
HO-1, Heme oxygenase 1
IF, Immunofluorescence
IHC, Immunohistochemistry
IL, Interleukin
INF-γ, Interferon gamma
iNOS, Inducible nitric oxide synthase
Keap1, Kelch-like ECH-associated protein 1
KO, Knockout
LBD, Ligand binding domain
LCFA, Long-chain fatty acid
MOPS, 3-(N-morpholino) propane sulfonic acid
MMP, Matrix metalloproteinase
ng, Nanograms
NO, Nitric oxide
Nrf2, Nuclear factor erythroid 2-related factor 2
$O_2 \cdot^-$, Superoxide radical
·OH, Hydroxyl radical

PBD Peroxisome biogenesis disorder
PBS, Phosphate-buffered saline
PBST, Phosphate-buffered saline with Tween
PCR, Polymerase chain reaction
PED, Peroxisomal enzyme deficiency
Pex, Gene encoding a peroxin (peroxisome biogenesis protein)
PFA, Paraformaldehyde
PPAR, Peroxisome proliferator-activated receptors
PTS, Peroxisomal targeting signal
PUFA, Polyunsaturated fatty acids
RNA, Ribonucleic acid
ROS, Reactive oxygen species
RT, Room temperature
RXR, Retinoic X receptor
RZG, Rosiglitazone
SDS-PAGE, Sodium dodecyl sulfate polyacrylamide gel electrophoresis
SLPI, Secretory leukocyte protease inhibitor
siRNA, Small interfering RNA
SOD, Superoxide dismutase
TAE, Tris-acetate EDTA buffer
TEMED, N, N, N, N-tetramethylethylenediamine
TGF-β, Transforming growth factor-beta
THIOLASE, Peroxisomal 3-ketoacyl-CoA Thiolase
TNF-α, Tumor necrosis factor alpha
Tris, Tris (hydroxymethyl) aminomethane
VLCFA, Very long-chain fatty acid
v/v Volume/volume
WHO World Health Organization
WT Wild-type
w/v Weight/volume
X-ALD X-linked Adrenoleukodystrophy
ZSS Zellweger syndrome spectrum

List of Figures

Fig. 1. Normal bronchus vs. narrowed bronchus with excess mucous build-up. 4
Fig. 2. Shows the normal alveoli vs. COPD alveoli with disrupted alveolar attachments. 4
Fig. 3. Mechanisms of molecular pathogenesis in COPD (From Barnes, *J Clin Invest.,* 2008) [72]. 8
Fig. 4. Schematic representation of the matrix protein import (From Colasante *et al*., *Thromb Haemost.*, 2015) [104]. 12
Fig. 5. Schematic representation of ROS homeostasis by peroxisomes (Modified from Bonekamp *et. al*., *Biofactors,* 2009) [115]. 14
Fig. 6. Illustration of different mechanisms of peroxisomal degradation (pexophagy) (Modified from Manjithaya *et. al*., *FEBS Lett.*, 2010) [121]. 15
Fig. 7. PPAR gene transcription mechanisms (From Kota *et al*., *Pharmacol Res*., 2005). [148] 18
Fig. 8. Cigarette smoke generation apparatus. 26
Fig. 9. CLSM images of IF preparations for mucin 5 (MUC5AC). 41
Fig. 10. CLSM images of IF preparations for the peroxisomal biogenesis enzyme PEX14 43
Fig. 11. CLSM images of IF preparations for the peroxisomal β-oxidation enzyme ACOX1 43
Fig. 12. CLSM images of IF preparations for the peroxisomal β-oxidation enzyme Thiolase 44
Fig. 13. CLSM images of IF preparations for the peroxisomal antioxidative enzyme catalase (CAT). 44
Fig. 14. Expression of peroxisomal biogenesis (PEX13 and PEX14) and peroxisomal targeting receptors (PEX5 and PEX7). 46
Fig. 15. Real-time PCR and Western blot of ether phospholipid synthesis enzyme. 46
Fig. 16. Real-time PCR of peroxisomal β-oxidation gene. 47
Fig. 17. Real-time PCR and Western blots of the transcription factors 47
Fig. 18. Real-time PCR of the pro-inflammatory cytokines. 47
Fig. 19. CLSM images IF preparations for the peroxisomal biogenesis enzyme Pex14. 50
Fig. 20. CLSM images of IF preparations for the peroxisomal antioxidative enzyme catalase (Cat). 51
Fig. 21. The expression levels of peroxisomal biogenesis gene mRNAs. 51
Fig. 22. Real-time PCR of peroxisomal β-oxidation (*Acoox1* and *Acaa1*) and ether lipid synthesis (*Agps*) gene 51
Fig. 23. The expression levels of antioxidative (A), and transcription factor (B) gene mRNAs 52
Fig. 24. The expression levels of inflammatory mediator. 52
Fig. 25. Cell viability of cigarette smoke extract-exposed HBE cells. 53
Fig. 26. CLSM images of IF stainings for peroxisomal biogenesis (A-D), β-oxidation (E-F) and ether lipid synthesis (G-H) proteins in HBE cells. 54
Fig. 27. CLSM images of IF stainings for the antioxidative enzyme CAT in HBE cells. 55
Fig. 28. The expression levels of peroxisomal gene mRNAs (A-C) and protein abundance (D). 56
Fig. 29. Real-time PCR of peroxisomal β-oxidation gene mRNAs. 56
Fig. 30. Real-time PCR and Western blot analyses of peroxisomal ether phospholipid synthesis gene mRNAs and proteins. 57
Fig. 31. Real-time PCR and Western blot analysis of peroxisomal antioxidative (CAT) and transcription factor (PPARγ) gene 57
Fig. 32. The expression levels of inflammatory mediators 57
Fig. 33. Cigarette smoke extract induced IL-8 production in HBE cells. 58
Fig. 34. Cell viability of cigarette smoke extract-exposed cells. 59
Fig. 35. CLSM images of IF stainings for peroxisomal biogenesis proteins in C22 cells 60
Fig. 36. CLSM images of IF stainings for peroxisomal β-oxidation (Thiolase) and antioxidative (CAT) proteins in C22 cells. 60
Fig. 37. The expression levels of peroxisomal biogenesis gene mRNAs (A) and protein abundance (B) 61

Fig. 38. Real-time PCR of peroxisomal β-oxidation gene mRNAs 61
Fig. 39. Real-time PCR and Western blot analysis of peroxisomal ether phospholipid synthesis *Agps* mRNA (A) and protein (B). 61
Fig. 40. Gene expression and protein abundance of transcription factors 62
Fig. 41. Real-time PCR and Western blot analysis of pro-inflammatory cytokines (A) and the inflammatory marker (B) 62
Fig. 42. Cigarette smoke extract induced cytokine release in C22 cells. 63
Fig. 43. Real-time PCR and Western blot analyses of antioxidative gene 63
Fig. 44. Real-time PCR and Western blot analysis of peroxisomal biogenesis gene 65
Fig. 45. Effects of *Pex13* gene knock-down as shown by immunofluorescence. 65
Fig. 46. Mistargeting of CAT into the cytoplasm after *Pex13* knock-down 65
Fig. 47. Real-time PCR and Western blot analysis of peroxisomal biogenesis gene. 66
Fig. 48. Real-time PCR and Western blot analysis of peroxisomal antioxidant and ether phospholipid synthesis gene mRNA and protein 67
Fig. 49. Real-time PCR of peroxisomal β-oxidation gene mRNAs 67
Fig. 50. Percentage of BrdU positive cells 68
Fig. 51. CSE increased the expression of pro-inflammatory mediators 69
Fig. 52. Cigarette smoke extract induced the release of pro-inflammatory cytokines (IL-6 and TNF-α) 69
Fig. 53. Measurement of ROS by dihydroethidium (DHE) staining after different siRNA treatments 70
Fig. 54. Cigarette smoke extract induced the mRNA expression and protein abundance of transcription factors in siRNA-*Pex13* transfected cells. 71
Fig. 55. Cigarette smoke extract induced the mRNA expression and protein abundance of Nrf2 regulated antioxidative enzymes SOD1 and HO-1 in *Pex13* siRNA transfected cells 71
Fig. 56. Increased ARE response element activity in *Pex13* knock-down cells. 72
Fig. 57. PPARγ knock-down. 72
Fig. 58. *Pparγ* knock-down downregulated Pex13 73
Fig. 59. *Pparγ* knock-down reduced the expression and abundance of the peroxisomal antioxidative enzyme catalase (CAT). 73
Fig. 60. Cigarette smoke extract induced expression and abundance of Nrf2 in *Pparγ* siRNA transfected cells. 74
Fig. 61. Cigarette smoke extract induced expression and abundance of Nrf2-regulated antioxidative enzymes SOD1 and HO-1 74
Fig. 62. *Pparγ* knock-down and CSE treatment. 75
Fig. 63. Increased ARE response element activity in PPARγ knock-down cells. 75
Fig. 64. Percentage of BrdU positive cells. 76
Fig. 65. RZG treatment induced the expression and abundance of PEX13 in the CSE treated cells 76
Fig. 66. RZG treatment induced the expression and abundance of antioxidative enzyme CAT in the CSE treated cells 77
Fig 67. RZG stimulation induced the peroxisomal β-oxidation (A) and ether phospholipid synthesis enzymes (B and C) 78
Fig. 68. RZG activation induced the expression (A) and abundance of the Nrf2 (B) and Nrf2 regulated antioxidant enzymes (C and D). 78
Fig. 69. Increased ARE response element activity in RZG treated cells. 79
Fig. 70. RZG treatment reduced the expression of pro-inflammatory mediators and prooxidant COX-2. 79
Fig. 71. RZG attenuated the release of pro-inflammatory cytokines (IL-6 and TNF-α) 80
Fig. 72. Measurements of ROS by dihydroethidium stain following RZG treatment. 81
Fig. 73. PPARγ overexpression promotes PPARγ activation. 81

Fig. 74. PPARγ overexpression induces down-regulation of the peroxisomal membrane protein PEX13 in the cells treated with CSE. 82
Fig. 75. PPARγ overexpression induces the down-regulation of peroxisomal antioxidative (A), β-oxidation (B) and ether phospholipid synthesis enzymes (C) in the cells treated with CSE. ... 83
Fig. 76. PPARγ overexpression provoked a decrease of Nrf2 (A) and of its regulated antioxidant enzymes (B&C) in the cells treated with CSE 84
Fig. 77. PPARγ expression attenuated the mRNA expression (A) and the release (B) of pro-inflammatory cytokines in the media of CSE treated cells 85
Fig. 78. Percentage of BrdU positive cells 85
Fig. 79 Cigarette smoke-extract (CSE) treatment. 98
Fig. 80 Rosiglitazone treatment. 99
Fig. 81 Cells with overexpressed PPARγ 100

List of Tables

Table 1. Spirometric classification of COPD severity based on FEV_1 (Adapted from Juvelekian and Stoller, 2012) [17]. 2
Table 2. Risk factors for COPD development (Adapted from the Global Initiative for COPD, 2005) [14]. 3
Table 3. Some of the important exogenous and endogenous PPARγ activators 18
Table 4. The chemicals used in the experiments with the corresponding providers. 22
Table 5. The chemicals used in the experiments with the corresponding providers. 23
Table 6. General materials and the cell culture medium used in the experiments 24
Table 7. Solutions for isolation of proteins for SDS PAGE and Western blotting 31
Table 8. Recipes for two 10% SDS-polyacrylamide gel with a comb thickness of 1.25mm 31
Table 9. The composition of the buffers used for western blotting 32
Table 10. List of primary antibodies used in this study 33
Table 11. The experimental procedure of immunofluorescence staining on paraffin-embedded tissue sections 35
Table 12. Solutions used for immunofluorescence staining of paraffin-embedded tissue sections 35
Table 13. Solutions used for immunofluorescence staining of cells grown on coverslips. 36
Table 14. Sequences of the human primers used for the qRT-PCR 38
Table 15. Sequences of the mouse primers used for the qRT-PCR 38
Table 16. Characteristics of the selected COPD patients and lung donors as control subjects. 41
Table 17. Peroxisomal enzymes in various cells of the control and COPD lungs, their localization and comparison 49

Table of Contents

List of Abbreviations i
List of Figures vi
1. Introduction 1
1.1. The History and Definition of COPD 1
1.2. Epidemiology 2
1.3. Risk Factors 2
1.3.1. Cigarette Smoke vs. Cigarette Smoke Extract 3
1.4. Pathophysiology 3
1.4.1. Chronic Bronchitis 3
1.4.2. Emphysema 4
1.5. Pathology 5
1.5.1. Airway Epithelium and Cigarette Smoke 5
1.5.2. Oxidative Stress 6
1.6. Molecular Mechanisms of COPD Pathogenesis 7
1.7. Therapeutic Approaches 9
1.8. Peroxisomes 10
1.8.1. Discovery and Morphology of Peroxisomes 10
1.8.2. Biogenesis of Peroxisomes 10
1.8.3. Peroxisomal Matrix Protein Import 11
1.8.4. Peroxisomal Topology 12
1.8.5. Peroxisome Degradation 14
1.8.6. Peroxisomal Disorders 15
1.9. Peroxisomes in the Lungs 16
1.9.1. Peroxisomes in the Lung Epithelium 16
1.9.2. Peroxisome Proliferator-activated Receptors 17
1.9.3. PPAR Transcription Machinery 18
1.9.4. Peroxisomes and COPD 19
1.9.5. PPARγ and COPD 20
2. Aims of the study 21
3. Materials and Methods 22
3.1. General Materials used in the laboratory 22
3.1.1. Routine materials used for molecular and morphological experiments 22
3.1.2. Laboratory instruments used 23
3.1.3. The materials used for culturing the cells 24
3.2. Human and animal tissue materials used 24
3.2.1. Human tissue samples 24
3.2.2. Mouse samples 25
3.3. Methods 25
3.3.1. Cell culturing of different cell lines 25
3.3.1.1. Cell culture of primary HBE cells 25
3.3.1.2. Cell culture of C22 cells 25
3.3.2. Preparation of Cigarette Smoke Extract (CSE) 26
3.3.3. MTT Assay 26
3.3.4. Treatment of cells 27
3.3.4.1. PPARγ agonist 27
3.3.4.2. Cigarette smoke extract 27
3.3.5. Transfection 27
3.3.6. Luciferase activity assay 28
3.3.6.1. Transfection 28
3.3.6.2. Preparation of cell lysates 28
3.3.7. Dihydroethidium (DHE) staining 29
3.3.8. BrdU cell proliferation assay 29
3.3.9. Cytokine and chemokine levels in supernatants 29
3.3.10. Western Blot 30
3.3.10.1. Lung tissue homogenate preparation for Western Blots 30
3.3.10.2. Cell preparation for Western Blots 30
3.3.10.3. SDS-PAGE and blotting 31
3.3.11. Indirect Immunofluorescence 35
3.3.11.1. Immunofluorescence of embedded tissues 35
3.3.11.2. Immunofluorescence of cells 36

3.3.12. RNA Isolation 37
3.3.12.1. RNA isolation from cells 37
3.3.12.2. RNA isolation from tissues 37
3.3.12.3. cDNA synthesis 37
3.3.12.4. qRT-PCR 37
3.3.13. Statistical Analysis 39
4. Results 40
4.1. Human COPD samples 40
4.1.1. Patient sample selection 40
4.1.2. Peroxisomal biogenesis, lipid metabolism and anti-oxidative enzymes are altered in COPD patients 42
4.1.3. Peroxisomal distribution in various cell types of control and COPD lungs 48
4.2. COPD mouse model 49
4.2.1. Peroxisomal biogenesis, lipid metabolism and antioxidative enzymes are altered in COPD mouse model as well 49
4.3. Human bronchial epithelial cells 52
4.3.1. Cigarette smoke exposed human cell culture model 52
4.3.2. CSE mediates upregulation of peroxisomes in the HBE cell culture COPD model 53
4.3.3. *PEX13* knockdown 58
4.4. Immortalized (Conditionally) Mouse Lung Club Cells (C22) cells 58
4.4.1. Cigarette smoke-exposed model 58
4.4.2. CSE treated C22 cells reveal an upregulation of peroxisomes 59
4.4.3. *Pex13* knockdown in C22 cells 63
4.4.3.1. Peroxisome deficiency in *Pex13* knockdown in C22 cells 63
4.4.3.2. *Pex13* deletion negatively affects cell proliferation 67
4.4.3.3. The *Pex13* deletion and CSE treatment induced a strong increase in the expression and the release levels of pro-inflammatory cytokines 68
4.4.3.4. Peroxisomal deficiency induces a much higher ROS production after CSE treatment 69
4.4.3.5. Peroxisomal dysfunction due to Pex13 knockdown induced an oxidative response 70
4.4.3.6. *Pparγ* regulates the *Pex13* expression 72
4.4.3.7. *Pparγ* silencing provoked a similar response of antioxidative enzymes as was observed after *Pex13* knock-down 73
4.4.4. PPARγ stimulation induces the elevation of peroxisomes 76
4.4.4.1. RZG treatment reduced the CSE induced pro-inflammatory and pro-oxidant reaction in the cells 79
4.4.4.2. RZG treatment attenuates the oxidative stress in the cells stimulated with cigarette smoke extract 80
4.4.5. PPARγ overexpression blocks the CSE-induced oxidative stress response 81
5. Discussion 86
5.1. The role of peroxisomes in scavenging ROS and attenuating oxidative stress and their possible effects in ameliorating the pathophysiology of COPD 87
5.2. The peroxisomal compartment and its corresponding genes are activated in COPD patients with high MUC5 expression 87
5.3. A similar pattern of peroxisomal induction was detected in a mouse COPD model 90
5.4. Generation of an *in vitro* cigarette smoke-extract COPD model 91
5.6. Peroxisome proliferation can be activated by PPARγ agonists reducing inflammation, oxidative stress and ROS release 94
6. Summary 101
7. Zusammenfassung 103
8. Appendix 105
X. PPARγ Cloning 105
9. References 121
Acknowledgements 135
Curriculum Vitae ..... Error! Bookmark not defined.

1. Introduction

1.1. The History and Definition of COPD

The clinical understanding of chronic obstructive pulmonary disease (COPD) has evolved over time, such that one of the first descriptions of emphysema was made by the Swiss physician Theophile Bonet in 1679 when he described a condition of 'voluminous lungs' [1]. Much later, in 1769, the Italian anatomist Giovanni Morgagni described 19 cases of "turgid" from air lungs [2] and only in 1789 Braille's illustrations of emphysematous lungs suggested that emphysema could be a part of a more complex disease [3]. In 1814, the British doctor Charles Badham used the word "catarrh" to describe chronic cough and mucous hypersecretion known today to be the characteristics of chronic bronchitis [4]. Moving ahead to 1821, Rene Laënnec, the French physician and inventor of the stethoscope, described a combination of emphysema and chronic bronchitis as; hyperinflated lungs where the bronchus is filled with mucus [5].

However, the diagnosis of COPD became possible only in 1846 when John Hutchinson invented the spirometer [6]; yet, it only measured the vital capacity. It took another 101 years until Tiffeneau and Pinelli added the concept of timed vital capacity as a measure of airflow [7]. Finally, in 1959, physicians at the CIBA Guest Symposium formally defined the terms 'chronic bronchitis' and 'emphysema' [8]. Couple of years later, Dr. William Briscoe used the word 'COPD', he is believed to be the first person establishing this term in his discussion at the 9th Aspen Emphysema Conference in 1965 [9]. Today, this is the preferred term for the disease.

In general, COPD is a progressive disorder which is characterized by airflow limitation that is not fully reversible [10]. It is a heterogeneous disease that affects central airways causing chronic bronchitis, peripheral airways leading to small airway disease, and lung parenchyma giving rise to emphysema [11]. Due to emphysema, the airway attachments in COPD patients are disrupted leading to airway closure and gas trapping in the alveoli [12]. Moreover, the peripheral airways in the patients are obstructed by inflammatory cell infiltration, fibrosis and mucus hypersecretion [13].

According to Global Initiative for Chronic Obstructive Lung Disease (GOLD), the diagnosis of COPD and of its severity is based on the spirometric criteria, where the ratio of forced expiratory volume in one second (FEV_1) to the forced vital capacity (FVC) is estimated [14]. FEV_1 is the volume expired in the first second of maximal

expiration after a maximal inspiration whereas FVC is a maximum volume of air that can be exhaled during a forced exhalation. The drop in the FEV_1/FVC ratio below 0.7 (FEV_1/FVC ratio <70%) indicates airflow limitation and the possibility of COPD [15,16]. Based on the FEV_1 degree (GOLD), the spirometric classification of severity of COPD includes four stages which are summarized in **Table 1** [17].

Disease Severity	GOLD
Stage I: mild	FEV_1 ≥80% of predicted
Stage II: moderate	FEV_1 50% to < 80% of predicted
Stage III: severe	FEV_1 30 to < 50% of predicted
Stage IV: very severe	FEV_1 <30% of predicted

Table 1. Spirometric classification of COPD severity based on FEV_1 (Adapted from Juvelekian and Stoller, 2012) [17].

1.2. Epidemiology

The prevalence of chronic obstructive pulmonary disease (COPD) is increasing and it is becoming one of the leading causes of morbidity and mortality all over the world [18]. In 2002, the World Health Organization (WHO) has predicted that COPD will become the fifth most common cause of disability and the third most common cause of death in the world by 2020 [19]. However, according to the WHO report in 2012, COPD has already become the third leading cause of death worldwide (**Fig. 1**) [20]. In addition to increased prevalence and mortality, there is currently no cure for this disease.

1.3. Risk Factors

Two types of risk factors are responsible for the development of COPD; environmental factors and genetic risk factors. The most commonly encountered risk factor for COPD is cigarette smoking which accounts for 80%-90% of COPD cases [21]. In smokers, the oxidant burden is enhanced due to the fact that cigarette smoke is a mixture of over 4,700 chemical compounds; it contains 10^{14} oxidants/puff and 3,000 ppm nitric oxide (NO) per puff [22]. Free radicals in cigarette smoke are in the gas and tar phase. The gas phase includes short lived oxidants like nitric oxide, peroxide, peroxynitrite and nitrogen dioxide, whereas the tar phase includes long-lived radicals such as: semiquinones, which react with oxygen to produce $\cdot O_2 \cdot^-$, $\cdot OH$ and H_2O_2 [23].

Another environmental factor that contributes to the pathogenesis of COPD is the exposure to indoor pollution in poorly ventilated houses due to accumulation of particulate matter arising from cooking and heating with biomass fuel [24]. In addition to this, occupational exposure to gases and fumes increases the risk of COPD

development [25]. This exposure to other risk factors has a cumulative effect with that from cigarette smoking [26]. Although smoking remains the main risk factor, genetics also plays a role. For instance, people suffering from alpha-1-antitrypsin deficiency, a major inhibitor of serine proteases, have a high risk of COPD development [27]. Environmental and inherited risk factors are summarized in **Table 2** [14].

Environmental factors	Genetic factors
Cigarette smoke	Genetic abnormalities
Indoor biomass exposure	Bronchial hyper-responsiveness
Occupational exposures	Reduced lung growth
Outdoor air pollution	Age

Table 2. Risk factors for COPD development (Adapted from the Global Initiative for COPD, 2005) [14].

1.3.1. Cigarette Smoke vs. Cigarette Smoke Extract

Cigarette smoke (CS) as was mentioned above is a mixture of a variety of chemical components. The exposure of mice to cigarette smoke in order to generate a model of human smoking is dated back to 1940s [28] and it continues nowadays, however, this method is time consuming as it is of extended duration. Cigarette smoke extract (CSE), that is used in this thesis, is an alternative for cigarette smoke as it contains most of particulate matter that is found is the cigarette smoke [29-31]. This method was first published by Miller and colleagues as they introduced cigarette smoke components intranasally through CSE exposure [32]. CSE is considered as a second hand smoke and it consists of 85% of smoke that rises from the tip of the burning cigarette between puffs, of 11% of the exhaled smoke from the smoker and from 4% of the contaminants diffused through the cigarette paper [33]. The CSE method has become very popular and it is used now in a wide range of pulmonary and cancer studies in order to unravel important biological cellular pathways. The method for generation of CSE is practically similar in most of the studies, however, the concentration of CSE, the media and the number of cigarettes used varies. The method for CSE generation is described in the methods (section 3.3.2) of this thesis.

1.4. Pathophysiology

1.4.1. Chronic Bronchitis

The presence of chronic productive cough for three months per year in two consecutive years is characterized as chronic bronchitis [34]. This persistent cough, a consequence of chronic irritation caused by gases and noxious particles like cigarette smoke, leads to excess mucous production and increased expression of the

MUC5AC gene [35,36]. Mucous hypersecretion is a result of goblet cell hyperplasia, an increase in the size of bronchial submucosal glands and the impairment in the mucous clearance [37]. Moreover, the accumulation of mucous leads to increased susceptibility to infection. The difficulty in mucous clearance is caused by squamous metaplasia and as a consequence of ciliary dysfunction leading to airway obstruction which is mechanically stimulating coughing [35]. The schematic drawings of the normal and inflamed bronchus with excess mucous are illustrated in the figure (**Fig. 1**).

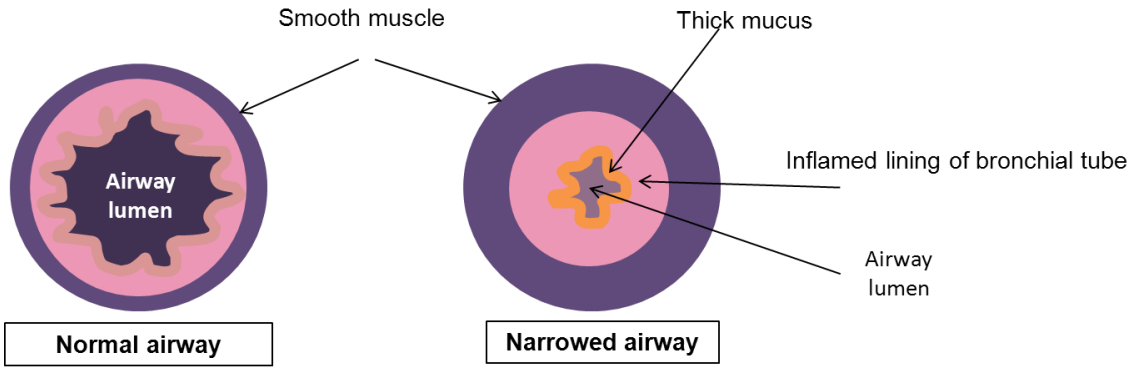

Fig. 1. Normal bronchus vs. narrowed bronchus with excess mucous build-up.

1.4.2. Emphysema

Emphysema is characterized by the destruction of the alveolar wall and permanent enlargement of the airspaces distal to the terminal bronchioles [38]. It is caused by the protease-antiprotease imbalance or by the inherited α1-antitrypsin deficiency [39,40]. Thus, continuous exposure to the cigarette smoke inactivates endogenous antiproteases triggering macrophages and neutrophils to release a variety of proteases, including neutrophil elastase, matrix metalloproteinases (MMPs), and cathepsins [41,42]. The released proteases bind to the lung extracellular matrix causing elastin and collagen degradation [43]. This leads to the damage and loss of alveolar attachments and consequently to the reduction of the elastic supporting structure of the lung resulting in collapse of airways and airflow limitation [44]. The comparison of the normal alveoli with the emphysematous is illustrated in the **Fig. 2**.

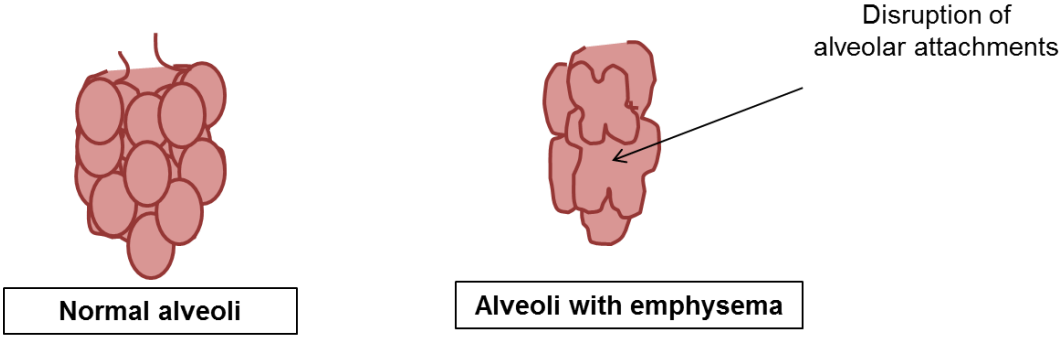

Fig. 2. Shows the normal alveoli vs. COPD alveoli with disrupted alveolar attachments (surface view).

1.5. Pathology

1.5.1. Airway Epithelium and Cigarette Smoke

The first line of defence against the harmful inhaled materials is the airway epithelium, it releases antioxidants which may be activated or inhibited depending on the degree of smoking thus trying to combat and counteract the cigarette-smoke induced stress [45]. Pulmonary epithelium is not only having a protective role, but it also provides communication between different compartments of vascular, interstitial and luminal parts of the lung. It is one of the first targets of cigarette smoke which disables the receptors and enzymes on the membrane of the epithelium and disrupts the tight junctions inducing epithelial changes [46-49]. This anti-oxidative capacity of the airway epithelium can be overwhelmed leading to inflammation, excess membrane permeability and tissue damage leading to disease risk [50]. There are several mechanisms, by which CSE damages the airway epithelium, one of the ways is that cigarette smoke causes the loss of the airway epithelium. Studies have shown that exposure of A549, human lung adenocarcinoma cells, and primary alveolar type II cells to CSE lead to cell senescence, which is an irreversible growth arrest [51]. Several other studies have demonstrated apoptosis of alveolar epithelial cells, inflammatory and endothelial cells in COPD lungs [52,53]. Other studies showed that exposure of A549 cells to lower concentrations of CSE demonstrated no apoptosis, but necrosis [54]**.** Even though that there is a proportionality between the concentration of cigarette smoke and the cell death, apoptosis of alveolar cells can lead to the loss of structure of alveoli, contributing to the onset of emphysema. Another possible mechanism by which CSE can damage the epithelial layer is by affecting its permeability, one of the studies showed that CS induced lung epithelial tight junction permeability in the human epithelial bronchial cell line Calu-3, leading to loss of the epithelial barrier [50]. Another possible mechanism is that CSE could interfere with repair mechanism of the lungs thus changing airway architecture and therefore contributing to COPD pathogenesis. A study using human bronchial epithelial cells (HBE) showed that CS inhibited the HBE proliferation, chemotaxis and the ability to remodel the extracellular matrix [55]. Another study showed that CS reduced the cell attachment, increased cell detachment and decreased cell proliferation in A549 cells [56]. In addition, many cytokines are implicated in the COPD pathogenesis. Human bronchial epithelial cells exposed to CS showed an increased inflammatory response

by release of pro-inflammatory mediators such as IL-1β, RANTES, IL-6, IL-8, and GM-CSF [57]. Altogether, cigarette smoke exerts an enormous impact on the epithelia.

1.5.2. Oxidative Stress

As was mentioned previously, the respiratory epithelium is a major target for oxidative injury from oxidants generated either exogenously or endogenously. The exogenous oxidants come from cigarette smoke or air pollutants like ozone, nitric and sulfur dioxide, whereas endogenous oxidants are generated from reactive oxygen (ROS) and nitrogen (RNS) species released from inflammatory/epithelial cells [23,58] or formed through mitochondrial respiration [59]. ROS and RNS are produced under normal conditions as by-products of metabolism, participating in physiological processes involved in intracellular signalling, angiogenesis, cell proliferation, and gene expression [60]. However, in order to combat the injurious effects of oxidants, the body possesses multiple antioxidant systems which are classified into enzymatic and non-enzymatic ones. The enzymatic system comprises catalase, superoxide dismutase (SOD) and glutathione peroxidase, whereas non-enzymatic includes β-carotene, mucin, vitamin E, ascorbic acid and albumin [61]. Moreover, many antioxidant enzymes are under the control of nuclear factor erythroid 2-related factor 2 (Nrf2). Nrf2 is expressed throughout the lung and is mainly found in epithelial cells and macrophages. Nrf2 plays a protective role in the lungs, under normal conditions Nrf2 exists in the cytoplasm where it is bound to the Kelch-like ECH-associated protein 1 (Keap1) which promotes its ubiquitination and degradation [62]. However, under stress conditions, Nrf2 dissociates from Keap1 and translocates to the nucleus, where it induces the transcription of downstream antioxidant genes (SOD, HO-1, thioredoxin reductase) by binding to the antioxidant response element (ARE) [63].

Despite that, any imbalance between oxidants and antioxidants towards pro-oxidant system leads to oxidative stress in cells and tissues [64]. This stress is not only a result of increased oxidants but also of a decreased antioxidative capacity. Chronic oxidative stress leads to DNA, lipid and protein damage [65] and is responsible for mucous hypersecretion, metaplasia, apoptosis, inactivation of surfactants and anti-proteases [61]. Consequently, the increased burden of oxidative stress is responsible for the inflammation and plays an important role in the development and progression of COPD [66].

Moreover, ROS can oxidize membrane phospholipids when produced close to the cell membranes generating lipid hydroperoxide molecules within the membrane [67]. This leads to tissue permeability, inactivation of membrane-bound receptors and impairment of membrane function [67]. As a result, reactive aldehydes (acrolein and 4-hydroxy-2-nonenal (4-HNE)) and other bioactive molecules, such as isoprostanes are formed. They are highly diffusible products of lipid peroxidation that can alter the function of histone deacetylase HDAC-2 [68] and extracellular proteins, such as collagen and fibronectin [69] by forming adducts with them due to their high affinity towards cysteine, histidine, and lysine residues. This, in turn, affects the cellular function.

In addition to this, ROS and RNS maintain the oxidative stress in the lungs through the activation of macrophages that in turn recruit other inflammatory cells (neutrophils, monocytes, lymphocytes) by releasing cytokines [58]. It was reported that patients with COPD exhibit high levels of oxidative stress markers in their blood, breath, lungs and sputum [70].

1.6. Molecular Mechanisms of COPD Pathogenesis

COPD is characterized by progressive chronic inflammation. The cells involved in its pathogenesis are neutrophils, macrophages and lymphocytes. Cigarette smoke activates the immune cells (neutrophils, macrophages and lymphocytes) to release pro-inflammatory mediators like cytokines, chemokines and chemoattractants thus leading to chronic inflammation [71].

The mechanism of COPD pathogenesis is explained in **Fig. 3** [72]. Inhaled cigarette smoke and other irritants stimulate macrophages and epithelial cells to release inflammatory mediators. Epithelial cells release TGF-β and FGFs which stimulate fibroblast proliferation, inducing fibrosis [72].

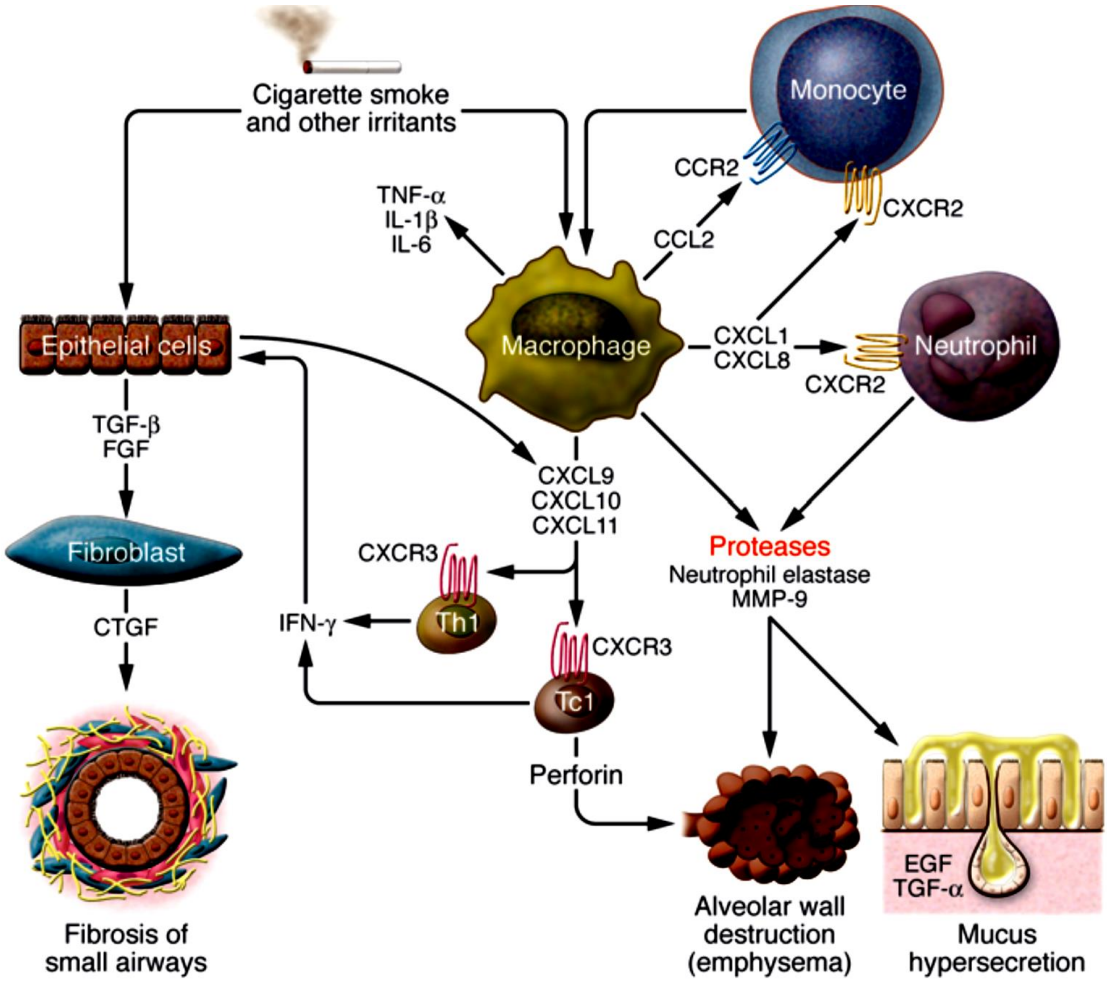

Fig. 3. Mechanisms of molecular pathogenesis in COPD (From Barnes, *J Clin Invest.,* 2008) [72].

Macrophages, in turn, release TNF-α, IL-6 and Il-1β which amplify the inflammation in COPD. Moreover, alveolar macrophages secrete proteases possessing an elastolytic activity such as MMP-9, MMP-12, and cathepsins K, L and S leading to emphysema [73]. In addition to this, alveolar macrophages express CCL2 (also known as monocyte chemotactic peptide MCP-1) which is a potent chemoattractant for monocytes acting via CCR2 [72]. CXC chemokines, CXCL1 (also known as GRO-α) and CXCL8, which are as well derived from alveolar macrophages and act on CXCR2, are responsible for monocyte and neutrophil recruitment [74]. Thereafter, monocytes differentiate into macrophages in the lung. In addition to this, destructive enzymes such as perforin and granzyme B are released from recruited CD8+ lymphocytes (Tc1), resulting in apoptosis of the alveolar epithelial cells [75]. Neutrophils in turn, release chemoattractants like IL-8 and leukotriene B4 (LTB4) to the site of inflammation in order to attract other neutrophils [76]. In addition to this, neutrophils release proteolytic enzymes, including neutrophil elastase (NE), cathepsin G as well as matrix

metalloproteinase MMP-8 and MMP-9, that cause the damage of the elastic lung tissue [77] and promote mucus hypersecretion [78].

1.7. Therapeutic Approaches

Although many approaches have been taken to cure COPD, currently no treatment has been found to prevent the progression of the disease. Some approaches that can alleviate the symptoms of COPD include:

- **Inhaled steroids**: although these locally applied steroids have no effect on the systemic inflammation, they can decrease the frequency of exacerbations and hence improve the health status of COPD patients [79].
- **Anticholinergics**: it was suggested that antagonising the release of acetylcholine from macrophages and epithelial cells and therefore blocking the activation of neutrophils and macrophages could play a role in decreasing the inflammation in COPD. However, it was shown that this only decreases the onset of exacerbations and has no effect on serum interleukins (ILs) in COPD patients [80].
- **Antioxidant intervention**: several antioxidants have been tested as potential candidates for treatment, however; none of them protected against oxidative stress and consequently against COPD onset. This could be due to the fact that most experimental approaches have investigated the effect of a single antioxidant agent, whereas COPD is a heterogeneous disease involving many antioxidant systems [65].
- **Antioxidative pharmacological mimetics**: experimental studies with SOD-mimicking activity agents showed significant antioxidant and anti-inflammatory properties. The studies have only been conducted in models of airway inflammation; the challenge is to find SOD mimetics which decrease airway inflammation, inflammatory cytokines and lipid peroxidation [81].
- **Thiols**: BRONCUS (Bronchitis Randomized on NAC Cost-Utility Study), was the largest antioxidant trial in COPD, however; it failed to show any beneficial effect of the oral administration of N-acetyl cysteine on the frequency of exacerbations and progression of disease [82].

Therefore, new treatment approaches are needed.

1.8. Peroxisomes

1.8.1. Discovery and Morphology of Peroxisomes

Peroxisomes are single membrane-bound organelles that were first discovered electron microscopically by Rhodin [83] and named ‘microbodies’ due to the lack of knowledge concerning their function and biological importance. Two years later, these organelles were identified in rat liver cells by Rouiller and Bernard who suggested that these organelles might be precursors of mitochondria [84]. Only in 1960, De Duve and his co-workers recognized them as a novel enzyme-containing organelle while doing fractionation experiments for lysosome isolation [85]. They noticed that this organelle contains catalase, D-amino acid oxidase, and uric acid oxidase and that it is different from lysosomes, mitochondria and microsomes. Based on the fact that it contains H_2O_2-degrading enzyme (catalase), as well as H_2O_2-producing (flavin-containing oxidases) enzymes, the name ‘peroxisome’ was proposed to this organelle [85].

With the introduction of the alkaline 3, 3′-diaminobenzidine (DAB) reaction for catalase, the peroxisomal detection became possible under the light and electron microscopy [86-88]. Using this method, peroxisomes were identified in every examined tissue except the spermatozoa [89] and the red blood cells . DAB reaction showed that peroxisomes vary in size (ranging from 0,2µm to 1µm in diameter) shape (angular, elongated, interconnected, and tubular) and abundance. This variation of the peroxisomal shape and the organelle’s enzyme content depends on the organ and the cells type and it differs during developmental, environmental and metabolic factors.

1.8.2. Biogenesis of Peroxisomes

All processes involved in the formation of the peroxisomal membrane, import of proteins into the peroxisomal matrix and the proliferation of the peroxisomes are summarized in the term “peroxisome biogenesis” [90]. Peroxisomes either arise *de novo* or multiply by fission from pre-existing peroxisomes [91]. However, it’s not clear yet how these both pathways contribute to the total number of peroxisomes in the wild-type cells [92]. Moreover, how the peroxisomal membrane is generated in the mammalian cells is still the matter of debate, even though, the membrane was described to be synthesized via budding from the endoplasmic reticulum in the yeast model [93,94].

All proteins required for the biogenesis of peroxisomes are termed “peroxins” (PEX proteins) and they are encoded by PEX genes (*Pex* in the mouse) which are numbered according to their date of discovery [90]. Moreover, these peroxins can be divided into different functional groups. For instance, PEX3, PEX16, and PEX19 are involved in the formation of the peroxisomal membrane. Hence, cells that are deficient in either of these peroxins have neither peroxisomes nor peroxisomal membrane remnants [95,96]. PEX5 and PEX7 are responsible for cytoplasmic translocation of peroxisomal matrix proteins [97] whereas PEX13, PEX14 and PEX17 facilitate the docking of receptor/cargo complexes [98]. PEX10 and PEX12 are important for import of proteins into the peroxisome, PEX11 for budding and fission of the organelles and PEX4 for the degradation of the organelle [98]. Nowadays, 31 known peroxins have been discovered, of which 14 peroxins have been identified in human [99].

Since peroxisomes do not contain DNA and ribosomes and therefore have no means of protein production, peroxisomal matrix proteins are synthesized on free ribosomes in the cytosol and then they are post-translationally transported into peroxisomes [97]. Before being imported into the pre-existing organelle, the synthesized peroxisomes are folded into their mature conformation [100].

1.8.3. Peroxisomal Matrix Protein Import

Peroxisomal matrix proteins possess peroxisomal targeting signals (PTS) that enable them to be targeted from the cytosol into the organelle [82]. These peroxisomal targeting signals (PTS) are the PTS1 with the amino-acid consensus sequence (S/C/A) (K/R/H) (L/M) that is located in protein carboxyl-terminal (C-terminus) [101] and the PTS2 that is located in protein amino-terminus (N-terminus) with the consensus sequence (R/K)(L/V/I)(X)5(H/Q)(L/A) [102,103].

Cytoplasmic shuttling receptors (PEX5p and PEX7p), that interact with PTS1 and PTS2 respectively, bind the peroxisomal matrix proteins in the cytoplasm (Cargo Receptor Binding) and translocate them to the docking complex (Docking) in the peroxisomal membrane as illustrated in the figure (**Fig. 4**) [104]. The docking complex comprises two peroxisomal membrane proteins PEX13 and PEX14 to which shuttling receptors bind and subsequently release the cargo into the peroxisome (Cargo Release) [104,105]. Then, the ubiquitination and recycling of PEX5p occurs (Ubiquitination and Translocation, Recycling) and this process requires

PEX1p/PEX6p that are anchored to the peroxisomal membrane by PEX26p in humans [104,106].

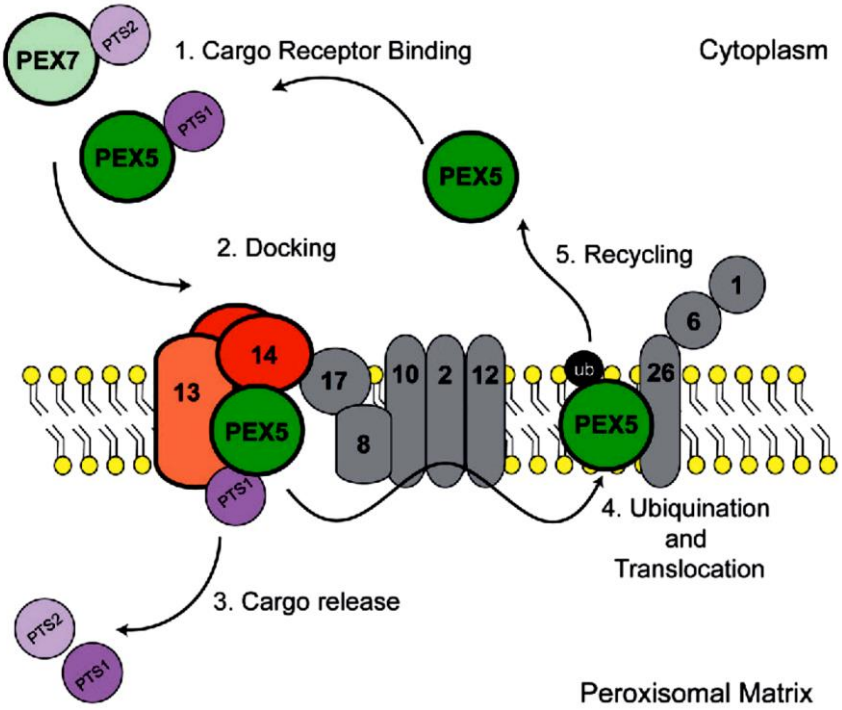

Fig. 4. Schematic representation of the matrix protein import (From Colasante *et al*., *Thromb Haemost.*, 2015) [104].

1.8.4. Peroxisomal Topology

The peroxisomal enzyme content is versatile. It varies from one species to another, even within the same species, and from one organ to another [107]. Peroxisome composition in mammals comprises various enzymes that are divided into different groups (**Fig. 5A**):

- **β-Oxidation enzymes:** peroxisomes catalyze the degradation of a variety of fatty acids that are not metabolized in the mitochondria. Peroxisomes degrade long-chain fatty acids (LCFA), very long-chain fatty acids (VLCFA), long branched-chain fatty acids and eicosanoids; by acyl-CoA oxidases (ACOX1, ACOX2, ACOX3), multi-functional protein 1 and 2 (MFP1,2) and peroxisome 3-ketoacyl-CoA Thiolase (ACAA1) [108,109].
- **Antioxidative enzymes:** peroxisomes degrade various reactive oxygen species (ROS). Catalase, glutathione peroxidase 1 (GPX) and peroxiredoxins 1, 5 (PRX1, PRX5) decompose H_2O_2 whereas superoxide dismutase 1 (SOD1) scavenges superoxide anions.

- **Ether lipid synthesis enzymes:** enzymes responsible for the synthesis of plasmalogens are dihydroxyacetone phosphate acyl-transferase (DHAPAT=GNPAT (glyceronephosphate O-acyltransferase)) and-alkylglycerone phosphate synthase (AGPS) [108].
- **Cholesterol synthesis enzymes:** 3-Hydroxy-3-methyl glutaryl-CoA (HMGCoA) reductase (localized in endoplasmic reticulum as well), Isopentenyl diphosphate delta isomerase (IDI1), mevalonate kinase (MVK), phosphor-mevalonate kinase (PMVK), mevalonate pyrophosphate decarboxylase (MPD), isopentenyl-diphosphate isomerase 2 (IPP) and farnesyl diphosphate (FPP) [110-112].

Specific transporters (e.g. ABCD1) are responsible for carrying various peroxisomal metabolites (VLCFA) across the membrane where these metabolites are broken down by peroxisomal oxidases (light purple) (**Fig. 5A**). During the process of β-oxidation, H_2O_2 is generated and further decomposed to H_2O and O_2 by peroxisomal antioxidative enzymes (light blue) (**Fig. 5A**). Superoxide anions ($O_2^{\bullet-}$), are scavenged by copper-zinc-superoxide dismutase (CuZnSOD) (**Fig. 5A**). In addition to this, M-LP (Mpv17-like protein) (dark blue) is a PMP that is involved in the metabolism of ROS [113]. Nitric oxide (•NO) that is produced from the oxidation of L-arginine by nitric oxide synthase (NOS, dark purple), reacts with $O_2^{\bullet-}$ radicals forming a powerful oxidant peroxynitrite (ONOO−) (**Fig. 5A**). Recent study in hepatocytes has shown that iNOS is also targeted to peroxisomes through interaction with PEX7 [114].

ROS as well as reactive nitrogen species (RNS) are not only scavenged by peroxisomes but they are also generated by this organelle (**Fig. 5B**) [115]. Two corrections have to be made concerning the diagram, Mn-superoxide dismutase (MnSOD) which was used to be recognized as the peroxisome antioxidant enzyme, has been found to be actually located solely within the mitochondrial matrix [116] whereas MPV17 encodes an inner mitochondrial membrane protein [117].

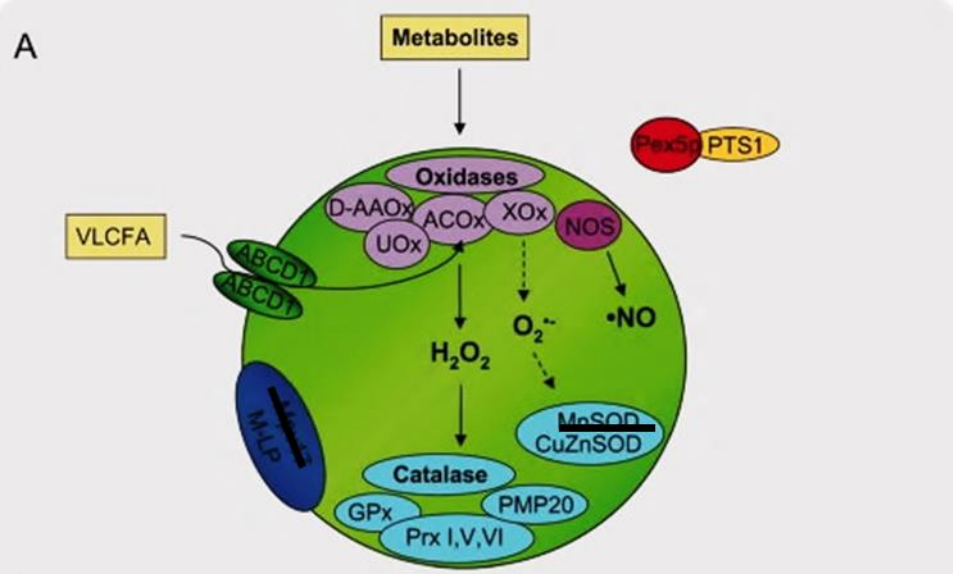

B

Type of ROS/RNS produced	Generating reaction	Produced in PO by	Scavenged in PO by
Hydrogen peroxide (H_2O_2)	$O_2^{\bullet-} + H^+ \rightarrow HO_2^{\bullet}$, $2HO_2^{\bullet} \rightarrow H_2O_2 + O_2$	Acyl-CoA oxidase (several types) Urate oxidase Xanthine oxidase D-amino acid oxidase D-aspartate oxidase Pipecolic acid oxidase Sarcosine oxidase L-alpha-hydroxy acid oxidase Polyamine oxidase	Catalase Glutathione Peroxidase Peroxiredoxin I PMP20
Superoxide anion ($O_2^{\bullet-}$)	$O_2 + e^- \rightarrow O_2^{\bullet-}$	Xanthine oxidase	MnSOD CuZnSOD
Nitric oxide (•NO)	L-Arg + NADPH + H^+ + O_2 → NOHLA + $NADP^+$ + H_2O, NOHLA + ½ NADPH + ½ H^+ + O_2 → L-citrulline + ½ $NADP^+$ + •NO + H_2O	Nitric oxide synthase	

Fig. 5. Schematic representation of ROS homeostasis by peroxisomes (Modified from Bonekamp *et. al*., *Biofactors,* 2009) [115].

1.8.5. Peroxisome Degradation

Peroxisomes have a half-life of around 2 days [118]. Hence, in order to maintain a proper functional peroxisome population, dysfunctional organelles have to be removed. Peroxisomes are degraded by autophagy, in a process called “pexophagy” [119]. The peroxisomal turnover has three important functions: 1) to recycle the cellular components in order to adapt to different environment (non-selective degradation), 2) to remove damaged or non-functional organelles (selective degradation) and 3) to get rid of exhausted peroxisomes (constitutive degradation) [120]. Two different mechanisms of pexophagy occur; macropexophagy and micropexophagy as illustrated in figure (**Fig. 6**) [121]. Macroautophagy involves the sequestration of the organelle by a double-membrane cytosolic structure known as autophagosomes that fuses with the vacuole releasing the autophagic bodies inside for further degradation

[122]. In contrast, micropexophagy involves the engulfment of the organelles by invagination of the vacuolar membrane and further degradation of the organelle in the vacuolar lumen [123].

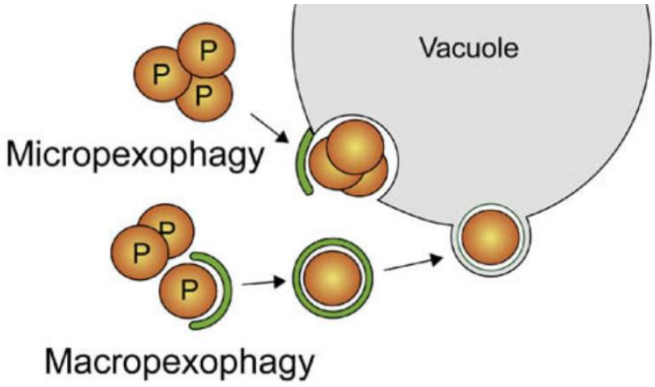

Fig. 6. Illustration of different mechanisms of peroxisomal degradation (pexophagy) (Modified from Manjithaya *et. al*., *FEBS Lett.*, 2010) [121].

1.8.6. Peroxisomal Disorders

The cause of the peroxisomal disorders may be associated either with peroxisome biogenesis disorders (PBDs) or with single peroxisomal enzyme/transporter deficiencies (PEDs).

Peroxisome biogenesis disorders (PBDs) are caused by the mutations in some peroxin genes (*PEX*) which are important for biogenesis of peroxisomes as well as for the peroxisomal carrier proteins [124]. The mutations of the *PEX* genes cause developmental and/or degenerative pathological disorders known as disorders of the Zellweger syndrome spectrum (ZSS) [124]. Peroxisome biogenesis disorders (PBDs) include; Zellweger syndrome (ZS), neonatal adrenoleukodystrophy (NALD) and infantile refsum disease (IRD). The Zellweger syndrome, known as cerebro-hepato-renal syndrome, is characterized by either a reduced number of functional peroxisomes or by a complete lack of peroxisomes [125-127]. Children with ZS suffer from general hypotonia, muscular weakness and are susceptible to life-threatening respiratory problems. They usually die before reaching their 1st year of age from the swallowing dysfunction and respiratory compromise or from cardiac problems [128,129]. Usually, these patients suffer from a decrease in plasmalogens (ether lipids) and polyunsaturated fatty acid (PUFA) as well as from the accumulation of branched-chain and VLC fatty acids [130].

In contrast to peroxisomal biogenesis disorders, in PEDs, peroxisomes are present and mostly intact but there is a deficiency in one of the enzymes, thus leading to

metabolic abnormality [131]. The best known peroxisomal diseases of this group are the ones with mutations in the GNPAT and AGPS genes, which encode the enzymes of the peroxisomal ether lipid synthesis, leading to the diseases such as; rhizomelic chondrodysplasia punctata type 2 and type 3 respectively [132]. The other diseases include: X-linked adrenoleukodystrophy (X-ALD) and acyl-CoA oxidase deficiency [131].

1.9. Peroxisomes in the Lungs

1.9.1. Peroxisomes in the Lung Epithelium

In the early studies published 30-40 years ago, peroxisomes were visualized with the help of DAB reaction in bronchiolar club cells (formerly called Clara cells) and alveolar type II cells (AECII) of different species such as man, mouse, rat, hamster, guinea pig, rabbit, cat, pig and monkey [133-135]. With the discovery of additional peroxisomal marker proteins and the introduction of a more sensitive catalase detection method, identification of peroxisomes became possible in all pulmonary cell types including alveolar type I cells (AECI) and alveolar macrophages of man and mice [136,137]. However, the distribution, size and protein composition of pulmonary peroxisomes showed heterogeneity in distinct cell types indicating the functional differences of this organelle. For instance, club cells, AECII cells and macrophages express higher levels of catalase as well as possess larger peroxisomes than AECI cells. In contrast, higher abundance of β-oxidation enzymes is found in AECI cells [136,137]. The presence of GNPAT in the peroxisomes of AECII cells suggests that they are involved in the synthesis and secretion of the surfactant, which is important for the alveolar function and prevention of alveolar collapse [138]. Moreover, the formation of inflammatory lipid mediators (leukotrienes and prostaglandins) as well as platelet activating factor (PAF, plasmalogens), secreted by macrophages and neutrophils, depends on peroxisomal ether lipid synthesis or peroxisomal β-oxidation [138].

The exposure of lungs to high oxygen concentrations makes them very susceptible to injury mediated by oxidative stress [139]. Nonenzymatic antioxidants, such as glutathione, vitamin C and β-carotene as well as ether lipids (plasmalogens) and polyunsaturated fatty acids (PUFA) in the plasma membranes of airway epithelial cells or in the surfactant film, covering the alveolar region, are the first line of defence against the oxidants [136]. Interestingly, the important steps in the synthesis of these lipids occur in peroxisomes. The second line of defence against oxidative stress includes antioxidative enzymes such as superoxide dismutases, catalase, glutathione

peroxidases and peroxiredoxins. The antioxidative enzymes are degrading various types of ROS and are localized in distinct intracellular subcompartments as well as in different pulmonary cell types [137]. Thus, if the balance between the antioxidative defensive mechanisms and the ROS production is disturbed, pathological changes are induced leading to lung injury and to various airway diseases such as COPD, asthma and pulmonary fibrosis [139]. Therefore, peroxisomes might protect the pulmonary airway epithelium by their high content in different antioxidative enzymes, their role in the synthesis of PUFA and plasmalogens and their ability to degrade toxic lipid derivatives through the β-oxidation systems [136].

1.9.2. Peroxisome Proliferator-activated Receptors

Peroxisome proliferator-activated receptors (PPARs) belong to the nuclear hormone receptor family that function as ligand-activated transcription factors [140]. PPARs play a role in the regulation of important processes, such as cellular differentiation, inflammation, and wound healing [141]. Three different subtypes of PPARs exist: PPARα (also known as NR1C3), PPARγ (also known as NR1C1) and PPARβ (also known as PPARδ or NR1C2). PPARγ was found to be expressed, within the lung in smooth muscle cells, in the epithelia, endothelium, fibroblasts, macrophages, eosinophils, dendritic cells, B cells and T cells [45]. PPARα was found to be localized in the heart, liver, kidneys and intestinal mucosa [142,143] whereas PPARβ is highly expressed in adipose tissue, heart, muscle, intestine, and macrophages [143].

PPARγ (peroxisome proliferator-activated receptor gamma) can be activated by endogenous as well as exogenous factors (**Table 3**). Among the endogenous ligands (natural) for PPARγ are polyunsaturated fatty acids (such as linoleic acid, arachidonic and eicosapentaenoic acid), oxidized lipids (13-HODE and 15-HETE) and prostaglandin (PG)-related compounds, such as 15-deoxy-delta12-14-PGJ2 (15d-PGJ2) [144]. The exogenous ligands (synthetic) include thiazolidinediones (TZDs) like troglitazone, ciglitazone, pioglitazone and rosiglitazone, non-thiazolidinediones (non-TZDs) such as isoxazolidinedione JTT-501 and tyrosine-based ligands, like GW-7845 [145,146].

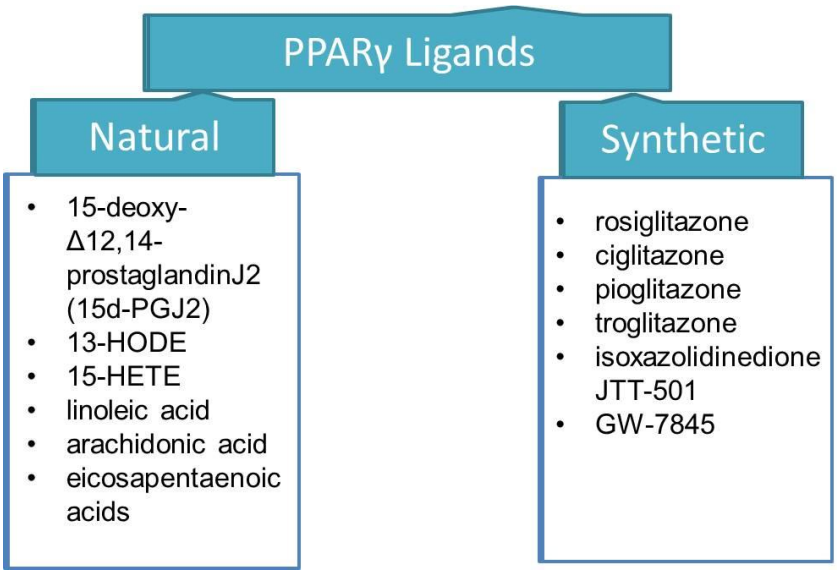

Table 3. Some of the important exogenous and endogenous PPARγ activators

1.9.3. PPAR Transcription Machinery

PPARs have two functional domains that are highly conserved in all the three receptors; a DNA binding domain (DBD) (promotes the binding of PPAR to the peroxisome proliferator response element (PPRE)) and a ligand-binding domain (LBD) (for binding to a wide range of ligands) [147]. As illustrated in the figure (**Fig. 7**) [148], in an inactive state, PPARs interact with the corepressor having histone deacetylase activity thus inhibiting the gene transcription. However, upon binding of endogenous or exogenous ligands to the PPAR, the PPAR-ligand bound complex heterodimerizes with the retinoid X receptor (RXR) forming a PPAR-RXR heterodimer [149]. This heterodimer binds to PPRE leading to recruitment of co-activators that have histone acetylase activity thus inducing the transcription of genes [149]

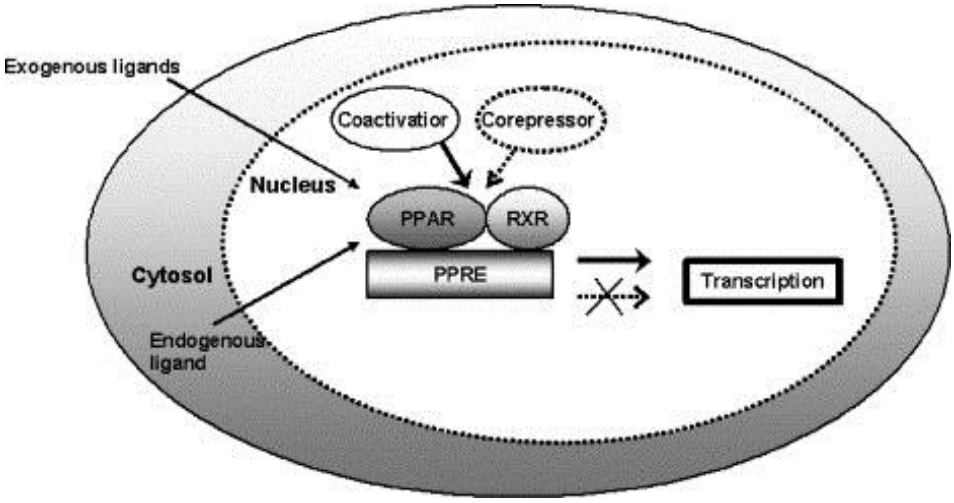

Fig. 7. PPAR gene transcription mechanisms (From Kota *et al*., *Pharmacol Res*., 2005). [148]

1.9.4. Peroxisomes and COPD

Cigarette smoke or cigarette smoke extract (CSE) contain massive amounts of oxidants (ROS and RNS) which provoke oxidative stress by an oxidant/antioxidant imbalance [150]. Therefore, peroxisomes could be easily affected in airway epithelial cells by components of cigarette smoke (e.g. oxidants and NO), since most of these organelles are indeed localized directly underneath of the apical surface of ciliated cells or in the apical region of club cells of the bronchiolar epithelium [136,137]. Moreover, peroxisomes are also very abundant in alveolar type II cells [137].

The role of peroxisomes in the bronchiolar epithelium (BE) as well as in the alveolar region is not well understood and their possible alterations in COPD patients are unknown. However, Karnati and Baumgart-Vogt (2008) [137] suggested that the high numerical abundance of peroxisomes in the ciliated cells of the respiratory epithelium of bronchi and the bronchiolar epithelium in humans may contribute to the protection of the epithelial cells against ROS.

It is of interest that in peroxisomes, lipid and ROS metabolism are intimately linked to each other, since they synthesize plasmalogens (ether lipids) that are able to trap ROS. It is clear, that oxidative stress in the COPD lungs exerts a major role in the aggravation of the disease and that the imbalance of oxidants and antioxidants plays a vital role in the molecular pathogenesis of COPD. It was found that oxidative stress induces alterations in the peroxisomal compartment, such as tubulation of the organelles [151]. Therefore, it is most likely, that the peroxisomal compartment is affected in the alveolar and bronchiolar region of COPD patients [136]. Furthermore, altered peroxisomal lipid metabolism, such as a reduced ether lipid synthesis or a reduced peroxisomal β-oxidation of eicosanoids, which are important lipid mediators of inflammation, might prolong the inflammatory response. In addition to catalase, peroxisomes contain a number of antioxidative enzymes, such as SOD1, glutathione peroxidase and peroxiredoxins I, V and VI [136]. Therefore, the activation of peroxisomal genes and peroxisomal proliferation by peroxisome proliferator-activated receptors (PPARs), could protect the pulmonary airways against the inflammatory onset [152].

Since peroxisomes are intimately involved both in the metabolism of ROS and of pro-inflammatory lipids, alterations in their numerical abundance or in the regulation of their metabolic pathways might, therefore, influence the pathogenesis of COPD.

1.9.5. PPARγ and COPD

Unfortunately, homozygous ablation of PPARγ *in vivo* has been hindered since the deletion of PPARγ caused impaired placental development leading to embryonic lethality [153,154]. PPARγ null mice demonstrated a lethal effect of placenta dysfunction starting from gestational day 9.5 (E9.5) [154], which is actually the time point when the lung development in mice begins [155,156]. Therefore, the dissection of PPARγ function has relied on generation of tissue-specific or isoform-specific knock-out mouse models [157-161].

A study with targeted deletion of PPARγ in the airway epithelium of mice led to enlargement of airway spaces, exhibited abnormal lung maturation, loss of elastic recoil and differences in parenchymal geometry in comparison to control mice [162]. Another study with PPARγ deletion in the airway epithelium promoted the influx of macrophages and produced more severe emphysema, after exposure to cigarette smoke, in comparison to mice possessing the PPARγ gene [163]. Similarly, activation of PPARγ in wild type mice protected against inflammation following the exposure to cigarette smoke [164,165]. PPARγ is found in immune and inflammatory lung cells, it is expressed in monocytes/macrophages, plays a role in differentiation and activation of monocytes and in the regulation of inflammatory activity [166,167]. Moreover, the release of pro-inflammatory cytokines from activated macrophages, eosinophils and airway epithelial cells can be inhibited by PPARγ ligands, resulting in anti-inflammatory and immuno-modulatory effects [45,168,169]. Agonists of PPARγ might regulate epithelial cell inflammation by decreasing cigarette smoke-induced mucin synthesis in the airway epithelium [170]. These PPARγ actions might be pathophysiologically relevant to COPD.

Moreover, it was shown that PPARγ expression is impaired in patients with COPD [171], acute lung injury [172], cystic fibrosis and sarcoidosis [173]. It has been suggested that PPARγ agonists might have potential for COPD treatment [165,174-176]. Therefore, PPARs might be novel targets in lung diseases such as; COPD, asthma and acute lung injury [45,177].

2. Aims of the study

No information is available so far on the role of peroxisomes in the molecular pathogenesis of COPD. As was stated previously in the introduction, the fact the peroxisomes are abundant in the airway epithelium and that they could be directly affected by cigarette smoke as they are located underneath the apical surface of airway epithelia made us hypothesize that they could play a role in COPD. Moreover, since peroxisomes are rich in different antioxidative enzymes, and they play an important role in β-oxidation of eicosanoids, hereby they could protect the pulmonary airway epithelium against ROS and lipotoxicity.

Due to these hypotheses, the aims of the thesis were;

1. To analyze the possible alterations of the peroxisomal compartment in lung samples of COPD patients in comparison to healthy control subjects.
2. To analyze the possible alterations of the peroxisomal compartment in lung samples of a COPD mouse model in comparison to control mice.
3. To study the functional consequences of cigarette smoke extract on the peroxisomal compartment in human HBE cells and mouse C22 cells.
4. To investigate whether impairment in peroxisomal metabolism could affect the molecular pathogenesis of COPD.
5. To evaluate the changes in the peroxisomal compartment, antioxidative enzymes and cytokines following PPARγ overexpression or knockdown in cigarette smoke-treated cells.

3. Materials and Methods

3.1. General Materials used in the laboratory

3.1.1. Routine materials used for molecular and morphological experiments

The chemicals used in the experiments and the corresponding suppliers are listed in **Table 4.**

Table 4. The chemicals used in the experiments with the corresponding providers.

Chemicals	Catalogue number	Providers
2X Rapid Ligation Buffer	C6711	Promega
3-(4,5-dimethylthiazol-2-yl)-2,5-diphenyltetrazolium bromide (MTT)	M5655	Sigma-Aldrich
AccuGENE™ water	51200	LONZA
Acrylamide	EC 890	ProtoGel
Agarose	11404	Serva
Agarose Universal	35-1020	Peqlab
Allstars negative siRNA	1027280	Qiagen
Ampicillin	A6352	Applichem
Bradford reagent	B6916	Sigma-Aldrich
BrdU cell proliferation assay	2750	Millipore
Bromophenol blue	15375.01	Serva
Deoxynucleotide Mix (dNTP)	2201210	5 Prime
Dihydroethidium (DHE)	D7008	Sigma-Aldrich
DNA ladder	10068-013	Invitrogen
DNA Stain G	39803	Serva
Dual luciferase reporter assay	E1910	Promega
ElectroMAX™ DH5α-E™ Competent Cells	11319019	Invitrogen
Ethanol	64-17-5	Merck
Ethylene diamine tetraacetic acid (EDTA)	O3690	Fluka
Gene Pulser®/MicroPulser™ Electroporation Cuvettes, 0.2	1652086	Bio-Rad
Glutaraldehyde	G7651	Sigma-Aldrich
Glycerol	GG1	Sigma-Aldrich
High-Capacity cDNA Reverse Transcription Kit	4368814	ThermoFisher
Human IL-8 ELISA Ready-SET-Go!® (2nd Generation)	88-8086-22	Affymetrix eBioscience
Human TNF alpha ELISA Ready-SET-Go!®	88-7346-88	Affymetrix eBioscience
Immun-Star™ AP Substrate	170-5018	Bio-Rad
MicroPulser™ electroporator	165-2100	Bio-Rad
Milk powder	T145.3	Carl Roth
Mouse IL-6 ELISA Ready-SET-Go!®	88-7064-22	Affymetrix eBioscience
Mouse TNF alpha ELISA Ready-SET-Go!®	88-7324-22	Affymetrix eBioscience
Mowiol 4-88	17951-500	Polysciences
3-[N-Morpholino]-propanesulfonic acid (MOPS)	M-8899	Sigma-Aldrich
N-Propyl-gallate	02370	Sigma-Aldrich
Neomycin	A7002	Applichem
NucleoBond® Xtra Midi EF	REF 740420.50	Macherey-Nagel
NucleoSpin® Gel and PCR Clean-up	Lot 1601/002	Macherey-Nagel
Paraformaldehyde (PFA)	604380	Sigma-Aldrich
Penicillin/Streptomycin	P06-07001	PAN Biotech
pGL2-basic vector	X65323	Promega
Plasmid PPARγ	IPAKp961L1324Q=	RZPD
pRL-SV40 Renilla luciferase (Rluc) control reporter	E2231	Promega
Precision Plus Protein™ Standards Dual Color	161-0374	Bio-Rad
Protease inhibitor mix M	39102	Serva
PVDF membranes	IPVH00010	Millipore
RNAzol® RT	R4533	Sigma-Aldrich

Rosiglitazone	R2408	Sigma-Aldrich
ScreenFect A	S3001	InCella
siRNA Pex13	GEHC1-000790 (SO-24886576)	Dharmacon
siRNA PPARγ isoform 2	S101385398	Qiagen
Sodium chloride	S6191	Merck
Sodium dodecyl sulfate (SDS)	L4390	Sigma
Subcloning Efficiency™ DH5α Competent Cells	18265-017	Invitrogen
TopTaq DNA Polymerase	200203	Qiagen
T4 DNA Ligase	M1804	Promega
Tetramethylethylenediamine (TEMED)	A1148,0025	BioChemica
Trishydroxymethylaminomethane (Tris)	4855.2	Carl Roth
Triton X-100	T8787	Sigma
Tween 20	822184	Merck
Xylene	97133	Carl Roth

3.1.2. Laboratory instruments used

All instruments used for the experimental parts with appropriate manufacturers are summarized in **Table 5.**

Table 5. The chemicals used in the experiments with the corresponding providers.

Instruments	Suppliers
Biocell A10 water system	Milli Q-Millipore
Biofuge Fresco	Heraeus
BioRad electrophoresis apparatus (Sub Cell GT) system	Bio-Rad
Centrifuge mini Uni-fuge	Roth
Dish washing machine (G 78 83 CD)	Miele
Fusion FX	Fisher Biotec
Gel-Doc 2000 gel documentation system	BioRad
Heating and drying table	Medax
Hera cell 240 incubator	Heraeus
Hera safe, clean bench KS-12	Heraeus
Ice machine, Scotsman AF-100	Scotsman Ice Systems
iCycler PCR machine MyiQ2 optical module	Bio-Rad
Leica DMRD fluorescence microscope	Leica
Leica DC 480 camera	Leica
Leica TCS SP2 confocal laser scanning microscope	Leica
Leica SM 2000R rotation microtome	Leica
Microwave oven MB-392445	LG
Mini-Protean 3 cell system	Bio-Rad
Mini Trans-Blot® Cell	Bio-Rad
Multifuge 3SR centrifuge	Heraeus
NanoDrop™ 8000	ThermoFisher
Oven HERAEUS T 5050 EKP	Heraeus
Paraffin tissue floating bath	Medax
pH meter E163649	IKA
Pipettes ErgoOne	Starlab
Potter-Elvehjem homogenizer 8533024	B.Braun
PowerPac 200	Bio-Rad
Pressure/Vacuum Autoclave FVA/3	Fedegari
Pump Drive PD 5001	Heidolph Instruments
Smartspec™ 3000 spectrophotometer	Bio-Rad
Thermostat Block HBT 130	HLC, BioTech
Trans-Blot SD semi dry transfer cell	Bio-Rad
Trimmer TM60	Reichert
TRIO-Thermoblock	Biometra
TriStar LB 941 Multimode Reader	Berthold

Ultra balance LA120S	Sartorius
Ultra Turrax T25 basic homogenizer	Junke & Kunkel
Universal balance	Sartorius
Vortex MELB 1719	Merck Eurolab
Water bath shaker GFL 1083	GFL

3.1.3. The materials used for culturing the cells

The general materials and the cell culture medium used for culturing of HBE and C22 are listed in **Table 6.**

Table 6. General materials and the cell culture medium used in the experiments

Material for cell culture	Suppliers
Cover slips	Menzel-Gläser, Germany
Culture dish (60mm)	BD Biosciences, Germany
Multi-well cell culture plates (6 wells)	BD Biosciences, Germany
Multi-well cell culture plates (12 wells)	BD Biosciences, Germany
Multi-well cell culture plates (24 wells)	BD Biosciences, Germany
Nalgene syringe filter (0.2µm)	ThermoFisher Scientific, Germany
HBE materials	
Airway Epithelial Cell Basal Medium	ATCC, Germany
Small Airway Epithelial Cell Growth Kit	ATCC, Germany
C22 media	
DMEM, high glucose, GlutaMAX™ supplement	ThermoFisher Scientific, Germany
Endothelin-1	Peninsula labs, USA
Recombinant mouse interferon gamma	Cell Sciences, USA
Insulin	Sigma-Aldrich, Germany
Transferrin	BD Biosciences, Germany
Endothelial cell growth supplement (ECGS)	Sigma-Aldrich, Germany
Epidermal growth factor	BD Biosciences, Germany
Hydrocortisone	BD Biosciences, Germany
T3 Triiodothyronine	Sigma-Aldrich, Germany
Fetal ovine serum	ThermoFisher Scientific, Germany
Penicillin-Streptomycin	Life technology, Germany

3.2. Human and animal tissue materials used

3.2.1. Human tissue samples

Lung-tissue samples from stage IV COPD patients (age range 50-70; females/males) as well as from donors (control) (age range 50-70, females/males) were obtained from the Giessen DZL-biobank at the UGMLC (Universities of Giessen and Marburg Lung Center). The study protocol was approved by the Ethics Committee of the Justus Liebig University school of Medicine (AZ 31/93) in accordance with the national law and with the “Good Clinical Practice/International Conference on Harmonization”. Informed consent for the study protocol was obtained in written form from each subject. For protein extraction, lung tissue was snap-frozen directly after explantation. For morphological studies, lung tissue was immersion-fixed and embedded in paraffin.

3.2.2. Mouse samples

Paraffin-embedded tissue samples from cigarette smoke-exposed and unexposed mice were kindly provided by Dr. Michael Seimetz (Excellence Cluster Cardio-Pulmonary System, ECCPS) from the group of Prof. Dr. Norbert Weissmann group. Briefly, animals were housed under controlled conditions with 12h day and night cycle, with food and water supply ad libitum. Animals were randomly assigned to smoke-exposed and unexposed groups consisting of 6 mice per group. A group of 6 wild type mice was exposed to the mainstream smoke of 3R4F cigarettes; (University of Kentucky, Lexington, KY, USA) for 6h/day, 5days/week for up to 3 months. The control group was kept under identical conditions as smoke-exposed mice but without exposure to the smoke [178].

3.3. Methods

3.3.1. Cell culturing of different cell lines

3.3.1.1. Cell culture of primary HBE cells

Human primary bronchial epithelial cells (HBE), isolated from epithelial lining of airways, were obtained from ATCC (PCS-300-010). Cells were cultured in Airway Epithelial Cell Basal Medium (ATCC, Germany) that was supplemented with the Small Airway Bronchial Epithelial Cell Growth Kit (ATCC, Germany) (**Table 6**). Cells were maintained at 37˚C in a humidified environment of 5% CO_2. Passages from 2 till 8 were used.

3.3.1.2. Cell culture of C22 cells

Mouse club cells are epithelial progenitor lung cells which line the bronchial airways down to the alveoli. The mouse C22 club cells are derived from transgenic H-2kb-tsA58 mice[179], which are conditionally immortalized, expressing a temperature-sensitive Simian Virus 40 (SV40) large T antigen. When the cells are cultured in the presence of IFN-γ (Interferon gamma) at 33°C, the expression of the SV40 large T antigen is induced and the cells proliferate. Cells were purchased from ECACC (Nb. 07021401). They were cultured in Dulbecco's modified Eagle's medium (Thermo Fisher Scientific, Germany), supplemented with 4% FBS, 0.25µg/ml endothelin-1, 0.01µg/ml Interferon gamma, 10µg/ml insulin, 5µg/ml tansferrin, 7.5µg/ml endothelial cell growth supplement (ECGS), 0.025µg/ml epidermal growth factor, 0.36µg/ml hydrocortisone, and 0.02µg/ml T3. The cells were maintained at 33˚C in a 5% CO_2 incubator.

3.3.2. Preparation of Cigarette Smoke Extract (CSE)

Special research cigarettes (3R4F) from the Kentucky Tobacco Research and Development Centre (University of Kentucky, Lexington, KY) were used for the generation of CSE (**Fig. 8**). Cigarette smoke from one research cigarette containing 9.4mg tar and 0.73mg nicotine was bubbled into 15ml of the appropriate medium required for each cell line (section 3.3.1.). Each puff being of 3s followed by a 20s break. After adjusting the pH of the CSE to 7.4, it was filtered through a 0.2µm filter (ThermoFisher). The extract, designated as 100% CSE, was diluted with the appropriate media for each cell type, to 2%, 4%, 8% and 16%. The CSE was either used immediately or stored at -80°C for a maximum of 3 days. For control experiments, air was bubbled into 15ml of the appropriate medium. Cells well treated with either DMSO or with different CSE concentrations for 4 hours.

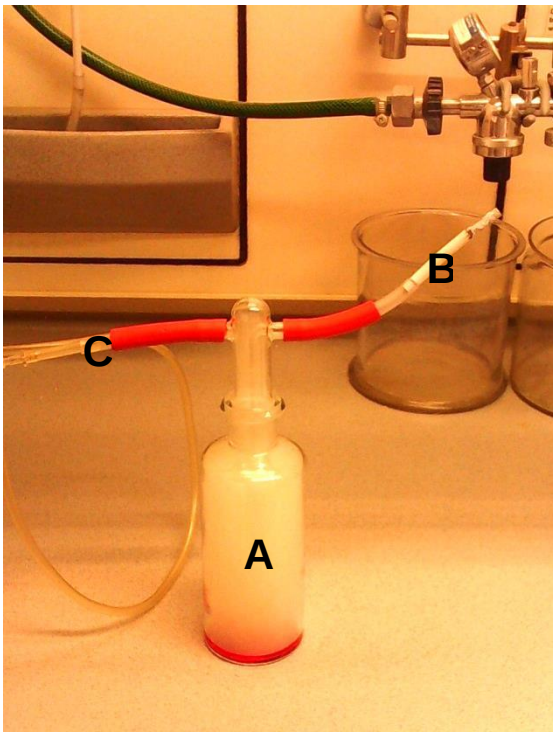

Fig. 8. Cigarette smoke generation apparatus consisting of a flask with the appropriate media (A), cigarette (B) and a connection to a pressure pump (C).

3.3.3. MTT Assay

In order to measure the cell viability in response to the CSE, the 3-(4,5-dimethylthiazol-2-yl)-2,5-diphenyltetrazolium bromide (MTT) (Sigma, Germany) assay was performed. Stock solution was prepared by dissolving 5mg/ml of MTT in a medium lacking phenol red (DMEM). The prepared solution was stored at -20°C. Prior to use, stock solutions were dissolved to equal 1/10th of the original culture volume.

Briefly, HBE and C22 cells were seeded in a 12-well plate, after 24h of seeding, the cells were treated with different concentrations of CSE (0%, 2%, 4%, 8% and 16%) for 4h. Then, the medium was aspirated and the cells were washed once with PBS. After that, 1ml of MTT was added to each well, and the cells were incubated in the incubator for an additional 2-3h to facilitate the conversion of MTT to formazan crystals in living cells by mitochondrial dehydrogenases. After incubation, MTT was removed and dark-violet formazan was solubilized by addition of 300µl/well of DMSO. The optical density was read at a wavelength of 570nm using a Smartspec^{TM} 3000 spectrophotometer (Bio-Rad, Germany).

3.3.4. Treatment of cells

3.3.4.1. PPARγ agonist

Rosiglitazone (RZG) solution was prepared by dissolving 10mg of the drug in dimethyl sulfoxide (DMSO) to obtain a 10mM stock solution. All working solutions were prepared fresh directly from stocks by dissolving (RZG) in the culture media to get the final concentration of 10uM (RZG) per 1ml of medium. Treatment was performed on the cells at 70% confluence after 24h of seeding. The cells were either treated with DMSO as a control or with RZG (10µM/ml media) for 24h prior to any experiment.

3.3.4.2. Cigarette smoke extract

The stock, designated as 100% CSE, was further diluted to 2%, 4%, 8% and 16% in the culture medium required for each cell line. After establishing the toxicity of CSE by MTT assay, the CSE concentration of 8% was further used for all the experiments. For the basal condition, the treatment with CSE was done on the cells at 70% confluence. The cells were either treated with DMSO as a control or with 8% CSE for 4h.

For further experiments, the cells that were previously treated with RZG for 24h or the cells that were transfected with siRNA (*siPex13* or *siPPARγ*) for 72h were thereafter incubated with 8% CSE for 4h or with DMSO as a control.

3.3.5. Transfection

In order to knockdown *Pex13* or *PPARγ* gene expression in C22 cells as well as in order to overexpress the PPARγ gene, the following siRNAs and plasmid were purchased: *Pex13* siRNA (sense GCUAUAGCCCUUAUAGUUATT, antisense

UAACUAUAAGGGCUAUAGCTT), *PPARγ* siRNA (Qiagen) and PCMV Sport PPARγ plasmid (RZPD). Allstars negative siRNA (sequence is proprietary to the company) from Qiagen was used as a control. Cells were transfected with ScreenFectA transfection reagent (InCella) according to the standard protocol from the manufacturer. Cells were seeded 24h prior to transfection in 6-well culture plates. In 2 separate Eppendorf tubes, the following mixtures were prepared: Tube 1 containing (4.5µl of ScreenFect A+120µl of buffer), Tube 2 (30nmol of siRNA+120µl buffer). The prepared mixtures were allowed to stand for 5min at RT. Thereafter, the reagents of the two tubes were mixed together and allowed to stand for an additional 20min at RT. Then, the complexes were transferred to one well of a 6-well plate containing 1250ul of freshly added medium. A similar protocol was used for the transfection with the PPARγ plasmid, where 2ug of the plasmid was used for a single well of a 6-well plate. The protein and RNA were collected 72 hours post transfection.

3.3.6. Luciferase activity assay

3.3.6.1. Transfection

Cells were seeded in 6-well plates 24h prior to transfection or until 60% confluence. In 2 separate Eppendorf tubes, the following mixtures were prepared: Tube 1 containing (4.5µl of ScreenFect A+120µl of buffer), Tube 2 (30nmol of siRNA+120µl buffer). In addition to this, Tube 2 also contained either 3ug of pARE luc and 0.25ug of renilla luciferase expression vector pRL-SV40 or 3ug of pGL3 basic vector and 0.25ug of renilla luciferase expression vector pRL-SV40. The prepared mixtures were allowed to stand for 5min at RT. Thereafter, the reagents of the two tubes were mixed together and allowed to stand for an additional 20min at RT. Then, the complexes were transferred drop by drop to one well of a 6-well plate containing 1250ul of freshly added medium. The plates were swirled gently to ensure even dispersal of the complexes and then incubated for 68h before 4hr CSE- or DMSO-treatment.

3.3.6.2. Preparation of cell lysates

The luciferase assay measurements were performed according to the standard protocol of the manufacturer (Promega). The growth medium was removed from the wells and the cells were rinsed with 1X PBS solution. Then, 150µl of 1X luciferase cell culture lysis reagent (CCLR) (5X CCLR provided within the Promega kit was mixed with 4 volumes of sterile water to prepare the working concentration 1X) was

added to each well of a 6-well plate and the plates were gently shaken for 5min to ensure that the complete surface was covered with lysis buffer. Cells were scraped and the lysate was transferred to Eppendorf tubes. Before the luciferase activity measurements, all samples were incubated on ice for 15s, vortexed afterwards for 15s and finally harvested by centrifugation at a speed of 13,000g for 30s at RT. Thereafter, the firefly or renilla luciferase activities were determined with the substrates provided in the dual luciferase reporter assay kit from Promega.

3.3.7. Dihydroethidium (DHE) staining

To detect the generation of intracellular ROS, the cell permeable dihydroethidium (DHE) dye (Sigma) was used. DHE reacts with superoxide forming the ethidium product which upon intercalating with DNA produces a red fluorescent color. Cells plated on coverslips were incubated with 5µM DHE in medium for 30min at 37°C and washed with PBS afterwards. Then, the cells were fixed with PFA for 20min, washed with PBS and counterstained with Hoechst 33342 for 10min. Thereafter, the cells were washed with PBS and mounted on a slide for further examination with a LEICA TCS SP5 confocal microscope (CLSM) (Leica Mikrosysteme Vertrieb GmbH).

3.3.8. BrdU cell proliferation assay

Cells were seeded into sterile 96-well culture plates 24h prior to the treatment. After 24h, the necessary treatments were performed and the cells were incubated with BrdU 2h (Millipore) prior to the end of the test reagent incubation. Thereafter, the cells were fixed and the DNA was denatured with 200µl/well of the fixing solution for 30min at RT. Then, the medium was aspirated and the plate was washed 3 times with 1X Wash Buffer. After washing, the buffer was removed and 100ul/well of anti-BrdU monoclonal antibody was added for 1hr at RT. Following the incubation, the microplate was washed again and 100µl/well of goat anti-mouse IgG was added for 30min at RT. The plate was then washed and incubated with 100µl/well of TMB peroxidase substrate for 30min at RT. Finally, the reaction was stopped with 100µl/well of stop solution and the plate was read at a dual wavelength of 450/550 nm.

3.3.9. Cytokine and chemokine levels in supernatants

Cell culture supernatants from different treatment groups were collected and stored at −80°C for further analysis. Levels of TNF-α, IL-6, and IL-8 were measured using ELISA kits (Affymetrix, eBioscience) according to the manufacturer's instructions.

Shortly, following the coating of the 96-well plate with specific capture antibody, the plate was washed and incubated with blocking ELISPOT diluent for 1hr at RT. Afterwards, the lyophilized standards, as well as supernatant samples, were added and the plate was incubated for 2h at RT. Then, the plate was washed and incubated for an additional 1hr with the detection antibody. Thereafter, the plate was washed and Avidin-HRP was added for 30min at RT. After the incubation, the plate was extensively washed and then incubated with TMB solution for 15min. Finally, stop solution was added and the absorbance was read at 450nm using a TriStar microplate reader (Berthold).

3.3.10. Western Blot

3.3.10.1. Lung tissue homogenate preparation for Western Blots

Lung tissue samples from COPD patients as well as from donors (control) (see section 3.2.1.) were snap-frozen directly after explantation and stored in liquid nitrogen until use. Prior to processing, lung tissue specimens were cut into small pieces where 2g of each tissue sample was homogenized with a Potter-Elvehjem homogenizer at 1,000rpm (1 stroke, 60s). The homogenization (2g of tissue per 2ml buffer) was carried out in an ice-cold homogenization buffer (**Table 7**) containing 1% protease inhibitor mix M (SERVA, Germany). Thereafter, lung homogenates were centrifuged (Biofuge Fresco, Heraeus, Germany) at 2,500g for 3min at 4°C and the supernatants were collected for further protein analysis. The protein concentration was determined by the Bradford method using the Bradford protein assay reagent (Sigma) [180].

3.3.10.2. Cell preparation for Western Blots

After washing HBE or C22 cell cultures once with phosphate buffered saline (1XPBS) (Sigma), 100µl of IPB lysis buffer (**Table 7**) containing 1% protease inhibitor mix M was added to each well of a 6 well culture plate. Cells were then scraped thoroughly using a rubber policeman and transferred to Eppendorf tubes. The whole isolation process was carried out on ice. The isolated protein homogenate was vortexed for a couple of times and then centrifuged (Biofuge Fresco, Heraeus, Germany) at 2,500g for 10min at 4°C. Supernatants were collected and the protein concentrations were measured by the Bradford method using the Bradford protein assay reagent (Sigma) [180].

Table 7. Solutions for isolation of proteins for SDS PAGE and Western blotting

Tissue homogenization buffer	0.25M sucrose and 5mM MOPS, pH 7.4, 1mM EDTA, 0.1% ethanol, 0.2mM DTT, 1mM aminocaproic acid, supplemented with 1% protease inhibitor mix M prior to use
Cell lysis buffer (IPB)	150mM NaCl, 50mM Tris, 1% Triton X-100 (pH 7.4), supplemented with 1% protease inhibitor mix M prior to use

3.3.10.3. SDS-PAGE and blotting

The protein samples (20µg) as well as 5µl of dual color precision plus protein Standard® (BioRad, Germany) were separated on 10% SDS-polyacrylamide gels using a BioRad gel electrophoresis apparatus. The recipes of the gels used for electrophoreses are provided in **Table 8.**

Table 8. Recipes for two 10% SDS-polyacrylamide gel with a comb thickness of 1.25mm

Resolving gel buffer A	0.4% SDS 1.5 M Tris-HCl, adjusted to pH 8.8
Stacking gel buffer B	0.4% SDS, 0.5 M Tris-HCl, adjusted to pH 6.8
Resolving gel (10%)	3.34ml of dH_2O, 10ml of buffer A, 6.68ml of 30% acrylamide,15µl of TEMED, 130µl of 10% APS
Stacking gel	3.75ml of dH2O, 5ml of buffer B, 1.25ml of 30% acrylamide, 8µl of TEMED, 60µl of 10% APS
10X Sample buffer	3.55ml dH_2O, 1.25ml 0.5M Tris-HCl (pH 6.8), 2.5ml 50% (w/v) glycerol, 2.0ml 10% (w/v) SDS, 0.05% bromophenol blue. Prior to use, add 50µl of β-mercaptoethanol to every 1ml of 10X Sample buffer

The electrophoresis was performed at a voltage of 150V using the PowerPac 200. Thereafter, proteins were transferred to a polyvinylidene membrane (PVDF) (Millipore, Germany) using either a semi-dry Trans-Blot® apparatus at a constant current of 120mA for 1hr or tank-blotted in cold Towbin buffer at 100V for 1hr.

The membranes were then blocked with 5% non-fat milk powder (Carl Roth, Germany) in TBST (TBS + 0.05% Tween-20) for 1hr at RT. Thereafter, the membranes were incubated overnight with the specific primary antibodies (**Table 10**) in 5% blocking solution at 4°C. Dilutions of primary antibodies used are listed in **Table 10**. The following day, membranes were washed twice with TBST for 15min and incubated with alkaline phosphatase conjugated secondary antibodies (Sigma, Germany) for 1hr at RT. To visualize the bands, membranes were incubated with chemiluminescent substrate (Immunostar^{TM} – AP, BioRad) for 5min and visualized with Fusion FX (Fisher Biotec, Australia).

Mouse anti-GAPDH antibody (Glyceraldehyde-3-Phosphate Dehydrogenase) (5G4, HyTest, Finland) was used to normalize the expression. For detection of different target proteins, the membranes were stripped and re-used by re-probing with different primary antibodies. All Western blot analyses were performed in triplicates to produce reliable results. The buffer recipes used for the Western Blot analysis are summarized in **Table 9.**

Table 9. The composition of the buffers used for western blotting

10X Electrophoresis buffer	250mM Tris, 2M glycin + 1% SDS
10X Towbin transfer buffer (tank blotting)	125mM Tris, 192mM glycine adjusted to pH 8.3 in 1l of dH_2O
1X Towbin	For 1L: 700ml dH_2O, 100ml Towbin, 200ml methanol
20X Transfer buffer (semi-dry transfer)	Bis-Tris-HCl buffered (pH 6.4) polyacrylamide gel, NuPAGE transfer buffer (Invitrogen, Heidelberg, Germany)
10X TBS	0.1MTris, 0.1M NaCl in 1l dH_2O, adjusted to pH 8.0
1X Washing buffer (TBST)	10 mM Tris/HCl, 0.15 M NaCl, 0.05% Tween 20, pH 8.0
5% Blocking buffer	5g fat free milk powder in 1X TBST solution
Stripping buffer (500ml)	62.5mM Tris (pH 6.8), 0.2% SDS, 500ml dH_2O, 50ml of buffer/membrane in the water-bath at 42°C for 40min with additional 350µl β-mercaptoethanol

Table 10. List of primary antibodies used in this study

Primary antibody against antigen	Host	Dilution IF (Cells)	Dilution IF (Tissues)	Dilution (WB)	Supplier
Peroxisomal biogenesis and metabolic protein					
Peroxin 13 (PEX13p), mouse	Rabbit, polyclonal	1:1,000	1:1,000	1:5,000	Gift from Denis I. Crane; School of Biomol. Biophys. Sci., Griffith Univ., Nathan, Brisbane, Australia
Peroxin 14 (PEX14p), mouse	Rabbit, polyclonal	1:1,000	1:1,000	1:8,000	Gift from Denis I. Crane; School of Biomol. Biophys. Sci., Griffith Univ., Nathan, Brisbane, Australia
Catalase (CAT), mouse	Rabbit, polyclonal	1:2,000	1:2,000	1:30,000	Gift from Denis I. Crane; School of Biomol. Biophys. Sci., Griffith Univ., Nathan, Brisbane, Australia
Acyl-CoA oxidases I, mouse	Rabbit, polyclonal	1:1,000	1:1,000	1:5,000	Gift from Paul P. van Veldhoven, Dept. of Molecular Cell Biology, Pharmacology, Catholic University Leuven, Belgium
Thiolase, human	Rabbit, polyclonal	1:1,000	1:1,000	1:5,000	Gift from Nancy E Bravermann; Depts. of Human Genetics and Pediatrics, McGill University-Montreal Montreal, QC, Canada
Alkylglycerone-phosphate synthase (AGPS), human	Mouse, monoclonal	-	-	1:500	Santa Cruz, Cat no: sc-374201
Glyceronephosphate O-acyltransferase (GNPAT), human	Rabbit, polyclonal	1:500	1:500	1:500	Proteintech, Cat no: 14931-1-AP
Transcription factors and signalling molecules					
Peroxisome proliferator-activated receptor gamma (PPARγ), rabbit	Rabbit, polyclonal	1:50	1:50	1:500	Santa Cruz, Cat no: sc-7196
Nuclear factor-erythroid-2 related factor 2 (Nrf2), human	Rabbit, polyclonal	-	-	1:1,000	Santa Cruz Biotechnology Inc., Heidelberg, Germany, Cat. no:sc-722
Other antioxidative enzymes					

Heme oxygenase 1 (HO-1)	Rabbit, polyclonal	-	-	1:1,000	Assay Designs, Inc. Michigan, USA, Cat.no:SPA-895
Superoxide dismutase 1 (SOD1), rat (partially in peroxisomes)	Rabbit, polyclonal	-	-	1:1,000	Research diagnostics, Cat no: RDI-RTSODMabR
Cell type-specific antigens					
Mucin 5AC, human	Mouse, monoclonal	-	1:500	-	AbD Serotec, Cat. no: 1695-0128
Pro-inflammatory antigens					
Cycloxygenase-2 (COX-2), goat	Rabbit, polyclonal	-	-	1:1,000	Santa Cruz Biotechnology Inc., Cat. no: sc-1747
Loading Control					
Glyceraldehyde-3-phosphate dehydrogenase (GAPDH), rabbit	Mouse, polyclonal	-	-	1:10,000	HyTest, Finland, Cat. no: 5G4
Secondary Antibodies					
Secondary detection system	**Host**	**Dilution (WB)**	**Dilution (Cells/ Tissues)**		**Supplier**
anti-Rabbit-IgG alkaline phosphatase conjugate	Goat, polyclonal	1:20,000	**-**		Sigma Aldrich, Cat. no: A0545
anti-Mouse-IgG alkaline phosphatase conjugate	Goat, polyclonal	1:20,000	**-**		Sigma Aldrich, Cat. no: A3562
anti-Rabbit-IgG AlexaFluor488	Donkey	-	1:1,000		Molecular Probes/Invitrogen, Cat. no: A21206
anti-Mouse-IgG AlexaFluor555	Donkey	-	1:1,000		Molecular Probes/Invitrogen, Cat. no: A31570
anti-Goat-IgG AlexaFluor594	Chicken	-	1:1,000		Molecular Probes/Invitrogen, Cat. no: A11058
Counterstaining of nuclei for immunofluorescence					
Hoechst 33342 (1 µg/ml)	-	-	1:1,000		Molecular Probes/Invitrogen, Cat. no: 33342
TOTO®-3 iodide	-		1:1,000		Molecular Probes/Invitrogen, Cat. no: T-3604

3.3.11. Indirect Immunofluorescence

3.3.11.1. Immunofluorescence of embedded tissues

Human and mouse (see section 3.2.1.) paraffin-embedded tissue blocks were cut into 2-3µm-thick sections using a rotation microtome (Leica RM2135). **Table 10** shows the dilutions of the primary and secondary antibodies used. The immunofluorescence procedure was carried out for 3 days and is summarized in **Table 11.** The components of the solutions used are summarized in **Table 12.**

Table 11. The experimental procedure of immunofluorescence staining on paraffin-embedded tissue sections

Time	Procedure
Day 1	Human and mouse tissue sections were placed overnight into a 50°C oven (Heraeus, Hanau,Germany) for deparaffinization
Day 2	• Sections were deparaffinized with xylene and rehydrated in a series of ethanol (absolute ethanol, 96% ethanol, 80% ethanol, 70% ethanol, and aqua dest.), each step was for 3min at RT • For antigen retrieval, sections were subjected to digestion with trypsin buffer for 10min at 37°C on a heating plate and then microwaved in citrate buffer for 15min at 900W (Table 12.) • Sections were blocked with 4% PBSA at RT for 2h • Sections were incubated overnight at RT with the primary antibody diluted (**Table 10**) in 1% PBSA
Day 3	• Sections were rinsed 3X for 5min with 1X PBS • Incubated with secondary antibody (**Table 10**) for 1hr at RT • Washed with 1X PBS, 3X for 5min at RT • Stained with Hoechst 33342 and TOTO-3 iodide for 10min at RT • Washed 3X with 1X PBS for 5min • Mounted with cover slips using Mowiol and propylgallate

For negative controls, the sections were incubated with PBSA instead of the primary antibody. The samples were analyzed by confocal laser scanning microscopy (CLSM) with a Leica TCS SP5 (Leica Mikrosysteme Vertrieb GmbH).

Table 12. Solutions used for immunofluorescence staining of paraffin-embedded tissue sections

Solution	Composition
10X PBS	1.5M NaCl, 131mM K_2HPO_4 , 50mM KH_2PO_4, pH 7.4
Trypsin (0.01%)	Fresh 0.01g trypsin in 100ml of 1X PBS buffer
Citrate buffer	Buffer A: 1mM $C_6H_8O_7.H_20$ Buffer B: 50mM $C_6H_5Na_3O_7.2H_20$ Final concentration: 0.15mM buffer A + 8.5mM buffer B (pH 6)
Blocking buffer: 4% PBSA + 0,05% Tween 20	To 8g BSA add 200ml of 1X PBS and 100µl of Tween 20
Dilution buffer: 1% PBSA + 0,05% Tween 20	To 2g BSA add 200ml of 1X PBS and 100µl of Tween 20
Mowiol 4-88 solution	Overnight stirring of 16.7% Mowiol 4-88 (w/v) and 80ml of 1X

	PBS, add 40ml of glycerol and stir overnight again; centrifuge at 15,000U/min for 1hr, take off the supernatant and store at -20°C
Anti-fading agent (2.5%)	2.5g N-propylgallate in 50ml of PBS and add 50ml of glycerol
Mounting medium	3 parts of Mowiol 4-88 and 1 part of anti-fading agent propylgallate

3.3.11.2. Immunofluorescence of cells

Cells were plated on coverslips and allowed to grow for 24h. After that, all the necessary manipulations (siRNA, plasmids, RZG, CSE) were performed. Thereafter, cells were washed with PBS and fixed with 4% paraformaldehyde (PFA) in PBS for 20min at RT. After fixation, the cells were washed with PBS, pH 7.4 and the coverslips containing the cells were incubated in 1% glycine in PBS for 10min. Thereafter, they were incubated for additional 10min in 1% glycine and 0.3% Triton X-100 for permeabilization. After incubation, samples were rinsed with PBS and incubated for 30min in 1% BSA and 0.05% Tween 20 in PBS to block non-specific protein binding sites. After blocking, the coverslips were incubated with primary antibodies (**Table 10**) at 4°C in a moist chamber overnight. The following day, the cells were washed extensively with PBS and incubated with secondary antibodies for 1h at RT. Thereafter, the cover slips were washed with PBS and the nuclei were counterstained with Hoechst 33342 (1µg/ml) and TOTO-3 iodide for 10min at RT. At last, the coverslips were washed with PBS and mounted on the slides. The composition of solutions used for immunofluorescence of cells grown on the cover-slips is shown in **Table 13.**

Table 13. Solutions used for immunofluorescence staining of cells grown on coverslips.

Solution	Composition
Fixative solution	4% PFA in 1X PBS (150mM NaCl, 13.1mM K_2HPO_4, 5mM KH_2PO_4), pH 7.4
Glycine (1%)	1g glycine in 100ml of 1X PBS buffer
Glycin (1%) + Triton X-100 (0.3%)	1g glycine in 100ml of 1X PBS buffer + 0.3ml Triton X-100
Blocking buffer- 1% PBSA + 0,05% Tween 20	To 2g BSA add 200ml of 1X PBS and 100µl of Tween 20
Mowiol 4-88 solution	Overnight stirring of 16.7 % Mowiol 4-88 (w/v) and 80ml of 1X PBS, add 40ml of glycerol, stir again overnight; centrifuge at 15,000 U/min for 1h and take off the supernatant and store at -20°C
Anti-fading agent (2.5%)	2.5g N-propylgallate in 50ml of PBS and 50ml of glycerol
Mounting medium	Mowiol 4-88 mixed with anti-fading agent in ratio of 3:1

3.3.12. RNA Isolation

3.3.12.1. RNA isolation from cells

For RNA isolation, the medium was aspirated from the cells and 1ml of RNAzol (RNAzol®, Sigma-Aldrich) was added to each well of a 6 well culture plate. The lysed cells were collected into 2ml tubes. Then, 0.4ml of RNase-free water per ml of RNazol was added to each tube and left for 15min at RT. The lysate was then centrifuged at 12,000g for 15min and the supernatant was transferred to a fresh tube followed by an addition of an equal volume of 100% isopropanol for RNA precipitation for 10min at RT. Thereafter, the lysate was centrifuged at 12,000g for 10min and the supernatant was discarded. The RNA pellet was washed twice with 0.5ml of 75% ethanol per ml of supernatant. Then, the RNA was centrifuged at 8,000g for 3min at RT and the ethanol was removed thereafter. Finally, the RNA pellet was solubilized in RNase-free water at a concentration of 1-2µg/ml. The quantity and integrity of the isolated RNA were assessed with the NanoDrop™ 8000 Spectrophotometer.

3.3.12.2. RNA isolation from tissues

Tissue samples were homogenized at RT with 1ml RNAzol per 100mg of tissue using an Ultra Turrax T25 basic homogenizer and allowed to stand for 15min prior to further steps. Thereafter, the isolation process was the same as mentioned in section 3.3.7.1.

3.3.12.3. cDNA synthesis

One µg of total isolated RNA was reverse transcribed to cDNA using the High Capacity cDNA Reverse Transcription Kit (Applied Biosystems, Germany) as described by the manufacturer. The reverse transcription mix contained 0.8µl of 25X dNTP Mix (100mM), 2µl 10X RT buffer, 2µl 10X RT random primers, 1µl MultiScribe™ reverse transcriptase, 1µl RNase inhibitor and 3.2µl nuclease-free H_2O. Thereafter, 1ug total RNA in nuclease-free water to a volume of 10ul was pipetted into 10µl reverse transcription mix. The reaction was incubated at 25 °C for 10 min, at 37 °C for 120 min and at 85 °C for 5 min in a Trio-Thermoblock.

3.3.12.4. qRT-PCR

The qRT-PCR of target genes, described in **Table 14-15**, was performed in the iCycler iQ5™ Real-Time PCR Detection System (BioRad). The reactions were set up with the SYBR™ Green PCR mix (Life technologies) according to the manufacturer's protocol. The PCR cycle consisted of an initial cycle of 95°C for 3min followed by 42 repeated cycles of 95°C for 15s, 60°C annealing temperature for 30s, and the primer extension

at 72°C for 30s. Then, 91 repeated cycles at the temperature between 50°C-95°C with increased set point temperature after cycle 2 by 0.5°C were performed. All reactions were run in triplicates. Mouse *Gapdh* and human *HPRT* were used as an endogenous reference. The comparison of relative expression values of each gene to the internal control gene was analyzed using the equation $2^{-ddC}{}_T$, where dC_T = ($C_T$target gene − $C_T$internal control gene).

Table 14. Sequences of the human primers used for the qRT-PCR

Gene name	Sense 5'-3'	Antisense 5'-3'
ACAA1	GATGCCTTCTTACCCCAACA	CCCAACCACTGCATAAGACC
ACOX1	ATTTCCTTCAGGGGAGCATC	GCCAAGTGTCACATCCTGAA
AGPS	AGGGGGATCGTGAGAAGGT	CCAAAGCCAAGTCTCGAATG
CAT	CGTGCTGAATGAGGAACAGA	TTGTCCAGAAGAGCCTGGAT
HPRT	GAAAAGGACCCCACGAAGTGT	AGTCAAGGGCATATCCTACAACA
GNPAT	GTGCAGAAAAACGCCTTAGC	GGCTGGTTTTCCTATTGGTG
IL6	AATTCGGTACATCCTCGACGG	TTGGAAGGTTCAGGTTGTTTTCT
IL8	TTTTGCCAAGGAGTGCTAAAGA	AACCCTCTGCACCCAGTTTTC
PEX5	TGGGAGTCCTTTTCAACCTG	CGCCTAGCTTATTCCACAGC
PEX7	GGCTCATGGGATCAAACTGT	ACCTGAGGCTGAAGCAAAAC
PEX13	CCATGTAGTTGCCAGAGCAG	CATCAAGGCTAGCCAGAAGC
PEX14	CTGCCTTTGGCTTTGATCTC	CGTGGTGTCACGGTAGTCAA
PPARG	ATCTTTCAGGGCTGCCAGT	TCGTGGACTCCATATTTGAGG
TNFα	CCTCTCTCTAATCAGCCCTCTG	GAGGACCTGGGAGTAGATGAG

Table 15. Sequences of the mouse primers used for the qRT-PCR

Gene name	Sense 5'-3'	Antisense 5'-3'
Acaa1	CAATGAACTGAAGCGTCGTG	CACCACTGTGGCACTCTCTG
Acox1	CCGCCACCTTCAATCCAGAG	CAAGTTCTCGATTTCTCGACGG
Agps	TGTCCTCCGTGTCTGTTCCT	CATGGTACAACCTGCCCTTC
Cat	GGAGAGGAAACGCCTGTGTGA	GTCAGGGTGGACGTCAGTGAAA
Cox2	GACTCTGCTCACGAAGGAAC	AGCAAGGATTTGCTGCCT
Ho-1	CGCCTTCCTGCTCAACATT	TGTGTTCCTCTGTCAGCATCAC
Gapdh	TGGCAAAGTGGAGATTGTTGCC	AAGATGGTGATGGGCTTCCCG
Il6	CTCTCTGCAAGAGACTTCCATC	CTCCGACTTGTGAAGTGGTATAG
Nrf2	CCAGCAGGACATGGATTTGA	ATAGTCCTTCTGTCGCTGACTA
Pex7	CGACAGCCTGTGTTTGAACT	AGAAGCGGATCAGGCTTTG
Pex5	AATGCAACTCTTGTATCCCGA	GGCGAAAGTTTGACTGTTCAATC
Pex13	TGGATATGGAGCCTACGG	CGGTTAAAGCCCAAACCATT

Pex14	GCCACCACATCAACCAACTG	GTCTCCGATTCAAAAGAAGTCCT
Pparg	TTTTCAAGGGTGCCAGTTTC	CATGGACACCATACTTGAGCA
Sod1	AAAATGAGGTCCTGCACTGG	AACCATCCACTTCGAGCAGA

3.3.13. Statistical Analysis

Each result is a representative of at least three experiments. Data are expressed as mean ± standard deviation. Differences between groups were evaluated by the analysis of variance (one-way ANOVA) and by the un-paired student t-test. Data were considered statistically significant if $p \leq 0.05$.

4. Results

4.1. Human COPD samples

4.1.1. Patient sample selection

There is growing evidence that the prevalence and incidence of COPD increase in the elderly and that the onset of COPD is higher in persons over 50 years of age [181-183]. Therefore, the lung tissue samples analysed in this study belong to the COPD patients and donors in the age range of 50-70 years. The samples belong to the patients diagnosed with either chronic bronchitis, emphysema, or both. In order to confirm the COPD characteristics, samples were analysed for the expression of MUC5AC. It is known that excessive mucous hypersecretion is a feature of a variety of chronic airway diseases including COPD and that the most abundant mucins present in the airways are MUC5B which is constitutively expressed and MUC5AC which is induced in response to pathogens and pollutants like cigarette smoke [184-186]. As a result, it has been shown that the expression of the MUC5AC is increased in the bronchial epithelium of COPD patients [187,188]. Thus, paraffin-embedded COPD lung tissue samples were selected based on MUC5AC upregulation.

Immunofluorescence analysis of COPD samples (**Fig. 9**) showed a heterogeneous distribution of the MUC5AC protein in the bronchial region of different patients, with the highest abundance of MUC5AC in patient number 3 (**Fig. 9K**). For further experiments, COPD patients exhibiting similar MUC5AC abundance as patient 3 were selected. Similarly, donors showing the absence of MUC5AC (**Fig. 9E**) were selected for further experiments. Interestingly, MUC5AC was detected in donor number 3; this could mean that the donor was having an inflammatory airway disease.

Characteristics of the 5 donors and 6 patients selected for further analysis are described in **Table 16.**

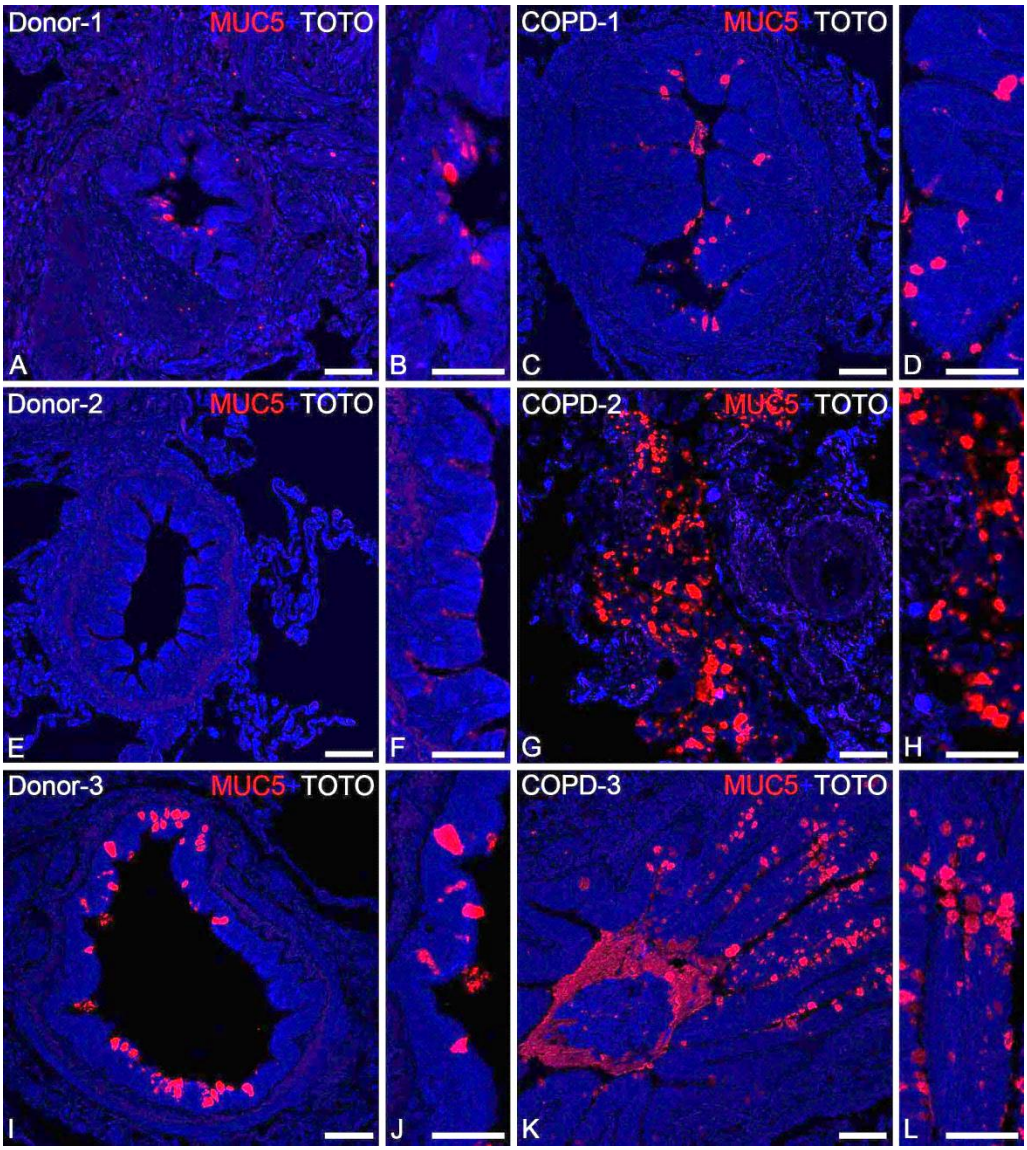

Fig. 9. CLSM images of IF preparations for mucin 5 (MUC5AC) in 3 human donor lungs (A, E and I) and (B, F and J represent the higher magnification) and 3 different COPD patients (C, G and K) and (D,H and L represent the higher magnification) in order to show the hyperplasia of goblet cell in the bronchiolar epithelium and to confirm the COPD characteristics. Nuclei were counterstained with TOTO-3-iodide. Bars represent 60μm for (B, F, J, D, H and L) and 20μm for (A, C, E, G, I and K).

Table 16. Characteristics of the selected COPD patients and lung donors as control subjects.

Gender	Age	Diagnosis
Female	58	COPD/Centrilobular emphysema and bronchitis
Female	52	COPD/ Bronchitis
Female	58	COPD/Centrilobular emphysema
Male	55	COPD/Emphysema
Male	56	COPD/Emphysema
Male	58	COPD/Centrilobular emphysema and bronchitis

Female	70	Donor
Female	60	Donor
Male	61	Donor
Male	58	Donor
Male	56	Donor

4.1.2. Peroxisomal biogenesis, lipid metabolism and anti-oxidative enzymes are altered in COPD patients

After the selection of five donors and five COPD patients, based on the MUC5AC expression, the second step was to analyze the peroxisomal distribution of the COPD and donor lung samples. As mentioned previously, cigarette smoke provokes oxidative stress by an oxidant/antioxidant imbalance [150]. Therefore, peroxisomes could be easily affected by components of cigarette smoke, since most of these organelles are indeed localized directly underneath of the apical surface of ciliated cells or in the apical region of club cells of the bronchiolar epithelium [136,137]. Thus, peroxisomal metabolism could be altered in COPD patients.

The analysis of paraffin embedded tissue samples revealed a high upregulation and proliferation of the peroxisome biogenesis protein PEX14 in the bronchiolar region of the COPD patient (**Fig. 10C and D**) compared to the control (**Fig. 10A and B**). Tissue staining with PEX13 antibody was not performed due to the cross-reactivity of this antibody with the elastic fibers of the tissue sample. Next, the abundance of the peroxisomal β-oxidation enzymes; ACOX1 and Thiolase (Acaa1) was analysed. ACOX1, the first rate-limiting enzyme of the peroxisomal β-oxidation pathway 1 was increased in bronchiolar epithelial cells **(Fig. 11C and D**) as well as in the alveolar region (**Fig. 11G and H**) of COPD patients in comparison to the control samples (**Fig. 11A, B, E and F**). Similarly, Thiolase which is the terminal enzyme of the β-oxidation pathway I, was strongly upregulated in the club cells (**Fig. 12E**), goblet cells (**Fig. 12F**), ciliated cells of the bronchiolar region (**Fig. 12G**) and in macrophages and type II cells (**Fig. 12H**) of the alveolar region in COPD tissue samples as compared to the donor samples. Double labelling of rabbit anti-Thiolase with mouse anti-MUC5AC; which is a marker of goblet cells, showed high abundance of mucin in the bronchi of COPD patients.

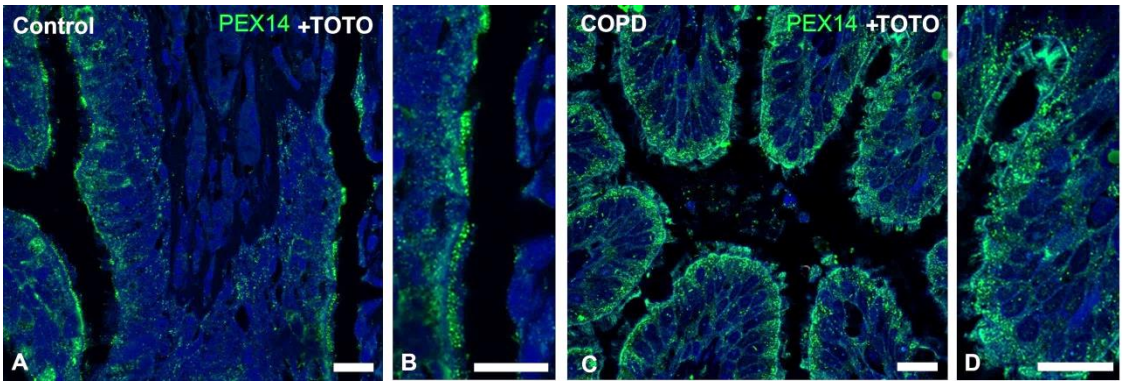

Fig. 10. CLSM images of IF preparations for the peroxisomal biogenesis enzyme PEX14 in the bronchiolar (A-D) epithelial regions of human donor (A-B) and COPD patient (C-D) lungs. Nuclei were counterstained with TOTO-3-iodide. Bars represent 20μm for (A and C) and 25μm for (B and D).

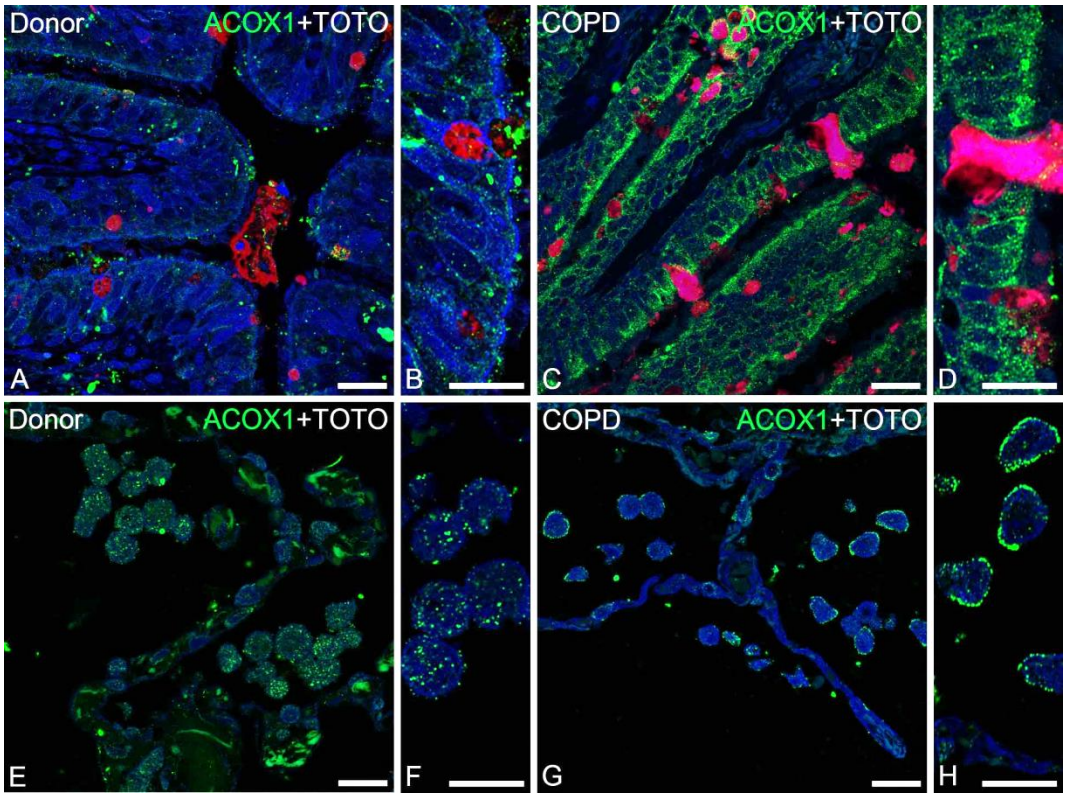

Fig. 11. CLSM images of IF preparations for the peroxisomal β-oxidation enzyme ACOX1 in the bronchiolar (A-D) and alveolar (E-H) epithelial regions of human donor and COPD patient lungs. Nuclei were counterstained with TOTO-3-iodide. Bars represent 20μm for (A, C, E and G) and 60μm for (B, D, F and H).

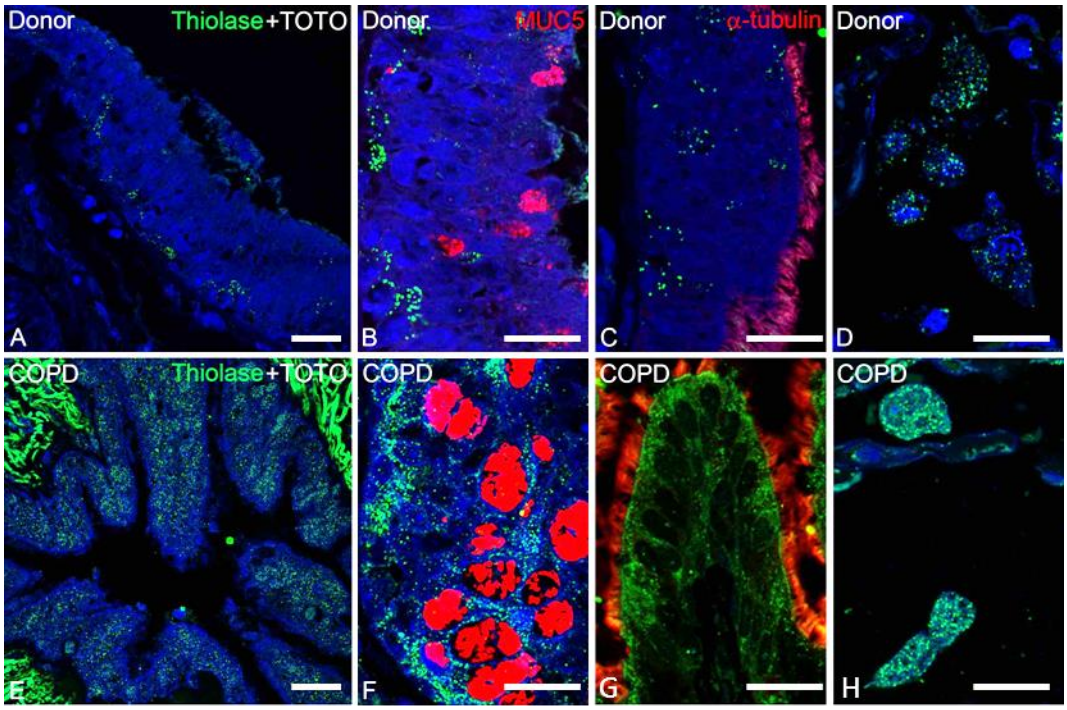

Fig. 12. CLSM images of IF preparations for the peroxisomal β-oxidation enzyme Thiolase in the bronchiolar and alveolar regions of human donor lungs and COPD patients. Double labelling with rabbit anti-thiolase and mouse anti-MUC5AC (B and F) or mouse anti-tubulin (C and G). Bars represent 20µm for (A and E) and 60µm for (B, C, D, F, G and H).

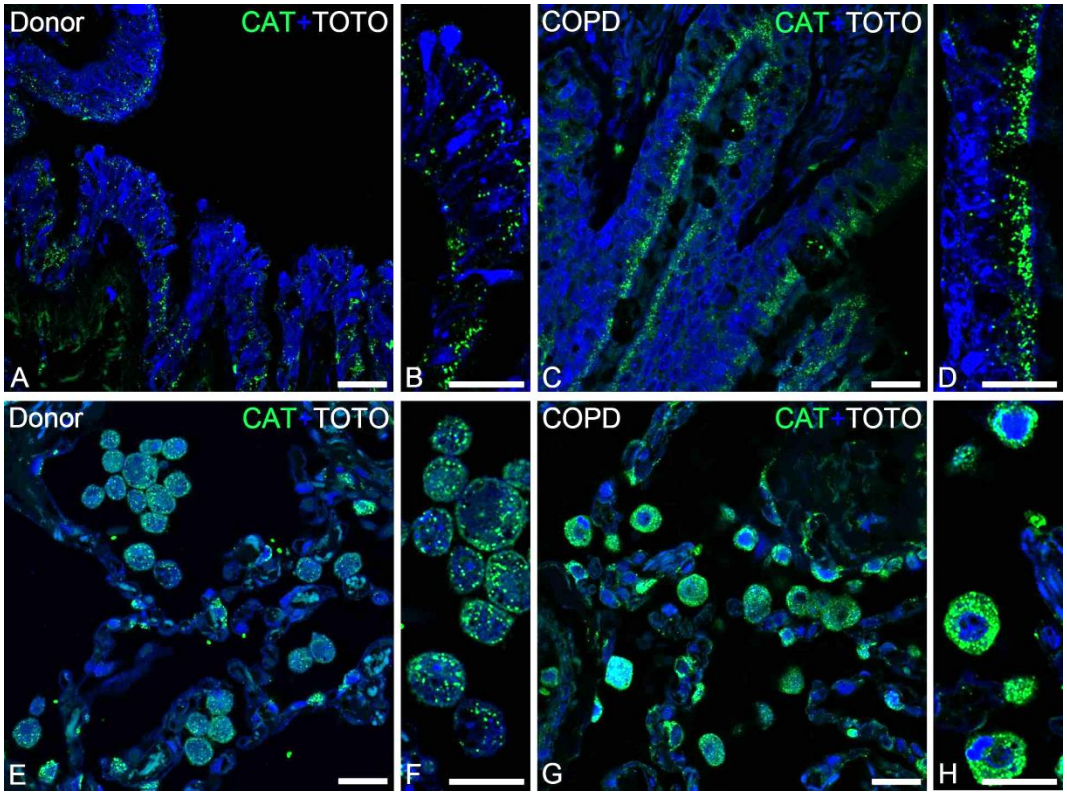

Fig. 13. CLSM images of IF preparations for the peroxisomal antioxidative enzyme catalase (CAT) in the bronchiolar (A-D) and alveolar regions (E-H) of human donor (A, B, E and F) and COPD patient lungs (C, D, G and H). Nuclei were counterstained with TOTO-3-iodide. Bars represent 20µm for (A, C, E and G) and 60µm for (B, D, F and H).

Peroxisomes contain a variety of anti-oxidative enzymes, of which catalase is the most abundant one. Therefore, in addition to the above-mentioned biogenesis and β-oxidizing enzymes, a staining with the peroxisomal anti-oxidative protein CAT revealed an upregulation of CAT in the bronchiolar epithelial cells of the COPD patients (**Fig. 13C and D**). Moreover, CAT was also upregulated in alveolar macrophages and alveolar type II cells of the patients (**Fig. 13G and H**) in comparison to the donor samples (**Fig. 13A, B, E and F**).

The increase in the abundance of peroxisomal enzymes in COPD patients was confirmed by Western blot analyses. Similarly, the increase in the expression of peroxisomal genes in the COPD patients was observed at mRNA level with the real-time PCR analyses. Western blot and real-time PCR analyses showed that the protein and mRNA levels of peroxisomal biogenesis proteins involved in matrix protein import (such as PEX5, PEX7, PEX13 and PEX14) were increased in their abundance and expression in the COPD patients as compared to the control samples (**Fig. 14**). Moreover, the protein and mRNA levels of peroxisomal enzymes in ether lipid synthesis (AGPS and GNPAT) (**Fig. 15**), peroxisomal β-oxidation (ACOX1 and ACAA1) (**Fig. 16A**) and ROS metabolism (CAT) (**Fig. 16B**) as well as transcription factors (**Fig. 17**) were shown to be significantly upregulated in the total tissue lysates and total RNA of the COPD lungs as compared to the lungs from healthy donor controls. Next, we analysed the samples on the expression of pro-inflammatory cytokines such as IL-6, IL-8 and TNF-α which have been proposed to play an important role in the pathogenesis of COPD. Real time PCR revealed a highly significant increase of the *IL-8* gene and a lower but still significant expression of *TNF-α* gene in the total RNA of the COPD patient (**Fig. 18**). The increase in the expression of IL-6 was shown to be insignificant (**Fig. 18**).

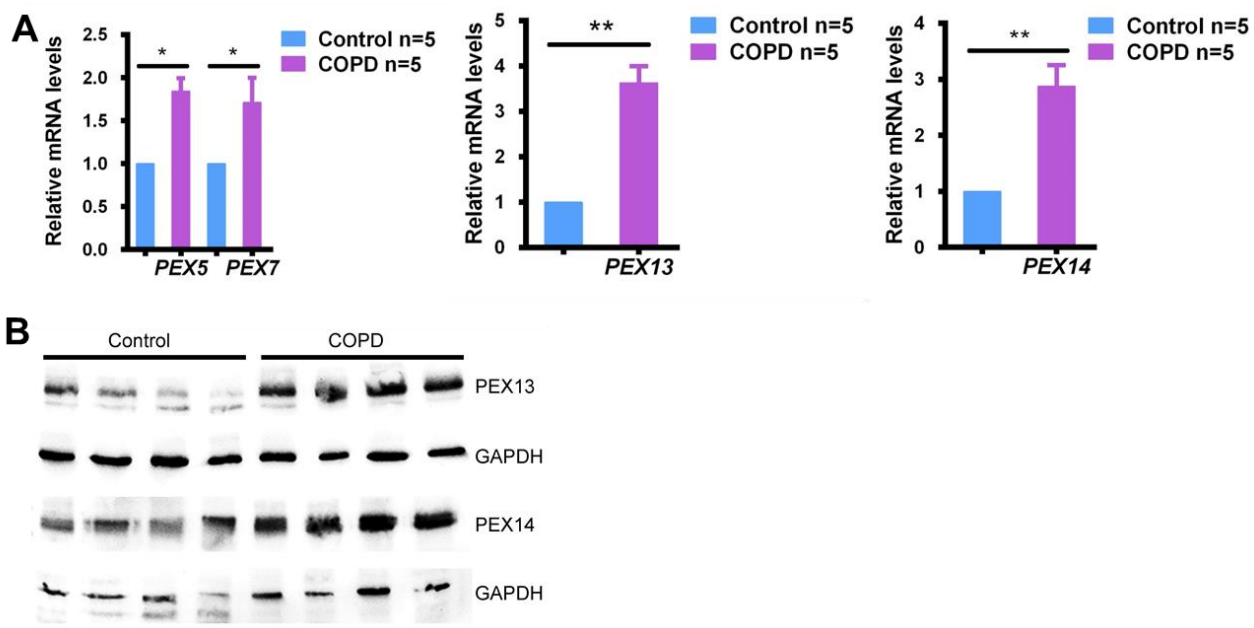

Fig. 14. Expression of peroxisomal biogenesis (PEX13 and PEX14) and peroxisomal targeting receptors (PEX5 and PEX7) at the mRNA and (A) protein (B) levels in the control and COPD samples by Western blot and real-time PCR analyses. P values were calculated by the unpaired student t-test. *p ≤ 0.05, **p ≤ 0.01.

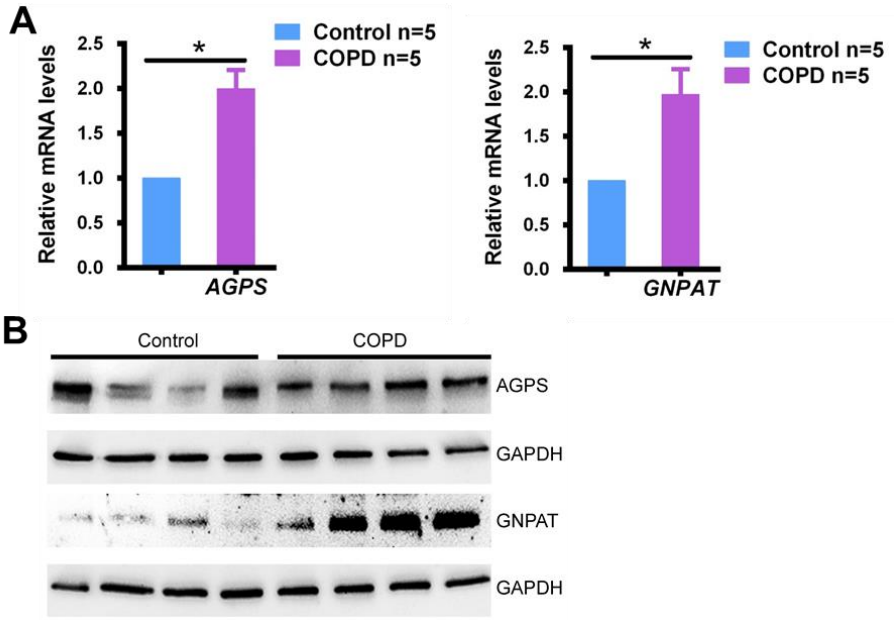

Fig. 15. Real-time PCR and Western blot of ether phospholipid synthesis enzyme mRNAs (A) and proteins (B) in total lysates and RNAs of healthy donor control and COPD lungs. P values were calculated by the unpaired student t-test.*p ≤ 0.05.

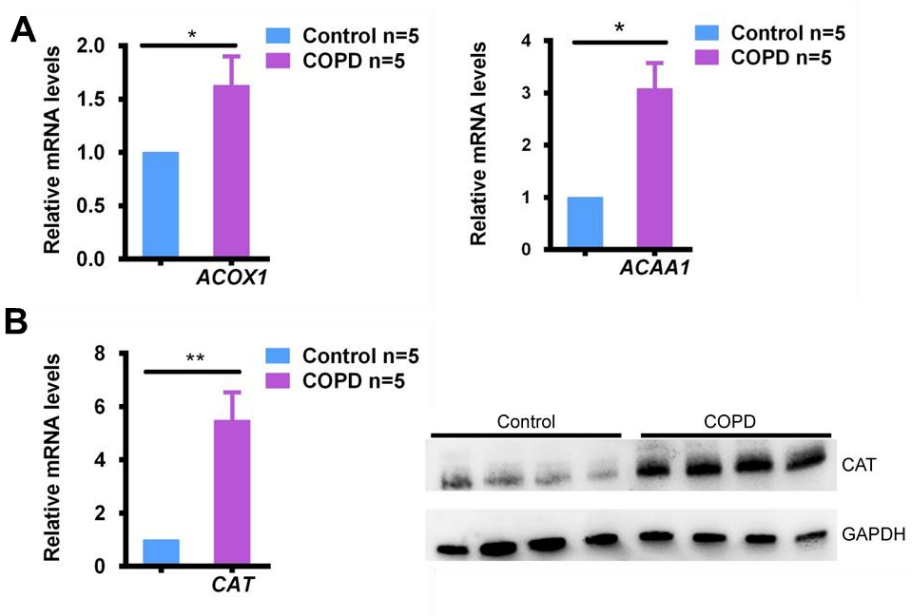

Fig. 16. Real-time PCR of peroxisomal β-oxidation gene mRNAs on total RNA of human lung tissue (A) and real-time PCR and Western blot of the peroxisomal antioxidant enzyme Catalase (B) on total RNAs and lysates of control and COPD lungs**.** P values were calculated by the unpaired student t-test.*p ≤ 0.05, **p ≤ 0.01.

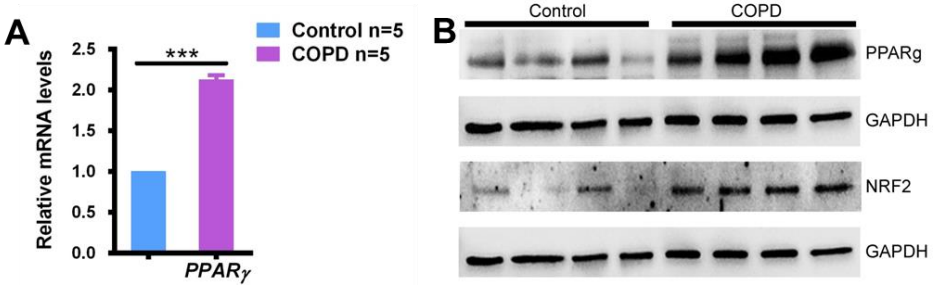

Fig. 17. Real-time PCR and Western blots of the transcription factors (A) on total RNAs and (B) lysates of control and COPD lungs. P values were calculated by the unpaired student t-test. *** p ≤ 0.001

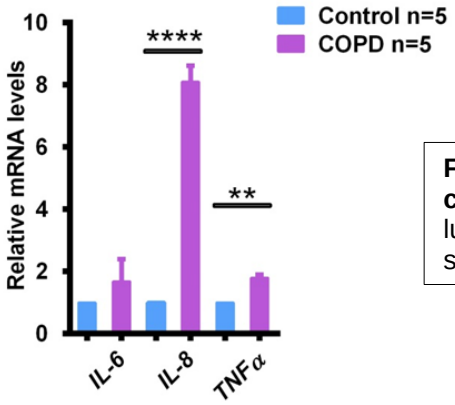

Fig. 18. **Real-time PCR of the pro-inflammatory cytokines** on total RNA of control and COPD lungs. P values were calculated by the unpaired student t-test. **p ≤ 0.01, **** p ≤ 0.0001.

To summarize, immunofluorescence, Western blot and real time PCR analyses of peroxisomal protein and gene expression levels revealed a strong upregulation of peroxisomal biogenesis, anti-oxidative and lipid metabolic (β-oxidation, plasmalogen

synthesis) enzymes as well as an increase in the abundance of peroxisome-related transcription factors (PPARγ and Nrf2) in the COPD patients, suggesting that the peroxisomal function is being more activated. Moreover, the observed increase in the level of pro-inflammatory cytokines is a typical characteristic feature of COPD.

4.1.3. Peroxisomal distribution in various cell types of control and COPD lungs

The next step was to check the distribution, localization and compartmentalization of different peroxisomal enzymes in various cell types of control and COPD lungs. By using immunofluorescence for the localization of peroxisomal marker proteins, five control and 5 COPD samples were analysed. **Table 17** provides a nice summary of the results obtained for different peroxisomal markers.

Immunofluorescence analysis revealed that MUC5AC only weakly stained goblet cells in the control tissues. The peroxisomal biogenesis protein PEX14 was highly abundant in macrophages in comparison to a much weaker abundance in AECII cells. Club cells and ciliated cells showed a similar middle high expression of PEX14. The staining for the antioxidative enzyme CATALASE (CAT) showed its high abundance in macrophages, club cells, and alveolar epithelial type II cells (AECII) of the control samples. Other cell types were only weakly stained for CAT. Acyl-CoA oxidase 1 (ACOX1), which is known to be responsible for the rate-limiting step of the peroxisomal β-oxidation pathway I, was equally and highly abundant in the club cells, macrophages and AECII cells whereas a lower abundance was observed in the ciliated cells of the control samples. Another β-oxidation enzyme, peroxisomal 3-oxo-acyl-CoA thiolase (Acaa1) was more prominent in AECII than in any other cell type of the control lungs. Interestingly, the pattern of peroxisomal distribution in various cell types of the COPD lungs was similar to that of the control lungs. However, the peroxisomal protein abundance in cells of COPD lungs was much higher as in the control lungs.

Thus, there exists a cell-type specific distribution of the peroxisomal proteins in different cells of the control lungs. The distribution pattern is similar in the COPD lungs but the abundance of peroxisomes in the COPD patients was observed to be very high in comparison to the control samples.

Table 17. Peroxisomal enzymes in various cells of the control and COPD lungs, their localization and comparison

Control lungs	Club cells	Ciliated cells	Goblet cells	Macrophages	AECII
MUC5AC	-	-	+	-	-
PEX14	+	+	-	++	+
CAT	++	+	-	++	++
ACOX1	++	+	-	++	++
THIOLASE (ACAA1)	+	+	-	+	+
COPD lungs					
MUC5AC	-	-	++++	-	-
PEX14	+++	+++	-	++++	++
CAT	++++	++	-	++++	++++
ACOX1	++++	+++	-	++++	+++
THIOLASE (ACAA1)	++	++	-	++	++

+weak, ++ significant, +++ very significant, ++++ extremely significant

4.2. COPD mouse model

4.2.1. Peroxisomal biogenesis, lipid metabolism and antioxidative enzymes are altered in COPD mouse model as well

It was interesting to check whether COPD mouse model displayed a similar pattern of peroxisomal alterations as it was observed in the human COPD patients. For this purpose, lung tissue samples (obtained from the group of Prof. Weissmann) from the wild-type (WT) mice exposed to cigarette smoke for 3 months were analysed and compared to the age-matched controls that were kept under identical conditions but without smoke exposure[178] (refer to section 3.2.2). Immunofluorescence analysis of paraffin sections revealed that the peroxisomal biogenesis protein PEX14 was strongly up-regulated in the bronchiolar region of the cigarette smoke (CS) exposed mice (**Fig. 19C and D**). Similarly, the alveolar region of the COPD mouse model (**Fig. 19G and H**) showed a high abundance of PEX14 when compared to the alveolar region of WT controls (**Fig. 19E and F**). Similar staining pattern was observed for the peroxisomal antioxidative protein CAT, such that the COPD mouse model showed a high abundance of CAT in the bronchiolar (**Fig. 20C and D**) and alveolar (**Fig. 20G and H**) regions in comparison to the control lungs (**Fig. 20A, B, E and F**). Moreover, the expression of peroxisomal mRNA for transcription factors as well as the expression for inflammatory mediators were analysed on total RNA by real-time PCR. As shown in **Fig. 21**, the expression levels of peroxisomal biogenesis genes are significantly up-regulated in the COPD model as compared to the WT controls. Similarly, β-oxidation (*Acox1* and *Acaa1*) and ether lipid biosynthesis (*Agps*) genes are highly expressed in

the CS treated model (**Fig. 22**). The antioxidative genes (**Fig. 23A**) as well as transcription factor mRNAs (**Fig. 23B**) were as well highly increased in the mouse COPD model. It is known that the various inflammatory mediators derived from the inflammatory and structural cells of the airways are increased in COPD. This was observed in our CS-exposed mice, where the levels of *Il-6*, *Tnfα* and *Cox-2* in the lungs of these mice were highly increased with the *Il-6* gene level showing the highest expression (**Fig. 24**). Thus, the results of the qRT-PCR analyses demonstrate that the expression levels of most of the peroxisomal genes as well as inflammatory mediators and transcription factors are significantly upregulated in the COPD model.

To summarize, in the COPD mouse model similar alterations were present concerning the peroxisomal compartment and its associated gene expression levels as in COPD patients.

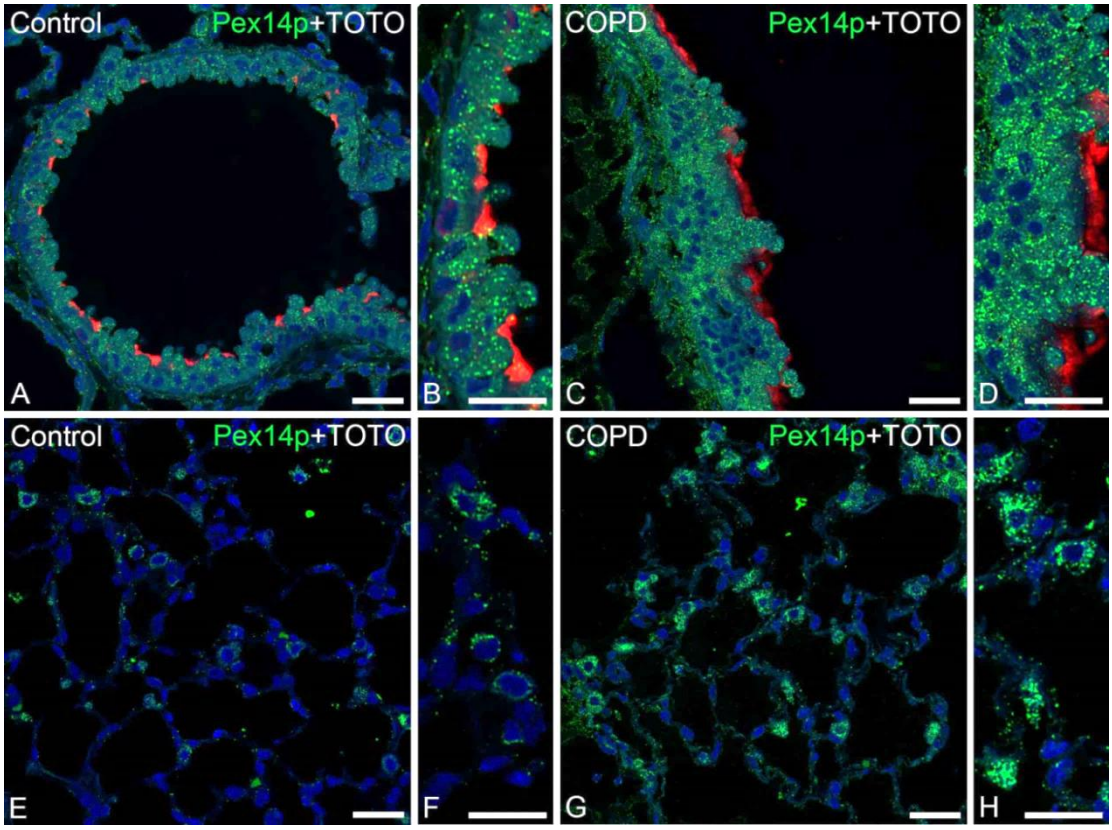

Fig. 19. CLSM images IF preparations for the peroxisomal biogenesis enzyme Pex14 in the bronchiolar (A-D) and alveolar epithelium (E- H) of the mouse control (A, B, E and F) and CS-exposed lungs (C, D, G and H). Nuclei were counterstained with TOTO-3-iodide. Bars represent 20µm for (A, C, E and G) and 60µm for (B, D, F and H).

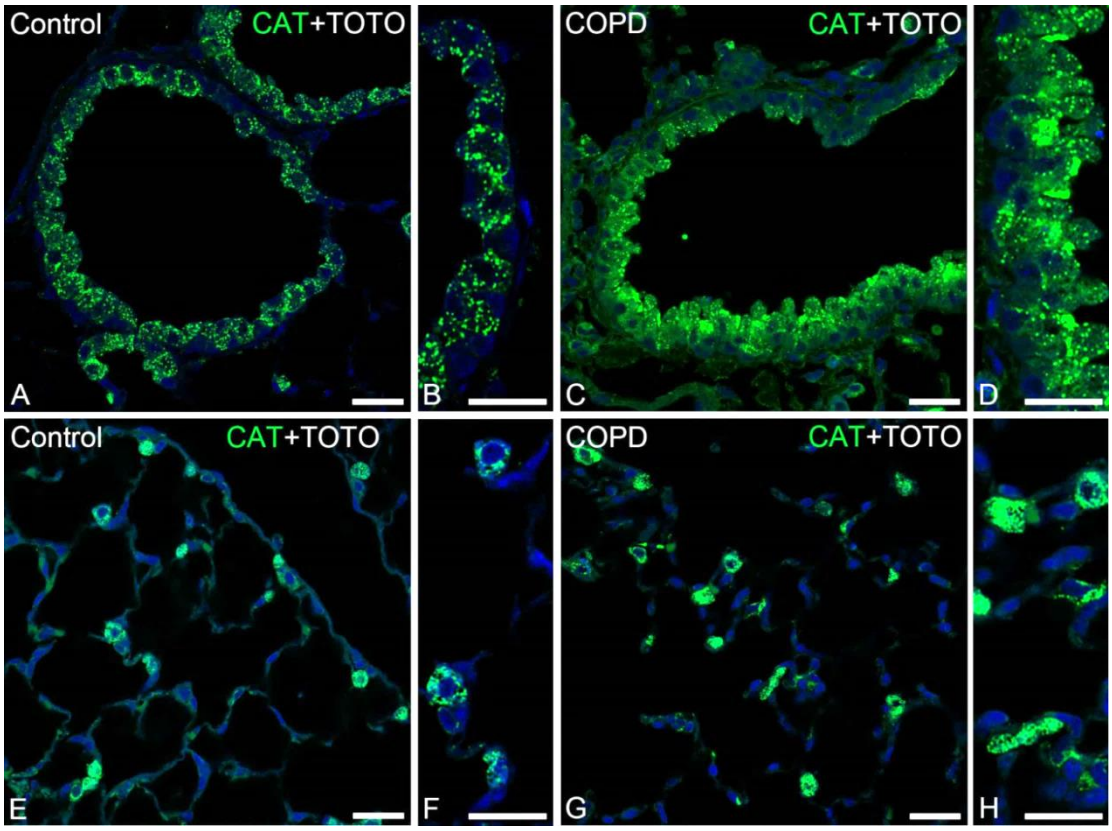

Fig. 20. CLSM images of IF preparations for the peroxisomal antioxidative enzyme catalase (Cat) in the bronchiolar (A-D) and alveolar epithelium (E- H) of mouse control lungs (A, B, E and F) and lungs of the COPD model (C, D, G and H). Nuclei were counterstained with TOTO-3-iodide. Bars represent 20µm for (A, C, E and G) and 60µm for (B, D, F and H).

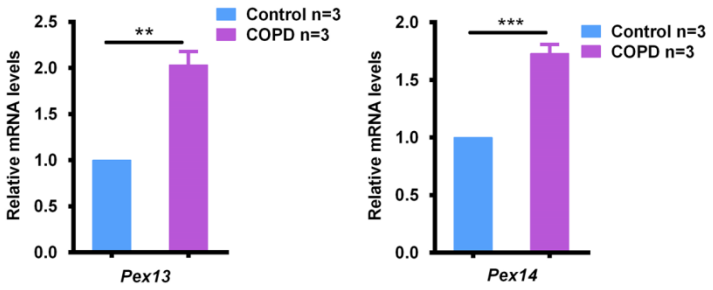

Fig. 21. The expression levels of peroxisomal biogenesis gene mRNAs on total RNA of control and CS-exposed mice. P values were calculated by the unpaired student t-test. *p ≤ 0.05, **p ≤ 0.01.

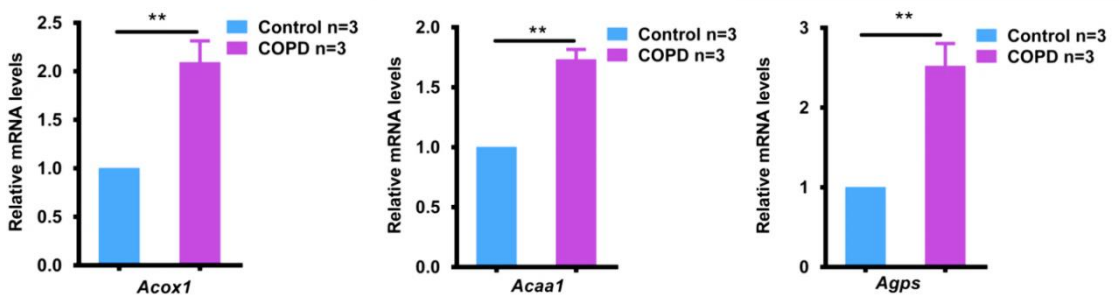

Fig. 22. Real-time PCR of peroxisomal β-oxidation (*Acoox1* and *Acaa1*) and ether lipid synthesis (*Agps*) gene mRNAs on total RNA of control and CS-exposed mice. P values were calculated by the unpaired student t-test. **p ≤ 0.01.

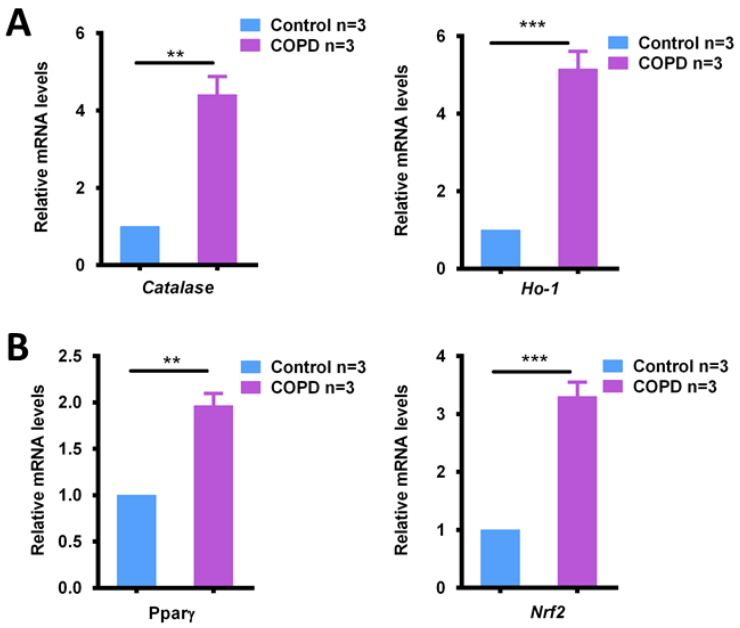

Fig. 23. The expression levels of antioxidative (A), and transcription factor (B) gene mRNAs on total RNA of control and CS-exposed mice as analysed by qRT-PCR. P values were calculated by the unpaired student t-test. ** p≤0.01, *** p≤0.001.

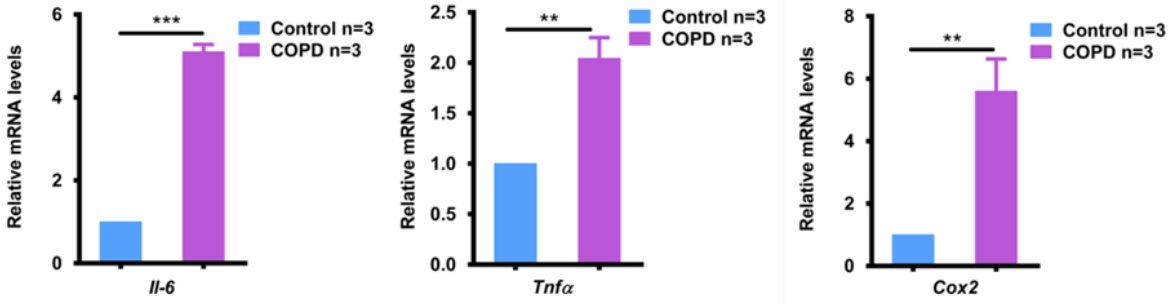

Fig. 24. **The expression levels of inflammatory mediator** mRNAs from total RNA of control and CS-exposed mice as analysed by qRT-PCR. P values were calculated by the unpaired student t-test. **p ≤ 0.01, *** p ≤ 0.001.

4.3. Human bronchial epithelial cells

4.3.1. Cigarette smoke exposed human cell culture model

Following the analysis of human COPD samples and CS-exposed mouse model, our next goal was to establish an *in vitro* model and to determine the effect of CS extract (CSE) on peroxisomal alterations in cultured cells. These cell culture models may provide vital information on molecular and functional mechanisms involved in the regulation of the peroxisomal or transcription factor alterations. For this purpose, primary human bronchial epithelial cells (HBE) were used.

In order to establish an optimal model, we determined the appropriate concentration of CSE that was necessary to stimulate the cells but without inducing cell death by applying MTT assay (**Fig. 25**). It was found that CSE reduced the cell viability in a

concentration dependent manner, such that a 4hr exposure to 16% CSE reduced cell viability by 50%. Only minor effects were observed with 4% CSE. Therefore, for our further experiments, 8% CSE was used because it was the highest concentration that showed still only minor cytotoxicity. Two concentrations of 4% and 8% CSE were used for the peroxisomal analysis in Western blots in order to detect whether these two concentrations affect peroxisome abundance in a concentration dependent manner.

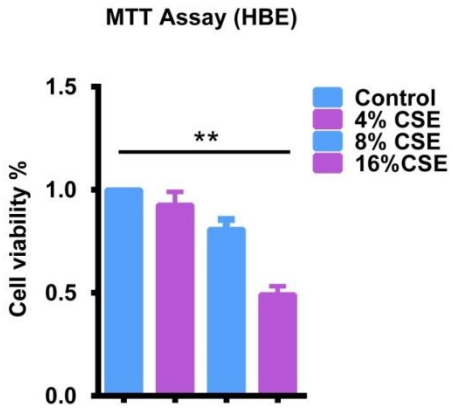

Fig. 25. Cell viability of cigarette smoke extract-exposed HBE cells. The viability is determined by MTT assay after a 4h exposure to different concentrations of CSE. Results are expressed as percentages of the unexposed control. P values were calculated by one way ANOVA. n=3, ** $p \leq 0.01$.

4.3.2. CSE mediates upregulation of peroxisomes in the HBE cell culture COPD model

After determination of the proper CSE concentration, we were interested to find whether the results of peroxisomal alterations in the cigarette smoke HBE cell culture model would correlate with the results obtained in the human and mouse COPD model. For this purpose, HBE cells were cultured until they reached 70% confluency and thereafter treated with 8% CSE for 4h. The abundance and expression of peroxisomal proteins was then investigated by immunofluorescence, Western blot and real time RT-PCR analyses.

Immunofluorescence analysis revealed a significant increase of peroxisomal biogenesis (**Fig. 26B and D**), β-oxidation (**Fig. 26F**) and ether phospholipid synthesis (**Fig. 26H**) proteins in CSE-treated cells in comparison to DMSO treated controls (**Fig. 26A, C, E and G**). Moreover, the peroxisomal antioxidative enzyme Cat was up-regulated as well in this cell culture COPD model **(Fig. 27B**).

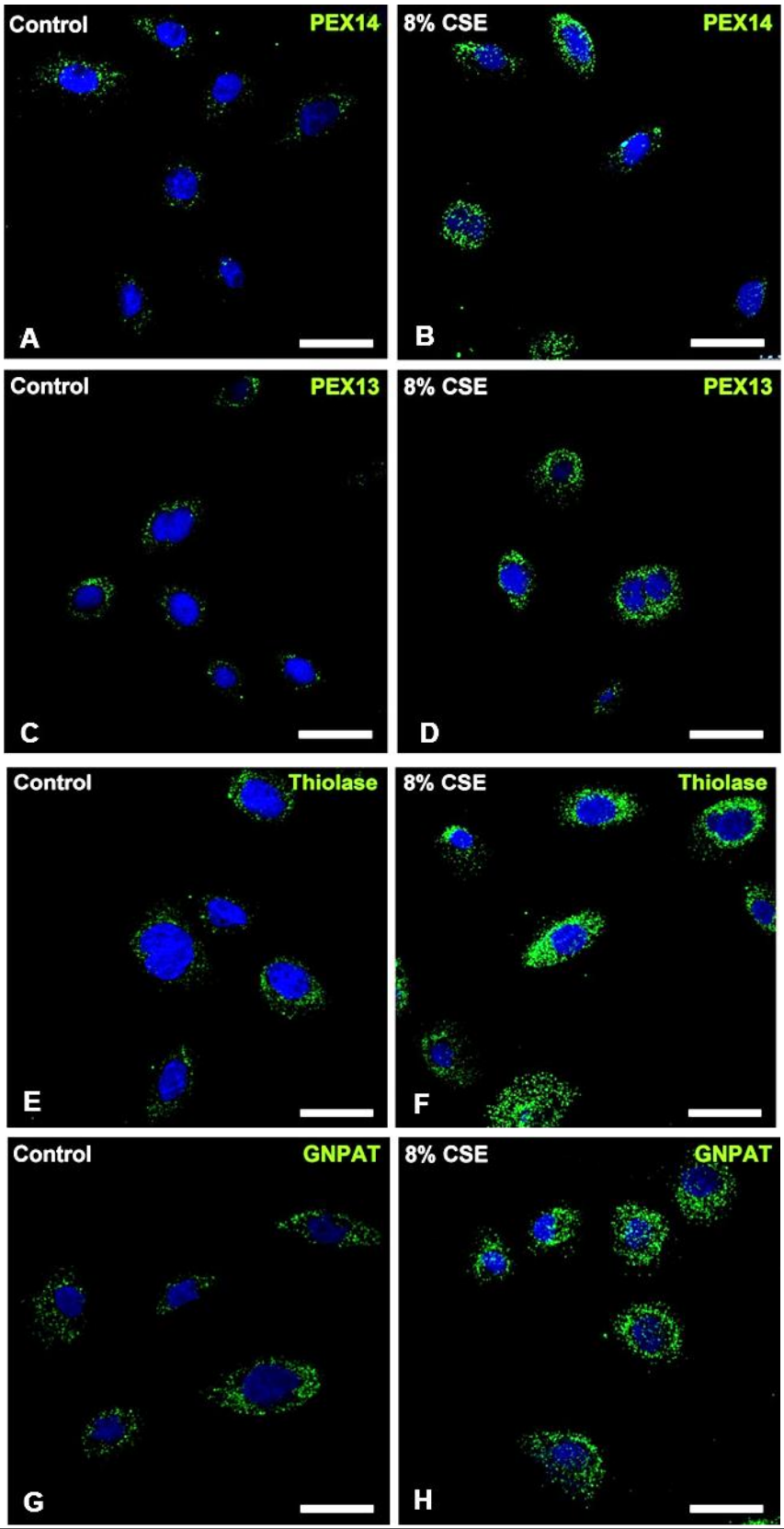

Fig. 26. CLSM images of IF stainings for peroxisomal biogenesis (A-D), β-oxidation (E-F) and ether lipid synthesis (G-H) proteins in HBE cells. Human HBE cells were treated with DMSO (A, C, E and G) for 4h prior to IF staining. Cells treated with 8% CSE (B, D, F and H) for 4h prior to IF. Bars represent 25μm.

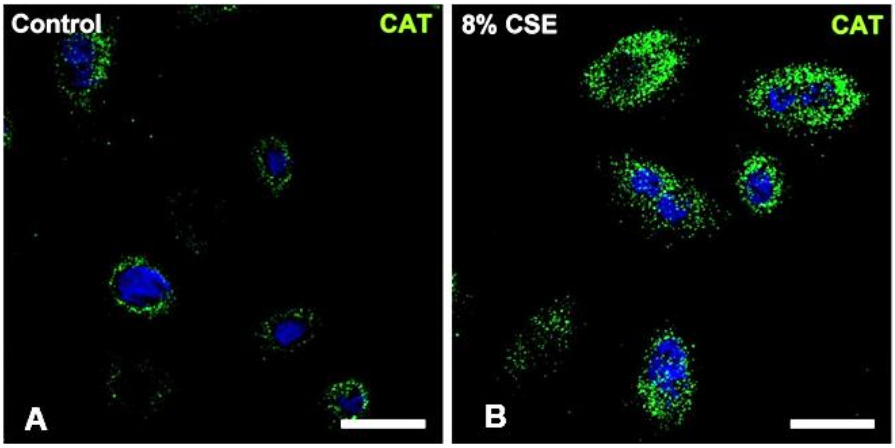

Fig. 27. CLSM images of IF stainings for the antioxidative enzyme CAT in HBE cells. HBE cells were treated with DMSO as a control (A) and with 8% CSE (B) for 4h prior to IF. Bars represent 25µm.

The upregulation of the peroxisomal compartment was also confirmed on the mRNA and protein level by qRT-PCR and Western blot analyses respectively. Significantly increased mRNA expression levels of the peroxisome-related genes involved in matrix protein import (PEX5, PEX7, PEX13 and PEX14) were observed in the 8% CSE treated cells (**Fig. 28A-C**) in comparison to the control. Similar upregulation of the corresponding proteins was observed (**Fig. 28D**). Moreover, peroxisomal β-oxidation genes (**Fig. 29**) as well as peroxisomal ether phospholipid synthesis genes (**Fig. 30A and B**) and proteins (**Fig. 30C**) were increased in expression/abundance in the *in vitro* smoke model as compared to DMSO treated cells. Furthermore, peroxisomal antioxidative enzyme catalase (CAT) and transcription factor (PPARγ) genes (**Fig. 31A and C**) and proteins (**Fig. 31B and D**) were highly upregulated in the 8% treated cells. Interestingly, Western blot analysis revealed that CSE triggered the upregulation of peroxisomal proteins in a concentration dependent manner.

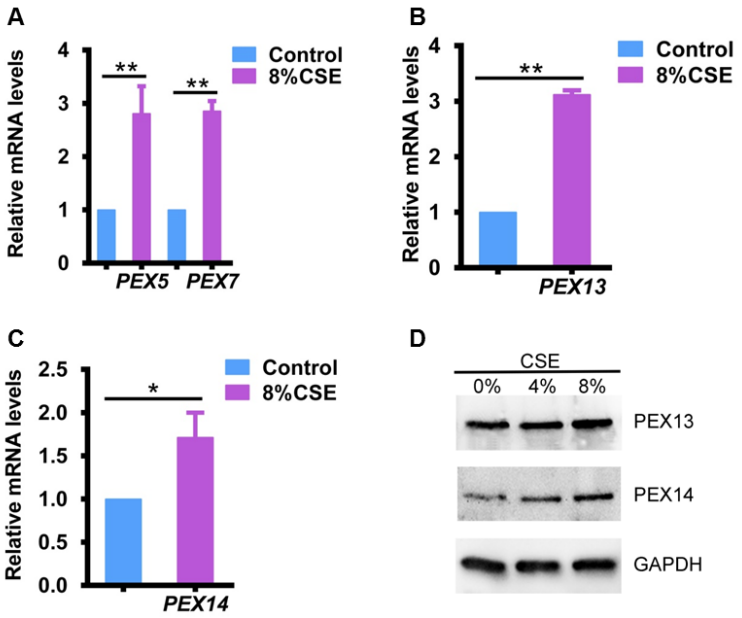

Fig. 28. The expression levels of peroxisomal gene mRNAs (A-C) and protein abundance (D) on total RNA and total lysate respectively. Western blot analyses and qRT-PCR were performed on the cells treated either with DMSO as a control or with 4-8% CSE for 4h. P values were calculated by the unpaired student t-test. n=3, *p ≤ 0.05, ** p ≤ 0.01.

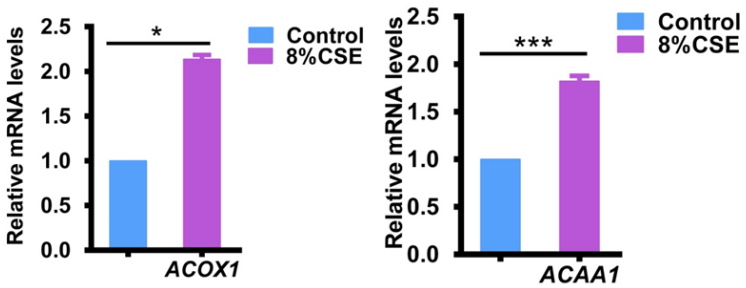

Fig. 29. Real-time PCR of peroxisomal β-oxidation gene mRNAs (*ACOX1* and *ACAA1*) on total RNA of control and CSE-treated cells. P values were calculated by the unpaired student t-test. n=3, *p ≤ 0.05, *** p ≤ 0.001.

It is known that in COPD, inflammatory cells are activated and produce inflammatory mediators like IL-6, IL-8 and TNFα [78,189]. Many studies demonstrated the elevation of these inflammatory cytokines in COPD patients. Similarly, our CS-exposed HBE cell culture model revealed an increase in the expression of inflammatory genes (**Fig. 32**) in comparison to the controls. Moreover, ELISA analysis of the supernatants from the DMSO or CSE treated cells showed a high release of IL-8 from the CSE treated HBE cells. In other words, CSE treatment induced IL-8 release into the medium (**Fig. 33**).

To summarize, our CS-exposed HBE cell culture model demonstrated a significant upregulation of the peroxisomal compartment. These results were in agreement with the results obtained in the COPD patients and the CS-exposed mouse model. This correlates with our goal which was to establish a good cell culture model that will allow

us to maintain as many physiologically-relevant factors as possible and to perform functional studies in future experiments.

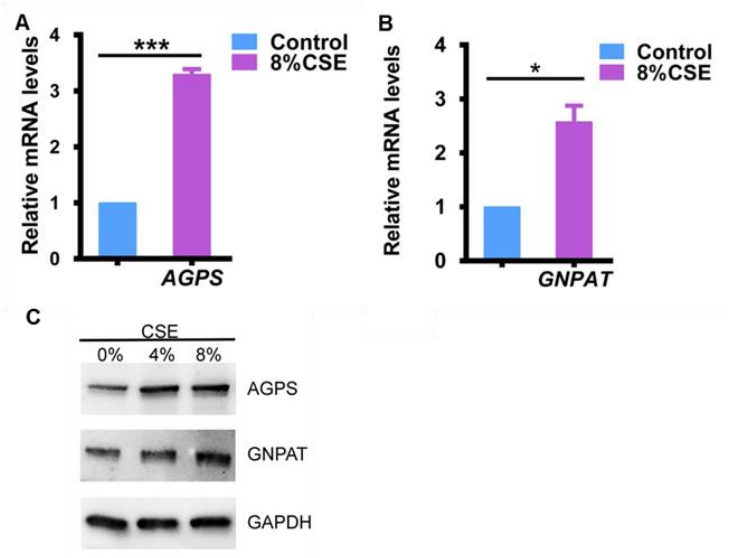

Fig. 30. Real-time PCR and Western blot analyses of peroxisomal ether phospholipid synthesis gene mRNAs and proteins on total RNA and total lysate respectively. Cells were either treated with DMSO as a control or with 4-8% CSE for 4h. P values were calculated by the unpaired student t-test. n=3, *p ≤ 0.05, *** p ≤ 0.001.

Fig. 31. Real-time PCR and Western blot analysis of peroxisomal antioxidative (CAT) and transcription factor (PPARγ) gene mRNAs and proteins on total RNA and total lysate respectively. Cells were either treated with DMSO as a control or with 4-8% CSE for 4h. P values were calculated by the unpaired student t-test. n=3, ** p ≤ 0.01.

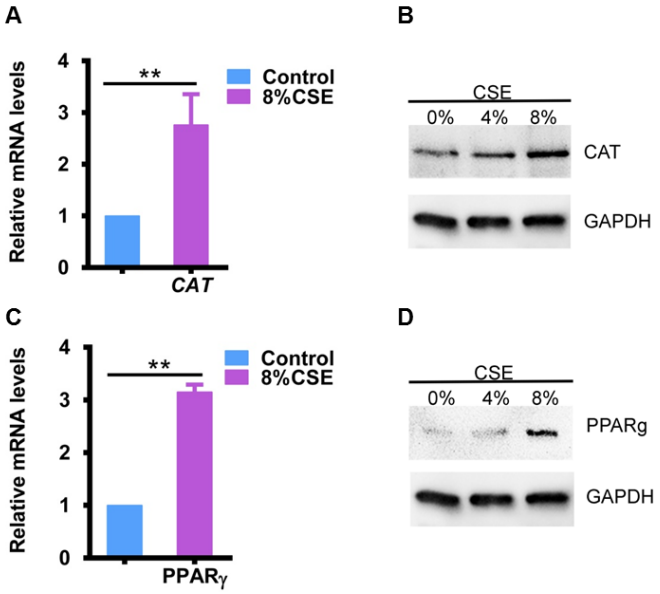

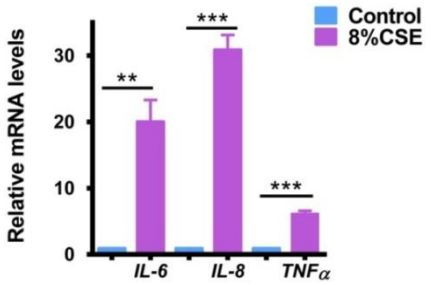

Fig. 32. The expression levels of inflammatory mediators mRNA from total RNA of control and CS-exposed cells as analysed by qRT-PCR. P values were calculated by the unpaired student t-test. n=3, ** p ≤ 0.01, ***p≤0.001.

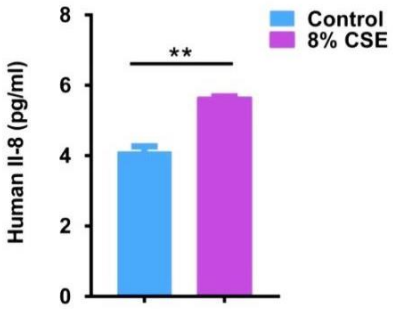

Fig. 33. Cigarette smoke extract induced IL-8 production in HBE cells. The supernatants of DMSO and CSE treated cells were collected after 4h of treatment and analysed by ELISA for the secretion of IL-8. P values were calculated by the unpaired student t-test. n=3, ** $p \leq 0.01$.

4.3.3. *PEX13* knockdown

The *PEX13* gene encodes a peroxisomal biogenesis protein in the peroxisomal membrane that belongs to the docking complex and is necessary for peroxisomal matrix protein import. Therefore, deletion of *PEX13* leads to a loss of matrix protein import via the PTS1 and PTS2 targeting signals [190]. Knockdown of the *PEX13* gene disrupts peroxisome biogenesis and would provide a good model to study the role of peroxisomes in the pathogenesis of COPD.

Establishment of the conditions for the *PEX13* knockdown was done with two different *PEX13* small interfering RNAs (siRNAs) over a range of 24-96h. We noticed that the knockdown drastically affected the survival of the cells even with the lower concentration of PEX13 siRNA used (10nmol). The delivery of siRNA into primary cells is considered to be challenging because primary cells are hard-to-transfect and after couple of unsuccessful attempts, we decided to use the mouse club cell line (C22 cells) for this purpose.

4.4. Immortalized (Conditionally) Mouse Lung Club Cells (C22) cells

4.4.1. Cigarette smoke-exposed model

Similarly like in experiments with HBE cells, it was important to determine the appropriate concentration of CSE to be used for the generation of CSE-exposed cell model. For this purpose, cell viability was measured with the MTT assay (**Fig. 34**). The results were similar to that of HBE cells where CSE treatment reduced cell viability in a concentration dependent manner, such that a 4hr exposure with 16% CSE reduced the cell viability by 50%. Only minor changes of cell viability were observed with 4% CSE. Therefore, for our further experiments, 8% CSE was chosen to be used because it was the highest concentration that still had low cytotoxicity.

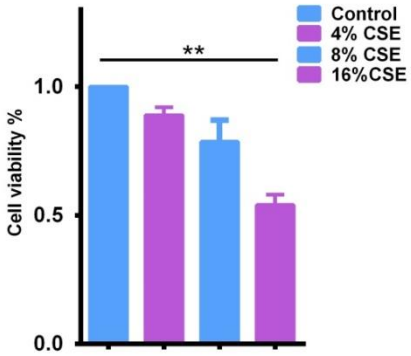

Fig. 34. Cell viability of cigarette smoke extract-exposed cells. The viability is determined by MTT assay after a 4hr exposure to different concentrations of CSE. Results are expressed as percentage of the unexposed control. P values were calculated by the one way ANOVA. n=3, ** $p \leq 0.01$.

4.4.2. CSE treated C22 cells reveal an upregulation of peroxisomes

Before knocking down *Pex13*, we wanted to confirm that our CSE-exposed C22 *in vitro* model would corroborate the results observed in COPD patients as well as in COPD mouse and HBE cell culture model. For this purpose, it was necessary to examined whether CSE would induce similar responses, at the protein and mRNA levels as the ones observed in the previous models.

Immunofluorescence stainings of C22 cells treated with 8%CSE for 4h demonstrated an elevation of the peroxisomal biogenesis protein PEX13 (**Fig. 35 B**) in comparison to the control cells treated with DMSO (**Fig. 35A**). The increase in PEX14 (**Fig. 35D**) abundance was very slight in comparison to control cells (**Fig. 35D**). In addition to this, the abundance of the peroxisomal antioxidative enzyme CAT (**Fig. 36D**) as well as the peroxisomal β-oxidation enzyme Thiolase (**Fig. 36B**) was drastically up-regulated in the cells stimulated with 8% CSE.

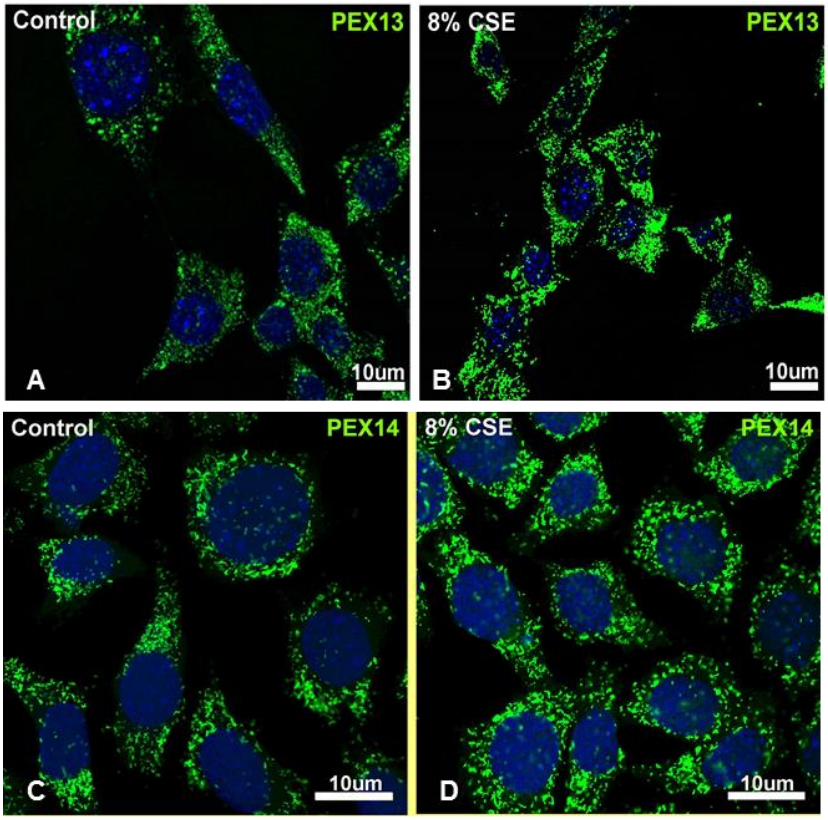

Fig. 35. **CLSM images of IF stainings for peroxisomal biogenesis proteins in C22 cells**. C22 cells were treated with DMSO as a control (A&C) and with 8% CSE (B&D) for 4h prior to IF. Bars represent 10μm.

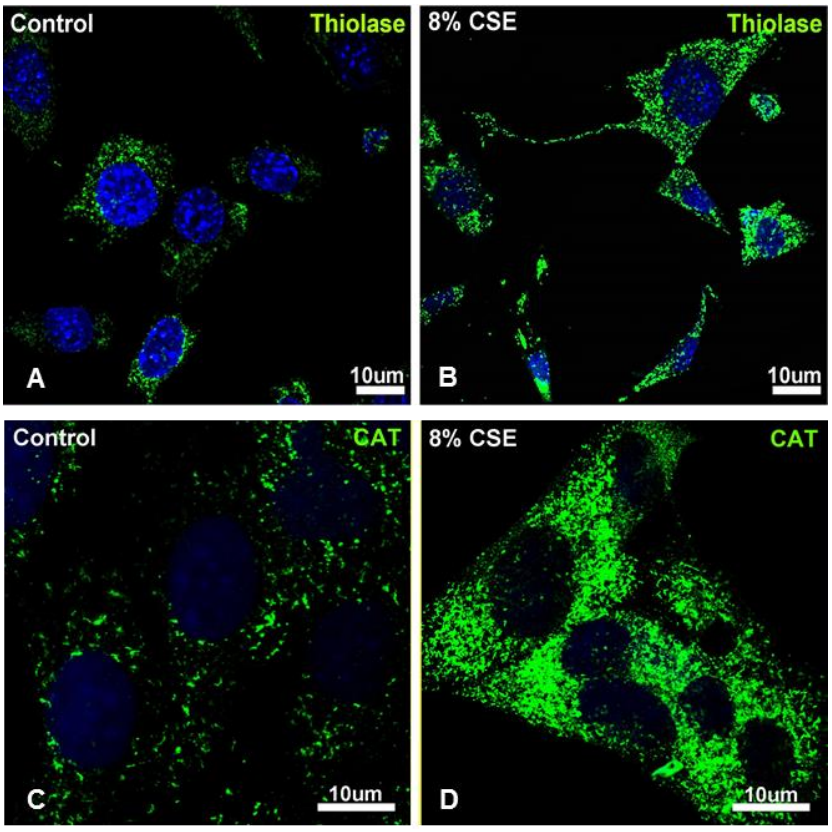

Fig. 36. **CLSM images of IF stainings for peroxisomal β-oxidation (Thiolase) and antioxidative (CAT) proteins in C22 cells**. C22 cells were treated with DMSO as a control (A&C) and with 8% CSE (B&D) for 4h prior to IF. Bars represent 10μm.

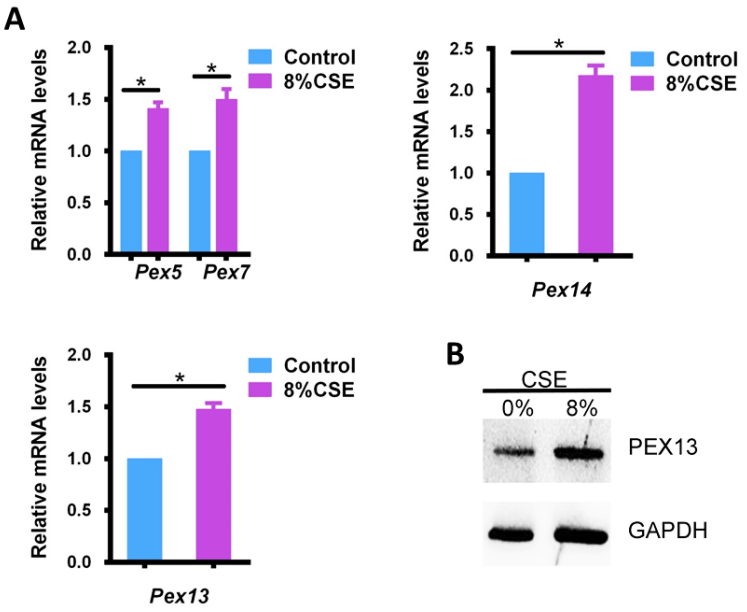

Fig. 37. The expression levels of peroxisomal biogenesis gene mRNAs (A) and protein abundance (B) on total RNA and total lysate respectively. qRT-PCR and Western blot were performed on the cells treated either with DMSO as a control or with 8% CSE for 4h. P values were calculated by the unpaired student t-test. n=3, * p ≤ 0.05.

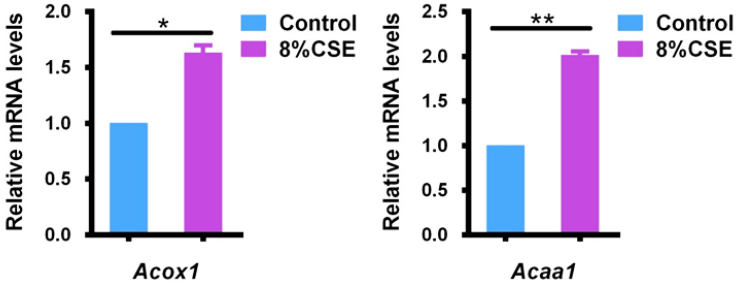

Fig. 38. Real-time PCR of peroxisomal β-oxidation gene mRNAs (*ACOX1* and *ACAA1*) on total RNA of control and CSE treated cells. P values were calculated by the unpaired student t-test. n=3, * p ≤ 0.05, **p≤0.01.

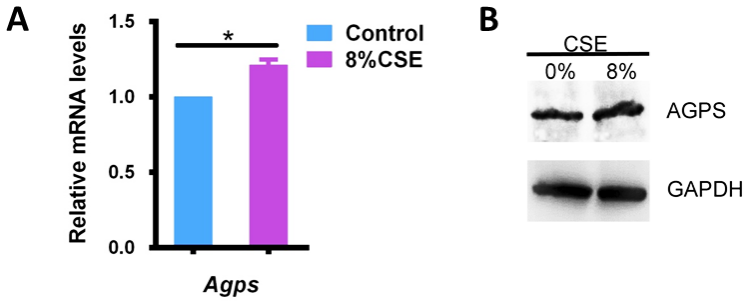

Fig. 39. Real-time PCR and Western blot analysis of peroxisomal ether phospholipid synthesis *Agps* mRNA (A) and protein (B) on total RNA and total lysates respectively. Cells were either treated with DMSO as a control or with 4-8% CSE for 4h. P values were calculated by the unpaired student t-test. n=3, * p ≤ 0.05.

Furthermore, Western blot and real time results were as well in accordance with the results shown in the previous models, where CSE induced a drastic upregulation in the peroxisomal biogenesis genes and protein (**Fig. 37A and B**), peroxisomal β-oxidation

gene mRNAs (**Fig. 38**) and peroxisomal ether phospholipid synthesis gene mRNA (**Fig. 39A**) and protein (**Fig. 39B**). Moreover, an increase in the transcription factors with 8% CSE in comparison to the DMSO control was observed with the Western blot and qPCR analysis (**Fig. 40A and B**). It is known that the oxidative stress caused by cigarette smoke triggers the release of various pro-inflammatory cytokines like IL-8, IL-6 and TNF-a and that COPD is characterized by abnormal increase of circulating cytokines such as CRP, IL-8, TNF-a, IL-6 [191,192]. Our results were in agreement with the COPD cytokine profile described in the previous studies such that; stimulation with 8%CSE for 4h increased the mRNA levels of pro-inflammatory cytokines, Il-6 and Tnf-α (**Fig. 41A**) and elevated the inflammatory protein level of COX-2 (**Fig. 41B**). Moreover, ELISA assay has shown a significant elevation of the secretory proteins TNF-α and IL-6 (**Fig. 42 A and B**). This implies that there is a strong oxidative stress which resulted in upregulation of antioxidant genes and enzymes CAT, HO-1 and SOD1 as shown by the qPCR and Western blot analysis (**Fig. 43A-C**).

To conclude, CSE treatment of mouse C22 cells recapitulated the results observed in samples taken from COPD patients, CS-exposed mouse model and samples generated from CSE-treated HBE cells. Therefore, C22 cells were used in the further knock-down experiments.

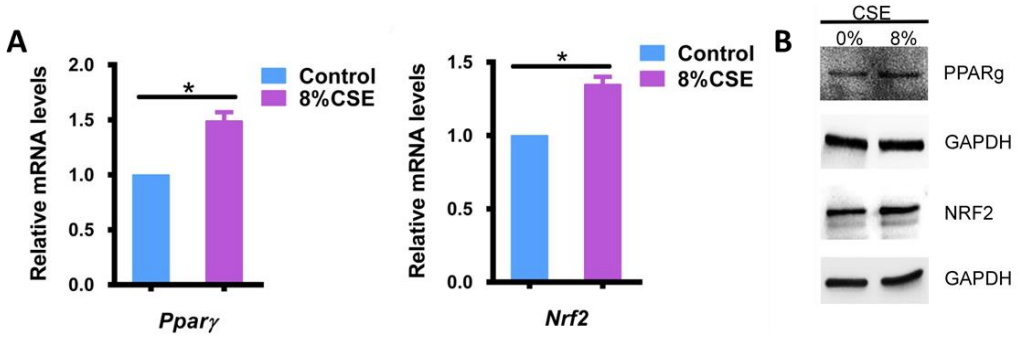

Fig. 40. Gene expression and protein abundance of transcription factors on total RNAs and total protein lysates respectively of control and CSE-treated cells as analysed by qRT-PCR and WB. P values were calculated by the unpaired student t-test. n=3, * p ≤ 0.05.

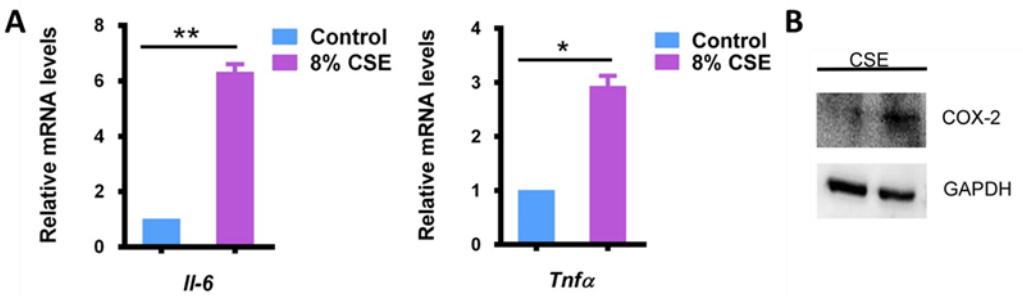

Fig. 41. Real-time PCR and Western blot analysis of pro-inflammatory cytokines (A) and the inflammatory marker (B) on total RNAs and total lysate respectively of DMSO control and 4hr CSE-treated cells. P values were calculated by the unpaired student t-test. n=3, * p ≤ 0.05, **p≤0.01.

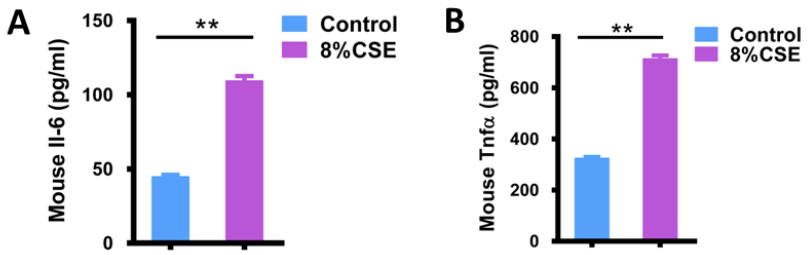

Fig. 42. Cigarette smoke extract induced cytokine release in C22 cells. The supernatants of DMSO and CSE-treated cells were collected after 4h of treatment and analysed by ELISA for the secretion of IL-6 and TNF-α. P values were calculated by the unpaired student t-test. n=3, **p≤0.01.

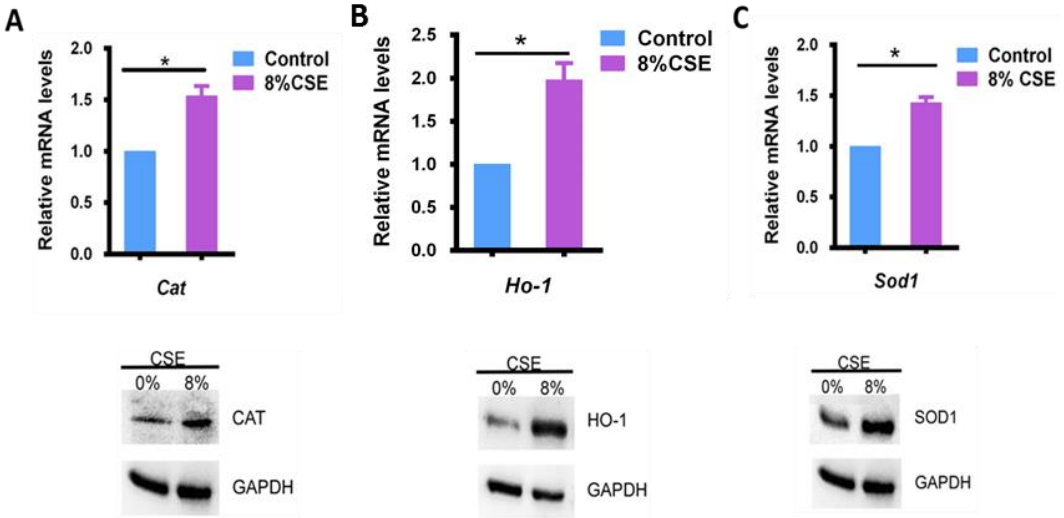

Fig. 43. **Real-time PCR and Western blot analyses of antioxidative gene** mRNAs and proteins on total RNAs and total lysates respectively of control and CSE-treated cells. . P values were calculated by the unpaired student t-test. n=3, * p ≤ 0.05.

4.4.3. *Pex13* knockdown in C22 cells

4.4.3.1. Peroxisome deficiency in *Pex13* knockdown in C22 cells

In order to understand the function of peroxisomes in the pathogenesis of COPD, the knock-down of *Pex13*, a peroxisomal biogenesis gene whose protein product acts as a docking factor in the peroxisomal membrane for the import of matrix proteins, was performed. Therefore, *Pex13* deletion disrupts the peroxisomal biogenesis preventing the matrix proteins from being imported into the organelle. Consequently, the matrix proteins are mislocalized into the cytoplasm in which many of them (except catalase) are degraded. Therefore, mistargeting of catalase to the cytoplasm is an excellent proof for the dysfunctional protein import into peroxisomes.

Establishment of the conditions for the Pex13 knockdown was done with *Pex13* small interfering RNA (siRNA) over a range of 24-96h with a single transfection of siRNA. Long times after transfection were necessary since the half-life of peroxisomes was estimated to be 3 days (in hepatocytes) and effects on protein levels can only be

observed around this time point. We found that the optimal conditions for siRNA transfection were as follows: single transfection of *Pex13* siRNA (30nmol) and then harvesting the cells 72h post transfection.

The cells transfected with siRNA specific for the *Pex13* gene and then treated with DMSO or 8%CSE, showed a significant reduction in the *Pex13* mRNA and protein levels after 72h of transfection (**Fig. 44A and B**). In contrast, a high expression in the level of *Pex13* mRNA was observed in the cells transfected with scr-siRNA and thereafter treated with CSE (**Fig. 44A**); this result is a confirmation of the previous results that CSE triggers upregulation of peroxisomes in un-transfected cells. Furthermore, in order to confirm the knock-down, immunofluorescence was performed 72h post transfection. Immunofluorescence for PEX13 in the *Pex13* siRNA transfected cells revealed a strong down-regulation in the PEX13 protein abundance in comparison to the scr-siRNA transfected cells (**Fig. 45B**). Moreover, the *Pex13* knockdown induced mistargeting of catalase (CAT), which is normally present in peroxisomes, into the cytoplasm of C22 cells as shown by IF (**Fig. 46B**). As was mentioned above, the cytoplasmic localization of peroxisomal matrix enzymes is a well-known phenomenon in cells with peroxisome deficiency [193]. The level of PEX14, which forms the docking complex together with PEX13 on the peroxisomal membrane, was not changed on the RNA (**Fig. 47A**) and protein (**Fig. 47B**) levels after siRNA transfection and this is reasonable as knock-down was *Pex13* specific.

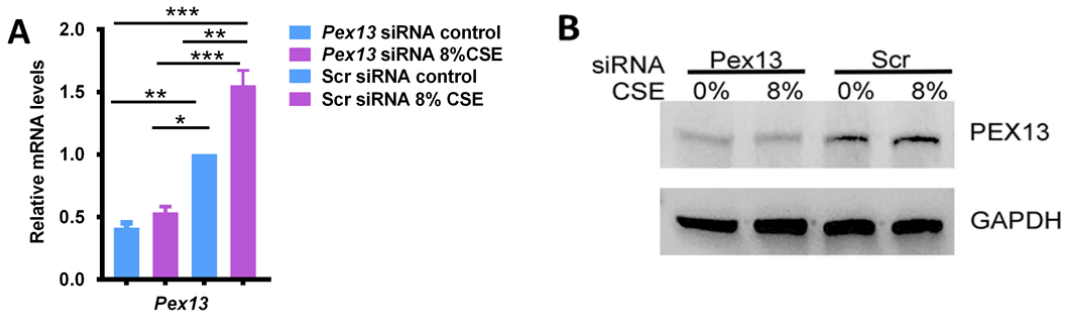

Fig. 44. Real-time PCR and Western blot analysis of peroxisomal biogenesis gene mRNA and protein of C22 cells transfected with either *Pex13*-siRNA or scr-siRNA followed by the DMSO (0%CSE) or CSE treatment. P values were calculated by the one way ANOVA. n=3, *p≤0.05, ** p≤0.01, *** p≤0.001.

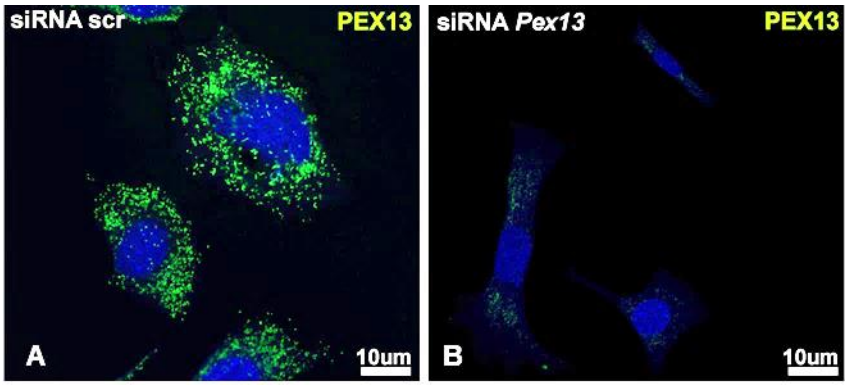

Fig. 45. Effects of *Pex13* gene knock-down as shown by immunofluorescence. C22 cells were transfected with scr- siRNA as a control (A) or with *Pex13* siRNA (B) for 72h prior to IF. Bars represent 10μm.

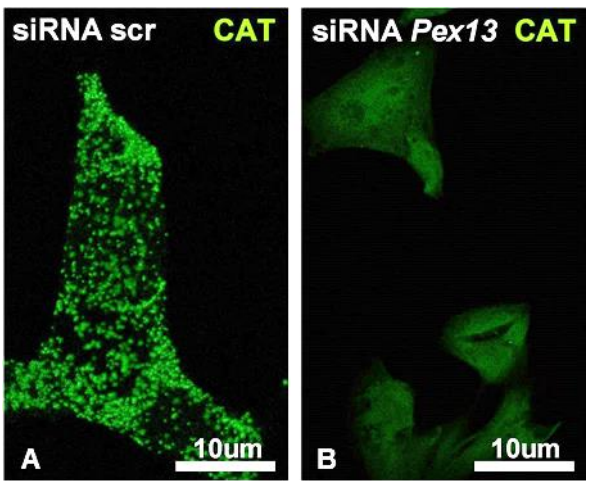

Fig. 46. Mistargeting of CAT into the cytoplasm after *Pex13* knock-down as shown by immunofluorescence. C22 cells were transfected with scr-siRNA as a control (A) or with *Pex13* siRNA (B) for 72h prior to IF. Bars represent 10μm.

Fig. 47. Real-time PCR and Western blot analysis of peroxisomal biogenesis gene mRNA and protein of C22 cells transfected with either Pex13-siRNA or scr-siRNA followed by the DMSO (0%CSE) or CSE treatment. P values were calculated by the one way ANOVA. n=3, *p≤0.05, ** p≤0.01.

As was mentioned before, proteins which are to be imported into the peroxisomal matrix contain either PTS1 or PTS2 peroxisomal targeting signals. Peroxisomal proteins harbouring either PTS1 or PTS2 signals are recognized by the PEX5 and PEX7 receptors respectively [194]. Once the cargo-receptor complex is formed, the complex is translocated to the peroxisomal membrane where it requires the peroxisomal membrane proteins (PEX13 and PEX14) for the initial binding step. Therefore, the knock-down of Pex13 will affect the import of PTS1 targeted proteins, such as catalase or PTS2 proteins, such as Thiolase into the peroxisome [195,196]. This is shown by the Western blot and real time PCR analyses where the peroxisomal antioxidative enzyme catalase (**Fig. 48A and C**) was reduced by more than 50% at the protein and mRNA level following the *Pex13* knock-down. In addition to catalase, the level of peroxisomal ether phospholipid synthesis enzyme AGPS was also reduced at the protein (**Fig. 48C**) and RNA (**Fig. 48B**) level after siRNA transfection. The peroxisomal β-oxidation enzymes ACOX1 and ACAA1 (Thiolase) (**Fig. 49A and B**) were as well decreased by 80% at the mRNA level in *Pex13* siRNA transfected cells. Therefore, peroxisome related gene expression and protein expression were strongly reduced in the *Pex13* knock-down model. How the mRNAs are down-regulated by the *Pex13* knock-down is not known until now. The degradation of peroxisomal matrix proteins in the cytoplasm is probably performed via the proteasome system.

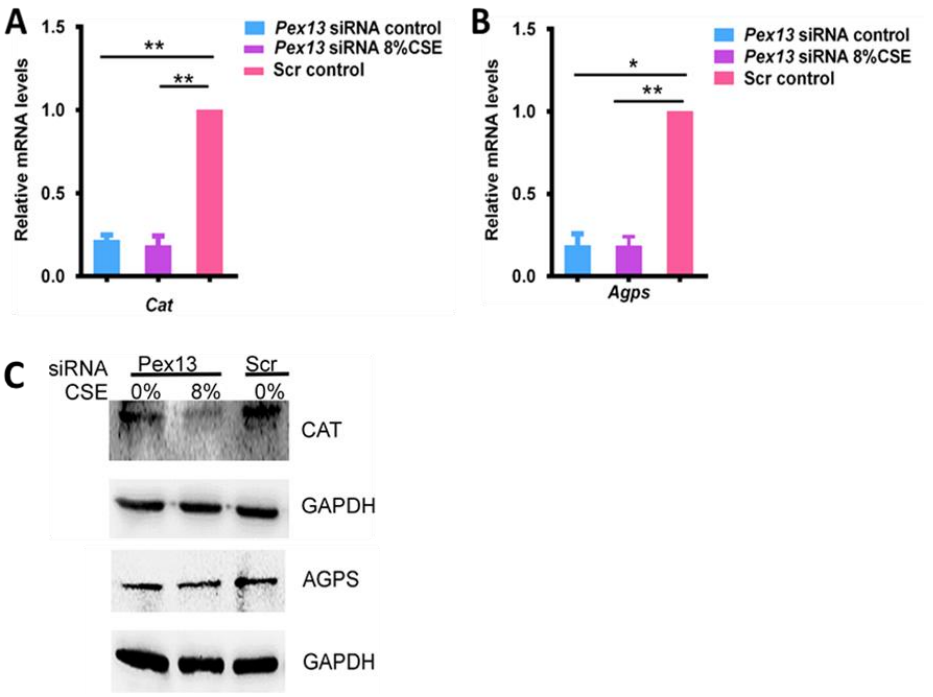

Fig. 48. Real-time PCR and Western blot analysis of peroxisomal antioxidant and ether phospholipid synthesis gene mRNA and protein of C22 cells transfected with either *Pex13*-siRNA or scr-siRNA followed by the DMSO (0%CSE) or 8%CSE treatment. P values were calculated by the one way ANOVA. n=3, *p≤0.05, ** p≤0.01.

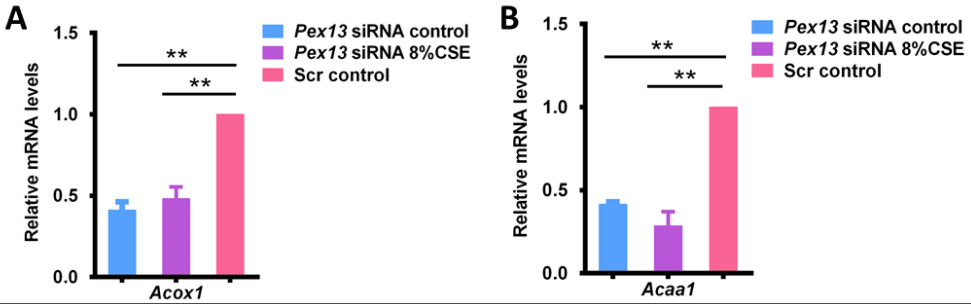

Fig. 49. Real-time PCR of peroxisomal β-oxidation gene mRNAs (*ACOX1* and *ACAA1*) on total RNA of scr-siRNA and *Pex13* siRNA transfected cells treated with either DMSO or CSE. P values were calculated by the one way ANOVA. n=3, ** p ≤ 0.01.

4.4.3.2. *Pex13* deletion negatively affects cell proliferation

To detect the effect of *Pex13* siRNA-treatment on cell proliferation, BrdU cell proliferation assays were performed. The calculation of the proliferation rate was based on measurements of BrdU incorporation during DNA synthesis in comparison to the scr-siRNA-treated groups. The *Pex13* knock-down together with CSE treatment reduced the cell proliferation by 20% in comparison to the DMSO treated scr-siRNA transfected cells (**Fig. 50**).

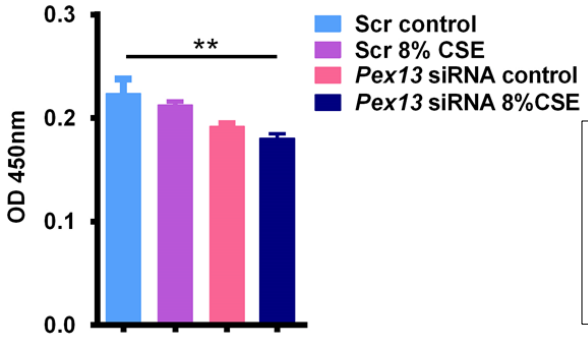

Fig. 50. Percentage of BrdU positive cells after either DMSO or CSE treatment following scr-siRNA or *Pex13* siRNA transfection. The extent of cell proliferation was measured by absorbance at 450nm. P values were calculated by the one way ANOVA. n=3, ** $p \leq 0.01$.

4.4.3.3. The *Pex13* deletion and CSE treatment induced a strong increase in the expression and the release levels of pro-inflammatory cytokines

A significant three and two fold increase was observed for the mRNA levels of *Il-6* (**Fig. 51A**) and *Tnf-α* (**Fig. 51B**) respectively in the cells transfected with *Pex13* siRNA and then treated for 4h with 8% CSE. Moreover, the abundance of the pro-inflammatory mediator COX-2 was up-regulated at the protein level in the *Pex13*-deleted cells (**Fig. 51C**) in comparison to cells treated with scr-siRNA. The upregulation of pro-inflammatory cytokines was confirmed by ELISA which revealed a much higher release of IL-6 and TNF-α into the medium after *Pex13* deletion and treatment with CSE. The supernatant of the cells transfected with *Pex13* siRNA for 68h showed a 3-fold increase in the released IL-6, from 44pg/ml in the unstimulated cells to 160pg/ml after CSE stimulation (**Fig. 52A**). Furthermore, the concentration of the released IL-6 in the supernatant of the cells transfected with *Pex13* siRNA and treated with CSE was 25% higher (160pg/ml) than in the supernatant of the cells transfected with scr-siRNA and thereafter treated with CSE (102pg/ml). In addition to this, the same pattern was observed for released TNF-α (**Fig. 52B**) where the transfected and then CSE treated cells showed a strong upregulation in TNF-α to approximately 1500pg/ml in comparison to 460pg/ml in the supernatant of *Pex13* siRNA transfected but untreated cells. Moreover, the TNF-α released was two-fold higher in the supernatant of *Pex13* deleted cells followed by CSE treatment than in the supernatant of the cells transfected with scrambled siRNA and treated with CSE (700pg/ml). In summary, the knock-down of *Pex13* together with CSE stimulation triggered a much higher release of pro-inflammatory mediators and this expression and release of the mediators was more significant than in scr-siRNA transfected and then CSE treated cells.

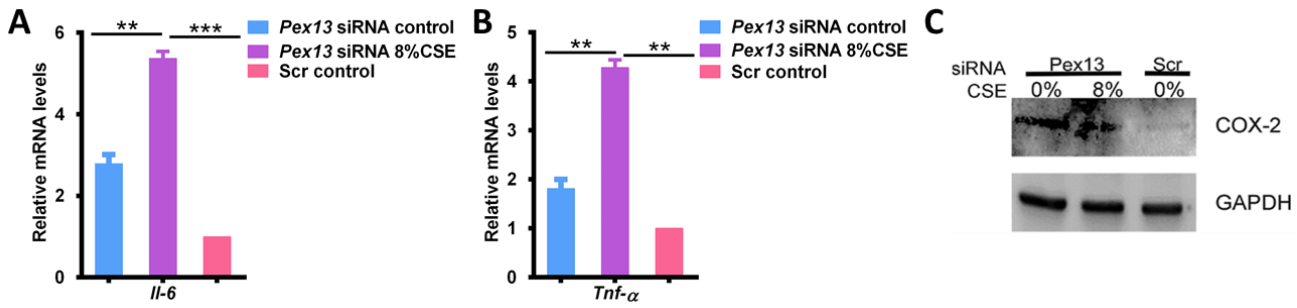

Fig. 51. CSE increased the expression of pro-inflammatory mediators at the mRNA level on total RNA of scr-siRNA and *Pex13* siRNA transfected cells, treated with either DMSO or CSE as estimated by qRT-PCR. P values were calculated by the one way ANOVA. n=3, ** p≤0.01, *** p≤0.001.

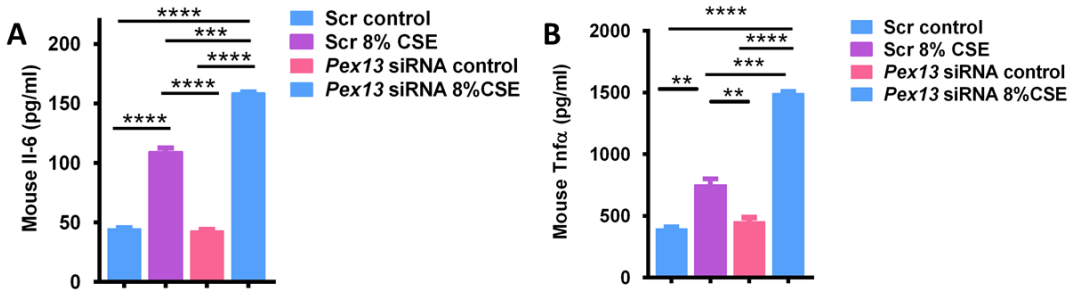

Fig. 52. Cigarette smoke extract induced the release of pro-inflammatory cytokines (IL-6 and TNF-α) in the supernatant of siRNA-Pex13 transfected cells as shown by ELISA assay. The C22 cells were transfected with either *Pex13* siRNA or scr-siRNA for 68h and then treated with DMSO or 8%CSE for 4h prior to supernatant collection. The released mediators were measured by ELISA. P values were calculated by the one way ANOVA. n=3, ** p ≤ 0.01, *** p≤0.001, **** p≤0.0001.

4.4.3.4. Peroxisomal deficiency induces a much higher ROS production after CSE treatment

As was shown above, the deletion of *Pex13* leads to downregulation of peroxisomal enzymes, decreases proliferation and induces the release of inflammatory mediators. In addition to this, the ROS production was analysed from differently treated cells by using dihydroethidium (DHE) staining. The ROS activity of scr-siRNA transfected cells treated with CSE (**Fig. 53B and B'**) was increased by 30% in comparison to the DMSO treated scr-siRNA transfected cells (**Fig. 53A and B'**), suggesting that the intracellular stress is caused by CSE. A slight increase in the ROS activity was already observed in *Pex13* siRNA transfected cells treated with DMSO (**Fig. 53C and B'**) in comparison to scr-siRNA transfected cells treated with DMSO (**Fig. 53A and B'**). However, in comparison to the value of scr-siRNA transfected and CSE treated cells, the *Pex13* knock-down and deficiency of the peroxisomal compartment lead to a further 80% increase in ROS suggesting that this increase was indeed exerted by the peroxisome deficiency (**Fig. 53D and B'**).

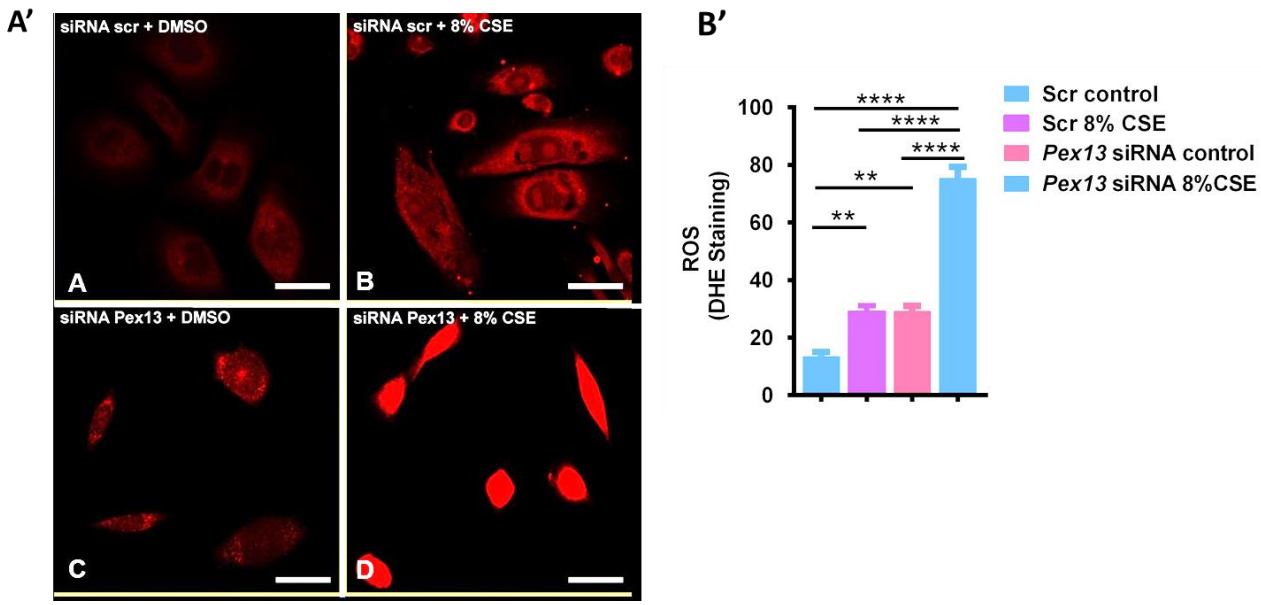

Fig. 53. Measurement of ROS by dihydroethidium (DHE) staining after different siRNA treatments (A'). Images were analyzed for DHE intensity using ImageJ (B'). The cells were transfected once with *Pex13*-siRNA and scr-siRNA. Following the siRNA transfection, the cells were treated with CSE and then stained with DHE for 30 min. The bars represent 10µm**.** P values were calculated by the one way ANOVA. n=3, ** p≤0.05, **** p ≤ 0.0001.

4.4.3.5. Peroxisomal dysfunction due to Pex13 knockdown induced an oxidative response

Oxidative stress mediates the expression of protective genes like *Nrf2, Pparγ, Ho-1* and *Sod1*. Moreover, it is known that Pparγ may modulate the expression of anti-inflammatory genes, apparently including antioxidant nuclear factor Nrf2 in response to oxidative stress [197].

It was found that *Pex13* deletion led to the upregulation of both transcription factors PPARγ and Nrf2. It also induced the protein expression and transcription of Nrf2 downstream genes HO-1 and SOD1. The highest increase in PPARγ was observed at the mRNA (**Fig. 54A**) and protein (**Fig. 54C**) level in the cells treated with 8% CSE after *Pex13* deletion. A similar pattern was detected at the mRNA (**Fig. 54B**) and protein level (**Fig. 54C**) for the transcription factor Nrf2 since it was strongly expressed in the cells treated with CSE following *Pex13* deletion. Indeed, the expression of these transcription factors was higher in *Pex13* transfected and CSE treated cells rather than in scrambled cells treated with CSE. The NRF2 regulated antioxidative enzymes SOD1 and HO-1, were as well highly expressed in *Pex13* knock-down cells treated with CSE at the mRNA (**Fig. 55A and B**) and protein levels (**Fig. 55C**). It is known that Nrf2 is a transcription factor that responds to oxidative stress by binding to the antioxidant response element (ARE). Therefore, a luciferase gene reporter assay was

performed with a reporter vector containing the antioxidant response element (ARE) (pARE-luc), the DNA-binding element for NRF2, in order to confirm that the *Pex13* knock-down induces oxidative stress. The results revealed that peroxisome deficiency by the *Pex13* knock-down, induced the activation of ARE (**Fig. 56**). This activation was the highest in cells treated thereafter with CSE. Similarly, the *Pex13* knock-down without CSE stimulation was also able to induce the ARE activity but to a lower extent than in the cells treated with CSE as demonstrated by the luciferase assay. In summary, the *Pex13* deletion induced peroxisome deficiency leading to reduction of the cell proliferation, a higher ROS production and oxidative stress.

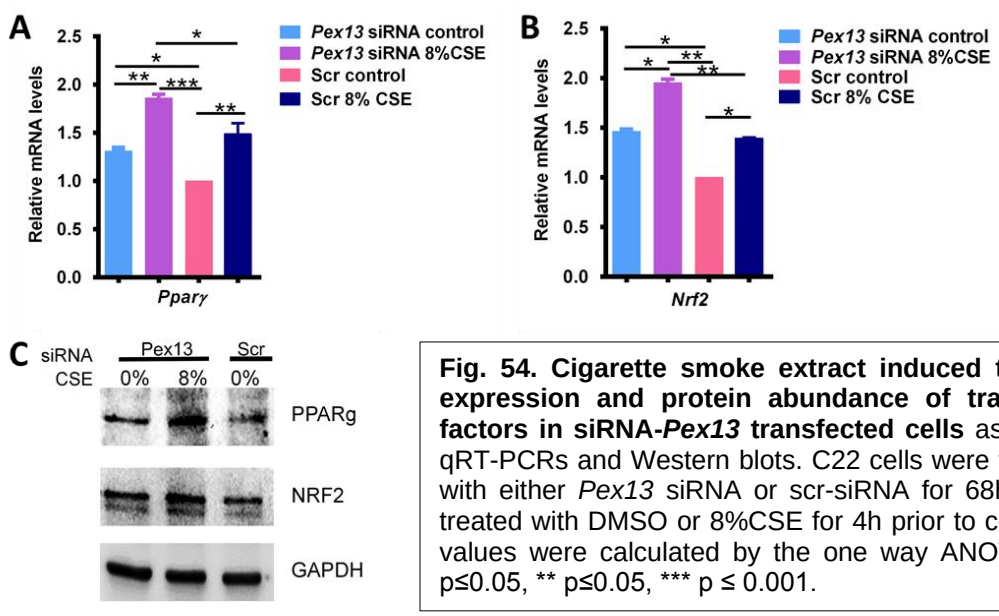

Fig. 54. Cigarette smoke extract induced the mRNA expression and protein abundance of transcription factors in siRNA-*Pex13* transfected cells as shown by qRT-PCRs and Western blots. C22 cells were transfected with either *Pex13* siRNA or scr-siRNA for 68h and then treated with DMSO or 8%CSE for 4h prior to collection. P values were calculated by the one way ANOVA. n=3, * p≤0.05, ** p≤0.05, *** p ≤ 0.001.

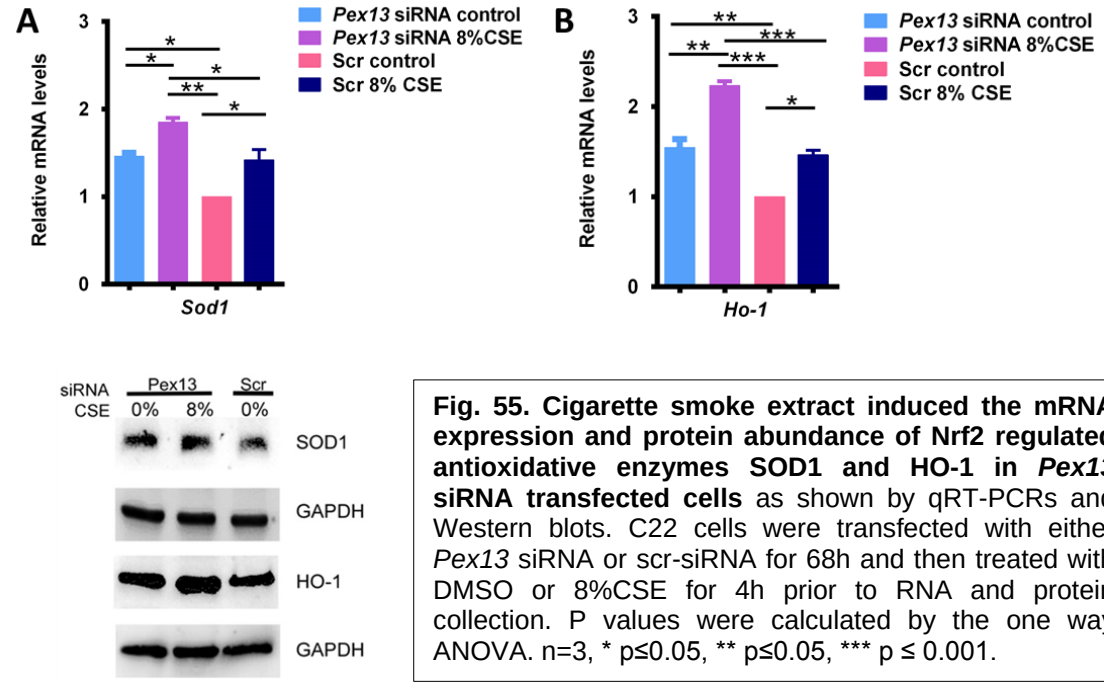

Fig. 55. Cigarette smoke extract induced the mRNA expression and protein abundance of Nrf2 regulated antioxidative enzymes SOD1 and HO-1 in *Pex13* siRNA transfected cells as shown by qRT-PCRs and Western blots. C22 cells were transfected with either *Pex13* siRNA or scr-siRNA for 68h and then treated with DMSO or 8%CSE for 4h prior to RNA and protein collection. P values were calculated by the one way ANOVA. n=3, * p≤0.05, ** p≤0.05, *** p ≤ 0.001.

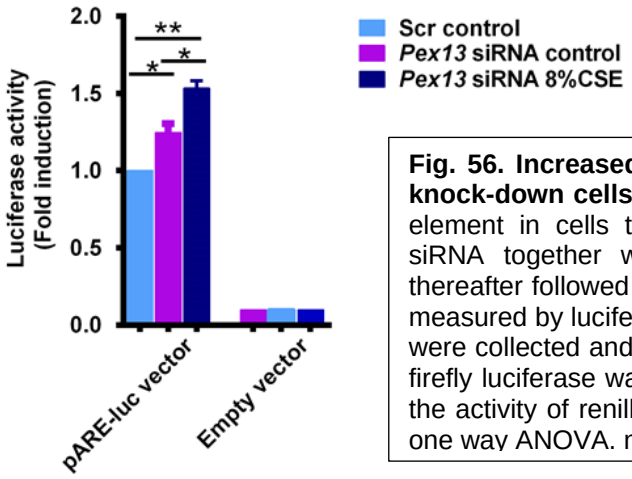

Fig. 56. Increased ARE response element activity in *Pex13* knock-down cells. Luciferase reporter activity of ARE promoter element in cells transfected with either *Pex13*-siRNA or scr-siRNA together with either pARE-luc or empty vector and thereafter followed by DMSO (0%CSE) or 8% CSE treatment as measured by luciferase assays. 72h post transfection cell lysates were collected and assayed for luciferase activity. The activity of firefly luciferase was measured in cell lysates and normalized to the activity of renilla luciferase. P values were calculated by the one way ANOVA. n=3, *p≤0.05, ** p≤0.01.

4.4.3.6. *Pparγ* regulates the *Pex13* expression

As shown above, the cells with *Pex13* knock-down were strongly affected by CSE treatment. This effect was significantly stronger than the one observed in the cells transfected with scr-siRNA stimulated with CSE. Moreover, these *Pex13* knock-down cells exhibited an elevation in oxidative stress, pro-inflammatory mediators, ROS levels and a decrease in proliferation. Therefore, we hypothesised that the activation and induction of peroxisomes could improve the cellular stress in COPD patients and therefore would reduce the severity of COPD symptoms. For this reason, it was important to prove that the peroxisome proliferator-activated receptor gamma (Pparγ) is upstream of the *Pex13* gene which would imply that the induction of PPARγ might activate the peroxisomal compartment. Therefore, a *Pparγ* knock-down was performed in order to check whether *Pex13* would be affected. As shown by the results, the knockdown was successful to silence 70% of the *Pparγ* gene in the cells transfected with *Pparγ* siRNA (**Fig. 57A**). A down-regulation of *Pparγ* was also observed at the protein level (**Fig. 57B**).

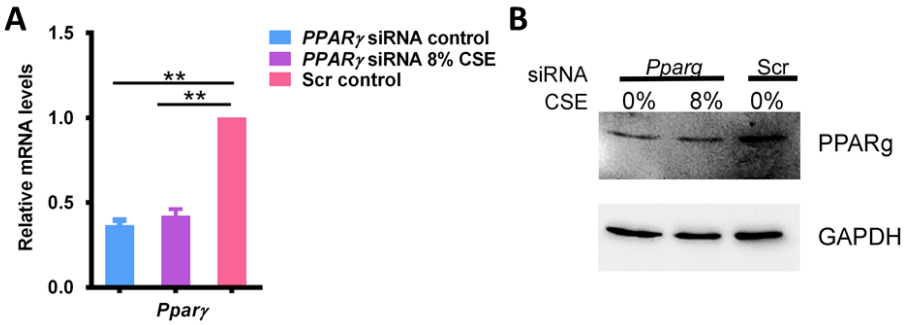

Fig. 57. PPARγ knock-down as shown by qRT- PCR and Western blot analysis. C22 cells transfected with either Pparγ-siRNA or scr-siRNA followed by the DMSO (0%CSE) or 8% CSE treatment. The RNA and protein was collected 72h post-transfection. P values were calculated by the one way ANOVA. n=3, ** p≤0.01.

The *Pparγ* siRNA silencing also reduced the *Pex13* gene expression (**Fig. 58A**) and reduced strongly its protein abundance (**Fig. 58B**) as shown by qRT-PCR and Western blot analyses.

Fig. 58. *Pparγ* knock-down downregulated Pex13 as demonstrated by the qRT-PCR and Western blot. C22 cells transfected with either Pparγ -siRNA or scr-siRNA followed by the DMSO (0%CSE) or CSE treatment. The RNA and protein was collected 72h post-transfection. P values were calculated by the one way ANOVA. n=3, * p≤0.05.

4.4.3.7. *Pparγ* silencing provoked a similar response of antioxidative enzymes as was observed after *Pex13* knock-down

Pparγ knock-down induced a similar pattern of the antioxidant response as was observed after *Pex13* knock-down. Catalase (CAT), a major peroxisomal antioxidative enzyme was analysed in *Pparγ* silenced cells. The results revealed a drastic down-regulation in peroxisomal CAT expression (**Fig. 59A**) and abundance (**Fig. 59B**) in the *Pparγ* silenced cells. This decrease in the level of CAT corroborated the strong down-regulation of the peroxisomal biogenesis protein PEX13 induced by the *Pparγ* knock-down.

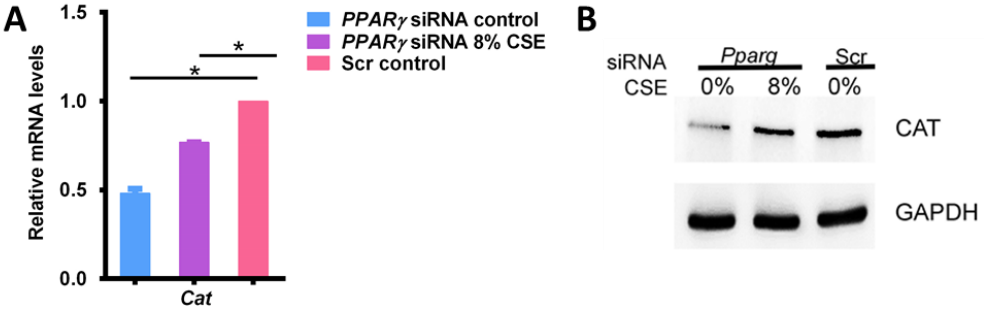

Fig. 59. *Pparγ* knock-down reduced the expression and abundance of the peroxisomal antioxidative enzyme catalase (CAT) as shown by qRT-PCR and Western blot. The C22 cells were transfected with either *Pparγ* siRNA or scr-siRNA for 68h and then treated with DMSO or 8%CSE for 4h prior to collection. P values were calculated by the one way ANOVA. n=3, * p≤0.05.

In contrast to catalase, *Pparγ* silencing provoked a different response of *Nrf2* and its downstream genes *Ho-1* and *Sod1*. Interestingly, the deletion of *Pparγ* led to the upregulation of the transcription factor Nrf2 and induced the protein expression and

transcription of the Nrf2-regulated genes encoding the antioxidative enzymes HO-1 and SOD1. A high increase in Nrf2 was observed at the mRNA (**Fig. 60A**) and protein (**Fig. 60B**) levels in the cells treated with 8% CSE after *Pparγ* deletion, whereas a slight increase in the abundance was seen in cells transfected with *Pparγ* and treated with DMSO thereafter in comparison to the cells transfected with scr-siRNA. A similar pattern was detected at the mRNA (**Fig. 61A and B**) and protein level (**Fig. 61C**) of Nrf2-regulated antioxidative enzymes SOD1 and HO-1, which were as well highly expressed in *Pparγ* knock-down cells treated with CSE. Moreover, *Pparγ* silencing provoked a drastic upregulation of COPD pro-inflammatory markers (*Il-6* and *Tnf-α*) (**Fig. 62**), suggesting an increase of the inflammatory response.

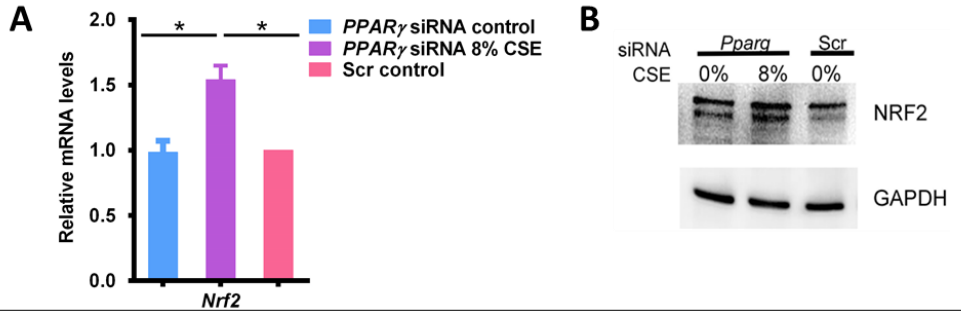

Fig. 60. Cigarette smoke extract induced expression and abundance of Nrf2 in *Pparγ* siRNA transfected cells as shown by qRT-PCR and Western blot analyses. The C22 cells were transfected with either *Pparγ* siRNA or scr-siRNA for 68h and then treated with DMSO or 8%CSE for 4h prior to collection. P values were calculated by the one way ANOVA. n=3, *p≤0.05.

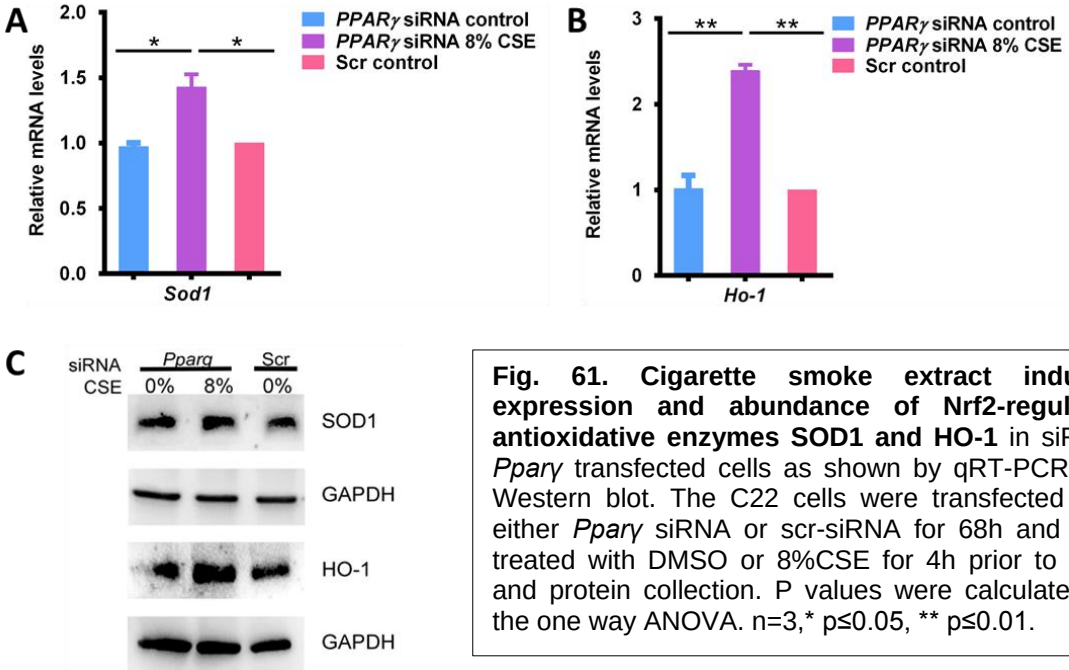

Fig. 61. Cigarette smoke extract induced expression and abundance of Nrf2-regulated antioxidative enzymes SOD1 and HO-1 in siRNA-*Pparγ* transfected cells as shown by qRT-PCR and Western blot. The C22 cells were transfected with either *Pparγ* siRNA or scr-siRNA for 68h and then treated with DMSO or 8%CSE for 4h prior to RNA and protein collection. P values were calculated by the one way ANOVA. n=3,* p≤0.05, ** p≤0.01.

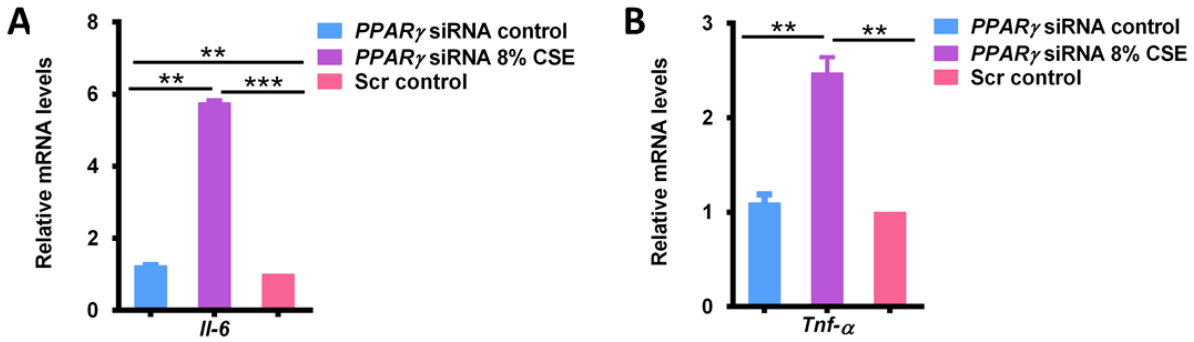

Fig. 62. *Pparγ* knock-down and CSE treatment increased the expression of the pro-inflammatory mediators *Il-6* and *Tnf-α* at the mRNA level on total RNA of scr-siRNA and *Pparγ* siRNA transfected cells, treated with either DMSO or CSE as estimated by qRT-PCR. P values were calculated by the one way ANOVA. n=3, ** p≤0.01, *** p≤0.001.

The ARE-luc reporter gene assay was already used to confirm that the *Pex13* knock-down induced the activation of the antioxidant response element (ARE) which upon Nrf2 binding leads to the expression of antioxidative enzymes and corresponding transcription factor genes (**Fig. 63**). In pro-oxidant conditions, Nrf2 binds to the antioxidant-responsive element (ARE) in the promoter region which activates the transcription of antioxidative genes, e.g. *Ho-1* and *Sod1*.

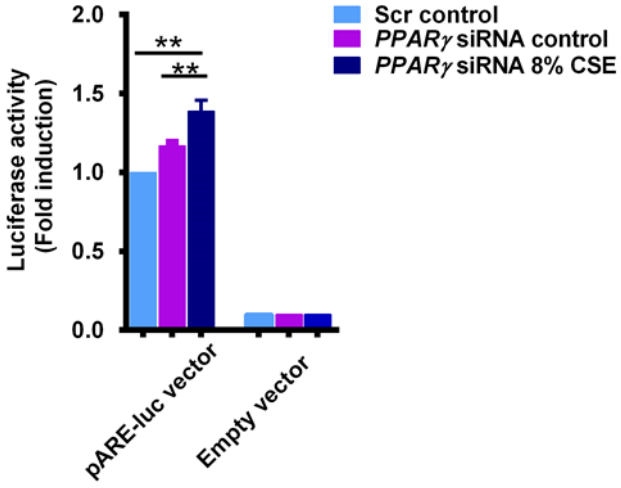

Fig. 63. Increased ARE response element activity in PPARγ knock-down cells. Luciferase reporter activity of ARE promoter element in cells transfected with either *Pparγ* -siRNA or scr-siRNA together with either pARE-luc or empty vector and thereafter followed by DMSO (0%CSE) or CSE treatment as measured by the luciferase assay. 72h post transfection cell lysates were collected and assayed for luciferase activity. The activity of firefly luciferase was measured in cell lysates and normalized to the activity of renilla luciferase. P values were calculated by the one way ANOVA. n=3, ** p≤0.01.

Our result on cell proliferation, could suggest that the knock-down of *Pparγ* is exerting a strong effect on the cells' ability to repair oxidative stress-induced damage caused by CSE, compromising cell proliferation as shown by the BrdU assay (**Fig. 64**), in which cell proliferation was reduced by 40% in comparison to the cells transfected with either scr-siRNA or *Pex13* siRNA.

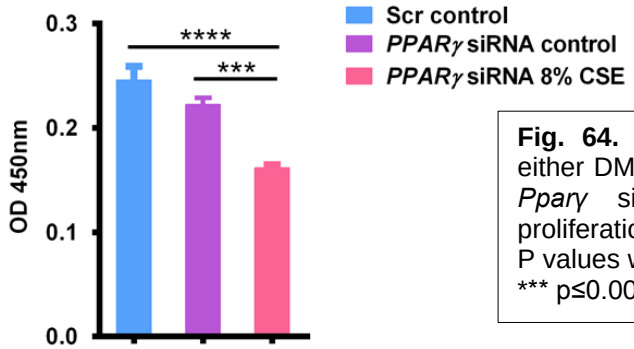

Fig. 64. Percentage of BrdU positive cells after either DMSO or CSE treatment following scr-siRNA or *Pparγ* siRNA transfection. The extent of cell proliferation was measured by absorbance at 450nm. P values were calculated by the one way ANOVA. n=3, *** p≤0.001, **** p≤0.0001.

4.4.4. PPARγ stimulation induces the elevation of peroxisomes

Since peroxisomal genes and proteins were down-regulated by the knock-down of *Pparγ*, the next step was to stimulate PPARγ in order to modulate the expression of peroxisomes in opposite direction and to check whether this would influence COPD markers. For this purpose, the treatment with rosiglitazone (RZG), a drug belonging to the class of thiazolidinediones was selected. RZG is a ligand for the nuclear receptor peroxisome proliferator-activated receptor gamma (PPARγ) which induces its activation. RZG-treatment was performed 24h before the CSE stimulation. The qRT-PCR (**Fig. 65A**) and Western blot (**Fig. 65B**) analyses revealed that the cells treated with RZG for 24h and then stimulated with 8% CSE showed a significant upregulation of the *Pex13* gene and PEX13 protein (**Fig. 65B**) in comparison to the DMSO treated and then CSE stimulated cells.

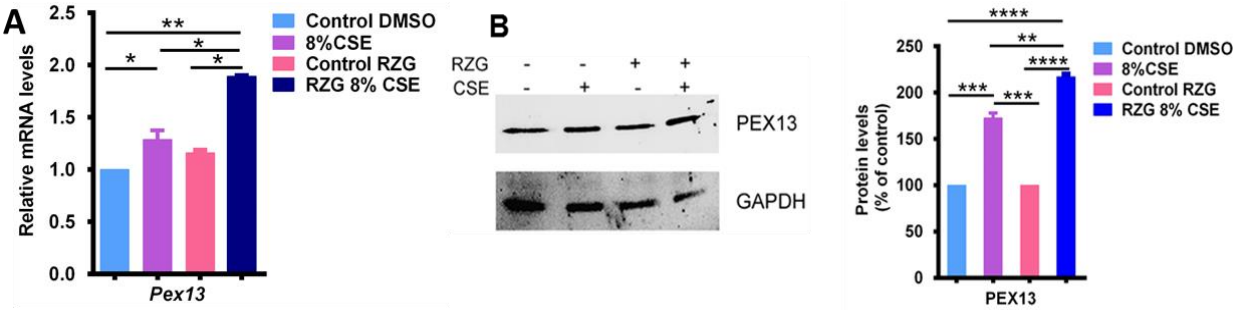

Fig. 65. **RZG treatment induced the expression and abundance of PEX13 in the CSE treated cells** as shown by qRT-PCR (A) and Western blot (B). Protein levels relative to GAPDH were quantified by densitometry with ImageJ. The C22 cells were treated with either DMSO or RZG for 24h and then stimulated with either 8%CSE or DMSO for 4h prior to protein and RNA collection. P values were calculated by the one way ANOVA. n=3, * p≤0.05, ** p≤0.01, *** p≤0.001, **** p≤0.0001.

Peroxisomal catalase as well exhibited a similar upregulation at the mRNA and protein levels (**Fig. 66A and B**) after RZG treatment and CSE stimulation as was observed with PEX13. Interestingly, RZG was only able to induce the higher upregulation of peroxisomes when the CSE treatment was applied whereas no clear difference was observed in peroxisomes in DMSO and RZG only treated groups. The cells treated

with DMSO as well as the cells stimulated with RZG showed no significant difference at the mRNA and protein levels for PEX13 and CAT.

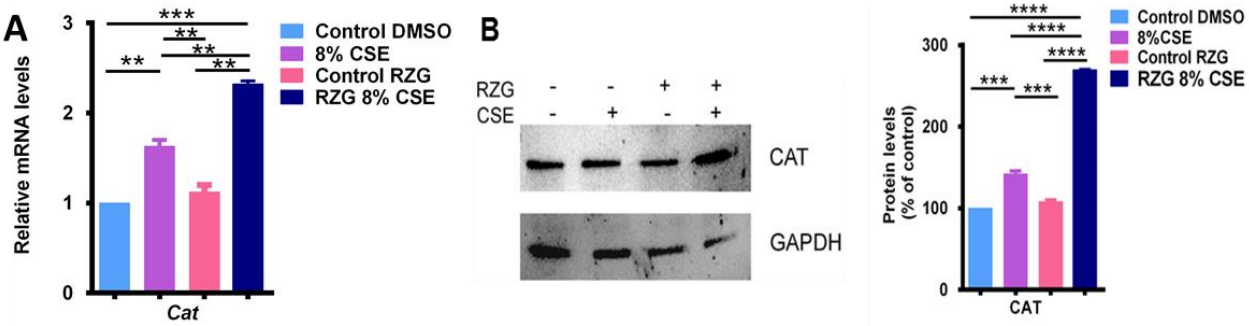

Fig. 66. RZG treatment induced the expression and abundance of antioxidative enzyme CAT in the CSE treated cells as shown by qRT-PCR (A) and Western blot (B). Protein levels relative to GAPDH were quantified by densitometry with ImageJ. The C22 cells were treated with either DMSO or RZG for 24h and then stimulated with either 8%CSE or DMSO for 4h prior to protein and RNA collection. P values were calculated by the one way ANOVA. n=3, ** p≤0.01, *** p≤0.001, **** p≤0.0001.

As was demonstrated by further experiments, RZG induced a significant upregulation of peroxisomal β-oxidation (**Fig. 67A**) and ether phospholipid synthesis enzyme (**Fig. 67B and C**) mRNAs and proteins when the CSE treatment was applied in comparison to the cells stimulated with CSE alone as shown by the qRT-PCR and Western blot analyses. Thereafter, it was interesting to check the Nrf2-mediated antioxidant response following CSE-treatment. Indeed, Nrf2 was significantly up-regulated at the mRNA and to a lesser extent at the protein level following the RZG treatment and CSE stimulation (**Fig. 68A and B**). This led to the drastic elevation of Nrf2-regulated genes encoding the antioxidative enzymes (HO-1 and SOD1) following RZG treatment and CSE stimulation at the mRNA (**Fig. 68C**) and protein levels (**Fig. 68D**). To summarize, the samples treated with RZG and then stimulated with CSE showed a significant upregulation of the peroxisomal compartment at the mRNA and protein levels in comparison to the samples stimulated with CSE alone. Similar results were observed for Nrf2 and its regulated genes *Ho-1* and *Sod1*. Thereafter, we checked the ARE activity by luciferase assays and found that the activity of the ARE-element-regulated promoter as well was significantly activated in the cells treated with CSE following the incubation with RZG (**Fig. 69**).

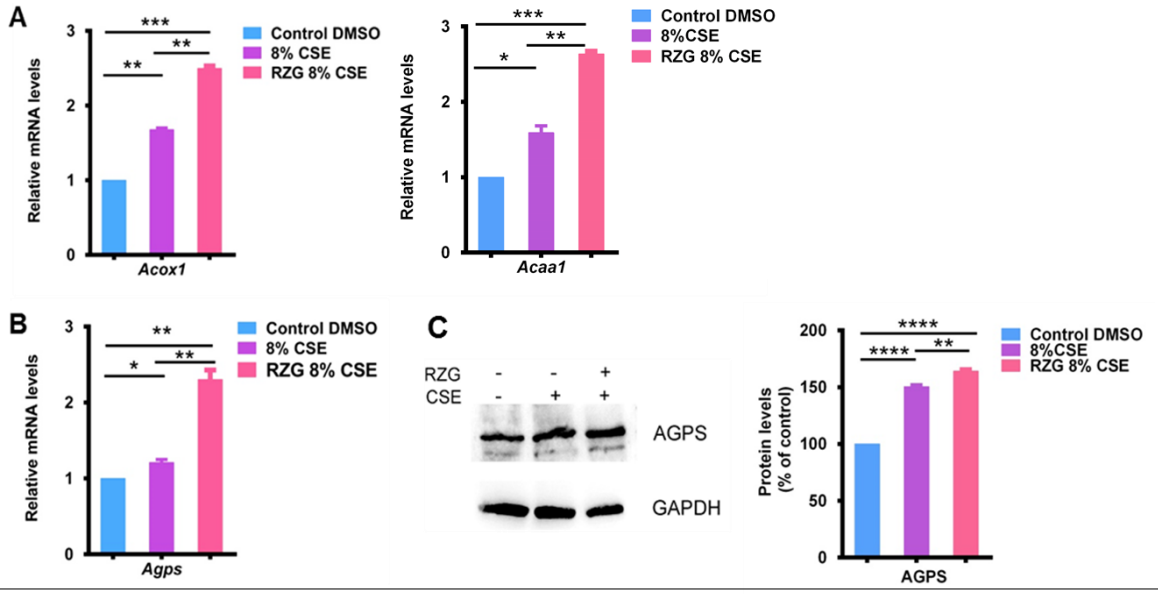

Fig 67. RZG stimulation induced the peroxisomal β-oxidation (A) and ether phospholipid synthesis enzymes (B and C) as shown by qRT-PCR and Western blot. Protein levels relative to GAPDH were quantified by densitometry with ImageJ. The C22 cells were treated with either DMSO or RZG for 24h and then stimulated with either 8%CSE or DMSO for 4h prior to protein and RNA collection. P values were calculated by the one way ANOVA. n=3, * p≤0.05, ** p≤0.01, *** p≤0.001, **** p≤0.0001.

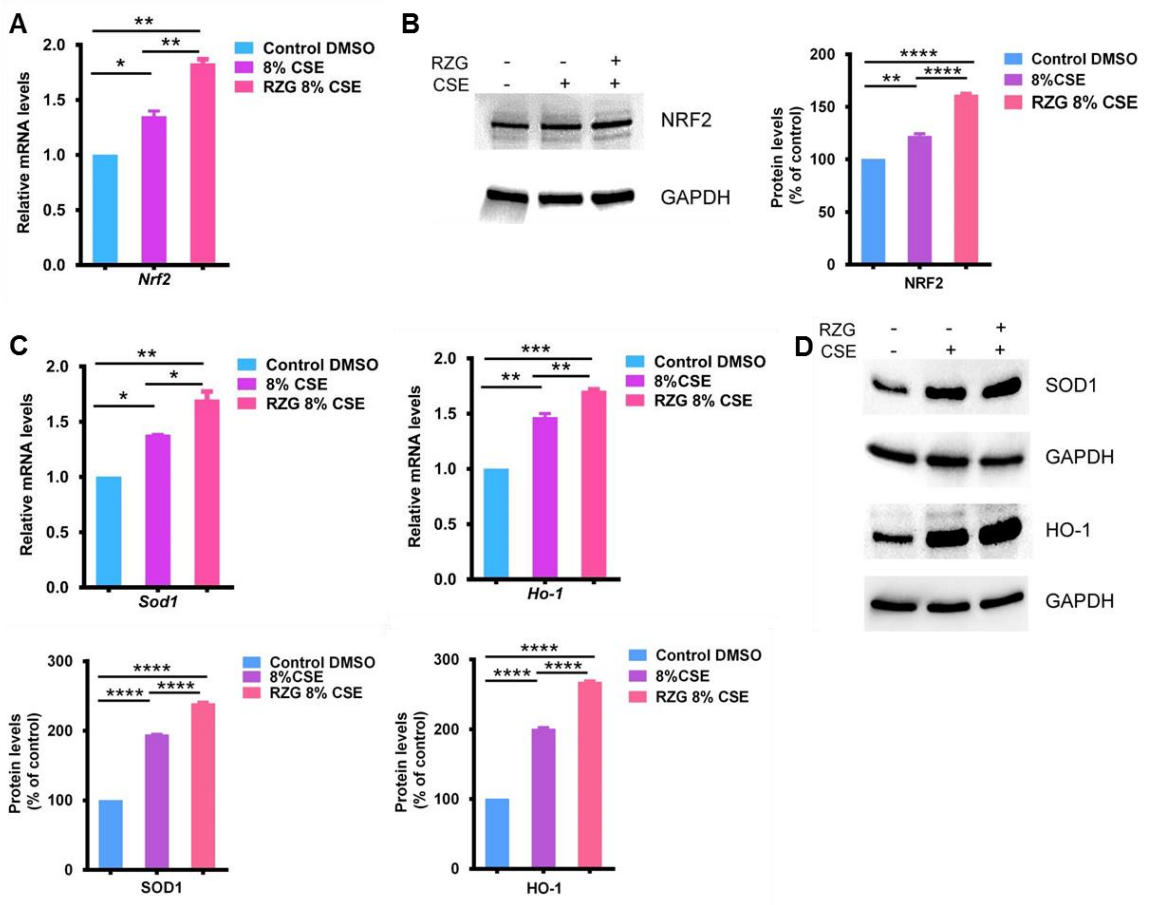

Fig. 68. RZG activation induced the expression (A) and abundance of the Nrf2 (B) and Nrf2 regulated antioxidant enzymes (C and D) as shown by qRT-PCR and Western blot. Protein levels relative to GAPDH were quantified by densitometry with ImageJ. The C22 cells were treated with either DMSO or RZG for 24h and then stimulated with either 8%CSE or DMSO for 4h prior to protein and RNA collection. P values were calculated by the one way ANOVA. n=3, * p≤0.05, ** p≤0.01, *** p≤0.001, **** p≤0.0001.

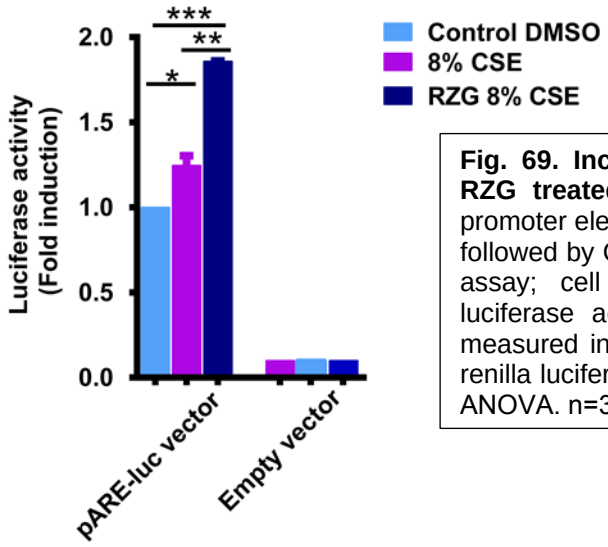

Fig. 69. Increased ARE response element activity in RZG treated cells. Luciferase reporter activity of ARE promoter element in cells treated with either RZG or DMSO followed by CSE stimulation as measured by the luciferase assay; cell lysates were collected and assayed for luciferase activity. The activity of firefly luciferase was measured in cell lysates and normalized to the activity of renilla luciferase. P values were calculated by the one way ANOVA. n=3, * p≤0.05, ** p≤0.01, *** p≤0.001.

4.4.4.1. RZG treatment reduced the CSE induced pro-inflammatory and pro-oxidant reaction in the cells

Il-6 and *Tnfα* were significantly downregulated by RZG treatment in the CSE stimulated cells (**Fig. 70A**). Similarly, RZG reduced the abundance of pro-oxidant COX-2 in the cells that were stimulated with CSE (**Fig. 70B**).

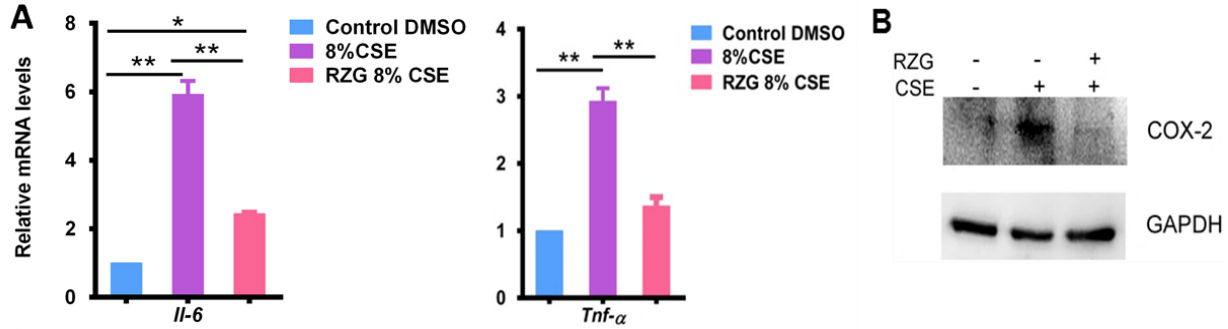

Fig. 70. RZG treatment reduced the expression of pro-inflammatory mediators and prooxidant COX-2 at the mRNA (A) and protein (B) level after incubation with RZG for 24h, cells were stimulated with CSE and the RNA and protein was collected thereafter. P values were calculated by the one way ANOVA. n=3, ** p≤0.01, *** p≤0.001.

For the confirmation of the beneficial effects of RZG, ELISAs were performed on the supernatants of the 3 groups for the detection of proinflammatory cytokines. As shown by ELISA, pre-treatment of cells with RZG attenuated the secretion of proinflammatory cytokines into the media when CSE stimulation was applied (**Fig. 71**).

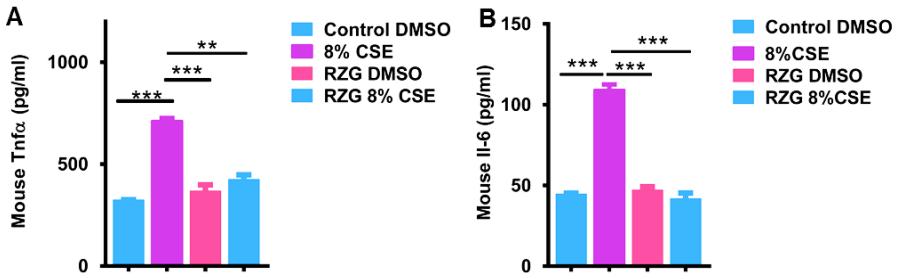

Fig. 71. RZG attenuated the release of pro-inflammatory cytokines (IL-6 and TNF-α) in the medium of CSE treated cells as shown by ELISA assays. C22 cells were incubated with RZG for 24h prior to a 4hr treatment with DMSO or 8%CSE, the supernatants were collected thereafter. The released mediators were measured by ELISA. P values were calculated by the one way ANOVA. n=3, ** p≤0.01, *** p≤0.001.

4.4.4.2. RZG treatment attenuates the oxidative stress in the cells stimulated with cigarette smoke extract

As was already shown above, CSE induced a drastic increase in oxidative stress as demonstrated by the elevation in DHE staining (**Fig. 72B**). In contrast, when RZG treatment was applied, this oxidative stress was reduced (**Fig. 72D**) to control level (**Fig. 72A**).

To summarize, RZG was able to attenuate the release of CSE induced pro-inflammatory and pro-oxidant mediators and it was as well capable to reduce the oxidative stress induced by CSE. We assume that the beneficial effect of RZG in protecting the cells against the CSE induced stress was due to its ability to upregulate the peroxisomal β-oxidation, ether phospholipid and antioxidative enzymes. In addition to this, peroxisome proliferator-activated receptor gamma upregulated Nrf2 and its antioxidative response element ARE which is a major defensive mechanism against oxidative stress. The upregulation of peroxisomal and antioxidative enzymes was much higher than the increase that was induced by the CSE treatment. This could suggest that this high upregulation was to protect the cells against inflammation and oxidative stress. In other words, CSE-induced upregulation of peroxisomes and antioxidative enzymes wasn't enough to battle or counteract the stress because the pro-oxidative effect was much stronger. However, the RZG induction of peroxisomes and antioxidants to the level that was higher than that caused by CSE was able to counteract the drastic CSE effects. To sum up, RZG by its upregulation of peroxisomes and other antioxidants induced the protective response.

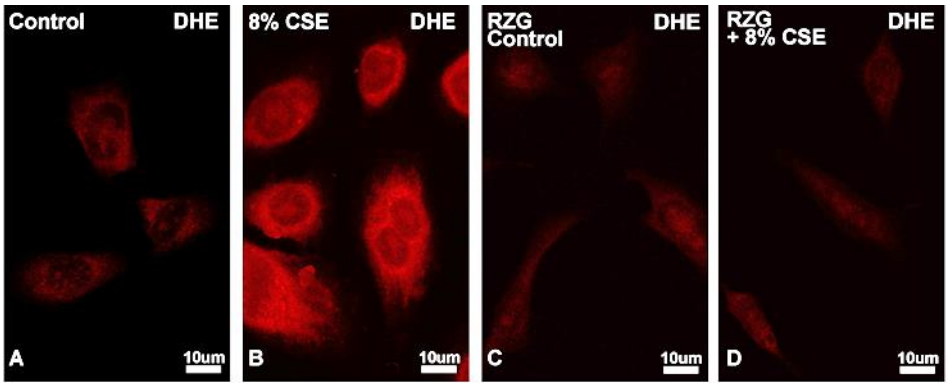

Fig. 72. Measurements of ROS by dihydroethidium stain following RZG treatment. The cells were incubated with either RZG (C&D) or DMSO (A&B) for 24h. Following the incubation, the cells were treated with DMSO (A&C) or CSE (B&D) and then stained with DHE for 30 min. The bars represent 10µm.

4.4.5. PPARγ overexpression blocks the CSE-induced oxidative stress response

We were wondering whether the overexpression of PPARγ would lead to comparable results as was observed with the PPARγ agonist RZG. For this purpose, we used the PCMV Sport PPARγ plasmid in order to overexpress PPARγ in C22 cells; PCMV-Sport6-GFP3b was used as a control vector. C22 cells were transfected either with the PPARγ overexpression plasmid or with the control plasmid for 68h prior to CSE or DMSO treatment. The first step was to examine mRNA expression levels of PPARγ. The qRT-PCR results showed a tremendous several hundred fold increase in *Pparγ* transcription factor mRNA expression (**Fig. 73A**). Western blot analysis as well revealed a much higher abundance of the PPARγ protein following the plasmid transfection in comparison to the control group (**Fig. 73B**).

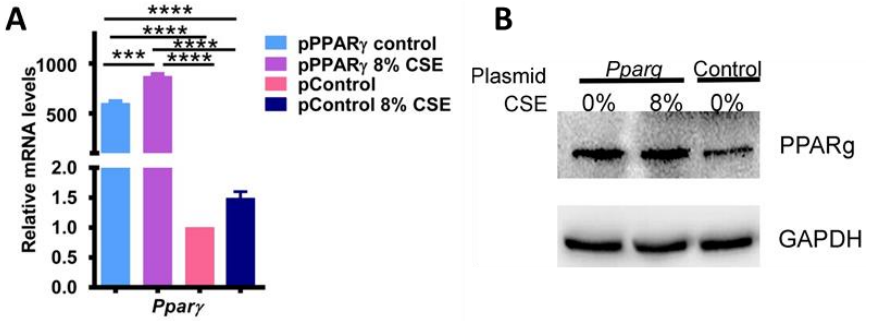

Fig. 73. PPARγ overexpression promotes PPARγ activation. The cells were either transfected with pPPARγ (PCMV Sport PPARγ) or with the pControl (PCMV-GFP3b) for 68h. Thereafter, DMSO or CSE stimulation was applied for 4h and the RNA and protein was collected afterwards and the results were analysed by qRT-PCR and Western blotting. P values were calculated by the one way ANOVA. n=3, *** p≤0.001, **** p≤0.0001.

The second step was to check the effect of PPARγ overexpression on the peroxisomal genes. The cells transfected with pPPARγ (control) showed a higher expression of

Pex13 mRNA than the cells transfected with the control plasmid (pControl) and then treated with CSE suggesting that possibly peroxisomes are highly proliferating in the pPPARγ overexpressing cells. The PEX13 protein was only slightly higher in the PPARγ overexpression group in comparison to the control group. To our surprise, we observed that the additional CSE-treatment of the PPARγ overexpressing group led to a down-regulation of the peroxisomal biogenesis gene *Pex13* (**Fig. 74A**) and its corresponding protein (**Fig. 74B**) in comparison to the cells transfected with pPPARγ and pControl.

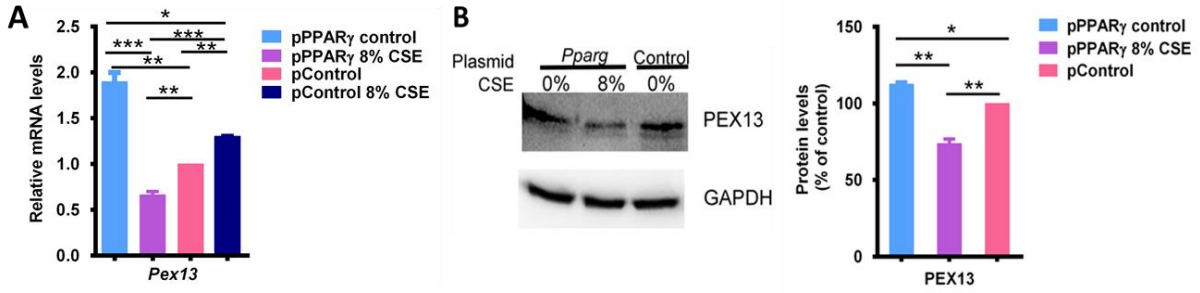

Fig. 74. PPARγ overexpression induces down-regulation of the peroxisomal membrane protein PEX13 in the cells treated with CSE. The cells were either transfected with pPPARγ (PCMV Sport PPARγ) or with the pControl (PCMV-GFP3b) for 68h. Thereafter, DMSO or CSE stimulation was applied for 4h and the RNA and protein was collected afterwards and the results were analysed by qRT-PCR (A) and Western blot (B). Protein levels relative to GAPDH were quantified by densitometry with ImageJ. P values were calculated by the one way ANOVA. n=3, * p≤0.05, ** p≤0.01, *** p≤0.001.

The down-regulation of the PEX13 protein could secondarily affect the peroxisomal matrix protein import (as was observed above under PEX13 knock-down conditions). Our hypothesis was confirmed by real time PCR and Western blot analyses where the expression and protein abundance of the peroxisomal antioxidative enzyme catalase (**Fig. 75A**) as well as the expression of peroxisomal β-oxidation (**Fig. 75B**) and ether phospholipid synthesis enzymes (**Fig. 75C**) was significantly down-regulated in pPPARγ overexpressing and then CSE treated cells in comparison to DMSO treated cells transfected with either pPPARγ or pControl plasmids.

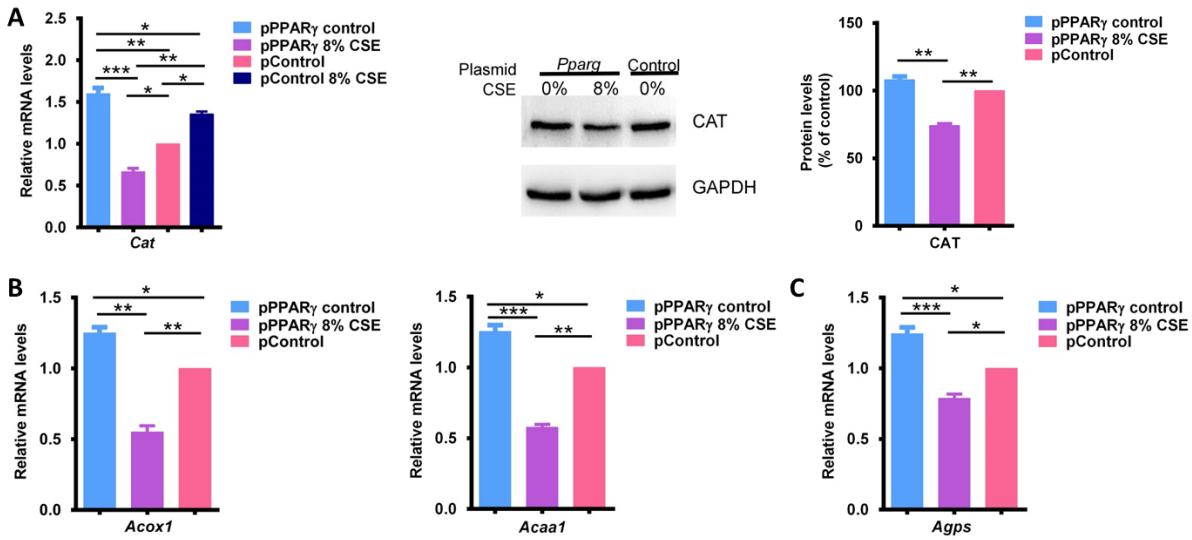

Fig. 75. PPARγ overexpression induces the down-regulation of peroxisomal antioxidative (A), β-oxidation (B) and ether phospholipid synthesis enzymes (C) in the cells treated with CSE. The cells were either transfected with pPPARγ (PCMV Sport PPARγ) or with the pControl (PCMV-GFP3b) for 68h. Thereafter, DMSO or CSE stimulation was applied for 4h and the RNA and protein was collected afterwards and the results were analysed by qRT-PCR and Western blotting. Protein levels relative to GAPDH were quantified by densitometry with ImageJ. P values were calculated by the one way ANOVA. n=3, *p≤0.05, ** p≤0.01, *** p≤0.001.

Moreover, we analysed Nrf2, some Nrf2-regulated genes and pro-inflammatory cytokines. Interestingly, overexpression of PPARγ followed by CSE treatment as shown by qRT-PCR and Western blot analyses downregulated Nrf2 at the mRNA and protein level (**Fig. 76A**) as well as the expression (**Fig. 76B**) and abundance (**Fig. 76C**) of its regulated enzymes in comparison to the control samples. This implies that indeed there is no oxidative stress even in the cells that were treated with CSE after the PPARγ has been overexpressed. If the results obtained with the *Pparγ* knock-down followed by CSE-treatment (**Fig. 57-61**) are compared to the ones with PPARγ overexpression and CSE-treatment (**Fig. 73-75**), a completely opposite pattern would be observed. Whereas *Pparγ* knock-down induced a significant upregulation of the peroxisomal compartment, Nrf2 and its regulated genes accompanied by an oxidative stress response and ROS production, overexpression of PPARγ down-regulated these genes, proteins and the oxidative stress.

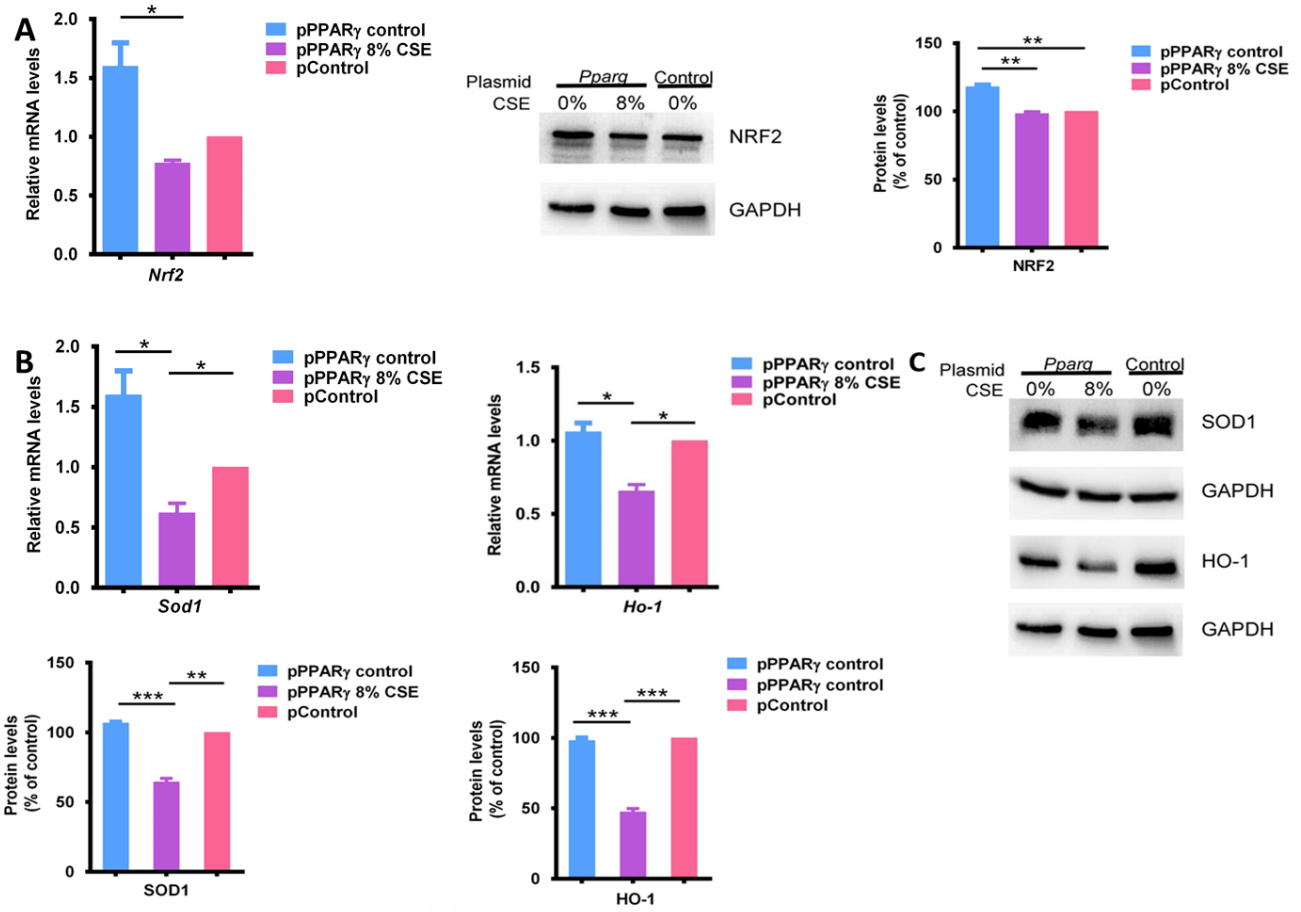

Fig. 76. PPARγ overexpression provoked a decrease of Nrf2 (A) and of its regulated antioxidant enzymes (B&C) in the cells treated with CSE. The cells were either transfected with pPPARγ (PCMV Sport PPARγ) or with the pControl (PCMV-GFP3b) for 68h. Thereafter, DMSO or CSE stimulation was applied for 4h and the RNA and protein was collected afterwards and the results were analysed by qRT-PCR and Western blot analyses. Protein levels relative to GAPDH were quantified by densitometry with ImageJ. P values were calculated by the one way ANOVA. n=3, * p≤0.05, ** p≤0.01, *** p≤0.001.

Moreover, qRT-PCR (**Fig. 77A**) and ELISA (**Fig. 77B**) results revealed that PPARγ overexpression attenuated the expression and release of pro-inflammatory cytokines in the CSE treated cells. These results again are a confirmation that there is no oxidative stress and inflammation in cells with overexpressed PPARγ even after the treatment with cigarette smoke extract. To summarize, no antioxidative stress response was observed in PPARγ overexpression groups and no stimulation of the proinflammatory cytokine release was detected. The PPARγ rather repressed the antioxidative enzyme genes to lower levels in CSE-treatment conditions (corresponding to control levels without CSE-treatment).

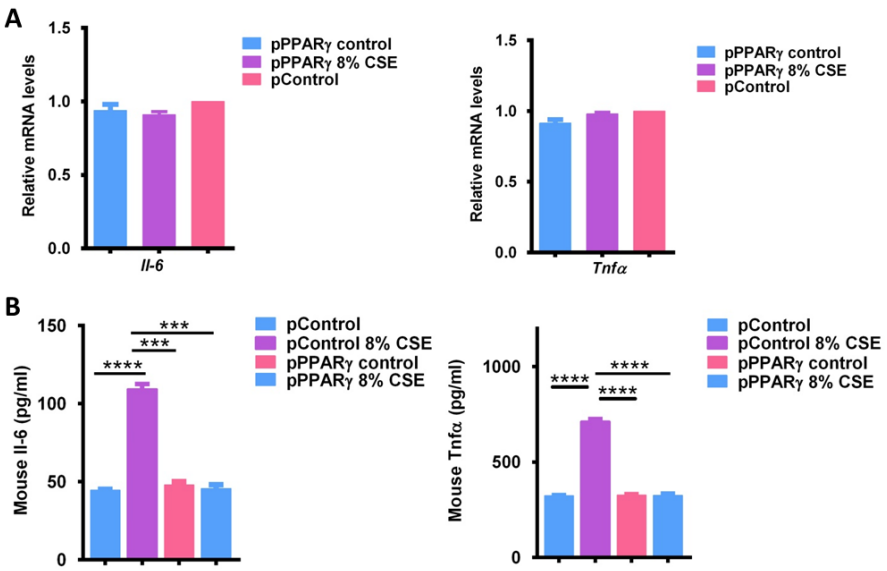

Fig. 77. PPARγ expression attenuated the mRNA expression (A) and the release (B) of pro-inflammatory cytokines in the media of CSE treated cells as shown by qRT-PCR and ELISA assay. The cells were either transfected with pPPARγ (PCMV Sport PPARγ) or with the pControl (PCMV-GFP3b) for 68h. Thereafter, DMSO or CSE stimulation was applied for 4h and the RNA supernatant was collected afterwards and the results were analysed by qRT-PCR and ELISA. P values were calculated by the one way ANOVA. n=3, *** p≤0.001, **** p≤0.0001.

PPARγ overexpression not only up-regulated peroxisomal genes when no CSE was applied, but also induced cells proliferation as was shown by the BrdU assay (**Fig. 78**).

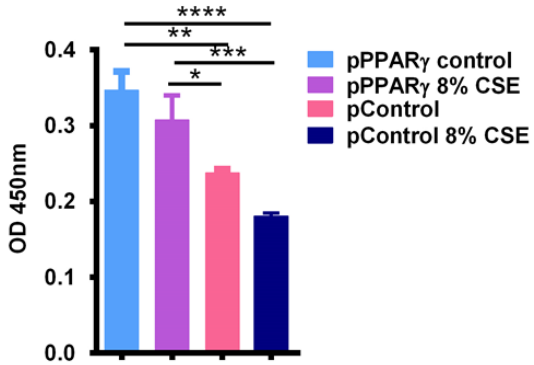

Fig. 78. Percentage of BrdU positive cells after pPPARγ overexpression. The cells were after either treated with DMSO or CSE.The extent of cell proliferation was measured by absorbance at 450nm. P values were calculated by the one way ANOVA. n=3, *p≤0.05, ** p≤0.01, *** p≤0.001, **** p≤0.0001.

PPARγ overexpression upon transfection into the cells exerts a preventive effect against the harmful CSE-induced proinflammatory cytokine release in the C22 cells under basal conditions, that's probably why the cells were not experiencing oxidative stress upon CSE treatment. On the contrary, RZG exerts a protective rather than preventive way of action. In another words, RZG protects the cells from oxidative stress by increasing antioxidative defence enzymes when the CSE stimulation is applied whereas specific PPARγ overexpression could have a preventive effect by inhibition or prevention of transcription activation of pro-inflammatory mediators.

5. Discussion

The prevalence of chronic obstructive pulmonary disease (COPD) is increasing worldwide. However, despite the increased prevalence and mortality, there is currently no cure available for this disease. It is well known that the most commonly encountered risk factor for COPD is cigarette smoking which accounts for 80%-90% of COPD cases [21]. Peroxisomes are organelles that are present in high numbers in secretory cells of bronchioli (club cells) as well as in type II cells of the alveolar region. Moreover, these organelles are located in the apical region in ciliated cells bordering lung airways. Therefore, peroxisomes could be easily affected in COPD by components of cigarette smoke. However, until the beginning of the experimental work of this thesis, no information was available on these cell organelles in the lung of COPD patients. It has been demonstrated, in this thesis, that cigarette smoke induces strong alterations of the peroxisomal compartment leading to the organelle proliferation and its enzyme upregulation in airway epithelial cells of COPD patients as well as in a COPD mouse model. Moreover, in order to analyse the role of peroxisomes in COPD pathogenesis, siRNA silencing of the mouse peroxisomal biogenesis protein PEX13 was applied provoking stronger oxidative stress in CSE treated samples. In contrast, the treatment of *in vitro* model with a PPARγ agonist induced the whole peroxisomal compartment and in consequence reduced oxidative stress, ROS and inflammatory mediators in the CSE-treated samples. Similarly, PPARγ overexpression attenuated oxidative stress and pro-inflammatory cytokines in the CSE treated samples. The results showed that both methods exert different mechanisms of action.

The results of this thesis suggest that peroxisomes could be key players in amelioration and protection against COPD progression. The discussion will concentrate on peroxisome abundance and enzyme composition as well as gene regulation in control samples in comparison to human and mouse COPD samples and *in vitro* models. Moreover, the pathological alterations exerted on the *in vitro* COPD models induced by *Pex13* and *Pparγ* gene knock-downs leading to peroxisome deficiency and all consequences thereafter will be discussed. Finally, the methods for peroxisomal activation in order to possibly reduce the disease progression and oxidative stress in COPD will be discussed.

5.1. The role of peroxisomes in scavenging ROS and attenuating oxidative stress and their possible effects in ameliorating the pathophysiology of COPD

The exposure of lungs to high oxygen concentrations makes them very susceptible to injury mediated by oxidative stress [139]. Non-enzymatic antioxidants, such as glutathione, vitamin C and β-carotene as well as ether lipids (plasmalogens) and polyunsaturated fatty acids (PUFA) in the plasma membranes of airway epithelial cells or in the surfactant film, covering the alveolar region, are the first line of defence against the oxidants [136]. Interestingly, the important steps in the synthesis of the antioxidant lipids occur in peroxisomes. The second line of defence against the oxidants consists of antioxidative enzymes such as superoxide dismutases, catalase, glutathione peroxidases and peroxiredoxins. These antioxidative enyzmes are degrading various types of ROS and are localized in distinct intracellular sub-compartments as well as in different pulmonary cell types [137]. If the balance between the antioxidant defensive mechanism and ROS production is disturbed, pathological alterations are induced leading to lung injury. It is well known that oxidative stress is central in the pathogenesis of a variety of respiratory diseases like COPD [49], cystic fibrosis [198], asthma [199] and idiopathic pulmonary fibrosis [200]. Moreover, ROS, which are released in the tunica mucosa, lead to oxidative stress in epithelial cells [199]. It has been shown that the bronchiolar epithelium and AECII in the alveolar region of human and murine lungs are rich in peroxisomes [137]. Therefore, peroxisomes might protect the pulmonary airway epithelium by their high content in different antioxidative enzymes, their role in the synthesis of PUFA and plasmalogens and their ability to degrade bioactive and toxic lipid derivatives through their β-oxidation systems [136]. The results of this thesis demonstrate that knocking down of the peroxisomal biogenesis gene *Pex13* generated a drastic increase in oxidative stress, ROS production and the release of inflammatory mediators in C22 cells. In this respect, peroxisomes could scavenge ROS induced by the CSE, attenuate oxidative stress and provide protection for the lung epithelium thereby possibly reducing the pathophysiology of COPD.

5.2. The peroxisomal compartment and its corresponding genes are activated in COPD patients with high MUC5 expression

As mentioned above, oxidative stress that arises from increased concentrations of reactive oxygen and nitrogen species (ROS/RNS) and from a reduction in their detoxification mechanism leads to the initiation and progression of chronic

inflammatory diseases such as COPD [23]. Numerous studies indicate that peroxisomes can respond to oxidative stress and ROS in order to protect the cells against oxidative damage [201]. Thus, in this thesis, it was first decided to analyse whether there would be any alterations in the peroxisomal compartment in COPD patients in comparison to the control samples. The selected lung tissue samples from patients were classified according to the Global Initiative for Chronic Obstructive Lung Disease (GOLD) as COPD stage IV [202]. All samples were selected according to their morphological characteristics and MUC5 abundance. Only tissues with high MUC5 abundance and comparable inflammatory reactions were selected. Whole lung homogenates and total RNA was analysed for peroxisomal gene expression and abundance.

Many of the peroxisomal genes are regulated by nuclear receptors of the PPAR family, the abundance and distribution of which are cell-type dependent. The activation of the peroxisome proliferator-activated receptor gamma (PPARγ), which is a ligand-activated nuclear transcription factor expressed in the lungs, exhibits antioxidative and anti-inflammatory effects [45,168,169]. Divers results are available from the literature concerning PPARγ expression in COPD. Some studies have shown that the activity and expression of PPARγ in the bronchial epithelial cells from COPD patients and from the CSE-exposed cell model was significantly down-regulated [203]. Several other studies have shown that the level of PPARγ was reduced in the lungs of patients with moderate COPD stages, whereas it was up-regulated in patients with mild COPD [176]. Another study has revealed that the alveolar macrophages from COPD patients and smokers showed a high PPARγ expression in comparison to never-smokers [204,205]. It was demonstrated, in human peripheral blood mononuclear cells, that PPARγ agonists inhibited the production of monocyte inflammatory cytokines such a IL-1β, IL-6 and tumour necrosis factor (TNF)-α [167] as well as suppressed COX-2 expression [206], reduced cigarette-smoke induced mucin production [170] and increased Nrf2 transactivation [207-209]. Our data revealed a strong upregulation in the expression and abundance of PPARγ in the samples of the patients with COPD in comparison to the non-COPD samples.

An elevation of the peroxisomal compartment in conditions of stress in the mammalian [210,211], yeast [212] and plant systems [213] has been demonstrated in several studies suggesting that this may be a common cellular mechanism for dealing with various stresses. Hence, cellular oxidative stress and peroxisomal metabolism are

intimately linked. The observation that stress increases peroxisomal abundance and expression brings the important question up whether this upregulation provides a protective effect against oxidative stress.

There is plenty of evidence that disturbance in peroxisomal redox balance puts the cells under oxidative stress [214]. Moreover, mice deficient in peroxisomes exhibit neurodegeneration [215] and show a decline in their motor and cognitive abilities leading to an early death [216]. In contrast, it was found that PPARγ agonists have the ability to increase catalase activity and expression in rat astrocytes [217]. Moreover, the results of this thesis revealed a significant increase in the expression and abundance of the major peroxisomal antioxidative enzyme catalase (CAT) in the lung. In this respect it is of interest that the *catalase* gene is regulated via Nrf2.

The results of this thesis demonstrated that Nrf2, a transcription factor which through its binding to the antioxidant response element (ARE) induces the expression of genes of antioxidative enzymes, is involved in the activation of the antioxidant response and in the protection against oxidative stress [218,219]. In unstressed conditions, Nrf2 transactivation is supressed by Keap1, whereas under oxidative stress conditions, Keap1 senses oxidative or electrophilic stress thus liberating Nrf2 which translocates into the nucleus and binds to ARE in order to induce the expression of cytoprotective genes [220,221]. Upon binding to ARE, Nrf2 induces the downstream target genes, such as heme oxygenase-1 (*Ho-1*), superoxide dismutase 1 (*Sod1*), catalase (*Cat*) and peroxiredoxin 1 (*Prxd1*) coding for a network of enzymatic antioxidative proteins protecting the cells against the oxidative stress as was shown in various *in vivo* [220,222,223] and *in vitro* [224-226] studies. Therefore, catalase which is considered to be a rather peroxisome-specific antioxidant enzyme is as well regulated by Nrf2 [223]. The results of this thesis demonstrated that COPD patients exhibit an increase in the gene expression and protein abundance of Nrf2 and its downstream target gene and protein catalase (CAT), suggesting the induction of the antioxidant response by high oxidative stress, as was demonstrated by the DHE-staining in this thesis.

Interestingly, cells that are deficient in the biosynthesis of plasmalogens, are more sensitive to ROS damage in comparison to control cells [227]. The antioxidative effect of plasmalogens has been discussed in various *in vitro* and *in vivo* studies [228-230]. The peroxisomal matrix enzymes glycerone-phosphate O-acyltransferase (GNPAT) and alkylglycerone phosphate synthase (AGPS) are the most crucial enzymes for the

plasmalogen biosynthesis. The results of this thesis show that the expression and abundance of GNPAT and AGPS were as well up-regulated in the patients with COPD.

COPD is not only characterized by high oxidative stress, but also by the inflammation that affects airways, pulmonary vessels and lung parenchyma. As shown in this thesis, this inflammation could be induced by the release of proinflammatory mediators like interleukin-8 (IL-8), IL-6 and tumor necrosis factor alpha (TNF-a) by the injured lung epithelial cells or from the activated inflammatory cells as shown in the literature [78,189]. Several studies found that levels of IL-6 are increased in plasma, exhaled breath and sputum of COPD patients in comparison to controls [231-234]. Similarly, TNF-α levels are increased in the induced sputum of patients with COPD and this cytokine was found as well to be implicated in cigarette smoke-induced emphysema in mouse models [235-237]. The expression of Il-6, Il-8 and Tnf-α, systemic inflammatory markers associated with COPD were analysed by qRT-PCR from the total RNA of COPD patients in comparison to the non-COPD lungs. Indeed the results of this thesis showed a significant increase in the expression levels of *Il-8* and *Tnfα* mRNA from the COPD lungs in comparison to the control samples as well as from CSE treated lung epithelial cells. It was suggested that these increased levels of cytokines provide an evidence of ongoing inflammatory processes in COPD [191].

Despite the increase of peroxisomes, as shown in the results of this thesis, oxidative stress and inflammatory cytokines were still highly elevated in the COPD patients suggesting that the net flux of ROS/RNS production exceeded the capacity of antioxidative enzymes of these organelles to eliminate harmful oxidants. Therefore, the increase of peroxisomes in COPD patients is not sufficient at this point to detoxify all potentially injurious oxidants.

5.3. A similar pattern of peroxisomal induction was detected in a mouse COPD model

Further, we wanted to check whether the pattern of peroxisomal expression in a COPD mouse model will be in accordance to the results obtained in the human samples. Therefore, paraffin-blocks from WT mice (obtained from Prof. Weissmanns's group, JLU Giessen) exposed to cigarette smoke for up to 3 months were analysed [178]. The samples from COPD mice indeed showed a similar increase in peroxisomal biogenesis proteins, antioxidative, β-oxidation, and ether phospholipid synthesis

enzymes. Therefore, despite the differences in lung maturation, development and anatomy among the species, the pattern of peroxisomal expression and abundance is similar in both models suggesting that this upregulation could be a characteristic feature of peroxisomes in COPD and that peroxisomes could play an important role in protecting the lung against harmful CS effects.

5.4. Generation of an *in vitro* cigarette smoke-extract COPD model

In addition to analysis of the tissue samples, the goal was to establish an *in vitro* model and to determine the effects of cigarette smoke extract (CSE) on peroxisomal alterations in cultured cells. CSE cell culture models could provide vital information on the molecular mechanisms taking part in the functional progression of the disease. Therefore, to get insights into the pathogenic mechanisms of the disease and to maintain as many physiological parameters *in vitro* as possible, we selected primary human bronchial epithelial cells (HBE). In order to determine a proper cigarette smoke extract (CSE) concentration, several concentrations were tested and the highest concentration which showed no toxicity for cell viability was used for the experimental treatment. The next step was to analyse the peroxisomal expression and abundance in order to find out whether this established *in vitro* model mimics the characteristics of the *in vivo* models. The increase in peroxisomal enzymes with the CSE treatment was a confirmation that the generation of the *in vitro* COPD model was successfully established and that it reflects the in situ situation in the lung of patients or in the COPD mouse model.

For better understanding of the role of peroxisomes in the pathogenesis of COPD, the first step was to disrupt the peroxisomal biogenesis by knocking down PEX13 which is a peroxisomal membrane protein that acts as a docking factor for the import of peroxisomal matrix proteins [190,195,238]. However, to our big disappointment, primary HBE cells didn't survive the siRNA transfection even when the smallest possible siRNA concentration was used. Therefore, for the further transfection experiments, the C22 mouse bronchial club cell-line was chosen. C22 cells are transformed murine club cells which secrete cell-type-specific proteins and possess morphological characteristics similar to club cells [239,240]. Moreover, our group showed that peroxisomes are abundant in C22 cells and that their corresponding gene expression and enzyme abundance are comparable to the one found in club cells in the mouse lung [241].

The CSE-model had to be adjusted for the second time, for C22 cells, in order to establish a good COPD model for the analysis of marker genes following the CSE treatment. The knock-down of *Pex13* in these cells was successful this time. The *Pex13* gene deletion was verified by a variety of methods in this thesis, such as qRT-PCR whereas PEX13 protein deletion was confirmed by IF staining and Western blot analysis. Real-time PCR analysis showed a strong down-regulation in the *Pex13* gene expression in the samples transfected with *Pex13* siRNA in comparison to the scr-siRNA samples. In addition to this, Western blot analysis showed a 90% decrease in the PEX13 protein abundance in the knock-down samples in comparison to the samples transfected with scr-siRNA. Similarly, immunofluorescence staining revealed a strong 90% downregulation of the PEX13 protein in the *Pex13* knock-down samples. In addition to this, the peroxisomal deficiency in the *Pex13* knock-down samples was confirmed, in immunofluorescence preparations, by the mistargeting of CAT into the cytoplasm due to a defect in the import machinery of CAT into peroxisomes upon *Pex13* deletion [242,243]. The cytoplasmic localization of peroxisomal matrix enzymes is a well-known phenomenon in cells with peroxisome deficiency [193].

Pex13 gene deletion leads to peroxisomal deficiency. The results of this thesis showed that the expression of genes encoding peroxisomal matrix enzymes (*Cat, Agps, Acox1* and *Acaa1*) and the abundance of the corresponding proteins (CAT and AGPS) were significantly down-regulated in *Pex13* siRNA transfected samples in comparison to the scr-siRNA transfected samples. Since PEX13 is involved in the import of peroxisomal matrix proteins with both PTS1 and PTS2 targeting signals, its deletion leads to a complete disruption of the peroxisomal matrix protein import leading to the complete loss of metabolic functions of these organelles [244]. Due to the mistargeting into the cytoplasm, most peroxisomal matrix proteins are degraded (most probably via the proteasome). However, it is not clear, how the down-regulation of mRNAs for peroxisomal proteins occurs. This has to be proven experimentally in future studies. Possibly, peroxisomal genes are co-ordinately down-regulated under conditions of peroxisomal deficiency in club cells via miRNAs or other molecular mechanisms. Moreover, the C22 cells with compromised peroxisomal biogenesis were more sensitive to the CSE treatment as was shown by BrdU assay.

Furthermore, silencing of *Pex13* followed by CSE treatment drastically increased ROS as was visible in fluorescence pictures of DHE-stained cells suggesting that the

increase was exerted by the *Pex13* knockdown. It is known that an antioxidative response is mediated via redox-sensitive transcription factors (e.g. Nrf2 or NfκB), which mediate the upregulation of transcription of protective genes, like *Pparγ*, *Ho-1* and *Sod1*. We found that *Pex13* deletion led to the upregulation of both transcription factors PPARγ and Nrf2 as well as it induced the transcription of Nrf2-regulated genes and its corresponding proteins HO-1 and SOD1 [245,246]. This mechanism was especially prominent in *Pex13* deleted and then CSE treated samples. Moreover, as was shown by ARE/luciferase assay, the ARE-driven reporter gene was highly activated when CSE stimulation was applied after *Pex13* knockdown revealing a strong oxidative stress in the knock-down samples, suggesting that peroxisomes are necessary to guarantee the cells' redox homeostasis.

In addition to this, cigarette smoke triggered the release of cytokines, such as TNF-α and IL-6 from C22 cells with *Pex13* knock-down. Our results demonstrated that *Pex13* knock-down indeed led to a drastic increase in pro-inflammatory cytokines as detected by qRT-PCR, Western blot and ELISA. Interestingly, this elevation was 2-3 folds higher in the *Pex13* siRNA transfected cells treated with CSE in comparison to scr-siRNA, scr-siRNA transfected cells treated with CSE and only *Pex13* siRNA transfected cells. Therefore, deletion of *Pex13* together with CSE stimulation triggers much stronger release of pro-inflammatory mediators like IL-6, TNF-α and COX-2 in comparison to scr-siRNA transfected and thereafter CSE treated cells suggesting that this upregulation is due to the *Pex13* deletion. These cytokines and pro-inflammatory mediators might be possibly activated via the Nf-κB pathway due to the oxidative stress in C22 cells. It is known that smoke derived oxidants can activate various intracellular signalling mechanisms, including the Nf-κB pathway. Nf-κB activation leads to its translocation into the nucleus subsequently inducing the production of chemokines, cytokines and adhesion molecules [247,248]. It was shown that neutrophils of COPD patients exhibit increasing Nf-κB signalling after cigarette smoke exposure [249]. Another study has shown that CSE exposure promotes the recruitment of RelB on pro-inflammatory gene promoters in the lungs of a COPD mouse model [250]. Moreover, it has been shown in the literature that the release of IL-6, IL-8 and TNF-α into the supernatant from CSE treated type II pneumocytes is mediated via the Nf-κB activation [251]. The exact mechanism behind the interleukin as well as COX-2 upregulation in this thesis has to be, however, proven by future experiments.

Taken together the results of this thesis suggest that down-regulation of peroxisome expression and abundance, as was shown with *Pex13* knock-down, exhibits an adverse effect on inflammation, wherefore in the pathophysiology of COPD peroxisomes could play an important role to protect the pulmonary cells against oxidative stress and the release of pro-inflammatory mediators.

5.6. Peroxisome proliferation can be activated by PPARγ agonists reducing inflammation, oxidative stress and ROS release

In order to show that PEX13 as well as peroxisomal enzymes are regulated by PPARγ and that the stimulation of PPARγ receptor by its agonist would trigger the activation of peroxisomal biogenesis and metabolism, silencing of *Pparγ* was performed. *Pparγ* silencing revealed that *Pex13* is significantly down-regulated in these cells and that our results on oxidative stress, inflammation and ROS, after *Pparγ* deletion, are in accordance with the results we observed following a *Pex13* knock-down. The next step was to possibly activate the peroxisomal compartment with the PPARγ agonist Rosiglitazone (RZG) in order to see whether peroxisomes would counteract the oxidative stress and whether this upregulation of peroxisomes would reduce the release of inflammatory cytokines.

PPARγ is a member of nuclear hormone receptor family that modifies gene expression upon ligand binding. It has been found that PPARγ ligands play an important role in the regulation of inflammatory processes and PPARγ agonists might become promising anti-inflammatory drugs [252-254]. It was shown that PPARγ ligands inhibit the M1 and M2 macrophage-activated pro- and anti- inflammatory gene transcription respectively [255,256]. In addition to this, the PPARγ ligands reduce the inflammatory response and regulate macrophage efferocytosis in the lungs of COPD patients [257]. Moreover, they were found to inhibit cigarette smoke-induced pulmonary neutrophilia [205,258] and reduce arthritis, colitis, and atherosclerosis in animal models [259-261].

Our results demonstrate that the cells incubated with RZG 24h prior to cigarette smoke extract indeed exhibited peroxisomal proliferation and upregulation of (peroxisomal proteins in comparison to control cells, cells treated with CSE and cells incubated with RZG without CSE treatment. RZG-only treated samples did not show any peroxisomal change and were similar to the control samples. Therefore, the peroxisomal upregulation was only seen in the samples stimulated with CSE after RZG incubation. Moreover, the samples treated with RZG and incubated with CSE showed decreased

ROS production, an attenuated cytokine release (IL-6, TNF-α) and an attenuated COX-2 increase, suggesting a reduced inflammatory response in the RZG samples with high peroxisomal gene expression and peroxisome proliferation. In these samples, the activation of Nrf2 based on the ARE luciferase analysis, Western blots and qRT-PCRs was demonstrated. Moreover, Nrf2-regulated genes and proteins were increased as was shown on the mRNA and protein levels, suggesting that Nrf2 is mediating, at least in part, the activation of the antioxidant response. These data suggest that PPARγ activation could provide a potential treatment for inflammatory airway diseases such as COPD and that this anti-inflammatory and ROS reducing action could be mediated through the activation of peroxisomes.

As was shown above, treatment with CSE activated the Nrf2 pathway but the oxidative stress was still present because the peroxisomes weren't as highly upregulated as they were after RZG treatment. However, RZG treatment activated peroxisomes and together with up-regulated Nrf2-controlled antioxidant genes balanced the antioxidant/oxidant redox homeostasis in the CSE treated samples as was confirmed by the DHE staining. This is a confirmation that for the homeostasis of the antioxidant/oxidant balance, peroxisomes are indispensable. Yet, since PPARγ agonists are implicated in the activation of several other pathways, as was mentioned in this discussion, under RZG treatment we can't exclude that the anti-inflammatory and antioxidative effects that we observed in our study were exclusively mediated by peroxisomes, but we can say for sure that up-regulated peroxisomes contributed strongly to the protective effect. Which other PPARγ dependent pathways contribute to the protection against CSE-induced oxidative stress has to be experimentally proven in the future.

To exclude non-specific activation by RZG, PPARγ was overexpressed in order to check whether this overexpression would corroborate the results obtained by RZG treatment. For this purpose, cells were transfected with PPARγ expression plasmid (PPARγ-pCMV-Sport6) for 68h and then treated with DMSO. Highly PPARγ overexpressing cells demonstrated an increase in peroxisomal gene expression in comparison to cells transfected with control plasmid. These results were indeed directly the opposite to the results observed with deleted *Pparγ* followed by DMSO treatment (*siPparγ* 0%CSE). Furthermore, these samples showed upregulation of Nrf2 and its dependent genes in comparison to PPARγ overexpression and CSE-treated

samples, which was as well opposite to what we have seen in the samples treated with DMSO following the *Pparγ* deletion (DMSO only group) and samples treated with CSE following the *Pparγ* knock-down respectively. Moreover, no inflammation was observed in these samples as was shown by qRT-PCR and ELISA analysis since the cytokine levels did not exceed the concentration of the control samples.

However, in comparison to PPARγ overexpressing cells treated with DMSO, cells with strong overexpression of PPARγ and additional CSE treatment, showed a significant reduction in peroxisomes, which was as well opposite to the results of Pparγ knock-down experiments. Similarly, the peroxisome biogenesis protein PEX13 was down-regulated in samples treated with CSE following PPARγ overexpression. Therefore, PTS1 and PTS2 containing peroxisomal antioxidative, β-oxidation and ether phospholipid synthesis enzymes were as well down-regulated in these cells. Interestingly, Nrf2 and its downstream genes and proteins HO-1 and SOD1 were also decreased which is a sign of to-the-control-levels balanced oxidative stress in these cells. Our results were confirmed by the decline in cytokine expression suggesting an attenuated inflammatory response in the CSE treated cells. The results of PPARγ overexpression were completely opposite to the results obtained by the *Pparγ* knock-down. Indeed the PPARγ overexpression for 68h exerted a preventive effect by attenuating the harmful CSE effects since it upregulated peroxisomes already in the samples before the CSE treatment was applied, thus blocking the CSE-driven oxidative stress in its initial steps. Overexpression of PPARγ leads, in many cases, to ligand-mediated trans-repression of genes by its SUMOylation. This could explain the observed down-regulation of peroxisomes, cytokines and Nrf2-driven enzymes. Indeed, different effects have been also observed between RZG-pretreated samples and the PPARγ overexpression for the regulation of the Nf-κB pathway [262]. Moreover, differences in overexpression times and high PPARγ protein levels in comparison to the RZG-treatment (24h) might also contribute to the distinct effect on the peroxisomal compartment. The exact mechanism leading to the different molecular regulation of peroxisomal gene transcription must be analysed in details in future experimental studies.

The results of this thesis demonstrated that PPARγ activation either by RZG or by overexpression plasmid attenuates the release of cytokines and reduces oxidative stress and ROS. The mechanism by which PPARγ agonists exert their anti-

inflammatory effects is poorly understood. Several studies showed that possible ways through which PPARγ ligands exert their actions could be by inhibition of TLR4 (toll like receptor 4) expression [263], by inhibition of the NF-κB pathway [164] by inhibition of ERK1/2 phosphorylation [264] by inhibition of ERK1/2/p38MAPK activation [265] or by upregulation of HDAC2 [203]. This thesis showed an upregulation and proliferation of peroxisomes under PPARγ stimulation. However, the exact molecular mechanism leading to the effects on the peroxisomal compartment has not yet been clarified. One study has shown that a functional cross-talk between NF-κB and Nrf2 exists [266], such that the Nrf2-regulated activation of the antioxidant machinery leads to the suppression of NF-κB [267]. In addition to this, reactive oxygen species activate Nrf2 and PPARγ which are linked by a positive feedback loop [268]. These interactions in connection to the peroxisomes have to be clarified in the further experiments.

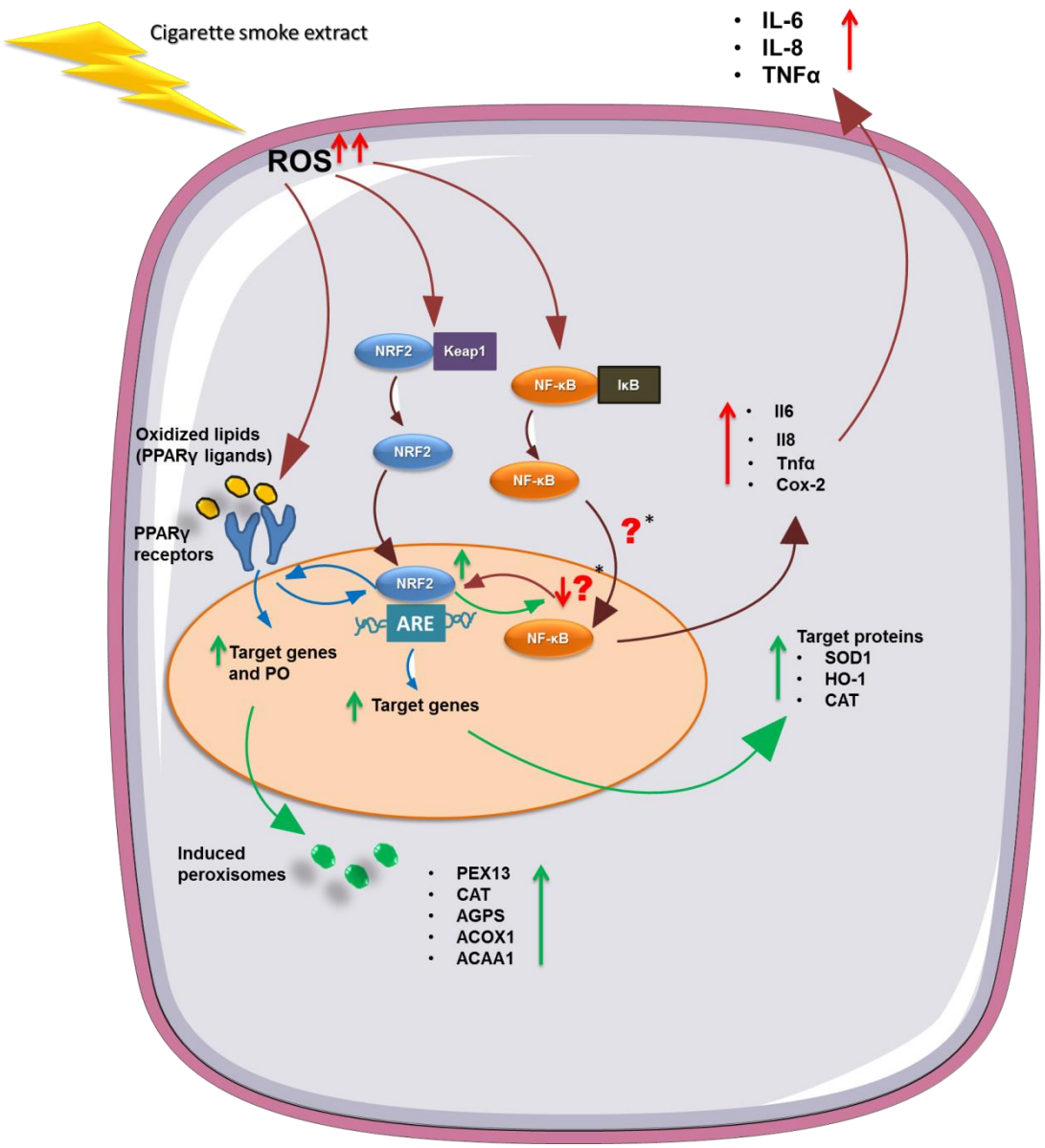

Fig. 79 Cigarette smoke-extract (CSE) treatment. Cigarette smoke generates ROS which leads to the translocation of the oxidative stress-activated Nrf2 transcription factor into the nucleus where it binds to ARE and mediates HO-1, SOD1 and CAT activation. In addition to this, cigarette smoke leads to a slight induction of the endogenous PPARγ ligands (eg. oxidized lipids) which activate the genes responsible for peroxisome proliferation leading to the increased abundance of peroxisomes. Furthermore, cigarette smoke induces proinflammatory cytokine production most probably by the activation of the NF-κB pathway. Several studies have shown that there is a functional cross-talk between NF-κB and Nrf2 [266], such that the Nrf2 regulated activation of the antioxidant machinery leads to the suppression of NF-κB [267]. In addition to this, ROS and other reactive species activate PPARγ and Nrf2 which are linked by a positive feedback loop. Under control conditions with CSE treatment, the expression and abundance of peroxisomes and antioxidative enzymes were probably not high enough to counteract the oxidative damage induced by the cigarette smoke extract (as was shown by the DHE staining). *Not analysed in this thesis, but known from the literature.

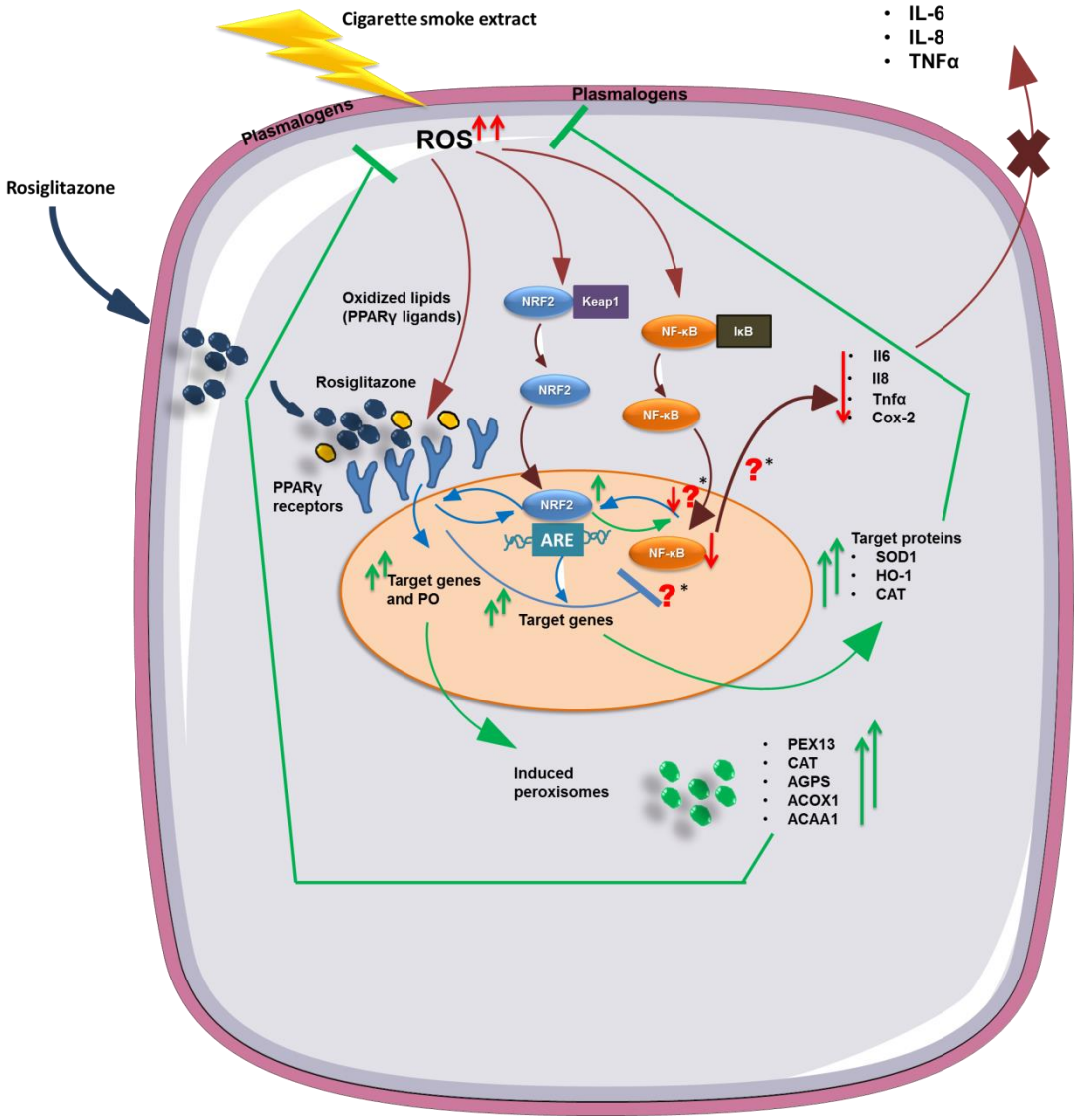

Fig. 80 Rosiglitazone treatment. The proposed mechanism is based on the results of the thesis and suggests that ROS and the pro-inflammatory cytokines (Ils, Tnfα) which are generated by the CSE-induced activation of NF-κB are suppressed by Rosiglitazone. This involves 2 pathways, such that 1) Rosiglitazone induces the expression of PPARγ which sustains the expression of Nrf2 via a positive feedback loop thus leading to the increased transcription of Nrf2 regulated antioxidative enzymes; 2) the strong up-regulation of Nrf2 or PPARγ possibly decrease the activation of NF-κB, suppressing the interleukin release. In addition to this, highly expressed PPARγ activates genes responsible for peroxisome induction leading to the increased number of peroxisomes as well as an increase in their metabolic functions. Peroxisomes, which are rich in antioxidative and β-oxidation enzymes and synthesize ROS trapping plasmalogens, reduce the amount of ROS and degrade oxidized lipids. The strong expression and abundance of peroxisomes and antioxidative enzymes was sufficient to counteract the oxidative damage induced by the cigarette smoke extract as was shown in this thesis by the DHE staining. Thus, we hypothesize that Rosiglitazone and peroxisomes play a protective role in attenuating the COPD pathophysiology.*Not analysed in this thesis, but known from the literature.

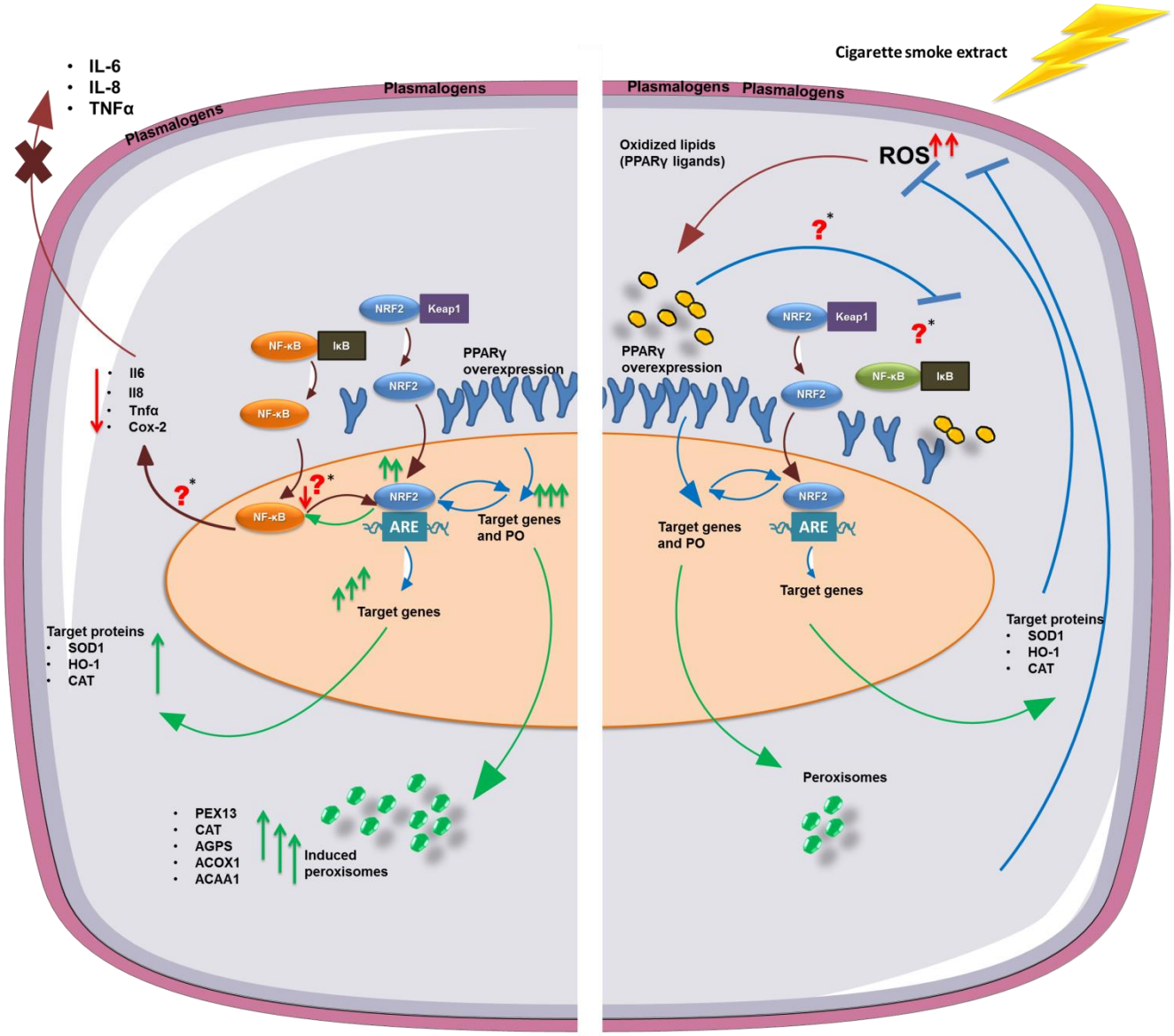

Fig. 81 Cells with overexpressed PPARγ either stimulated with DMSO (left) or CSE (right). The proposed mechanism is based on the results of the thesis and suggests that PPARγ overexpression leads to upregulation of peroxisomes and Nrf2-regulated genes thus bringing the level of proinflammatory cytokines to the control level as was observed in the absence of CSE treatment. This upregulation suggests that with PPARγ overexpression, cells are very rich in the antioxidative enzymes thus they are capable of preventing the accumulation of oxidative products even after the CSE-treatment. Future experiments are necessary to clarify the difference. Under PPARγ overexpression followed by CSE-treatment, peroxisomal genes as well as other antioxidant enzymes are downregulated. Moreover, Nrf2 is also decreased, suggesting that high PPARγ overexpression reduces the activation of the antioxidant and proinflammatory response. *Not analysed in this thesis, but known from the literature.

6. Summary

Chronic obstructive pulmonary disease (COPD) is a leading cause of mortality and morbidity globally, and its development is mainly associated with tobacco-induced oxidative stress. In the lung, pulmonary epithelia are the first targets of cigarette smoke components overwhelming the antioxidative capacity of the epithelial cells and contributing strongly to COPD pathogenesis.

Peroxisomes are single membrane-bound organelles that possess heterogeneous functions and enzyme composition depending on the organ and cell type. Until the beginning of experimental work of this thesis, no information was available so far on the role of peroxisomes in the molecular pathogenesis of COPD. The fact that peroxisomes are abundant in the airway epithelia and that they could be directly affected by CS, as they are located underneath the apical surface of the epithelial cells, made us hypothesize that they could alter the molecular-pathogenesis of COPD. Peroxisomes could protect the pulmonary airway epithelium against ROS and lipotoxicity since they are rich in different antioxidative enzymes, they synthesize plasmalogens (ROS trapping lipids) and play an important role in β-oxidation of eicosanoids.

Therefore, the main goal of the thesis was to analyze the possible alterations of the peroxisomal compartment in lung samples of COPD patients and a mouse COPD model in comparison to control samples, and to study the functional consequences of cigarette smoke extract-treatment on the peroxisomal compartment in human HBE cells and mouse C22 cells in culture. Studying the peroxisomal alterations would clarify whether the impairment in peroxisomal metabolism could affect the molecular pathogenesis of COPD. Moreover, changes in the peroxisomal compartment, antioxidative enzymes and cytokines following Pex13 deletion, RZG treatment, PPARγ overexpression or knockdown in cigarette smoke-treated cells could be detected.

To get a complete overview of the peroxisomal compartment and its alteration in the pathogenesis of COPD, several techniques were used, such as: immunofluorescence with a variety of antibodies against peroxisomal and cell marker proteins, cell and lung tissue homogenization, Western blot analysis, total RNA isolation, qRT-PCR, molecular cloning, transfections, luciferase assays and ELISAs

The results of this thesis indicate that a peroxisomal gene expression (*Cat*, *Pex13*, *Pex14*, *Acox1*, *Acaa1*, *Agps*, *Gnpat*) and corresponding protein upregulation occurs in human and mouse COPD samples. Moreover, the knock-down of the peroxisomal biogenesis gene *Pex13* provoked strong oxidative stress and a release of pro-inflammatory mediators suggesting a protective role of peroxisomes in preventing the chronification of inflammation in the disease pathogenesis. Furthermore, treatment with the PPARγ agonist Rosiglitazone and PPARγ overexpression were able to reverse the effects produced by cigarette smoke extract in C22 cells by inducing peroxisome proliferation by PPARγ activation. These results revealed the important role of PPARγ and the PPARγ regulated peroxisomal response for the protection against chronification and aggravation of the inflammation in COPD.

7. Zusammenfassung

Die Chronisch Obstruktive Lungenkrankheit (Chronic Obstructive Pulmonary Disease/COPD) ist eine führende Ursache für Mortalität und Morbidität weltweit, und deren Entwicklung ist hauptsächlich mit Tabakrauchen-induziertem oxidativen Stress verbunden. In der Lunge stellen pulmonale Epithelien die ersten Schàdigungsziele von Zigarettenrauchbestandteilen dar, die die antioxidative Kapàzitat der Epithelzellen überwàltigen und stark zur COPD-Pathogenese beitragen.

Peroxisomen sind von einer Einheitsmembran begrenzte Organellen, die je nach Organ und Zelltyp unterschiedliche Funktionen und Enzymzusammensetzung besitzen. Bis zum Beginn der experimentellen Studien dieser Doktorarbeit lagen jedoch keine Informationen über die Rolle der Peroxisomen in der molekularen Pathogenese von COPD vor. Die Tatsache, dass die Peroxisomen im apikalen Bereich der Atemwegsepithelien reichlich vorhanden sind und dadurch direkt durch Zigarettenrauch beeinflusst werden könnten, lässt vermuten, dass sie eine Rolle in der molekularen Pathogenese der COPD spielen könnten. Da Peroxisomen außerdem reich an verschiedenen antioxidativen Enzymen sind und eine wichtige Rolle in der Plasmalogensynthese (ROS-bindende Lipide) sowie bei der β-Oxidation von Eicosanoiden spielen, könnten sie die pulmonalen Atemwegsepithelien gegen ROS und Lipotoxizität schützen.

Das Hauptziel dieser Doktorarbeit war es, die möglichen Veränderungen des peroxisomalen Kompartiments in Lungenproben von COPD-Patienten und einem Maus-COPD-Modell im Vergleich zu Kontrollproben zu analysieren und die funktionellen Konsequenzen von Zigarettenrauchextrakt auf das peroxisomale Kompartiment in humanem HBE-Zellen und Maus-C22-Zellen zu untersuchen. Das Studium der peroxisomalen Veränderungen würde zur Klärung beitragen, ob die Beeinträchtigung des peroxisomalen Metabolismus die molekulare Pathogenese der COPD beeinflussen könnte und um Veränderungen im peroxisomalen Kompartiment, antioxidativen Enzymen und Zytokinen entweder nach Pex13-Deletion, Rosiglitazon-Behandlung, PPARγ-Überexpression oder entsprechendem PPARγ-Knockdown von Zigarettenrauch-behandelten Zellen zu erkennen.

Um einen vollständigen Überblick über das peroxisomale Kompartiment und seine Veränderungen in der Pathogenese der COPD zu erhalten, wurden verschiedene Techniken verwendet: Immunfluoreszenz mit einer Vielzahl von Antikörpern gegen peroxisomale und Zellmarkerproteine, Zell- und Lungengewebe-Homogenisierung, Western-Blot-Analyse, RNA-Isolierung, qRT-PCR, molekularbiologische Klonierungs- und Transfektionsverfahren, Luziferase-Assays und ELISAs.

Die Ergebnisse dieser Doktorarbeit zeigen, dass eine peroxisomale Gen- (*Cat*, *Pex13*, *Pex14*, *Acox1*, *Acaa1*, *Agps*, *Gnpat*) und entsprechende Protein-Hochregulierung in menschlichen und Maus-COPD-Proben vorhanden ist. Darüber hinaus führt ein Knockdown des peroxisomalen Biogenese-Gens Pex13 zu starkem oxidativen Stress und der erhöhten Freisetzung von Entzündungsmediatoren, die auch bei COPD-Patienten vorliegen. Deshalb lässt sich bei der Pathogenese dieser Erkrankung auf eine schützende Rolle der Peroxisomen schließen. Darüber hinaus konnten die Behandlung mit dem PPARγ-Agonisten Rosiglitazon und die PPARγ-Überexpression die Effekte, die durch Zigarettenrauchextrakt in C22-Zellen hervorgerufen wurden, umkehren, was die wichtige Rolle von PPARγ und der über PPARs-regulierten Peroxisomen bei der Protektion gegen die Chronifizierung und Verschlechterung der Entzündung bei COPD bestätigte.

8. Appendix

X. PPARγ Cloning

X.1 Materials and methods

X.1.1 PCR reaction

In order to amplify the insert of interest and to clone it into pGEM-T Easy, a PCR reaction was used. The primers (**Table 1**) for this PCR reaction were designed in order to amplify the entire open reading frame. The restriction sites SrfI (forward primer) and XhoI (reverse primer) (underlined in **Table 1**) were inserted in the primer sequence and will be subsequently used to clone the fragment into the final vector PCMV-Tag.

Table 1. Primers used for the amplification of PPARγ

Oligoname	Forward	Reverse
FVmmPPARγ 3b	ATAgcccgggcATGGGTGAAACTCTGG	TATctcgagCTAATACAAGTCCTTGTAGATCTC
FVmmPPARγ 5b	ATAgcccgggcATGGGTGAAACTCTGG	TATctcgagATACAAGTCCTTGTAGATCTCCTG

Table 2. Vector used for the amplification of the PCR-product

Gene Description	I.M.A.G.E. Fully Sequenced cDNA Clone
Peroxisome proliferator activated receptor gamma	IRAVp968E0327D

For the PCR reaction, two PCR master mixes were prepared using 2 different reverse primers as indicated in **Table 3**. The reactions were mixed and centrifuged before being put in the PCR machine. The steps of the program for the PCR are described in **Table 4**.

Table 3. Components of the PCR reaction

	Final concentration	Standard reaction
10X PCR buffer	1X	5µl
DNA (PCMV sport PPARγ)	10ng or 20 ng it is 100ng	1µl
Primer (forward – FVmm PPARγ 35b)	2pmol	2µl
Primer (reverse – RVmm PPARγ 5b or RVmm PPARγ 3b)	2pmol	2µl
dNTP	0.4mM	0.4µl
Taq polymerase	5u	0.5µl
Water	-	Till 50µl
Total	-	50ul

Table 4. The PCR program

Step	Temperature	Time
Denaturing	95°C	5min
Denaturing	95°C	30sec
Annealing	55°C	30sec
Extension	72°C	1min
Final extension	72°C	7min
Final hold	4°C	Hold

After completion of the program, the PCR reaction was analysed by agarose-gel electrophoresis to assess that only one PCR product of the correct size was synthesised.

X.1.2 DNA Gel electrophoresis

X.1.2.1 Preparation of an agarose gel

For a 1% agarose gel, 0.4g of agarose (SERVA) were dissolved in 40ml 1XTAE buffer (1X Tris-Acetate-EDTA). Thereafter, the agarose was melted in the microwave and left to cool down (hand-cold). Then, 1.5µl of stain G was added and the agarose was poured into a gel tray.

X.1.2.2 Preparation and loading of the DNA samples and gel running

For a small gel, 4µl of 6X DNA loading dye were added to the DNA sample and mixed by pipetting. The gel tray was transferred into a gel running tank and covered with 1XTAE buffer. Then, the ladder and the samples were loaded and the gel electrophoresis (Sub Cell GT, BioRad) was run at 100V for 30min. Finally, the gel was examined under UV light (Gel-Doc 2000 gel documentation system).

X.1.3 DNA extraction from the gel

The DNA fragments were purified by DNA gel electrophoresis followed by DNA extraction from the gel. After the electrophoresis, the DNA fragments were excised under the UV-light using a scalpel. The excised DNA fragments were placed into Eppendorf tubes and weighed. To each 100mg of the agarose gel fragments, 200µl of NTI buffer from the gel purification kit were added according to the DNA extraction protocol (Macherey-Nagel). The reaction tubes were incubated at 50°C for 10min and the samples were vortexed every 3min until the gel was completely dissolved. For DNA binding, 700µl of the sample were placed on the NucleoSpin® Column, centrifuged twice for 30s at 10,000g and the flow through was discarded. To wash the silica membrane, 700µl of Buffer NT3 were added to the NucleoSpin® Gel and PCR Clean-up Column, the column was centrifuged at 11,000g for 30s and the flow through was discarded. Thereafter, the NucleoSpin® Column was centrifuged twice at 11,000g for 1min to remove the buffer NT3 and to dry the column. Finally, the DNA was incubated with 30µl of buffer NE for 1min and then eluted by centrifuging twice for 1min at 11,000g.

X.1.3.1 PCR clean-up

In this thesis the PCR clean-up kit from Macherey-Nagel was used to remove enzymes and salts from the restriction enzyme reactions. One volume of the sample was mixed with 2 volumes of Buffer NTI. For DNA binding, 700µl of the sample were placed on the NucleoSpin® Gel and PCR Clean-up Column, centrifuged twice for 30s at 10,000g and the flow-through was discarded. To wash the silica membrane, 700µl of Buffer NT3 were added to the NucleoSpin® Gel and PCR Clean-up Column, the column was centrifuged at 11,000g for 30s and the flow through was discarded. Thereafter, the NucleoSpin® Column was centrifuged twice at 11,000g for 1min to remove the buffer NT3 and to dry the column. Finally, the DNA was incubated with 30µl of buffer NE for 1min and then eluted by centrifuging twice for 1min at 11,000g.

X.1.4 Ligation reactions

X.1.4.1 Ligation of the PCR product into pGEM-T Easy

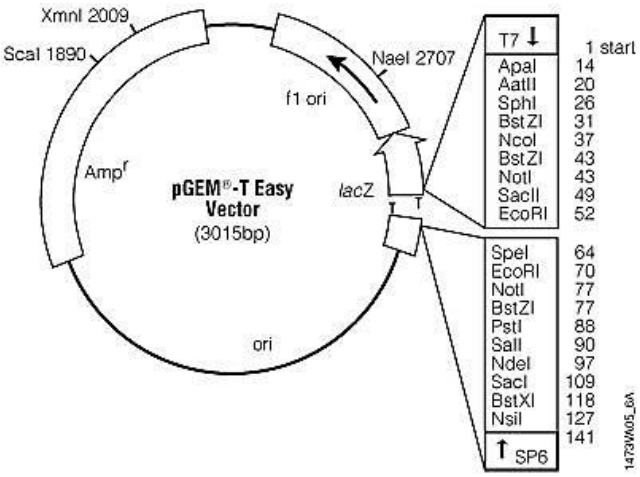

Fig. 1. Map of pGEM-T Easy vector. From www.promega.com

To facilitate the ligation into the final vector, the purified PCR product was first cloned into pGEM-T Easy plasmid vector. For the ligation, the reaction was set up as described in **Table 5** and incubated at 16°C overnight. The ligation reaction was then used to transform competent *E.coli* DH5α and for positive clones screening.

Table 5. Components of the ligation reaction

	Standard reaction
2X ligation buffer	5µl
pGEM-T easy vector	1µl
PCR product (gel extracted DNA)	2.5µl or 5µl
T4 ligase	0.5µl
Deionized water (LONZA)	1µl or 0µl
Total volume	10µl or 11.5µl

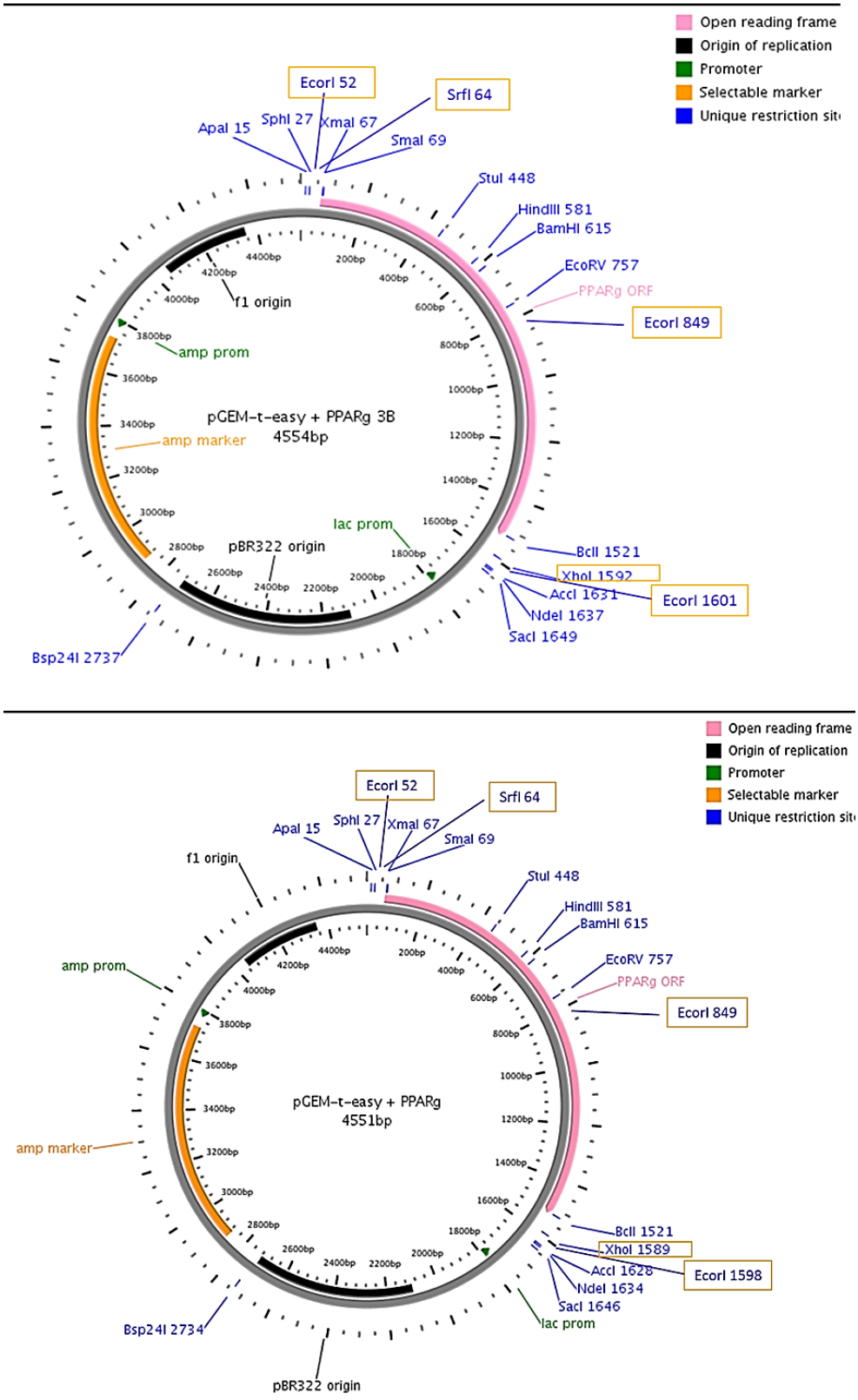

Fig. 2. The map of 3B and 5B inserts cloned into pGEM-T Easy vector. The purified PCR product was first cloned into pGEM-T Easy.

X.1.4.2 Ligation of the PPAR fragment into pCMV-Tag3B and 5B

The DNA fragments obtained from the restriction enzyme digest of pGEM-T Easy containing the PPARγ PCR-product were ligated into both the pCMV-Tag 3B and the 5B expression vectors. The reaction was set-up as described in **Table 6** and incubated at 16°C overnight.

Table 6. Components of the ligation reaction

Components	Reaction 1	Reaction 2	Reaction 3
10X T4 DNA ligase buffer	2µl	2µl	2µl
PCMV (3b or 5b)	1µl	1µl	-
Insert (3b or 5b)	5µl	-	5µl
T4 DNA ligase	1µl	1µl	1µl
Deionized water	11µl	16µl	12µl
Total volume	20µl	20µl	20µl

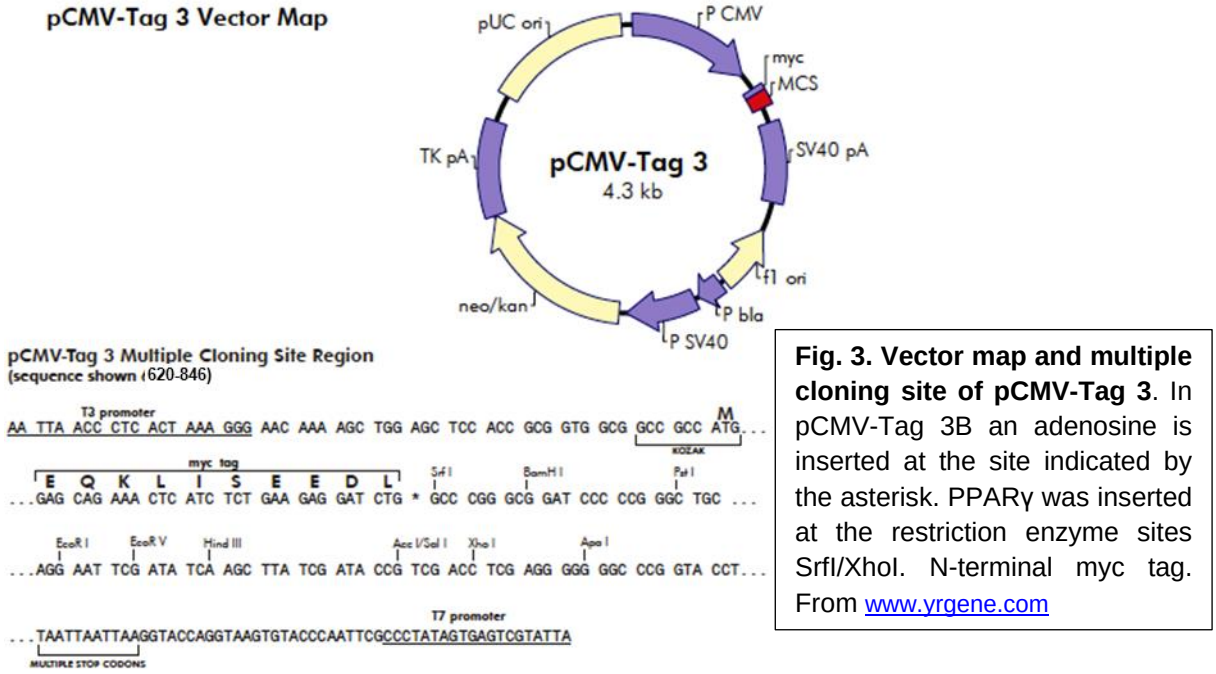

Fig. 3. Vector map and multiple cloning site of pCMV-Tag 3. In pCMV-Tag 3B an adenosine is inserted at the site indicated by the asterisk. PPARγ was inserted at the restriction enzyme sites SrfI/XhoI. N-terminal myc tag. From www.yrgene.com

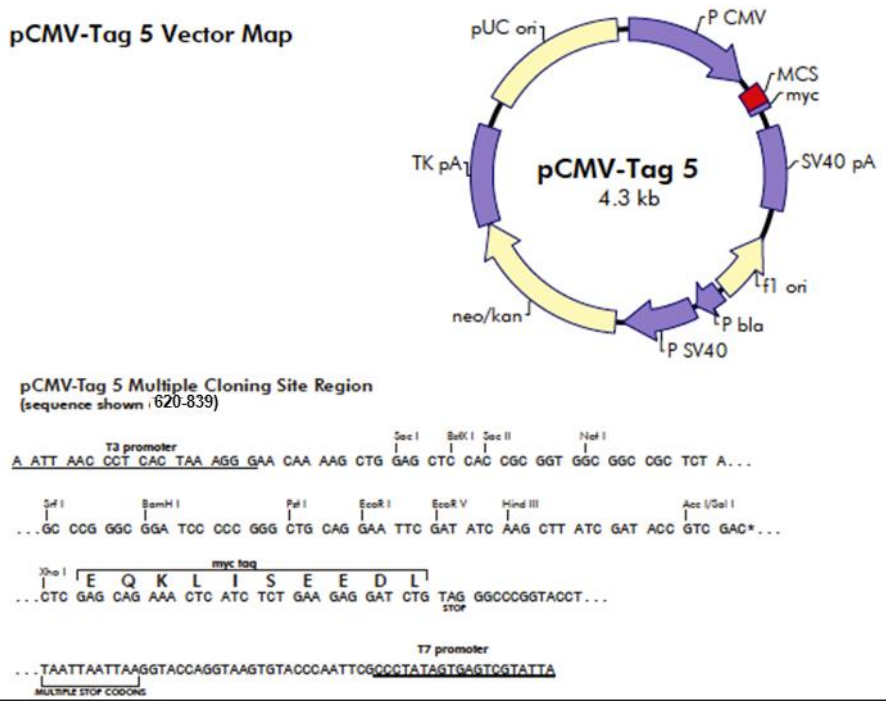

Fig. 4. Vector map and multiple cloning site of pCMV-Tag 5. In pCMV-Tag 5B, an adenosine is inserted at the site indicated by the asterisk. PPARγ was inserted at the restriction enzyme sites SrfI/XhoI. C-terminal myc tag. From www.yrgene.com

X.1.5 Restriction enzyme reactions

Table 7. Restriction enzymes

Restriction enzymes	Company	Buffer	Company
EcoRI	R601A, Promega	H buffer	R008A, Promega
XhoI	R6161, Promega	D buffer	R004A, Promega
SrfI	R0629S, New England Biolabs	CutSmart® Buffer	B7204S, New England Biolabs

The restriction enzyme reactions were set up as described in **Table 8, 9** and **10** and incubated at 37°C for 3h. Following the incubation, the restriction products were separated on a 1% agarose gel.

Table 8. The restriction enzyme reaction mix

	Standard reaction
Plasmid DNA (pGEM-T-Easy)	5µl
Restriction buffer	5µl
Enzyme (EcoR1 or XhoI)	1µl
Deionized water	39µl
Total volume	50µl

Table 9. Restriction enzyme reaction mix

	Standard reaction
XhoI restriction enzyme	1µl
pCMV-tag	30µl
10X Buffer D	5µl
Deionized water	14µl
Total volume	50µl

Table 10. Restriction enzyme reaction mix

	Standard reaction
SrfI restriction enzyme	1µl
pCMV-tag or pGEM-T-Easy	15µl

Restriction enzyme buffer	5µl
Deionized water	29µl
Total volume	50µl

X.1.6 *Escherichia coli* DH5αTransformation

Table 11. Mediums for bacterial growth and transfection

Transfer buffer 10X (TAE)	40mM Tris base, 20mM acetic acid, 1mM EDTA, pH 7.6
LB medium	0.17 M sodium chloride, 1% trypton, 0.5% yeast extract, pH 7.0
LB-Agar	LB medium, 1g/50ml agar, 100µg/ml ampicillin or 50µg/ml neomycin
6X-Agarose loading dye	0.025% (w/v) bromophenol blue without xylene cyanol, 30% (v/v) glycerol
SOC	Tryptone 2% (w/v), yeast extract 0.5% (w/v), NaCl 10mM, KCl 2.5mM, pH 7.0, the solution was autoclaved, then 20mM of glucose was added

X.1.6.1 *Escherichia coli* DH5α Electroporation and blue-white screening

Fifty µl of competent *E.coli* DH5α were used for one ligation reaction. Five µl of the ligation product were added to the tube containing bacteria and incubated for 15min on ice. After the incubation, the mixture was transferred to Electroporation Cuvettes and a single pulse (Ec2, 2.5kV) was applied (Gene Pulser®/MicroPulser™). As positive control, 1µl PUC-Vector was used. Following the electroporation, the mixture was put on ice for 10min. Thereafter, 500µl of SOC were added to each cuvette and the bacteria were incubated at 37°C for 30min. Then, the bacteria were spread on LB-ampicillin 100mg/ml (pGEM) or neomycin 50mg/ml (pCMV-Tag) plates and the plates were incubated upside-down at 37°C overnight.

X.1.6.2 *Escherichia coli* DH5α blue-white screening

To identify clones containing pGEM-t easy vector with the correct insert the electroporated *E.coli* DH5α were subjected to blue/white screening. For blue/white screening, 100µl of LB medium with 40µl X-Gal (20mg/ml) and 20µl of IPTG (0.8M) was prepared. The mixture was spread using glass beads on ampicillin agar plates and allowed to dry with half-open lids before plating the transformed bacteria.

X.1.6.3 Transformation of *Escherichia coli* DH5α by heat shock

50µl *E.coli* DH5α were mixed with 1µl PCMV sport PPARγ plasmid (1µl) by gently tapping the tube and incubated for 15min on ice. After the incubation, the cells in the tube were subjected to a heat-shock at 42°C for 90s and the tube was then placed on ice for 2min. Thereafter, 500µl of SOC were added to each tube and the bacteria were incubated at 37°C for 30min at 300rpm. Then, the cells were spread on LB-ampicillin plates and the plates were incubated upside-down at 37°C overnight. The following

day, single colonies were picked and cultured overnight in tubes containing 3ml LB media with 3µl neomycin (50mg/ml) at 37°C in a shaking incubator.

X.1.7 Preparation of cultures for the colony PCR

In order to identify positive clones from the ligation of the PPARγ insert into PCMV tag vector we have used colony PCR. The PCR master mix was prepared according to **Table 7** with either 3b or 5b primers, 50µl of the mix were added per PCR tube.

Table 12. Components of the PCR reaction

	Final concentration	Standard reaction
10X PCR buffer	1X	5µl
Bacterial DNA from colony	------	------
Primer (forward – FVmm PPARγ 35b)	2pmol	2µl
Primer (reverse – RVmm PPARγ 5b or RVmm PPARγ 3b)	2pmol	2µl
dNTP	0.4mM	0.4µl
Taq polymerase	5u	0.5µl
Water	-	Till 50µl
Total	-	50µl

The colonies from the overnight culture were picked using a pipette tip (**Fig. 5**), dipped into PCR tubes containing 50µl of PCR master mix, and immersed thereafter into tubes containing 100µl of LB media containing 50mg/ml neomycin for 5h at room temperature for later culture. Clones resulting to be positive were then incubated in 3ml of LB media containing 50mg/ml neomycin and cultured at 37°C in a shaker overnight and thereafter subjected to miniprep plasmid isolation.

The tubes containing the PCR master mix were subjected to PCR amplification with the same conditions as explained in **Table 2**. The obtained product was separated on an agarose gel.

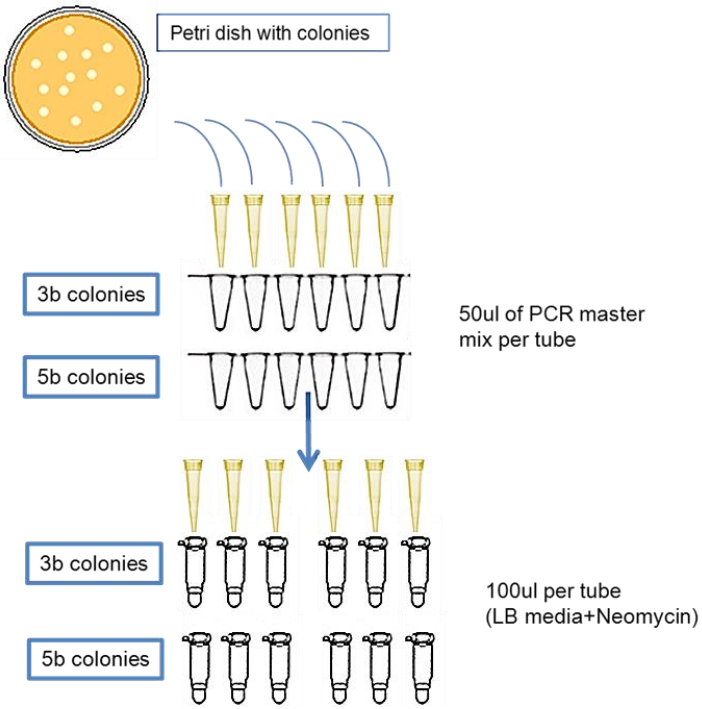

Fig. 5. Colony PCR procedure

X.1.8 Isolation of high-copy plasmid DNA from *E. coli*

X.1.8.1 Miniprep plasmid preparation

For the isolation of the high copy plasmid after ligation procedures the overnight cultures derived from positive clones screened by colony PCR were transferred into 2ml Eppendorf tubes and centrifuged for 30s at 11,000g and the supernatant was discarded. The pellet was resuspended (according to the NucleoSpin® Plasmid protocol from Macherey-Nagel) in 250µl of Buffer A1, followed by the addition of 250µl of buffer A2 and incubated at RT for 5min until the lysate cleared. Thereafter, 300µl of buffer A3 were added to neutralize the blue colour and the lysate was clarified by centrifugation for 10min at 11,000g at room temperature. Then, the supernatant was loaded onto a NucleoSpin® Plasmid/Plasmid Column and centrifuged for 1min at 11,000g to bind the DNA. In order to wash the membrane, 500µl of Buffer AW were pre-warmed to 50°C and added to the column, which was then centrifuged for 1min at 11,000g. Afterwards 600µl of buffer A4 were added and the column centrifuged for 1min at 11,000g. The membrane was dried by centrifugation for 2min at 11,000g. Finally, the DNA was eluted with 50µl of buffer AE following the incubation for 1min at room temperature and centrifugation at 11,000g.

X.1.8.2 Midiprep plasmid preparation

The overnight culture was pelleted by centrifugation at 6,000rpm for 10min at 4°C according to the ‘High-copy plasmid purification protocol’ (Macherey-Nagel). The pellet was then resuspended in 8ml of Res-EF buffer followed by the addition of 8ml of lysis buffer. The mixture was gently inverted for 5 times and the tube was incubated for 5min at RT. Meanwhile, the NucleoBond® Xtra Column together with the inserted filter was equilibrated with 15ml of EQU-EF Buffer. After the incubation, 8ml of the neutralization buffer NEU-EF were added to the lysate, which was then gently mixed by inverting until the blue sample turned colourless. The lysate was incubated on ice for 5min and loaded thereafter onto the column. The column and the filter containing the sample were then washed with 5ml of buffer FIL-EF and the filter was removed afterwards. The column was then washed twice with 35ml of ENDO-EF buffer followed by 15ml of Wash-EF buffer. The DNA was eluted with 5ml of ELU-EF buffer. The eluted plasmid was precipitated with 3.5ml of 2-propanol and then centrifuged at 8,500rpm for 1hr at 4°C. The pellet was washed with 2ml of 70% Ethanol-EF and centrifuged at 8,500rpm for 30min at 4°C. After the centrifugation, the ethanol was removed and the tube was inverted in order to facilitate the drying of the pellet. At last, the pellet was dissolved in an appropriate volume of buffer TE-EF.

X.2 Results

X.2.1 PPARγ Amplification

In order to overexpress PPARγ in C22 cells and to investigate the role of its overexpression in the pathogenesis of COPD, we decided to clone PPARγ into a mammalian expression vector bearing a protein-tag. For this purpose, three different vectors, pGEM-t Easy and pCMV tag 3B and 5B, were used. pGEM-T Easy is a subcloning vector that allows the ligation of the fragment without previous restriction enzyme digestion of vector and DNA fragment. It therefore facilitates downstream restriction digest and cloning procedures by capturing the PCR product into a “stiff” frame. The pCMV tag vectors are the mammalian expression vectors used for this cloning procedure. The transfection of these vectors produces a protein product bearing a myc-tag at either the N- or C-terminal side of the protein (pCMV 3B and 5B respectively). The advantage of using the myc-tag is that the protein can be detected with a standard anti myc-tag antibody and that this allows the differentiation between the endogenous and the overexpressed protein. We opted further to clone PPARγ with either C- or N-terminal myc-tag to exclude disturbances of the protein function caused by the location of the tag (eg. effects on subcellular localisation or protein folding).

The first step in the cloning procedure was the amplification of PPARγ by PCR. For this purpose we designed 2 primers bearing SrfI and XhoI restriction sites, which will be required later for the final ligation into PCMV-Tag. As mentioned above, PCMV-Tag 3B bears the myc-tag at the N-terminus while PCMV-5B at the C-terminus of the protein. Therefore, for the PCR-amplification of PPARγ we needed to design two different reverse primers, one of which did not contain the natural STOP codon present in the PPARγ-cDNA sequence and therefore will be used for the amplification of the PPARγ that will be cloned into PCMV-Tag 5B.

PPARγ was amplified from the original plasmid PCMV-Sport containing PPARγ. To make sure that the right amount of DNA was employed during the PCR-reaction, we used either 2.5µl or 5µl of the PCMV-Sport PPARγ plasmid corresponding to respectively 50ng and 100ng of plasmid DNA. After the PCR reaction, the PPARγ product (3b and 5b) containing the added restriction sites was analysed by gel-electrophoresis on a 1% agarose gel. For this purpose, the whole PCR product was loaded on the agarose gel. For both amounts of used PCMV-Sport PPARγ plasmid the electrophoresis revealed a single DNA band, of the expected size of 2,000bp (**Fig.1**),

corresponding to our amplified product (for both PPARγ). The fragments 3b and 5b were excised under the UV-light using a scalpel and thereafter subjected to the purification.

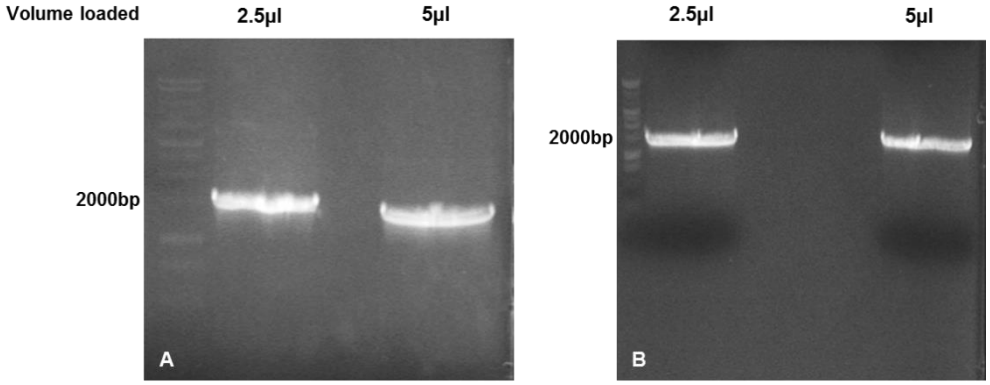

Fig. 1 PCR product from the amplified 3b and 5b PCR reaction. The whole PCR reaction was loaded on an agarose gel and subjected to electrophoreses for 30min at 100V. The separated fragments corresponded to the expected size of 2,000bp.

The purified product was used for ligation into pGEM-T Easy. The pGEM-T Easy vector system allows a direct PCR product ligation into a plasmid without previous restriction enzyme digestion reactions since it has "T" overhangs at the insertion site. The Taq polymerase adds an additional "A" at the end of the amplified DNA in the PCR reaction, so that the PCR product is complementary to the vector´s “T” overhangs and can ligate directly. The ligation reaction of the purified PCR product into pGEM-T Easy was set-up as described in **Table 5** and the product used to transform competent *E. coli* DH5α.

X.2.2 *Escherichia coli* DH5α transformation and blue white screening

E.coli DH5α were transformed with the ligation product by electroporation (section X.1.6.1) in order to identify clones containing pGEM-T Easy vectors with the PPARγ-insert. The transformed *E.coli* DH5α were subjected to blue/white screening which allows the identification of recombinant bacteria based on their ability to hydrolize X-Gal by β-galactosidase. Using the pGEM-T Easy system the PPARγ-fragment was ligated into the multiple cloning site (MCS) of the vector that contains the coding region for the β-galactosidase enzyme. Therefore, if the PPARγ-fragment was correctly inserted into the pGEM-T Easy plasmid, the bacteria should not be capable to hydrolize X-Gal by β-galactosidase and the colonies appear white (**Fig. 2B** and **C**). Colonies containing bacteria with active β-galactosidase (pGEM-T Easy without insert) can hydrolyze X-Gal and generate a blue product (**Fig. 2A**). We transformed the *E.coli* DH5α with pUC plasmid containing active β-galactosidase, as the positive control,

giving, as expected plenty of blue colonies on the agar plate (**Fig. 2A**). The number of colonies on the plates transformed with the pGEM-T easy ligations (**Fig 2B** and **C**) was 50% lower than the one observed for pUC (**Fig. 2A**). However, the number of white colonies in **Fig. 2B** and **C** was much higher than the number of blue colonies. This suggested that the PCR product was successfully transformed into *E.coli* disrupting the β-galactosidase gene and rendering the colonies to appear white in color.

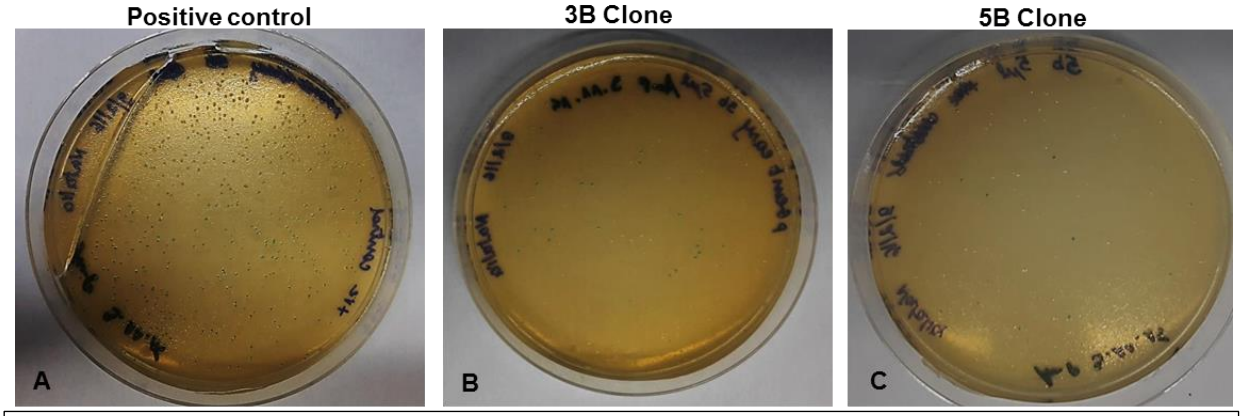

Fig. 2 Blue/white screening. Transformed *E.coli* DH5α were plated on agar plates with LB medium containing ampicillin and supplemented with X-gal. Colonies containing the ligated product are white, whereas those containing unligated plasmids are blue. A) Positive control, B) 3B clone, C) 5B clone

X. 2.3 Plasmid isolation and restriction enzyme digestion

From the white colonies obtained in section X.2.1 overnight cultures were set up and subjected to miniprep for the isolation of high copy plasmid. In order to determine whether the eluted DNA contains indeed the PPARγ insert, the isolated pGEM-T easy plasmids were subjected to restriction enzyme digestion with EcoRI followed by gel-electrophoresis. pGEM-T Easy contains 2 EcoRI sites flanking the DNA-fragment insertion sites. When this enzyme is used for the restriction enzyme digest of pGEM-T-easy, the inserted fragment is excised form the vector generating two products. In our case, the PPARγ insert contained an additional EcoRI site, and therefore 3 products were expected from this digest: two bands of approximately 1,000bp each representing PPARγ cut in half and one band of 3,000bp corresponding to pGEM-T Easy plasmid. The results of the digest are shown in **Fig. 3** and display the expected 3 bands. All clones that we had picked from the blue/white screening proved to be positive. For the next step, the digest with the restriction enzymes SrfI and XhoI, we therefore picked only one clone for 3B and one for 5B

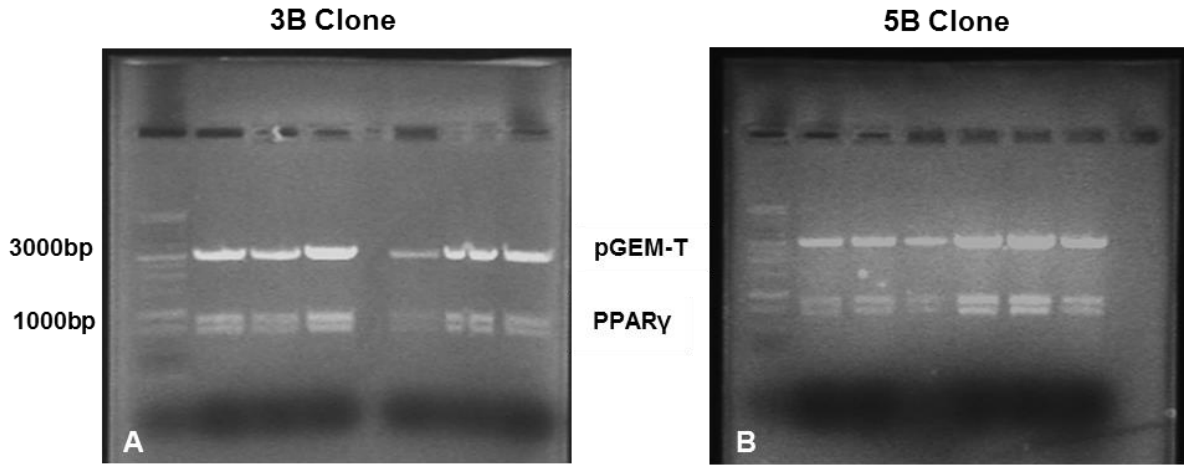

Fig. 3 Restriction enzyme digestion product Agarose gel electrophoresis after digestion with the restriction enzyme EcoRI presenting 3 bands. The band of 3,000bp corresponds to pGEM-T Easy and the 2 bands of 1,000bp correspond to the 2 fragments of PPARγ. A) 3B clone, B) 5B clone.

X. 2.4 Restriction enzyme digestion with SrfI and XhoI digestion

After the confirmation of a successfully ligated PPARγ insert, our next purpose was to subclone the insert into the pCMV vector. For this, we had to digest the pGEM-T Easy and the pCMV vector with the restriction enzymes SrfI and XhoI. Since the enzymes were bought from different companies and required two different restriction enzyme buffers, we had to perform the two digestion reactions subsequentially. All the vectors were first digested with SrfI and 5µl of this digest were analysed on a gel to assess the correct linearization of the plasmids. The SrfI digest resulted, as expected, in one single band on the agarose gel representing the linearized vectors of approximately 4,000 bp (**Fig. 4**). Following the SrfI digestion, the digested product was subjected to a PCR clean-up to remove the previous restriction enzyme buffer. Thereafter, the purified products (pGEM-T Easy containing PPARγ and pCMV) were digested using XhoI and then analysed on an agarose gel. This digest generated 2 bands (**Fig. 5**) for the pGEM-T Easy digests, eg one for pGEM-T-easy (3,000bp) and one for the PPARγ insert (2,000bp). On the other hand, for the pCMV-Tag digest, only one band of 3,000bp could be detected, corresponding well to the linearized vector. Following the electrophoresis, the bands corresponding to pCMV-Tag 3B and 5B and to PPARγ 3B and 5B were excised from the gel and purified.

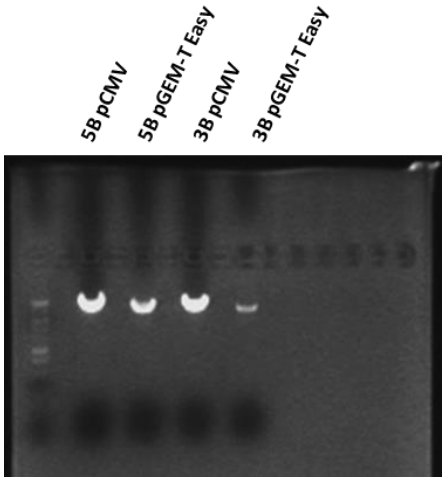

Fig. 4 SrfI digestion product. Agarose gel electrophoresis after digestion with the restriction enzyme SrfI presenting 1 band corresponding to pGEM-T Easy and pCMV vectors.

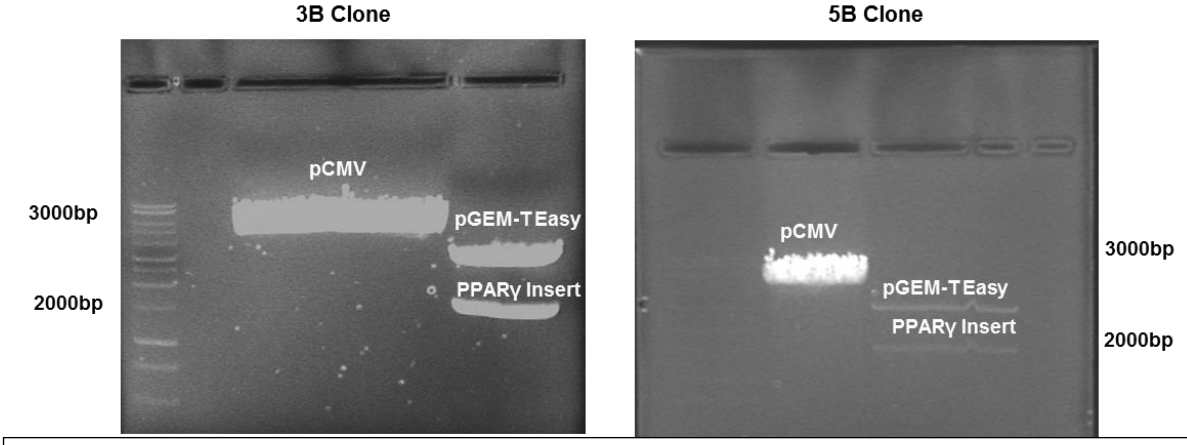

Fig. 5 XhoI digestion product. Agarose gel electrophoresis of a product after digestion with the restriction enzyme XhoI resulting in 3 bands. The bands correspond to pCMV (3000bp), pGEM-T Easy, and PPARγ insert (2000bp).

X. 2.5 Colony PCR Reaction

The purified DNA was further used for the final ligation reaction of the PPARγ fragments into pCMV-Tag 3B and 5B. The ligation reaction was set-up and then used to transform competent *E.coli* DH5α (section X.1.6.1). pCMV-Tag 3B-GFP was used as a positive control. The bacteria were plated on agar plates supplemented with LB media and neomycin as a selection marker. The clones containing PPARγ ligated into pCMV-Tag as well as clones containing pCMV-Tag without insert (self-ligated plasmid) are able to grow on the plates and cannot be differentiated as previously done using blue-white screening (**Fig. 4B** and **C**). Therefore, the next step was to identify, among the grown colonies, the positive clones containing PPARγ ligated into pCMV-Tag; for this purpose we used colony PCR. The colony PCR allows the identification of the presence or absence of the insert in the plasmid. Whole bacteria were used for the colony PCR since the initial 95°C heating step of the PCR reaction allows the release of the plasmid DNA from the bacterial cell. The released plasmid DNA containing the

insert is then used as a template for the amplification reaction. Insert-specific primers were used for the PCR amplification. Gel electrophoresis of the obtained PCR-products revealed a single band corresponding to 2,000bp, this suggested that all the clones were PPARγ positive. The clones that were positive were incubated in 3ml of LB media supplemented with neomycin and cultured at 37°C overnight in a shaker. Thereafter, DNA was isolated and purified from the overnight culture by miniprep.

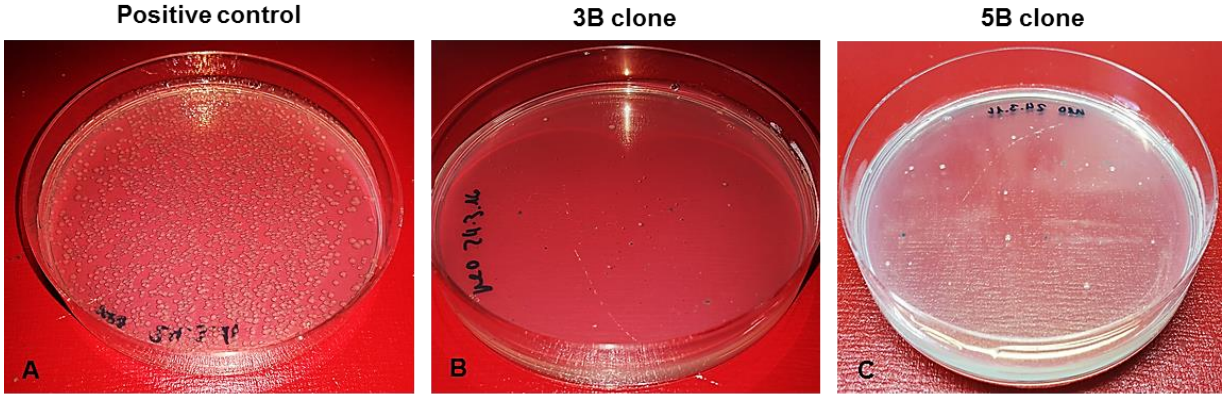

Fig. 4 Neomycin clones. Transformed *E.coli* DH5α were plated on agar plates with LB medium containing neomycin. Colonies containing the ligated PPARγ fragment into pCMV-tag were identified on the plates (B&C). A) Positive control, B) 3B clone, C) 5B clone

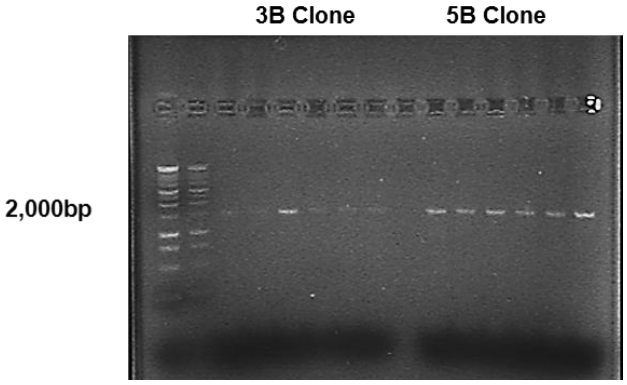

Fig. 5 Colony PCR product. Agarose gel electrophoresis of the colony PCR presenting 1 band corresponding to the pPPARγ insert.

To double-check that indeed the clones contained the right insert, a PCR reaction was set-up with the eluted DNA. Following the PCR, the products were separated on the agarose. Unfortunately, no bands were observed on the agarose gel and we had to conclude that either the isolated DNA was not of good enough quality to perform a PCR-reaction or that the results of the colony-PCR were “false positives”. However, even after several repetitions of the ligation and screening procedure we were unable to obtain the final PCMV-Tag vectors containing PPARγ. We therefore finally decided to use the original PCMV sport PPARγ plasmid that we used for the amplification of the PPARγ ORF for the transfection and overexpression experiments, despite the fact that the PCMV sport vector does not contain a myc tag.

9. References

1. Bonet T. Sepulchretum sive Anatomia practica, ex cadaveribus morbo denatis, proponens historias et observationes omnium penè humani corporis affectuum, ipsorumque causas reconditas revelans. Geneva; 1679.
2. Morgagni G. The seats and causes of disease. investigated by anatomy; in five books, containing a great variety of dissections, with remarks. London: Johnson and Payne; 1769.
3. Baillie M. The morbid anatomy of some of the past important parts of the human body divided into 10 fasciculi. London: W Blum R and Co.; 1799.
4. Badham C. An essay on bronchitis: with a supplement containing remarks on simple pulmonary abscess. London: J Callow 1814.
5. Laënnec R. A treatise on the diseases of the chest (English translation from the French). London: Forbes J. , editor. T and G Underwood; 1821.
6. Hutchinson J. On the capacity of the lungs, and on the respiratory functions, with a view of establishing a precise and easy method of detecting disease by the spirometer. Med Chir Trans 1846;29:137-252.
7. Tiffeneau R, Pinelli. Air circulant et air captif dans l'exploration de la function ventilatrice pulmonaire. Paris Med 1947;37(52):624-628.
8. CibaGuestSymposium. Terminology, definitions, and classification of chronic pulmonary emphysema and related conditions. Thorax 1959(14):286-299.
9. Briscoe WA, Nash ES. The slow space in chronic obstructive pulmonary diseases. Ann N Y Acad Sci 1965;121:706-722.
10. Pauwels RA, Buist AS, Calverley PM, Jenkins CR, Hurd SS. Global strategy for the diagnosis, management, and prevention of chronic obstructive pulmonary disease. NHLBI/WHO Global Initiative for Chronic Obstructive Lung Disease (GOLD) Workshop summary. Am J Respir Crit Care Med 2001;163(5):1256-1276.
11. Chronic obstructive pulmonary disease. National clinical guideline on management of chronic obstructive pulmonary disease in adults in primary and secondary care. Thorax 2004;59 Suppl 1:1-232.
12. Barnes PJ. Alveolar macrophages in chronic obstructive pulmonary disease (COPD). Cell Mol Biol (Noisy-le-grand) 2004;50 Online Pub:OL627-637.
13. Hogg JC, Chu F, Utokaparch S, Woods R, Elliott WM, Buzatu L, Cherniack RM, Rogers RM, Sciurba FC, Coxson HO, Pare PD. The nature of small-airway obstruction in chronic obstructive pulmonary disease. N Engl J Med 2004;350(26):2645-2653.
14. Global Initiative for Chronic Obstructive Lung Disease strategy for the diagnosis, management and prevention of chronic obstructive pulmonary disease: an Asia-Pacific perspective. Respirology 2005;10(1):9-17.
15. Siafakas NM, Vermeire P, Pride NB, Paoletti P, Gibson J, Howard P, Yernault JC, Decramer M, Higenbottam T, Postma DS, et al. Optimal assessment and management of chronic obstructive pulmonary disease (COPD). The European Respiratory Society Task Force. Eur Respir J 1995;8(8):1398-1420.
16. American Thoracic Society/European Respiratory Society Task Force. Standards for the diagnosis and management of patients with COPD. Version 1.2. New York: American Thoracic Society; 2004.
17. Juvelekian G, Stoller J. Chronic obstructive Pulmonary Disease Cleveland: The Cleveland Clinic Foundation; 2012
18. Lopez AD, Murray CC. The global burden of disease, 1990-2020. Nat Med 1998;4(11):1241-1243.
19. Brundtland GH. From the World Health Organization. Reducing risks to health, promoting healthy life. JAMA 2002;288(16):1974.
20. World Health Organization. The top 10 causes of death fact sheet N°310. Overview 2013 (Updated 2014).

21. Sethi JM, Rochester CL. Smoking and chronic obstructive pulmonary disease. Clin Chest Med 2000;21(1):67-86, viii.
22. Church DF, Pryor WA. Free-radical chemistry of cigarette smoke and its toxicological implications. Environ Health Perspect 1985;64:111-126.
23. Rahman I, MacNee W. Role of oxidants/antioxidants in smoking-induced lung diseases. Free Radic Biol Med 1996;21(5):669-681.
24. Salvi SS, Barnes PJ. Chronic obstructive pulmonary disease in non-smokers. Lancet 2009;374(9691):733-743.
25. Kauffmann F, Drouet D, Lellouch J, Brille D. Occupational exposure and 12-year spirometric changes among Paris area workers. Br J Ind Med 1982;39(3):221-232.
26. Pauwels RA, Rabe KF. Burden and clinical features of chronic obstructive pulmonary disease (COPD). Lancet 2004;364(9434):613-620.
27. Eriksson S. Studies in alpha 1-antitrypsin deficiency. Acta Med Scand Suppl 1965;432:1-85.
28. Lorenz E, Stewart H, Daniel J, Nelson C. The effects of breathing tobacco smoke on strain A mice. Cancer Res 1943;3:123.
29. Smith CJ, Hansch C. The relative toxicity of compounds in mainstream cigarette smoke condensate. Food Chem Toxicol 2000;38(7):637-646.
30. Hecht SS. Tobacco smoke carcinogens and breast cancer. Environ Mol Mutagen 2002;39(2-3):119-126.
31. Stabbert R, Voncken P, Rustemeier K, Haussmann HJ, Roemer E, Schaffernicht H, Patskan G. Toxicological evaluation of an electrically heated cigarette. Part 2: Chemical composition of mainstream smoke. J Appl Toxicol 2003;23(5):329-339.
32. Miller LM, Foster WM, Dambach DM, Doebler D, McKinnon M, Killar L, Longphre M. A murine model of cigarette smoke-induced pulmonary inflammation using intranasally administered smoke-conditioned medium. Exp Lung Res 2002;28(6):435-455.
33. Wong LS, Green HM, Feugate JE, Yadav M, Nothnagel EA, Martins-Green M. Effects of "second-hand" smoke on structure and function of fibroblasts, cells that are critical for tissue repair and remodeling. BMC Cell Biol 2004;5:13.
34. Smith J, Woodcock A. Cough and its importance in COPD. Int J Chron Obstruct Pulmon Dis 2006;1(3):305-314.
35. MacNee W. Pathology, pathogenesis and pathophysiology. BMJ 2006 (332):1202-1204.
36. Shao MX, Nakanaga T, Nadel JA. Cigarette smoke induces MUC5AC mucin overproduction via tumor necrosis factor-alpha-converting enzyme in human airway epithelial (NCI-H292) cells. Am J Physiol Lung Cell Mol Physiol 2004;287(2):L420-427.
37. Kim V, Criner GJ. Chronic bronchitis and chronic obstructive pulmonary disease. Am J Respir Crit Care Med 2013;187(3):228-237.
38. Standards for the diagnosis and care of patients with chronic obstructive pulmonary disease. American Thoracic Society. Am J Respir Crit Care Med 1995;152(5 Pt 2):S77-121.
39. Churg A, Wright JL. Proteases and emphysema. Curr Opin Pulm Med 2005;11(2):153-159.
40. Boschetto P, Miniati M, Miotto D, Braccioni F, De Rosa E, Bononi I, Papi A, Saetta M, Fabbri LM, Mapp CE. Predominant emphysema phenotype in chronic obstructive pulmonary. Eur Respir J 2003;21(3):450-454.
41. Shapiro SD. Proteinases in chronic obstructive pulmonary disease. Biochem Soc Trans 2002;30(2):98-102.
42. Cavarra E, Lucattelli M, Gambelli F, Bartalesi B, Fineschi S, Szarka A, Giannerini F, Martorana PA, Lungarella G. Human SLPI inactivation after cigarette smoke exposure in a new in vivo model of pulmonary oxidative stress. Am J Physiol Lung Cell Mol Physiol 2001;281(2):L412-417.
43. Cantin A, Crystal RG. Oxidants, antioxidants and the pathogenesis of emphysema. Eur J Respir Dis Suppl 1985;139:7-17.
44. Linhartova A, Anderson A, Jr., Foraker AG. Radial traction and bronchiolar obstruction in pulmonary emphysema. Observed and theoretical aspects. Arch Pathol 1971;92(5):384-391.

45. Belvisi MG, Hele DJ, Birrell MA. Peroxisome proliferator-activated receptor gamma agonists as therapy for chronic airway inflammation. Eur J Pharmacol 2006;533(1-3):101-109.
46. Vestbo J, Hogg JC. Convergence of the epidemiology and pathology of COPD. Thorax 2006;61(1):86-88.
47. Jones JG, Minty BD, Lawler P, Hulands G, Crawley JC, Veall N. Increased alveolar epithelial permeability in cigarette smokers. Lancet 1980;1(8159):66-68.
48. Hulbert WC, Walker DC, Jackson A, Hogg JC. Airway permeability to horseradish peroxidase in guinea pigs: the repair phase after injury by cigarette smoke. Am Rev Respir Dis 1981;123(3):320-326.
49. Rahman I. Oxidative stress in pathogenesis of chronic obstructive pulmonary disease: cellular and molecular mechanisms. Cell Biochem Biophys 2005;43(1):167-188.
50. Olivera DS, Boggs SE, Beenhouwer C, Aden J, Knall C. Cellular mechanisms of mainstream cigarette smoke-induced lung epithelial tight junction permeability changes in vitro. Inhal Toxicol 2007;19(1):13-22.
51. Tsuji T, Aoshiba K, Nagai A. Cigarette smoke induces senescence in alveolar epithelial cells. Am J Respir Cell Mol Biol 2004;31(6):643-649.
52. Segura-Valdez L, Pardo A, Gaxiola M, Uhal BD, Becerril C, Selman M. Upregulation of gelatinases A and B, collagenases 1 and 2, and increased parenchymal cell death in COPD. Chest 2000;117(3):684-694.
53. Yokohori N, Aoshiba K, Nagai A. Increased levels of cell death and proliferation in alveolar wall cells in patients with pulmonary emphysema. Chest 2004;125(2):626-632.
54. Wickenden JA, Clarke MC, Rossi AG, Rahman I, Faux SP, Donaldson K, MacNee W. Cigarette smoke prevents apoptosis through inhibition of caspase activation and induces necrosis. Am J Respir Cell Mol Biol 2003;29(5):562-570.
55. Wang H, Liu X, Umino T, Skold CM, Zhu Y, Kohyama T, Spurzem JR, Romberger DJ, Rennard SI. Cigarette smoke inhibits human bronchial epithelial cell repair processes. Am J Respir Cell Mol Biol 2001;25(6):772-779.
56. Lannan S, Donaldson K, Brown D, MacNee W. Effect of cigarette smoke and its condensates on alveolar epithelial cell injury in vitro. Am J Physiol 1994;266(1 Pt 1):L92-100.
57. Hellermann GR, Nagy SB, Kong X, Lockey RF, Mohapatra SS. Mechanism of cigarette smoke condensate-induced acute inflammatory response in human bronchial epithelial cells. Respir Res 2002;3:22.
58. Rahman I, Adcock IM. Oxidative stress and redox regulation of lung inflammation in COPD. Eur Respir J 2006;28(1):219-242.
59. Kirkham P, Rahman I. Oxidative stress in asthma and COPD: antioxidants as a therapeutic strategy. Pharmacol Ther 2006;111(2):476-494.
60. Rajendrasozhan S, Yang SR, Edirisinghe I, Yao H, Adenuga D, Rahman I. Deacetylases and NF-kappaB in redox regulation of cigarette smoke-induced lung inflammation: epigenetics in pathogenesis of COPD. Antioxid Redox Signal 2008;10(4):799-811.
61. MacNee W. Oxidants/antioxidants and COPD. Chest 2000;117(5 Suppl 1):303S-317S.
62. Kobayashi A, Kang MI, Watai Y, Tong KI, Shibata T, Uchida K, Yamamoto M. Oxidative and electrophilic stresses activate Nrf2 through inhibition of ubiquitination activity of Keap1. Mol Cell Biol 2006;26(1):221-229.
63. Kensler TW, Wakabayashi N, Biswal S. Cell survival responses to environmental stresses via the Keap1-Nrf2-ARE pathway. Annu Rev Pharmacol Toxicol 2007;47:89-116.
64. Kalyanaraman B. Teaching the basics of redox biology to medical and graduate students: Oxidants, antioxidants and disease mechanisms. Redox Biol 2013;1:244-257.
65. Biswas S, Hwang JW, Kirkham PA, Rahman I. Pharmacological and dietary antioxidant therapies for chronic obstructive pulmonary disease. Curr Med Chem 2013;20(12):1496-1530.
66. Kirkham PA, Barnes PJ. Oxidative stress in COPD. Chest 2013;144(1):266-273.
67. Gutteridge JM. Lipid peroxidation and antioxidants as biomarkers of tissue damage. Clin Chem 1995;41(12 Pt 2):1819-1828.

68. Marwick JA, Kirkham PA, Stevenson CS, Danahay H, Giddings J, Butler K, Donaldson K, Macnee W, Rahman I. Cigarette smoke alters chromatin remodeling and induces proinflammatory genes in rat lungs. Am J Respir Cell Mol Biol 2004;31(6):633-642.
69. Kirkham PA, Spooner G, Rahman I, Rossi AG. Macrophage phagocytosis of apoptotic neutrophils is compromised by matrix proteins modified by cigarette smoke and lipid peroxidation products. Biochem Biophys Res Commun 2004;318(1):32-37.
70. Rahman I. The role of oxidative stress in the pathogenesis of COPD: implications for therapy. Treat Respir Med 2005;4(3):175-200.
71. Barnes PJ. Immunology of asthma and chronic obstructive pulmonary disease. Nat Rev Immunol 2008;8(3):183-192.
72. Barnes PJ. The cytokine network in asthma and chronic obstructive pulmonary disease. J Clin Invest 2008;118(11):3546-3556.
73. Tetley TD. Macrophages and the pathogenesis of COPD. Chest 2002;121(5 Suppl):156S-159S.
74. Traves SL, Culpitt SV, Russell RE, Barnes PJ, Donnelly LE. Increased levels of the chemokines GROalpha and MCP-1 in sputum samples from patients with COPD. Thorax 2002;57(7):590-595.
75. Barnes PJ, Cosio MG. Characterization of T lymphocytes in chronic obstructive pulmonary disease. PLoS Med 2004;1(1):e20.
76. Mannino DM, Buist AS. Global burden of COPD: risk factors, prevalence, and future trends. Lancet 2007;370(9589):765-773.
77. Stockley RA. Neutrophils and the pathogenesis of COPD. Chest 2002;121(5 Suppl):151S-155S.
78. Barnes PJ, Shapiro SD, Pauwels RA. Chronic obstructive pulmonary disease: molecular and cellular mechanisms. Eur Respir J 2003;22(4):672-688.
79. Calverley PM, Anderson JA, Celli B, Ferguson GT, Jenkins C, Jones PW, Yates JC, Vestbo J. Salmeterol and fluticasone propionate and survival in chronic obstructive pulmonary disease. N Engl J Med 2007;356(8):775-789.
80. Powrie DJ, Wilkinson TM, Donaldson GC, Jones P, Scrine K, Viel K, Kesten S, Wedzicha JA. Effect of tiotropium on sputum and serum inflammatory markers and exacerbations in COPD. Eur Respir J 2007;30(3):472-478.
81. Domej W, Oettl K, Renner W. Oxidative stress and free radicals in COPD--implications and relevance for treatment. Int J Chron Obstruct Pulmon Dis 2014;9:1207-1224.
82. Decramer M, Rutten-van Molken M, Dekhuijzen PN, Troosters T, van Herwaarden C, Pellegrino R, van Schayck CP, Olivieri D, Del Donno M, De Backer W, Lankhorst I, Ardia A. Effects of N-acetylcysteine on outcomes in chronic obstructive pulmonary disease (Bronchitis Randomized on NAC Cost-Utility Study, BRONCUS): a randomised placebo-controlled trial. Lancet 2005;365(9470):1552-1560.
83. Rhodin J. Correlation of ultrastructural organization and function in normal and experimentally changed proximal convoluted tubule cells of the mouse kidney. Stockholm: Sweden; 1954.
84. Rouiller C, Bernard W. Microbodies and the problem of mitochondrial regeneration in liver cell. J Biophys Biochem Cytol 1956:355-358.
85. De Duve C, Baudhuin P. Peroxisomes (microbodies and related particles). Physiol Rev 1966;46(2):323-357.
86. Fahimi HD. Cytochemical localization of peroxidase activity in rat hepatic microbodies (peroxisomes). J Histochem Cytochem 1968;16(8):547-550.
87. Fahimi HD. Cytochemical localization of peroxidatic activity of catalase in rat hepatic microbodies (peroxisomes). J Cell Biol 1969;43(2):275-288.
88. Novikoff AB, Goldfischer S. Visualization of peroxisomes (microbodies) and mitochondria with diaminobenzidine. J Histochem Cytochem 1969;17(10):675-680.
89. Nenicu A, Luers GH, Kovacs W, David M, Zimmer A, Bergmann M, Baumgart-Vogt E. Peroxisomes in human and mouse testis: differential expression of peroxisomal proteins in germ cells and distinct somatic cell types of the testis. Biol Reprod 2007;77(6):1060-1072.

90. Distel B, Erdmann R, Gould SJ, Blobel G, Crane DI, Cregg JM, Dodt G, Fujiki Y, Goodman JM, Just WW, Kiel JA, Kunau WH, Lazarow PB, Mannaerts GP, Moser HW, Osumi T, Rachubinski RA, Roscher A, Subramani S, Tabak HF, Tsukamoto T, Valle D, van der Klei I, van Veldhoven PP, Veenhuis M. A unified nomenclature for peroxisome biogenesis factors. J Cell Biol 1996;135(1):1-3.
91. Anthonio EA, Brees C, Baumgart-Vogt E, Hongu T, Huybrechts SJ, Van Dijck P, Mannaerts GP, Kanaho Y, Van Veldhoven PP, Fransen M. Small G proteins in peroxisome biogenesis: the potential involvement of ADP-ribosylation factor 6. BMC Cell Biol 2009;10:58.
92. Nagotu S, Saraya R, Otzen M, Veenhuis M, van der Klei IJ. Peroxisome proliferation in Hansenula polymorpha requires Dnm1p which mediates fission but not de novo formation. Biochim Biophys Acta 2008;1783(5):760-769.
93. Hoepfner D, Schildknegt D, Braakman I, Philippsen P, Tabak HF. Contribution of the endoplasmic reticulum to peroxisome formation. Cell 2005;122(1):85-95.
94. Tam YY, Fagarasanu A, Fagarasanu M, Rachubinski RA. Pex3p initiates the formation of a preperoxisomal compartment from a subdomain of the endoplasmic reticulum in Saccharomyces cerevisiae. J Biol Chem 2005;280(41):34933-34939.
95. Honsho M, Tamura S, Shimozawa N, Suzuki Y, Kondo N, Fujiki Y. Mutation in PEX16 is causal in the peroxisome-deficient Zellweger syndrome of complementation group D. Am J Hum Genet 1998;63(6):1622-1630.
96. Shimozawa N, Suzuki Y, Zhang Z, Imamura A, Ghaedi K, Fujiki Y, Kondo N. Identification of PEX3 as the gene mutated in a Zellweger syndrome patient lacking peroxisomal remnant structures. Hum Mol Genet 2000;9(13):1995-1999.
97. Lazarow PB, Fujiki Y. Biogenesis of peroxisomes. Annu Rev Cell Biol 1985;1:489-530.
98. Eckert JH, Erdmann R. Peroxisome biogenesis. Rev Physiol Biochem Pharmacol 2003;147:75-121.
99. Smith JJ, Aitchison JD. Peroxisomes take shape. Nat Rev Mol Cell Biol 2013;14(12):803-817.
100. Lazarow PB. Peroxisome structure, function, and biogenesis--human patients and yeast mutants show strikingly similar defects in peroxisome biogenesis. J Neuropathol Exp Neurol 1995;54(5):720-725.
101. Gould SJ, Keller GA, Hosken N, Wilkinson J, Subramani S. A conserved tripeptide sorts proteins to peroxisomes. J Cell Biol 1989;108(5):1657-1664.
102. Rachubinski RA, Subramani S. How proteins penetrate peroxisomes. Cell 1995;83(4):525-528.
103. Flynn CR, Mullen RT, Trelease RN. Mutational analyses of a type 2 peroxisomal targeting signal that is capable of directing oligomeric protein import into tobacco BY-2 glyoxysomes. Plant J 1998;16(6):709-720.
104. Colasante C, Chen J, Ahlemeyer B, Baumgart-Vogt E. Peroxisomes in cardiomyocytes and the peroxisome / peroxisome proliferator-activated receptor-loop. Thromb Haemost 2015;113(3):452-463.
105. Dammai V, Subramani S. The human peroxisomal targeting signal receptor, Pex5p, is translocated into the peroxisomal matrix and recycled to the cytosol. Cell 2001;105(2):187-196.
106. Islinger M, Lüers GH, Li KW, Loos M, Völkl A. Rat liver peroxisomes after fibrate treatment. A survey using quantitative mass spectrometry. J Biol Chem 2007;282(32):23055-23069.
107. de Duve C, Palade GE. Albert Claude, 1899-1983. Nature 1983;304(5927):588.
108. Hajra AK, Bishop JE. Glycerolipid biosynthesis in peroxisomes via the acyl dihydroxyacetone phosphate pathway. Ann N Y Acad Sci 1982;386:170-182.
109. Wanders RJ, Waterham HR. Biochemistry of mammalian peroxisomes revisited. Annu Rev Biochem 2006;75:295-332.
110. Thompson SL, Krisans SK. Rat liver peroxisomes catalyze the initial step in cholesterol synthesis. The condensation of acetyl-CoA units into acetoacetyl-CoA. J Biol Chem 1990;265(10):5731-5735.

111. Kovacs WJ, Olivier LM, Krisans SK. Central role of peroxisomes in isoprenoid biosynthesis. Prog Lipid Res 2002;41(5):369-391.
112. Kovacs WJ, Tape KN, Shackelford JE, Duan X, Kasumov T, Kelleher JK, Brunengraber H, Krisans SK. Localization of the pre-squalene segment of the isoprenoid biosynthetic pathway in mammalian peroxisomes. Histochem Cell Biol 2007;127(3):273-290.
113. Iida R, Yasuda T, Tsubota E, Takatsuka H, Masuyama M, Matsuki T, Kishi K. M-LP, Mpv17-like protein, has a peroxisomal membrane targeting signal comprising a transmembrane domain and a positively charged loop and up-regulates expression of the manganese superoxide dismutase gene. J Biol Chem 2003;278(8):6301-6306.
114. Loughran PA, Stolz DB, Barrick SR, Wheeler DS, Friedman PA, Rachubinski RA, Watkins SC, Billiar TR. PEX7 and EBP50 target iNOS to the peroxisome in hepatocytes. Nitric Oxide 2013;31:9-19.
115. Bonekamp NA, Volkl A, Fahimi HD, Schrader M. Reactive oxygen species and peroxisomes: struggling for balance. Biofactors 2009;35(4):346-355.
116. Karnati S, Luers G, Pfreimer S, Baumgart-Vogt E. Mammalian SOD2 is exclusively located in mitochondria and not present in peroxisomes. Histochem Cell Biol 2013;140(2):105-117.
117. Spinazzola A, Viscomi C, Fernandez-Vizarra E, Carrara F, D'Adamo P, Calvo S, Marsano RM, Donnini C, Weiher H, Strisciuglio P, Parini R, Sarzi E, Chan A, DiMauro S, Rotig A, Gasparini P, Ferrero I, Mootha VK, Tiranti V, Zeviani M. MPV17 encodes an inner mitochondrial membrane protein and is mutated in infantile hepatic mitochondrial DNA depletion. Nat Genet 2006;38(5):570-575.
118. Huybrechts SJ, Van Veldhoven PP, Brees C, Mannaerts GP, Los GV, Fransen M. Peroxisome dynamics in cultured mammalian cells. Traffic 2009;10(11):1722-1733.
119. Klionsky DJ, Cuervo AM, Dunn WA, Jr., Levine B, van der Klei I, Seglen PO. How shall I eat thee? Autophagy 2007;3(5):413-416.
120. Aksam EB, Koek A, Kiel JA, Jourdan S, Veenhuis M, van der Klei IJ. A peroxisomal lon protease and peroxisome degradation by autophagy play key roles in vitality of Hansenula polymorpha cells. Autophagy 2007;3(2):96-105.
121. Manjithaya R, Nazarko TY, Farre JC, Subramani S. Molecular mechanism and physiological role of pexophagy. FEBS Lett 2010;584(7):1367-1373.
122. Mizushima N, Yoshimori T, Ohsumi Y. The role of Atg proteins in autophagosome formation. Annu Rev Cell Dev Biol 2011;27:107-132.
123. Chen Y, Klionsky DJ. The regulation of autophagy - unanswered questions. J Cell Sci 2011;124(Pt 2):161-170.
124. Braverman NE, D'Agostino MD, Maclean GE. Peroxisome biogenesis disorders: Biological, clinical and pathophysiological perspectives. Dev Disabil Res Rev 2013;17(3):187-196.
125. Waterham HR, Ebberink MS. Genetics and molecular basis of human peroxisome biogenesis disorders. Biochim Biophys Acta 2012;1822(9):1430-1441.
126. Pineda M, Giros M, Roels F, Espeel M, Ruiz M, Moser A, Moser HW, Wanders RJ, Pavia C, Conill J, Aracil A, Amat L, Pampols T. Diagnosis and follow-up of a case of peroxisomal disorder with peroxisomal mosaicism. J Child Neurol 1999;14(7):434-439.
127. Gootjes J, Schmohl F, Mooijer PA, Dekker C, Mandel H, Topcu M, Huemer M, Von Schutz M, Marquardt T, Smeitink JA, Waterham HR, Wanders RJ. Identification of the molecular defect in patients with peroxisomal mosaicism using a novel method involving culturing of cells at 40 degrees C: implications for other inborn errors of metabolism. Hum Mutat 2004;24(2):130-139.
128. Goldfischer S, Moore CL, Johnson AB, Spiro AJ, Valsamis MP, Wisniewski HK, Ritch RH, Norton WT, Rapin I, Gartner LM. Peroxisomal and mitochondrial defects in the cerebro-hepato-renal syndrome. Science 1973;182(4107):62-64.
129. Barkovich AJ, Peck WW. MR of Zellweger syndrome. AJNR Am J Neuroradiol 1997;18(6):1163-1170.

130. Jansen GA, van den Brink DM, Ofman R, Draghici O, Dacremont G, Wanders RJ. Identification of pristanal dehydrogenase activity in peroxisomes: conclusive evidence that the complete phytanic acid alpha-oxidation pathway is localized in peroxisomes. Biochem Biophys Res Commun 2001;283(3):674-679.
131. Wanders RJ, Waterham HR. Peroxisomal disorders I: biochemistry and genetics of peroxisome biogenesis disorders. Clin Genet 2005;67(2):107-133.
132. Wanders RJ, Ferdinandusse S, Brites P, Kemp S. Peroxisomes, lipid metabolism and lipotoxicity. Biochim Biophys Acta 2010;1801(3):272-280.
133. Petrik P. Fine structural identification of peroxisomes in mouse and rat bronchiolar and alveolar epithelium. J Histochem Cytochem 1971;19(6):339-348.
134. Schneeberger EE. A comparative cytochemical study of microbodies (peroxisomes) in great alveolar cells of rodents, rabbit and monkey. J Histochem Cytochem 1972;20(3):180-191.
135. Goldenberg H, Huttinger M, Kollner U, Kramar R, Pavelka M. Catalase positive particles from pig lung. Biochemical preparations and morphological studies. Histochemistry 1978;56(3-4):253-264.
136. Karnati S, Baumgart-Vogt E. Peroxisomes in airway epithelia and future prospects of these organelles for pulmonary cell biology. Histochem Cell Biol 2009;131(4):447-454.
137. Karnati S, Baumgart-Vogt E. Peroxisomes in mouse and human lung: their involvement in pulmonary lipid metabolism. Histochem Cell Biol 2008;130(4):719-740.
138. Ossendorp BC, Voorhout WF, van Golde LM, Wirtz KW, Batenburg JJ. Identification of the non-specific lipid-transfer protein (sterol carrier protein 2) in peroxisomes of lung type II cells. Biochem Biophys Res Commun 1994;205(3):1581-1588.
139. Rahman I, MacNee W. Oxidative stress and regulation of glutathione in lung inflammation. Eur Respir J 2000;16(3):534-554.
140. Evans RM. The steroid and thyroid hormone receptor superfamily. Science 1988;240(4854):889-895.
141. Calkin AC, Giunti S, Jandeleit-Dahm KA, Allen TJ, Cooper ME, Thomas MC. PPAR-alpha and -gamma agonists attenuate diabetic kidney disease in the apolipoprotein E knockout mouse. Nephrol Dial Transplant 2006;21(9):2399-2405.
142. Kliewer SA, Forman BM, Blumberg B, Ong ES, Borgmeyer U, Mangelsdorf DJ, Umesono K, Evans RM. Differential expression and activation of a family of murine peroxisome proliferator-activated receptors. Proc Natl Acad Sci U S A 1994;91(15):7355-7359.
143. Braissant O, Foufelle F, Scotto C, Dauca M, Wahli W. Differential expression of peroxisome proliferator-activated receptors (PPARs): tissue distribution of PPAR-alpha, -beta, and -gamma in the adult rat. Endocrinology 1996;137(1):354-366.
144. Nagy L, Tontonoz P, Alvarez JG, Chen H, Evans RM. Oxidized LDL regulates macrophage gene expression through ligand activation of PPARgamma. Cell 1998;93(2):229-240.
145. Shibata T, Matsui K, Nagao K, Shinkai H, Yonemori F, Wakitani K. Pharmacological profiles of a novel oral antidiabetic agent, JTT-501, an isoxazolidinedione derivative. Eur J Pharmacol 1999;364(2-3):211-219.
146. Suh N, Wang Y, Williams CR, Risingsong R, Gilmer T, Willson TM, Sporn MB. A new ligand for the peroxisome proliferator-activated receptor-gamma (PPAR-gamma), GW7845, inhibits rat mammary carcinogenesis. Cancer Res 1999;59(22):5671-5673.
147. Berger J, Moller DE. The mechanisms of action of PPARs. Annu Rev Med 2002;53:409-435.
148. Kota BP, Huang TH, Roufogalis BD. An overview on biological mechanisms of PPARs. Pharmacol Res 2005;51(2):85-94.
149. IJpenberg A, Jeannin E, Wahli W, Desvergne B. Polarity and specific sequence requirements of peroxisome proliferator-activated receptor (PPAR)/retinoid X receptor heterodimer binding to DNA. A functional analysis of the malic enzyme gene PPAR response element. J Biol Chem 1997;272(32):20108-20117.
150. Repine JE, Bast A, Lankhorst I. Oxidative stress in chronic obstructive pulmonary disease. Oxidative Stress Study Group. Am J Respir Crit Care Med 1997;156(2 Pt 1):341-357.

151. Schrader M, Fahimi HD. Mammalian peroxisomes and reactive oxygen species. Histochem Cell Biol 2004;122(4):383-393.
152. Paola RD, Cuzzocrea S. Peroxisome proliferator-activated receptors and acute lung injury. PPAR Res 2007;2007:63745.
153. Kubota N, Terauchi Y, Miki H, Tamemoto H, Yamauchi T, Komeda K, Satoh S, Nakano R, Ishii C, Sugiyama T, Eto K, Tsubamoto Y, Okuno A, Murakami K, Sekihara H, Hasegawa G, Naito M, Toyoshima Y, Tanaka S, Shiota K, Kitamura T, Fujita T, Ezaki O, Aizawa S, Kadowaki T, et al. PPAR gamma mediates high-fat diet-induced adipocyte hypertrophy and insulin resistance. Mol Cell 1999;4(4):597-609.
154. Barak Y, Nelson MC, Ong ES, Jones YZ, Ruiz-Lozano P, Chien KR, Koder A, Evans RM. PPAR gamma is required for placental, cardiac, and adipose tissue development. Mol Cell 1999;4(4):585-595.
155. Bogue CW, Lou LJ, Vasavada H, Wilson CM, Jacobs HC. Expression of Hoxb genes in the developing mouse foregut and lung. Am J Respir Cell Mol Biol 1996;15(2):163-171.
156. Warburton D, El-Hashash A, Carraro G, Tiozzo C, Sala F, Rogers O, De Langhe S, Kemp PJ, Riccardi D, Torday J, Bellusci S, Shi W, Lubkin SR, Jesudason E. Lung organogenesis. Curr Top Dev Biol 2010;90:73-158.
157. Koutnikova H, Cock TA, Watanabe M, Houten SM, Champy MF, Dierich A, Auwerx J. Compensation by the muscle limits the metabolic consequences of lipodystrophy in PPAR gamma hypomorphic mice. Proc Natl Acad Sci U S A 2003;100(24):14457-14462.
158. He W, Barak Y, Hevener A, Olson P, Liao D, Le J, Nelson M, Ong E, Olefsky JM, Evans RM. Adipose-specific peroxisome proliferator-activated receptor gamma knockout causes insulin resistance in fat and liver but not in muscle. Proc Natl Acad Sci U S A 2003;100(26):15712-15717.
159. Hevener AL, He W, Barak Y, Le J, Bandyopadhyay G, Olson P, Wilkes J, Evans RM, Olefsky J. Muscle-specific Pparg deletion causes insulin resistance. Nat Med 2003;9(12):1491-1497.
160. Zhang J, Fu M, Cui T, Xiong C, Xu K, Zhong W, Xiao Y, Floyd D, Liang J, Li E, Song Q, Chen YE. Selective disruption of PPARgamma 2 impairs the development of adipose tissue and insulin sensitivity. Proc Natl Acad Sci U S A 2004;101(29):10703-10708.
161. Tsai YS, Kim HJ, Takahashi N, Kim HS, Hagaman JR, Kim JK, Maeda N. Hypertension and abnormal fat distribution but not insulin resistance in mice with P465L PPARgamma. J Clin Invest 2004;114(2):240-249.
162. Simon DM, Tsai LW, Ingenito EP, Starcher BC, Mariani TJ. PPARgamma deficiency results in reduced lung elastic recoil and abnormalities in airspace distribution. Respir Res 2010;11:69.
163. Simon DM, Arikan MC, Srisuma S, Bhattacharya S, Andalcio T, Shapiro SD, Mariani TJ. Epithelial cell PPARgamma is an endogenous regulator of normal lung maturation and maintenance. Proc Am Thorac Soc 2006;3(6):510-511.
164. Solleti SK, Simon DM, Srisuma S, Arikan MC, Bhattacharya S, Rangasamy T, Bijli KM, Rahman A, Crossno JT, Jr., Shapiro SD, Mariani TJ. Airway epithelial cell PPARgamma modulates cigarette smoke-induced chemokine expression and emphysema susceptibility in mice. Am J Physiol Lung Cell Mol Physiol 2015;309(3):L293-304.
165. Shan M, You R, Yuan X, Frazier MV, Porter P, Seryshev A, Hong JS, Song LZ, Zhang Y, Hilsenbeck S, Whitehead L, Zarinkamar N, Perusich S, Corry DB, Kheradmand F. Agonistic induction of PPARgamma reverses cigarette smoke-induced emphysema. J Clin Invest 2014;124(3):1371-1381.
166. Tontonoz P, Nagy L, Alvarez JG, Thomazy VA, Evans RM. PPARgamma promotes monocyte/macrophage differentiation and uptake of oxidized LDL. Cell 1998;93(2):241-252.
167. Jiang C, Ting AT, Seed B. PPAR-gamma agonists inhibit production of monocyte inflammatory cytokines. Nature 1998;391(6662):82-86.
168. Spiegelman BM. PPARgamma in monocytes: less pain, any gain? Cell 1998;93(2):153-155.
169. Reddy RC. Immunomodulatory role of PPAR-gamma in alveolar macrophages. J Investig Med 2008;56(2):522-527.

170. Lee SY, Kang EJ, Hur GY, Jung KH, Jung HC, Kim JH, Shin C, In KH, Kang KH, Yoo SH, Shim JJ. Peroxisome proliferator-activated receptor-gamma inhibits cigarette smoke solution-induced mucin production in human airway epithelial (NCI-H292) cells. Am J Physiol Lung Cell Mol Physiol 2006;291(1):L84-90.
171. Lee JH, Hanaoka M, Kitaguchi Y, Kraskauskas D, Shapiro L, Voelkel NF, Taraseviciene-Stewart L. Imbalance of apoptosis and cell proliferation contributes to the development and persistence of emphysema. Lung 2012;190(1):69-82.
172. Cho HY, Gladwell W, Wang X, Chorley B, Bell D, Reddy SP, Kleeberger SR. Nrf2-regulated PPAR{gamma} expression is critical to protection against acute lung injury in mice. Am J Respir Crit Care Med 2010;182(2):170-182.
173. Culver DA, Barna BP, Raychaudhuri B, Bonfield TL, Abraham S, Malur A, Farver CF, Kavuru MS, Thomassen MJ. Peroxisome proliferator-activated receptor gamma activity is deficient in alveolar macrophages in pulmonary sarcoidosis. Am J Respir Cell Mol Biol 2004;30(1):1-5.
174. Belvisi MG, Hele DJ. Peroxisome proliferator-activated receptors as novel targets in lung disease. Chest 2008;134(1):152-157.
175. Shen Y, Chen L, Wang T, Wen F. PPARgamma as a Potential Target to Treat Airway Mucus Hypersecretion in Chronic Airway Inflammatory Diseases. PPAR Res 2012;2012:256874.
176. Li J, Dai A, Hu R, Zhu L, Tan S. Positive correlation between PPARgamma/PGC-1alpha and gamma-GCS in lungs of rats and patients with chronic obstructive pulmonary disease. Acta Biochim Biophys Sin (Shanghai) 2010;42(9):603-614.
177. Becker J, Delayre-Orthez C, Frossard N, Pons F. Regulation of inflammation by PPARs: a future approach to treat lung inflammatory diseases? Fundam Clin Pharmacol 2006;20(5):429-447.
178. Seimetz M, Parajuli N, Pichl A, Veit F, Kwapiszewska G, Weisel FC, Milger K, Egemnazarov B, Turowska A, Fuchs B, Nikam S, Roth M, Sydykov A, Medebach T, Klepetko W, Jaksch P, Dumitrascu R, Garn H, Voswinckel R, Kostin S, Seeger W, Schermuly RT, Grimminger F, Ghofrani HA, Weissmann N. Inducible NOS inhibition reverses tobacco-smoke-induced emphysema and pulmonary hypertension in mice. Cell 2011;147(2):293-305.
179. Jat PS, Noble MD, Ataliotis P, Tanaka Y, Yannoutsos N, Larsen L, Kioussis D. Direct derivation of conditionally immortal cell lines from an H-2Kb-tsA58 transgenic mouse. Proc Natl Acad Sci U S A 1991;88(12):5096-5100.
180. Bradford MM. A rapid and sensitive method for the quantitation of microgram quantities of protein utilizing the principle of protein-dye binding. Anal Biochem 1976;72:248-254.
181. Buist AS, McBurnie MA, Vollmer WM, Gillespie S, Burney P, Mannino DM, Menezes AM, Sullivan SD, Lee TA, Weiss KB, Jensen RL, Marks GB, Gulsvik A, Nizankowska-Mogilnicka E. International variation in the prevalence of COPD (the BOLD Study): a population-based prevalence study. Lancet 2007;370(9589):741-750.
182. Fukuchi Y, Nishimura M, Ichinose M, Adachi M, Nagai A, Kuriyama T, Takahashi K, Nishimura K, Ishioka S, Aizawa H, Zaher C. COPD in Japan: the Nippon COPD Epidemiology study. Respirology 2004;9(4):458-465.
183. Van Schayck CP, Loozen JM, Wagena E, Akkermans RP, Wesseling GJ. Detecting patients at a high risk of developing chronic obstructive pulmonary disease in general practice: cross sectional case finding study. BMJ 2002;324(7350):1370.
184. Rubin BK. Mucus and mucins. Otolaryngol Clin North Am 2010;43(1):27-34, vii-viii.
185. Rose MC, Nickola TJ, Voynow JA. Airway mucus obstruction: mucin glycoproteins, MUC gene regulation and goblet cell hyperplasia. Am J Respir Cell Mol Biol 2001;25(5):533-537.
186. Chen Y, Zhao YH, Di YP, Wu R. Characterization of human mucin 5B gene expression in airway epithelium and the genomic clone of the amino-terminal and 5'-flanking region. Am J Respir Cell Mol Biol 2001;25(5):542-553.
187. Caramori G, Di Gregorio C, Carlstedt I, Casolari P, Guzzinati I, Adcock IM, Barnes PJ, Ciaccia A, Cavallesco G, Chung KF, Papi A. Mucin expression in peripheral airways of patients with chronic obstructive pulmonary disease. Histopathology 2004;45(5):477-484.

188. Caramori G, Casolari P, Di Gregorio C, Saetta M, Baraldo S, Boschetto P, Ito K, Fabbri LM, Barnes PJ, Adcock IM, Cavallesco G, Chung KF, Papi A. MUC5AC expression is increased in bronchial submucosal glands of stable COPD patients. Histopathology 2009;55(3):321-331.
189. Shapiro SD. Evolving concepts in the pathogenesis of chronic obstructive pulmonary disease. Clin Chest Med 2000;21(4):621-632.
190. Gould SJ, Kalish JE, Morrell JC, Bjorkman J, Urquhart AJ, Crane DI. Pex13p is an SH3 protein of the peroxisome membrane and a docking factor for the predominantly cytoplasmic PTs1 receptor. J Cell Biol 1996;135(1):85-95.
191. Gan WQ, Man SF, Senthilselvan A, Sin DD. Association between chronic obstructive pulmonary disease and systemic inflammation: a systematic review and a meta-analysis. Thorax 2004;59(7):574-580.
192. Wouters EF, Groenewegen KH, Dentener MA, Vernooy JH. Systemic inflammation in chronic obstructive pulmonary disease: the role of exacerbations. Proc Am Thorac Soc 2007;4(8):626-634.
193. Baumgart E, Fahimi HD, Steininger H, Grabenbauer M. A review of morphological techniques for detection of peroxisomal (and mitochondrial) proteins and their corresponding mRNAs during ontogenesis in mice: application to the PEX5-knockout mouse with Zellweger syndrome. Microsc Res Tech 2003;61(2):121-138.
194. Terlecky SR, Nuttley WM, McCollum D, Sock E, Subramani S. The Pichia pastoris peroxisomal protein PAS8p is the receptor for the C-terminal tripeptide peroxisomal targeting signal. EMBO J 1995;14(15):3627-3634.
195. Erdmann R, Blobel G. Identification of Pex13p a peroxisomal membrane receptor for the PTS1 recognition factor. J Cell Biol 1996;135(1):111-121.
196. Girzalsky W, Rehling P, Stein K, Kipper J, Blank L, Kunau WH, Erdmann R. Involvement of Pex13p in Pex14p localization and peroxisomal targeting signal 2-dependent protein import into peroxisomes. J Cell Biol 1999;144(6):1151-1162.
197. Kostadinova R, Wahli W, Michalik L. PPARs in diseases: control mechanisms of inflammation. Curr Med Chem 2005;12(25):2995-3009.
198. Galli F, Battistoni A, Gambari R, Pompella A, Bragonzi A, Pilolli F, Iuliano L, Piroddi M, Dechecchi MC, Cabrini G. Oxidative stress and antioxidant therapy in cystic fibrosis. Biochim Biophys Acta 2012;1822(5):690-713.
199. Reddy PH. Mitochondrial Dysfunction and Oxidative Stress in Asthma: Implications for Mitochondria-Targeted Antioxidant Therapeutics. Pharmaceuticals (Basel) 2011;4(3):429-456.
200. Walters DM, Cho HY, Kleeberger SR. Oxidative stress and antioxidants in the pathogenesis of pulmonary fibrosis: a potential role for Nrf2. Antioxid Redox Signal 2008;10(2):321-332.
201. Schrader M, Fahimi HD. Peroxisomes and oxidative stress. Biochim Biophys Acta 2006;1763(12):1755-1766.
202. Rabe KF, Hurd S, Anzueto A, Barnes PJ, Buist SA, Calverley P, Fukuchi Y, Jenkins C, Rodriguez-Roisin R, van Weel C, Zielinski J. Global strategy for the diagnosis, management, and prevention of chronic obstructive pulmonary disease: GOLD executive summary. Am J Respir Crit Care Med 2007;176(6):532-555.
203. Lakshmi SP, Reddy AT, Zhang Y, Sciurba FC, Mallampalli RK, Duncan SR, Reddy RC. Down-regulated peroxisome proliferator-activated receptor gamma (PPARgamma) in lung epithelial cells promotes a PPARgamma agonist-reversible proinflammatory phenotype in chronic obstructive pulmonary disease (COPD). J Biol Chem 2014;289(10):6383-6393.
204. Amoruso A, Bardelli C, Gunella G, Fresu LG, Ferrero V, Brunelleschi S. Quantification of PPAR-gamma protein in monocyte/macrophages from healthy smokers and non-smokers: a possible direct effect of nicotine. Life Sci 2007;81(11):906-915.
205. Lea S, Plumb J, Metcalfe H, Spicer D, Woodman P, Fox JC, Singh D. The effect of peroxisome proliferator-activated receptor-gamma ligands on in vitro and in vivo models of COPD. Eur Respir J 2014;43(2):409-420.

206. Inoue H, Tanabe T, Umesono K. Feedback control of cyclooxygenase-2 expression through PPARgamma. J Biol Chem 2000;275(36):28028-28032.
207. Park EY, Cho IJ, Kim SG. Transactivation of the PPAR-responsive enhancer module in chemopreventive glutathione S-transferase gene by the peroxisome proliferator-activated receptor-gamma and retinoid X receptor heterodimer. Cancer Res 2004;64(10):3701-3713.
208. Wang X, Wang Z, Liu JZ, Hu JX, Chen HL, Li WL, Hai CX. Double antioxidant activities of rosiglitazone against high glucose-induced oxidative stress in hepatocyte. Toxicol In Vitro 2011;25(4):839-847.
209. Graeser AC, Boesch-Saadatmandi C, Lippmann J, Wagner AE, Huebbe P, Storm N, Hoppner W, Wiswedel I, Gardemann A, Minihane AM, Doring F, Rimbach G. Nrf2-dependent gene expression is affected by the proatherogenic apoE4 genotype-studies in targeted gene replacement mice. J Mol Med (Berl) 2011;89(10):1027-1035.
210. Lopez-Huertas E, Charlton WL, Johnson B, Graham IA, Baker A. Stress induces peroxisome biogenesis genes. EMBO J 2000;19(24):6770-6777.
211. Delmaghani S, Defourny J, Aghaie A, Beurg M, Dulon D, Thelen N, Perfettini I, Zelles T, Aller M, Meyer A, Emptoz A, Giraudet F, Leibovici M, Dartevelle S, Soubigou G, Thiry M, Vizi ES, Safieddine S, Hardelin JP, Avan P, Petit C. Hypervulnerability to Sound Exposure through Impaired Adaptive Proliferation of Peroxisomes. Cell 2015;163(4):894-906.
212. Kumar S, Singh R, Williams CP, van der Klei IJ. Stress exposure results in increased peroxisomal levels of yeast Pnc1 and Gpd1, which are imported via a piggy-backing mechanism. Biochim Biophys Acta 2016;1863(1):148-156.
213. Tiew TW, Sheahan MB, Rose RJ. Peroxisomes contribute to reactive oxygen species homeostasis and cell division induction in Arabidopsis protoplasts. Front Plant Sci 2015;6:658.
214. Ivashchenko O, Van Veldhoven PP, Brees C, Ho YS, Terlecky SR, Fransen M. Intraperoxisomal redox balance in mammalian cells: oxidative stress and interorganellar cross-talk. Mol Biol Cell 2011;22(9):1440-1451.
215. Muller CC, Nguyen TH, Ahlemeyer B, Meshram M, Santrampurwala N, Cao S, Sharp P, Fietz PB, Baumgart-Vogt E, Crane DI. PEX13 deficiency in mouse brain as a model of Zellweger syndrome: abnormal cerebellum formation, reactive gliosis and oxidative stress. Dis Model Mech 2011;4(1):104-119.
216. Bottelbergs A, Verheijden S, Van Veldhoven PP, Just W, Devos R, Baes M. Peroxisome deficiency but not the defect in ether lipid synthesis causes activation of the innate immune system and axonal loss in the central nervous system. J Neuroinflammation 2012;9:61.
217. Khoo NK, Hebbar S, Zhao W, Moore SA, Domann FE, Robbins ME. Differential activation of catalase expression and activity by PPAR agonists: implications for astrocyte protection in anti-glioma therapy. Redox Biol 2013;1:70-79.
218. Hirotsu Y, Katsuoka F, Funayama R, Nagashima T, Nishida Y, Nakayama K, Engel JD, Yamamoto M. Nrf2-MafG heterodimers contribute globally to antioxidant and metabolic networks. Nucleic Acids Res 2012;40(20):10228-10239.
219. Motohashi H, Katsuoka F, Engel JD, Yamamoto M. Small Maf proteins serve as transcriptional cofactors for keratinocyte differentiation in the Keap1-Nrf2 regulatory pathway. Proc Natl Acad Sci U S A 2004;101(17):6379-6384.
220. Itoh K, Chiba T, Takahashi S, Ishii T, Igarashi K, Katoh Y, Oyake T, Hayashi N, Satoh K, Hatayama I, Yamamoto M, Nabeshima Y. An Nrf2/small Maf heterodimer mediates the induction of phase II detoxifying enzyme genes through antioxidant response elements. Biochem Biophys Res Commun 1997;236(2):313-322.
221. Nguyen T, Sherratt PJ, Pickett CB. Regulatory mechanisms controlling gene expression mediated by the antioxidant response element. Annu Rev Pharmacol Toxicol 2003;43:233-260.
222. Hayes JD, Chanas SA, Henderson CJ, McMahon M, Sun C, Moffat GJ, Wolf CR, Yamamoto M. The Nrf2 transcription factor contributes both to the basal expression of glutathione S-transferases in mouse liver and to their induction by the chemopreventive synthetic antioxidants, butylated hydroxyanisole and ethoxyquin. Biochem Soc Trans 2000;28(2):33-41.

223. Chan K, Kan YW. Nrf2 is essential for protection against acute pulmonary injury in mice. Proc Natl Acad Sci U S A 1999;96(22):12731-12736.
224. Alam J, Stewart D, Touchard C, Boinapally S, Choi AM, Cook JL. Nrf2, a Cap'n'Collar transcription factor, regulates induction of the heme oxygenase-1 gene. J Biol Chem 1999;274(37):26071-26078.
225. Venugopal R, Jaiswal AK. Nrf2 and Nrf1 in association with Jun proteins regulate antioxidant response element-mediated expression and coordinated induction of genes encoding detoxifying enzymes. Oncogene 1998;17(24):3145-3156.
226. Ishii T, Itoh K, Takahashi S, Sato H, Yanagawa T, Katoh Y, Bannai S, Yamamoto M. Transcription factor Nrf2 coordinately regulates a group of oxidative stress-inducible genes in macrophages. J Biol Chem 2000;275(21):16023-16029.
227. Zoeller RA, Morand OH, Raetz CR. A possible role for plasmalogens in protecting animal cells against photosensitized killing. J Biol Chem 1988;263(23):11590-11596.
228. Khaselev N, Murphy RC. Structural characterization of oxidized phospholipid products derived from arachidonate-containing plasmenyl glycerophosphocholine. J Lipid Res 2000;41(4):564-572.
229. Morand OH, Zoeller RA, Raetz CR. Disappearance of plasmalogens from membranes of animal cells subjected to photosensitized oxidation. J Biol Chem 1988;263(23):11597-11606.
230. Zommara M, Tachibana N, Mitsui K, Nakatani N, Sakono M, Ikeda I, Imaizumi K. Inhibitory effect of ethanolamine plasmalogen on iron- and copper-dependent lipid peroxidation. Free Radic Biol Med 1995;18(3):599-602.
231. Kishimoto T. The biology of interleukin-6. Blood 1989;74(1):1-10.
232. Kolsum U, Roy K, Starkey C, Borrill Z, Truman N, Vestbo J, Singh D. The repeatability of interleukin-6, tumor necrosis factor-alpha, and C-reactive protein in COPD patients over one year. Int J Chron Obstruct Pulmon Dis 2009;4:149-156.
233. Vanfleteren LE, Spruit MA, Groenen M, Gaffron S, van Empel VP, Bruijnzeel PL, Rutten EP, Op 't Roodt J, Wouters EF, Franssen FM. Clusters of comorbidities based on validated objective measurements and systemic inflammation in patients with chronic obstructive pulmonary disease. Am J Respir Crit Care Med 2013;187(7):728-735.
234. Bucchioni E, Kharitonov SA, Allegra L, Barnes PJ. High levels of interleukin-6 in the exhaled breath condensate of patients with COPD. Respir Med 2003;97(12):1299-1302.
235. Churg A, Wang RD, Tai H, Wang X, Xie C, Wright JL. Tumor necrosis factor-alpha drives 70% of cigarette smoke-induced emphysema in the mouse. Am J Respir Crit Care Med 2004;170(5):492-498.
236. Keatings VM, Collins PD, Scott DM, Barnes PJ. Differences in interleukin-8 and tumor necrosis factor-alpha in induced sputum from patients with chronic obstructive pulmonary disease or asthma. Am J Respir Crit Care Med 1996;153(2):530-534.
237. Aaron SD, Angel JB, Lunau M, Wright K, Fex C, Le Saux N, Dales RE. Granulocyte inflammatory markers and airway infection during acute exacerbation of chronic obstructive pulmonary disease. Am J Respir Crit Care Med 2001;163(2):349-355.
238. Elgersma Y, Kwast L, Klein A, Voorn-Brouwer T, van den Berg M, Metzig B, America T, Tabak HF, Distel B. The SH3 domain of the Saccharomyces cerevisiae peroxisomal membrane protein Pex13p functions as a docking site for Pex5p, a mobile receptor for the import PTS1-containing proteins. J Cell Biol 1996;135(1):97-109.
239. Ryerse JS, Hoffmann JW, Mahmoud S, Nagel BA, deMello DE. Immunolocalization of CC10 in Clara cells in mouse and human lung. Histochem Cell Biol 2001;115(4):325-332.
240. Demello DE, Mahmoud S, Ryerse J, Hoffmann JW. Generation and characterization of a conditionally immortalized lung clara cell line from the H-2Kb-tsA58 transgenic mouse. In Vitro Cell Dev Biol Anim 2002;38(3):154-164.
241. Karnati S, Palaniswamy S, Alam MR, Oruqaj G, Stamme C, Baumgart-Vogt E. C22-bronchial and T7-alveolar epithelial cell lines of the immortomouse are excellent murine cell culture model

systems to study pulmonary peroxisome biology and metabolism. Histochem Cell Biol 2016;145(3):287-304.
242. Sheikh FG, Pahan K, Khan M, Barbosa E, Singh I. Abnormality in catalase import into peroxisomes leads to severe neurological disorder. Proc Natl Acad Sci U S A 1998;95(6):2961-2966.
243. Ahlemeyer B, Vogt JF, Michel V, Hahn-Kohlberger P, Baumgart-Vogt E. Microporation is an efficient method for siRNA-induced knockdown of PEX5 in HepG2 cells: evaluation of the transfection efficiency, the PEX5 mRNA and protein levels and induction of peroxisomal deficiency. Histochem Cell Biol 2014;142(5):577-591.
244. Maxwell M, Bjorkman J, Nguyen T, Sharp P, Finnie J, Paterson C, Tonks I, Paton BC, Kay GF, Crane DI. Pex13 inactivation in the mouse disrupts peroxisome biogenesis and leads to a Zellweger syndrome phenotype. Mol Cell Biol 2003;23(16):5947-5957.
245. Kansanen E, Kuosmanen SM, Leinonen H, Levonen AL. The Keap1-Nrf2 pathway: Mechanisms of activation and dysregulation in cancer. Redox Biol 2013;1:45-49.
246. Milani P, Ambrosi G, Gammoh O, Blandini F, Cereda C. SOD1 and DJ-1 converge at Nrf2 pathway: a clue for antioxidant therapeutic potential in neurodegeneration. Oxid Med Cell Longev 2013;2013:836760.
247. Pahl HL. Activators and target genes of Rel/NF-kappaB transcription factors. Oncogene 1999;18(49):6853-6866.
248. Krakauer T. Molecular therapeutic targets in inflammation: cyclooxygenase and NF-kappaB. Curr Drug Targets Inflamm Allergy 2004;3(3):317-324.
249. Brown V, Elborn JS, Bradley J, Ennis M. Dysregulated apoptosis and NFkappaB expression in COPD subjects. Respir Res 2009;10:24.
250. Yang SR, Yao H, Rajendrasozhan S, Chung S, Edirisinghe I, Valvo S, Fromm G, McCabe MJ, Jr., Sime PJ, Phipps RP, Li JD, Bulger M, Rahman I. RelB is differentially regulated by IkappaB Kinase-alpha in B cells and mouse lung by cigarette smoke. Am J Respir Cell Mol Biol 2009;40(2):147-158.
251. Lixuan Z, Jingcheng D, Wenqin Y, Jianhua H, Baojun L, Xiaotao F. Baicalin attenuates inflammation by inhibiting NF-kappaB activation in cigarette smoke induced inflammatory models. Pulm Pharmacol Ther 2010;23(5):411-419.
252. Blanquart C, Barbier O, Fruchart JC, Staels B, Glineur C. Peroxisome proliferator-activated receptors: regulation of transcriptional activities and roles in inflammation. J Steroid Biochem Mol Biol 2003;85(2-5):267-273.
253. Ricote M, Li AC, Willson TM, Kelly CJ, Glass CK. The peroxisome proliferator-activated receptor-gamma is a negative regulator of macrophage activation. Nature 1998;391(6662):79-82.
254. Xu J, Zhu YT, Wang GZ, Han D, Wu YY, Zhang DX, Liu Y, Zhang YH, Xie XM, Li SJ, Lu JM, Liu L, Feng W, Sun XZ, Li MX. The PPARgamma agonist, rosiglitazone, attenuates airway inflammation and remodeling via heme oxygenase-1 in murine model of asthma. Acta Pharmacol Sin 2015;36(2):171-178.
255. Ghisletti S, Huang W, Ogawa S, Pascual G, Lin ME, Willson TM, Rosenfeld MG, Glass CK. Parallel SUMOylation-dependent pathways mediate gene- and signal-specific transrepression by LXRs and PPARgamma. Mol Cell 2007;25(1):57-70.
256. von Knethen A, Neb H, Morbitzer V, Schmidt MV, Kuhn AM, Kuchler L, Brune B. PPARgamma stabilizes HO-1 mRNA in monocytes/macrophages which affects IFN-beta expression. Free Radic Biol Med 2011;51(2):396-405.
257. Majai G, Sarang Z, Csomos K, Zahuczky G, Fesus L. PPARgamma-dependent regulation of human macrophages in phagocytosis of apoptotic cells. Eur J Immunol 2007;37(5):1343-1354.
258. Birrell MA, Patel HJ, McCluskie K, Wong S, Leonard T, Yacoub MH, Belvisi MG. PPAR-gamma agonists as therapy for diseases involving airway neutrophilia. Eur Respir J 2004;24(1):18-23.
259. Su CG, Wen X, Bailey ST, Jiang W, Rangwala SM, Keilbaugh SA, Flanigan A, Murthy S, Lazar MA, Wu GD. A novel therapy for colitis utilizing PPAR-gamma ligands to inhibit the epithelial inflammatory response. J Clin Invest 1999;104(4):383-389.

260. Jackson SM, Parhami F, Xi XP, Berliner JA, Hsueh WA, Law RE, Demer LL. Peroxisome proliferator-activated receptor activators target human endothelial cells to inhibit leukocyte-endothelial cell interaction. Arterioscler Thromb Vasc Biol 1999;19(9):2094-2104.
261. Pfutzner A, Schneider CA, Forst T. Pioglitazone: an antidiabetic drug with cardiovascular therapeutic effects. Expert Rev Cardiovasc Ther 2006;4(4):445-459.
262. Remels AH, Langen RC, Gosker HR, Russell AP, Spaapen F, Voncken JW, Schrauwen P, Schols AM. PPARgamma inhibits NF-kappaB-dependent transcriptional activation in skeletal muscle. Am J Physiol Endocrinol Metab 2009;297(1):E174-183.
263. Yin Y, Hou G, Li E, Wang Q, Kang J. PPARgamma agonists regulate tobacco smoke-induced Toll like receptor 4 expression in alveolar macrophages. Respir Res 2014;15:28.
264. Lombardi A, Cantini G, Piscitelli E, Gelmini S, Francalanci M, Mello T, Ceni E, Varano G, Forti G, Rotondi M, Galli A, Serio M, Luconi M. A new mechanism involving ERK contributes to rosiglitazone inhibition of tumor necrosis factor-alpha and interferon-gamma inflammatory effects in human endothelial cells. Arterioscler Thromb Vasc Biol 2008;28(4):718-724.
265. Bai YP, Liu YH, Chen J, Song T, You Y, Tang ZY, Li YJ, Zhang GG. Rosiglitazone attenuates NF-kappaB-dependent ICAM-1 and TNF-alpha production caused by homocysteine via inhibiting ERK1/2/p38MAPK activation. Biochem Biophys Res Commun 2007;360(1):20-26.
266. Lin W, Wu RT, Wu T, Khor TO, Wang H, Kong AN. Sulforaphane suppressed LPS-induced inflammation in mouse peritoneal macrophages through Nrf2 dependent pathway. Biochem Pharmacol 2008;76(8):967-973.
267. Jeong WS, Kim IW, Hu R, Kong AN. Modulatory properties of various natural chemopreventive agents on the activation of NF-kappaB signaling pathway. Pharm Res 2004;21(4):661-670.
268. Pi J, Leung L, Xue P, Wang W, Hou Y, Liu D, Yehuda-Shnaidman E, Lee C, Lau J, Kurtz TW, Chan JY. Deficiency in the nuclear factor E2-related factor-2 transcription factor results in impaired adipogenesis and protects against diet-induced obesity. J Biol Chem 2010;285(12):9292-9300.

Acknowledgements

This dissertation would not have been accomplished without the support of many people. Herein, I would like to thank those who have contributed in various ways to make this dissertation a reality.

First, I would like to express my sincere gratitude to my awesome supervisor Prof. Baumgart-Vogt for her constant support, guidance, patience and immense knowledge. I am thankful for her understanding and for always being ready to listen to the research (and other) problems. I am grateful for her time and for all the late nights and early mornings that she spent with me; suggesting, discussing and correcting.

I am very grateful to my postdoc, Dr. Srikanth Karnati, who always had time for the fruitful advices and discussions concerning work. I highly acknowledge his help in taking the best possible pictures as well as in providing the necessary materials for the experiments.

I would like to thank my wonderful friend and colleague Dr. Claudia Colasante for her guidance, discussions, our trips, laughter, chats, outings, fun and for all the wonderful time spent together. I want to thank my dear friends and office-mates Shan and Eistine for their support, care, scientific discussions, our experiments together and for the crazy and fun moments that we had. I always enjoyed being in the laboratory with you. I love you guys and I hope that we will always keep in touch.

I would like to sincerely thank PD. Dr. Barbara Ahlemeyer for the scientific discussions, kind advices and valuable suggestions.

I am grateful to my former colleagues, Harshavardhan Janga and Dr. Vijith Vijayan for the opportunity to learn many skills. Thank you for being great teachers.

I would like to warmly thank Andrea Textor who had the patience to go with me through the transformation experiments, bacterial cultures and many other things. I will miss your delicious cakes.

I am thankful to Bianca Pfeiffer who helped me to learn tissue immunofluorescence technique. Furthermore, I am grateful to Susanne Pfreimer, Petra Hahn-Kohlberger, Elke Rodenberg-Frank and Silvia Heller for the technical support and for the nice and friendly work atmosphere.

Finally, my deepest thanks go to my loving family, who always encourage, motivate and believe in me - to my parents Ludmila and Fayez, my grandma Valentina, my sister Amira and to all my relatives. I dedicate this thesis to you.